1986

Flow in asymmetrical compound channels with and without a floating cover.

Sisir Kumar. Ray
University of Windsor

CANADIAN THESES

THÈSES CANADIENNES

NOTICE

The quality of this microfiche is heavily dependent upon the quality of the original thesis submitted for microfilming. Every effort has been made to ensure the highest quality of reproduction possible.

If pages are missing, contact the university which granted the degree.

Some pages may have indistinct print especially if the original pages were typed with a poor typewriter ribbon or if the university sent us an inferior photocopy.

Previously copyrighted materials (journal articles, published tests, etc.) are not filmed.

Reproduction in full or in part of this film is governed by the Canadian Copyright Act, R.S.C. 1970, c. C-30.

AVIS

La qualité de cette microfiche dépend grandement de la qualité de la thèse soumise au microfilmage. Nous avons tout fait pour assurer une qualité supérieure de reproduction.

S'il manque des pages, veuillez communiquer avec l'université qui a conféré le grade.

La qualité d'impression de certaines pages peut laisser à désirer, surtout si les pages originales ont été dactylographiées à l'aide d'un ruban usé ou si l'université nous a fait parvenir une photocopie de qualité inférieure.

Les documents qui font déjà l'objet d'un droit d'auteur (articles de revue, examens publiés, etc.) ne sont pas microfilmés.

La reproduction, même partielle, de ce microfilm est soumise à la Loi canadienne sur le droit d'auteur, SRC 1970, c. C-30.

THIS DISSERTATION
HAS BEEN MICROFILMED
EXACTLY AS RECEIVED

LA THÈSE A ÉTÉ
MICROFILMÉE TELLE QUE
NOUS L'AVONS REÇUE

NL-339 (r. 86/06)

Canada

FLOW IN ASYMMETRICAL COMPOUND CHANNELS WITH AND WITHOUT A FLOATING COVER

by

Sisir Kumar Ray
B.C.E., M.E.

A Thesis
submitted to the Faculty of Graduate Studies through the
Department of Civil Engineering in Partial Fulfillment
of the requirements for the Degree of
Master of Applied Science at
The University of Windsor

Windsor, Ontario, Canada
1986

ISBN 0-315-31979-8

To my parents

ABSTRACT

In a stream flow system accurate prediction of discharge is a challenging problem. The problem becomes complex in the case of a compound channel with overbank flow due to the existence of differential boundary conditions. It becomes more serious in cold region stream flow due to the formation of an ice cover on it.

There is not a single method of solution existing so far which can handle all these problems.

In the present study a serious attempt has been made through theoretical as well as experimental investigations to establish a generalized and comprehensive two-dimensional method of solution with due consideration of momentum transfer mechanism in both vertical and lateral directions.

The proposed method is generalized because it can be used in solving many stream flow problems irrespective of the cross-sectional shape, size and boundary conditions.

It is comprehensive because the forms of the proposed equations are such that one single numerical scheme can solve for the velocity profiles, boundary shear stress distributions, and thus would enable it to predict more accurately the discharge at any portion of channel cross-section (viz., flood discharge in the case of overbank flow) with determination of composite roughness and energy slope.

The theory is developed with a concept that in case of a non-uniform flow the discharge of any part of a cross-sectional flow can be calculated without recourse to a common energy gradient.

In the present study laboratory investigation was performed in a series of compound channel cross-section with one flood plain by changing its shape, size, boundary roughnesses, and discharge rate under both free-surface and floating covered surface flow conditions.

Two design curves, one each for two flow conditions, are proposed for their application in solving real value problems within some specified limits.

Theoretical investigation was extended for the analysis of experimental data of previous research on simple and complex channel cross-sections.

ACKNOWLEDGEMENTS

The author wishes to express his thanks and gratitude to his advisor, Dr. S. P. Chee for his constant guidance and for critically reviewing this thesis.

In addition, many thanks to Dr. J. A. McCorquodale, for his careful review of the text and suggestions for improvement; these are greatly appreciated.

The research grant provided by the Natural Sciences and Engineering Research Council, Canada, is gratefully acknowledged.

Thanks to friends and colleagues for their direct and indirect help and best wishes.

He is very thankful to Mrs. Zeleney for her effort in typing this thesis.

TABLE OF CONTENTS

LIST OF FIGURES

LIST OF TABLES

Table | Page

Appendix C (cont.d)

LIST OF APPENDICES

NOMENCLATURE

The nomenclature, subscripts, and abbreviations used in this thesis are presented. The terms, which are used for any specific expression or equation in section or subsection and are already defined thereof, may not be repeated here.

A	cross-sectional area of a channel
B	bottom width of channel cross-section
B'	average width of channel cross-section
BT	top width of channel cross-section
E1& E2	velocity coefficients of the proposed velocity model
e	exponent
f	Darcy's coefficient of roughness
g	acceleration due to gravity
H	maximum flow depth of an overall channel flow
Hl	height of the flood plain bed from the main channel bed
H_s	maximum flow depth of any strip under free-surface or equivalent free-surface condition
h_s	local height of any elementary fluid from the boundary of any strip or substrip
h_{fp}	flow depth of flood plain
k	roughness height
L,M,N	total number of subdivisions, nodal points, etc. and are self-explanatory whenever these are used.
n	Manning's roughness
n_c	Manning's roughness of coarser mesh

Subscripts

1	subsection governed by the bed in case of a vertical stip and subsection governed by the left hand side boundary in case of a horizontal strip
2	subsection governed by the cover in case of a vertical stip and subsection governed by the right hand side boundary in case of a horizontal strip
b	related to channel bed
e	related to elementary fluid
fp	flood plain in case of compound channel with one flood plain
fpℓ	left hand side flood plain in case of compound channel with two flood plains
fpr	right hand side flood plain
h or hs	horizontal strip
mh or mhs	horizontal substrip
mc	main channel
ℓv or ℓvs	vertical substrip
's'	general notation of any strip - vertical or horizontal
v or vs	vertical strip
yx	action of force in the X-direction on the plane perpendicular to the Y-direction
zx	action of force in the X-direction on the plane perpendicular to the Z-direction

Abbreviations

CM	coarse mesh
FM	fine mesh
FP	flood plain cross-section

n_F	Manning's roughness of finer mesh
n_P	Manning's roughness of plywood
n_m	Manning's roughness of any roughness material
P	Hydraulic parameter
Q	total flow rate
R	hydraulic radius
S	Energy slope and/or bed slope
T	temperature of water flow
U	two-dimensional local velocity of a fluid element
u	one-dimensional local velocity of a fluid element in X-direction
V	mean velocity of a channel cross-section
v	one-dimensional local velocity in Y-direction
V_*	shear velocity
w	one-dimensional local velocity in Z-direction
Y	local flow depth in vertical or Y-direction - used in general with any vertical strip
y	flow depth of any elementary fluid in vertical strip
Z	local flow depth in horizontal or Z-direction - used in general with any horizontal strip
Z	ratio of horizontal to vertical for denoting inclination of side wall of a channel cross-section
$\bar{u},\bar{v},\bar{w}$	average velocity components in X-, Y-, and Z-directions, respectively
u',v',w'	velocity fluctuations or variations of the $\bar{u}$, $\bar{v}$, and $\bar{w}$ values, respectively

α	hydraulic perimeter ratio (i.e., ratio between the hydraulic parameter of bed and the total parameter) of any strip flow
α_f	relative flow depth (i.e., ratio between the flow depths of flood plain and main channel of a compound channel)
β_f	relative top width (i.e., ratio between the top width of flood plain and main channel)
γ	specific weight of water
δ	thickness of boundary layer
ε	relative depth of a fluid element related to strip flow
κ	Von Karman's constant
θ	(without subscript) - channel bed slope
θ	(with subscript) - inclination of side wall of channel cross-section to horizontal
λ	hydraulic radius ratio = R_2/R_1
μ	dynamic viscosity of water
ρ	density of water
ν	kinematic viscosity of water
ν_t	eddy-viscosity
σ	standard deviation
τ	shear stress at any nodal point
τ_ϕ	boundary shear stress
τ_a	apparent shear stress
ψ	energy slope ratio = S_2/S_1
ϕ, ϕ_1, ϕ_2	shape factors as defined by the author and other researchers
Φ	function of dimensionless velocity profile as defined in Equation 3.47

Abbreviations (cont'd)

FP(L)	left hand side flood plain
CP(R)	right hand side flood plain
L.S.W.	left hand side wall
MC	main channel cross-section
OC	overall channel cross-section

N.B. In all the cases notations used without any subscripts are related with the overall channel cross-section except where it is indicated otherwise.

CHAPTER I

INTRODUCTION

1.1 GENERAL

A simplified, yet very generalized, method of computation has been developed to determine some of the important characteristics of stream flow in a channel cross-section, of any shape and size, with or without flood plain(s) in one or both side(s) of it, and under free-surface or free-bouyant (covered surface) condition; the channel flow is to be considered steady, uniform or nearly uniform and incompressible.

The term "characteristics of stream flow", centers mainly on the velocity profiles, 'discharge','boundary shear stress distributions', 'composite roughness' and 'energy slope' of a channel cross-section as a whole or as a part.

Also, three types of channel cross-sections which will be used hereafter, are defined as:

1. A channel cross-section of simple geometry, viz., a rectangular, trapezoidal, triangular, semi-circular, or an arc of a circle, will be denoted by 'Simple Channel' (Figure 1.1(a)).

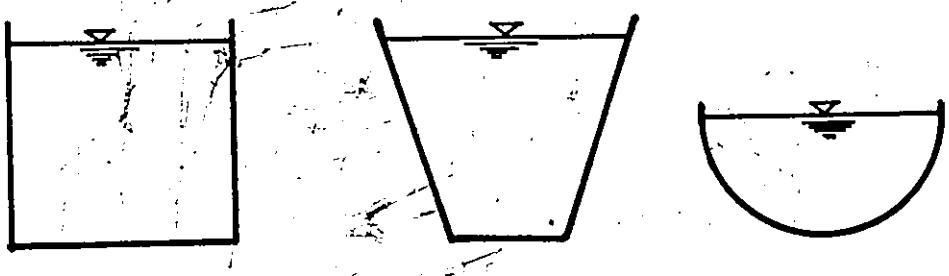

(a) Simple channels

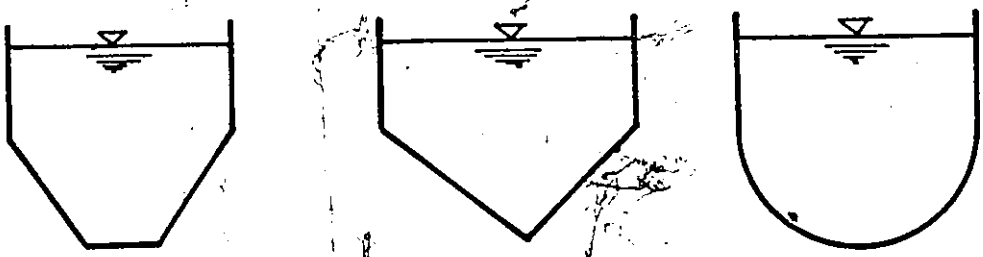

(b) Complex Channels

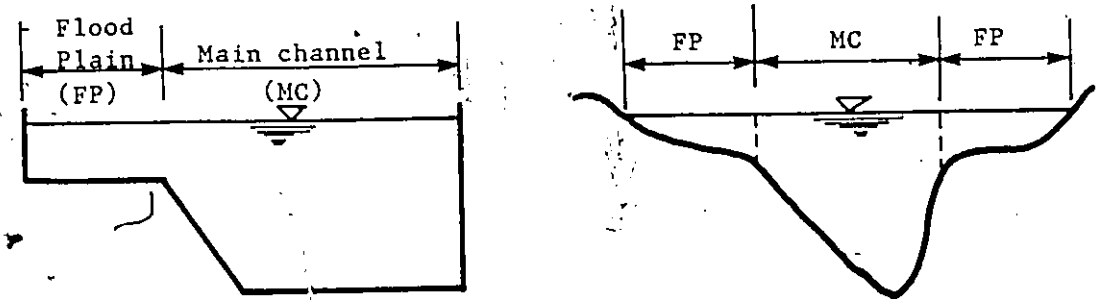

(c) Compound Channels

Fig. 1.1 Definition of Channels.

2. A channel cross-section with a combination of two or more simple geometries will be termed as a '<u>Complex Channel</u>' (Figure 1.1(b).

3. A simple channel or a complex channel together with flood plain(s) in one or both side(s) of the channel will be defined as a '<u>Compound Channel</u>' (Figure 1.1(c)).

1.2 CONCEPT OF THE THEORY

For a channel flow under a conventionally defined uniform flow condition, it is universally accepted that the energy slope of an entire channel flow is equal to the bed slope of the channel. It is common practice that the energy slope of an elementary fluid flow within a uniform flow system is also considered to be equal to the bed slope or the overall energy slope of the channel flow. This consideration will result in errors of computation of the gradually varied flow characteristics if the flow equation is to be developed from first principles or from the basic equations, such as the Reynolds form of the Navier Stokes equations.

Because of the existence of vertical and lateral momentum transfers of the prime flow in the longitudinal direction (in a three dimensional Cartesian coordinate system, Figure 3.1) of a channel, no two consecutive fluid elements at any cross-sectional flow will possess the same velocity. Hence, there will exist a vertical as well as a

lateral (i.e., horizontal) energy gradient. Therefore, the longitudinal energy slope of an elementary fluid motion is the resultant of vertical and lateral components of energy dissipation or head loss; it has a different value than that of the overall energy slope or bed slope (see Fig. 1.2).

In fact, Chow (17), in 1959, had mentioned one generalized equation for the determination of composite roughness of a channel section with multiple boundary roughnesses by assuming that the energy slope of each subarea is directly proportionate to the square of its boundary roughness (i.e., $s_i \alpha n_i^2$); the expression is given in equation 2.15 of Chapter II.

Moris and Wiggert (52) described in their text book, 'Applied Hydraulics in Engineering' that in case of overbank flow in a natural channel the total discharge will be affected by two causes: (1) the roughness coefficient for the overbanks flow is different from that of the river channel, and (2) the channel length for the flow on the overbanks is shorter than in the main channel because of the meanderings of the latter, causing the hydraulic slope to be higher for the overbank flow. This is the case of an unsteady flow.

In the present study the theory is developed on the basis of the concept mentioned hereby and with the assumption that the flow is a "quasi-uniform" and not strictly conforming to the "classical uniform" flow concept.

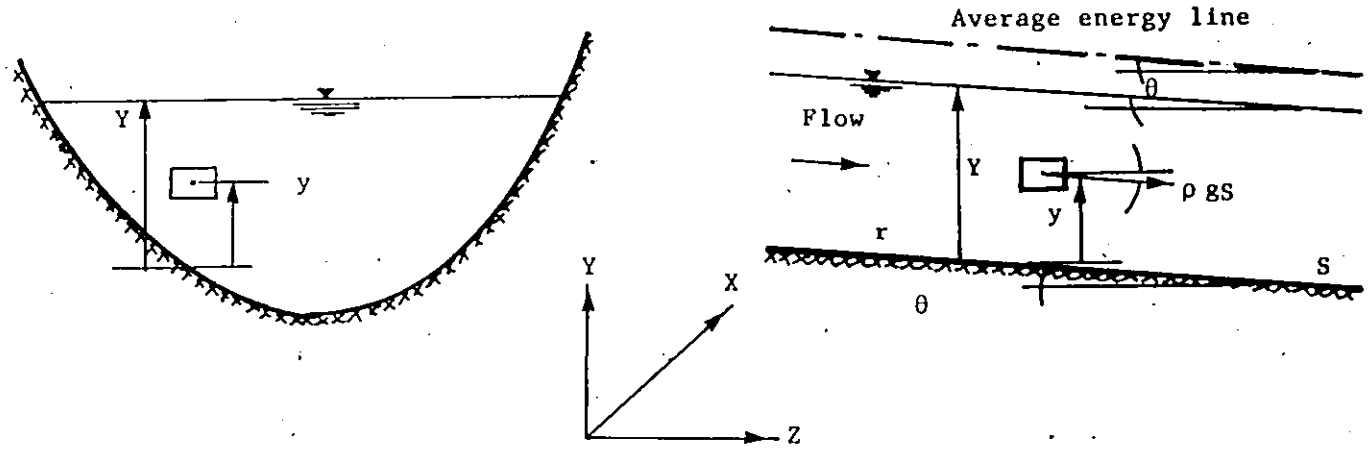

(a) Conventional Uniform Flow System

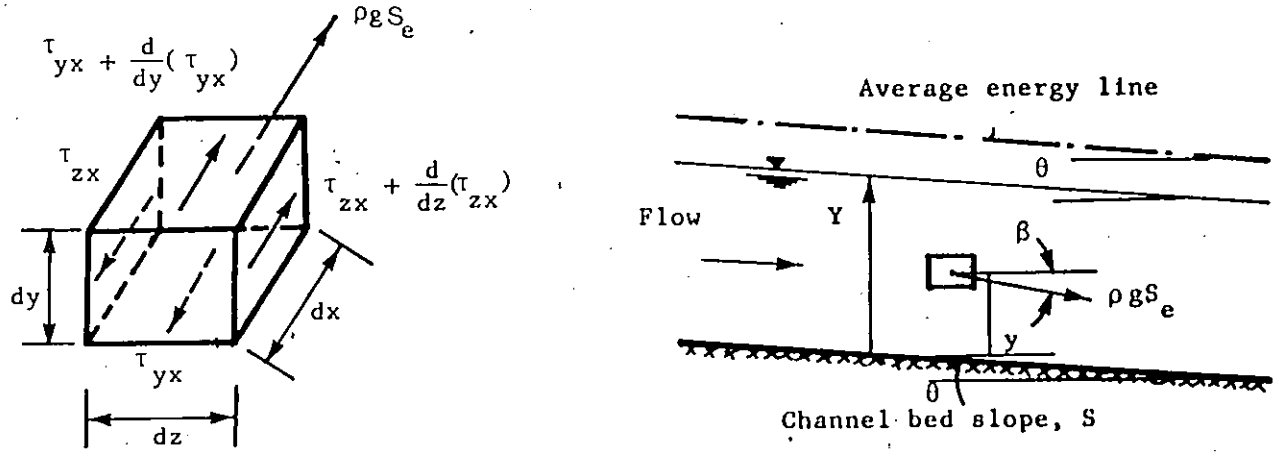

(b) Conceptual Uniform Flow System

Fig. 1.2. An Elementary Fluid in Motion.

1.3 PURPOSE OF THE RESEARCH

The successful solution of the above concept enables us to determine the velocity profile more accurately. The importance of obtaining accurate velocity profiles will allow us to determine the boundary shear stress distributions indirectly by using the widely accepted Prandtl theory of mixing length. For any part of a channel cross-section, the discharge can be computed from the velocity profiles while the energy slope is to be determined from the boundary shear stress distributions by using uniform flow equations. Hence, Manning's equation can be used for the determination of the composite roughness of the channel cross-section in question.

In case of a compound channel with overbank flow, the interaction between the generally slower moving water on the flood plains and the faster moving water in the main channel, that was explained by many researchers, is due to the existence of the apparent shear stress at an imaginary (vertical) interface plane between the two sections and affects the flow condition in a number of ways and makes the prediction of the stage-discharge relationship difficult.

In the present method the existence of the momentum transfer mechanism (irrespective of its degree of sensitivity) is considered significant between any two elemen-

tary fluid flows within the control volume of a two-dimensional channel flow. Therefore, no special requirements are to be considered for the imaginery (vertical) interface plane between the flood plain and the main channel cross-sections only.

The main objective of the present study is to establish the proposed velocity profile equation by determining the unknown coefficients analytically with the help of laboratory obtained data.

Laboratory investigation was programmed in such a way so that meaningful practical values of unknown coefficients could be obtained with a view to apply it in solving real value problems.

This is because of the practical difficulties involved in obtaining sufficient detailed measurements of velocity and boundary shear stress in the field during unsteady flood flow conditions.

With the limited scope of the present laboratory facilities, investigation was performed on a series of compound channel cross-sections with one flood plain by constructing them inside the existing test flume.

The tests were performed on a total of eleven channel cross-sections by changing its size and shape. The size was changed by varying the relative top widths of the flood

plain and the main channel. In total three different ratios (0.5, 1 and 2) were observed. The shape of the channel was changed by changing the inclination of the main channel's side wall with flood plain from 90° to 45° at an interval of 15°, while the other side wall of the main channel and that of the flood plain wall kept vertical. Each section was observed for both free- and covered-surface flows. Besides the study of the effects of shape, size and depth of flow, the effects of the multiple boundary roughness were also investigated by using two types of wire meshes.

Measurements of velocity distributions across the channel flow cross-sections were performed with a view to compare the results with velocity profiles, that were obtained from the solution of the proposed equation.

In Chapter II, the major research contributions of past years are presented in thematic order.

In Chapter III, theoretical considerations are established in more general forms.

In Chapter IV application of the generalized equations of Chapter III are expanded for the specific areas including the steps for its solutions.

Chapter V describes the experimental channels and ancillary apparatus together with the instrumentation used and the procedures followed in the experimental programme.

Chapter VI presents the discussion on the results of the laboratory study and its theoretical analysis.

Chapter VII discusses the application of the equations in solving actual problems through workout examples and comparing it with the other methods.

Conclusions and proposals for future research are dealt with in Chapter VIII.

CHAPTER II

LITERATURE REVIEW

2.1 GENERAL

The main concern of the present research is compound channels under free- as well as covered surface flow conditions. Most of the past research work on compound channels have been dealt with free-surface flow concentrating to establish the proper stage-discharge relationships. The analysis of composite roughness or equivalent roughness of the entire compound channel section often has not been given prominence.

To have a better understanding of the flow behaviour of a compound channel under covered-surface flow with multiple boundary roughnesses, this chapter will describe the major research contributions of past years mainly on compound channels under free-surface flow with an overview of the past works on composite roughness in case of non-compound channels both under covered and free-surface flows.

2.2 COMPOSITE ROUGHNESS

It is more than fifty years ago that researchers have attempted to develop equations for determining

composite roughness of channels with multiple boundary roughnesses. Most of these works are in the determination of composite or equivalent roughness of ice-covered channel flow, where only two boundary roughnesses exist; one for the ice-cover and the other for the bed including the side walls. Later, some researchers had tried to establish more generalized equations for determining composite roughness of both ice-covered and open channel flow with more than two boundary roughnesses.

2.2.1 Composite Roughness of Covered Channel Flow with Two Boundary Roughnesses

It is observed that all the equations of composite roughness are established by using one or more basic channel flow equations including uniform flow equations (Manning, Chezy, etc.), continuity equations, momentum equations together with simple geometrical relations and certain practical assumptions as well.

In all the cases, the basic assumptions that had been made to develop these equations are:

1. An ice-cover is a floating rigid boundary of homogeneous roughness.
2. The flow is incompressible, and uniform.
3. Influences or effects of secondary flows are neglected.
4. The cross-sectional flow is divided into two sub-

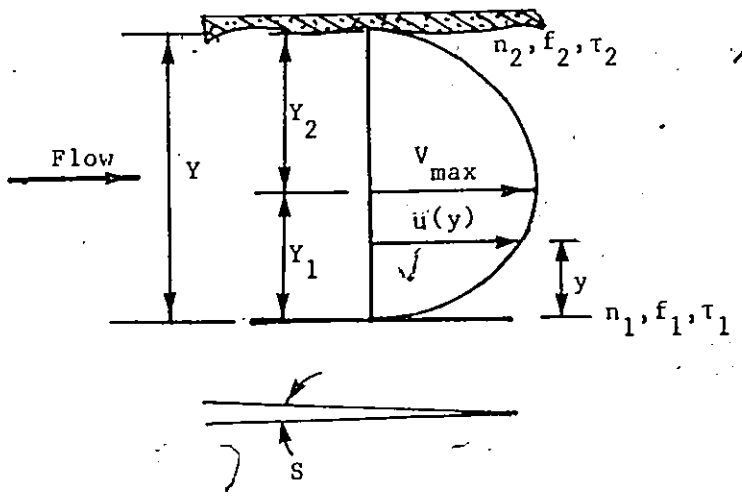

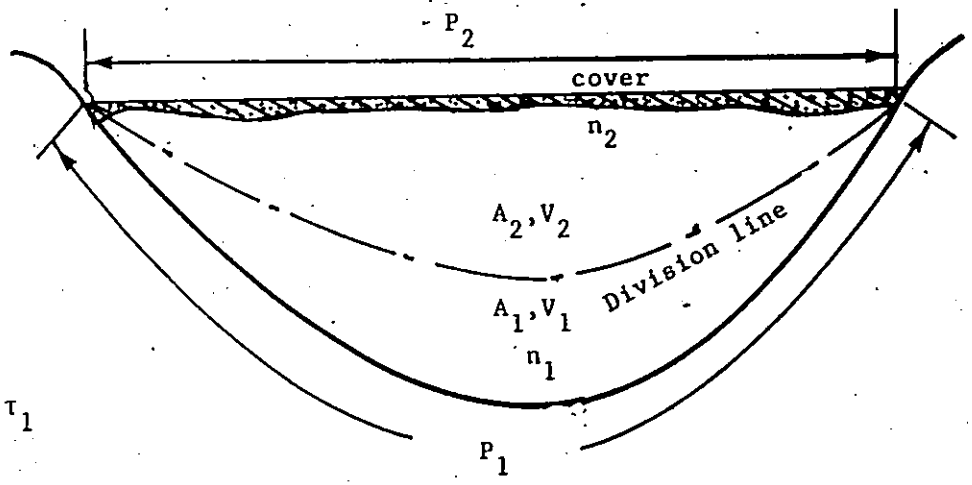

$$R_1 = \frac{A_1}{P_1},\ R_2 = \frac{A_2}{P_2},\ A_1 + A_2 = A,\ P = P_1 + P_2$$

Fig. 2.1. Schematic Depictation for the Determination of Composite Roughness of Channel Flow Under Covered Surface

section flows with an existence of an imaginary division line separating the two sub-section flows. Each sub-section flow is a channel with free-surface flow having single boundary roughness (see Figure 2.1).

Other assumptions vary from one researcher to another in the development of their equations; the most common are:

1. Hydraulic radius of each sub-section flow is equal to that of the entire channel flow (i.e., $R_1 = R_2 = R$).
2. Mean velocity of each sub-section flow is equal to that of the channel flow (i.e., $V_1 = V_2 = V$).
3. Summation of two hydraulic radii of two sub-sections is equal to the hydraulic radius of the channel (i.e., $R = R_1 + R_2$).

Table 2.1 shows some of these significant equations including the name of the main researchers, year of their publication, basic equations and the assumptions (Figure 2.2).

2.2.2 Composite Roughness - Generalized Equations

There are three principal equations mentioned by Chow (17) in 1959, which can be considered more generalized because of its application to determine composite roughness of a channel flow with more than two boundary

TABLE 2.1

Equation of Composite Roughness for Covered Channels

Researcher	Dimensionless Equation of Composite Roughness	Equation Number	Basic Equation(s)	Assumptions and Remarks
Pavlovskiy (1941)	$\frac{n}{n_1} = \left[\frac{1+a(n_2/n_1)^2}{1+a}\right]^{1/2}$	2.1	$\tau_\phi P = \tau_{\phi 1} P_1 + \tau_{\phi 2} P_2$ and Manning's Equation	$R_1=R_2=R$, and $V_1=V_2=V$
Lotter (1933)	$\frac{n}{n_1} = \frac{1+a}{1+a(n_1/n_2)}$	2.2	$AV=A_1V_1 + A_2V_2$ and Chezy's Equation	$R_1=R_2=R$ $V_1=V_2=V$
Sabaneev (1948)	$\frac{n}{n_1} = \left[\frac{1+a(\frac{n_2}{n_1})^{\frac{2}{2r+1}}}{1+a}\right]^{\frac{2r+1}{2}}$	2.3	$AV = A_1V_1 + A_2V_2$ and generalized equation of Chezy: $C_i = 1.486\, R_i^r/n_i$, $i = 1, 2$ and $r = 1/6$	$V_1=V_2=V$ $A = A_1+A_2$
Levi (1948)	$\frac{n}{n_1} = \frac{\kappa(y/2)^{1/4}}{n_1 g^{1/2}[\mathrm{Ln}(y/2k_m)-1]}$	2.4	Logarithmic velocity distribution: $u_i(y) = \frac{1}{\kappa}\frac{(gyS)^{1/2}}{2}\mathrm{Ln}(\frac{y_i}{k_i})$ $i = 1, 2$; the continuity and Chezy equations	$k_i=\frac{y}{2}\exp[-1-\frac{\kappa}{n_i g^{1/2}}(\frac{y}{2})^{1/4}]$ and, $k_m=(k_1+k_2)/2$
Chow (1959)	$\frac{n}{n_1} = \frac{1}{(1+a)^{1/2}}(n_2/n_1)[a^{3/4} + (\frac{n_1}{n_2})^{3/2}]^{2/3}$	2.5	$\tau_\phi P = \tau_{\phi 1} P_1 + \tau_{\phi 2} P_2$ and the Chezy equation	$R=R_1+R_2$ and the maximum discharge condition; $\frac{d(n)}{d(R_1/R_2)} = 0$

TABLE 2.1 (cont'd.)

Researcher	Dimensionless Equation of Composite Roughness	Equation Number	Basic Equation(s)	Assumption and Remarks
Shiperko (1961)	$\frac{n}{n_1} = \left(\frac{1+a}{1+a(n_1/n_2)^2}\right)^{1/2}$	2.6	Chezy's equation and minimal head loss equation: $C^2 = \frac{P_1}{P}C_1^2 + \frac{P_2}{P}C_2^2$	$R_1=R_2=R$
Sinotin (1965)	$\frac{n}{n_1} = \frac{0.6}{(\frac{Y_1}{Y})^{1.75} + \frac{n_1}{n_2}(\frac{Y_1}{Y})^{1.75}}$ where $\frac{Y_1}{Y} = 0.6 \log(\frac{n_2}{n_1}) + 0.5$	2.7	Nikitin's logarithmic velocity distributions: $(\frac{u}{V_*}) = 6.45 \log(\frac{y}{y_i}) + 5.6 + 2.8(\frac{y}{y_i}) - 1)/(\frac{y}{y_i})$	$V_1=V_2=V$ and considering the channel as a "Wide Channel"
Larsen (1966)	$\frac{n}{n_1} = \frac{0.63(\frac{Y_2}{Y_1} + 1)^{5/3}}{\frac{n_1}{n_2}(\frac{Y_2}{Y_1})^{5/3} + 1}$	2.8	Velocity profiles: $u_i(y_i) = 2.5 V_{*i} \mathrm{Ln}(30\frac{y_i}{k_i}F_i$, $i = 1,2$, and $AV = A_1V_1 + A_2V_2$	It is valid for $0.2 < \frac{n_1}{n_2} < 1.0$ and flow depth not less than 5.0 ft. cr 1.6 meter.
Komora and Sumbal (1967)	$\frac{n}{n_1} = \left[\frac{(\frac{n_2}{n_1})^{3/2} + 1}{2}\right]^{2/3}$ with the equation for hydraulic division ratio, $Y_1/Y = a_{h1} = \frac{n_1^{3/2}}{n_1^{3/2}+n_2^{3/2}}$	2.9(a)	Manning-Strickler Equation.	Pavlovskiy's assumptions

TABLE 2.1 (cont'd.)

Researcher	Dimensionless Equation of Composite Roughness	Equation Number	Basic Equation(s)	Assumption and Remarks
Komora and Sumbal (1967)	$\frac{n}{n_1} = \frac{0.63}{(1-a_{h1})^{5/3} + \frac{n_1}{n_2} a_{h1}}$	2.9(b)	Generalized form of hydraulic division ratio: $(1-a_{h1})^{1/2}(\frac{6Y^{1/2}}{n_2}6(1-a_{h1})^{1/2} + \frac{q}{k}^{1/2})$ $= (a_{h1})^{1/2}\frac{6Y^{1/2}}{n_1}6(a_{h1})^{1/2} + \frac{q}{k}^{1/2}$ and equation 2.9(a)	a_{h1} can be obtained from the monograph developed by the authors
Hancu (1967)	$\frac{n}{n_1} = \frac{1}{\sqrt{2}}(\frac{Y}{Y_1})^{1/6}((\frac{V_1}{V})^2 + (\frac{V_2}{V_1})^2(\frac{n_2}{n_1})^2(\frac{Y_1}{Y_2})^{1/3})^{1/2}$	2.10	Velocity defect law, $V_{max}-u_i(y) = V_{*i}\frac{1}{k}Ln\frac{Y_i}{Y_i}$. and $YV = V_1Y_1 + V_2Y_2$	Applied to wide channels only
Yu, Graf and Livien (1968)	$\frac{n}{n_1} = (\frac{1+az(n_2/n_1)}{(1+a)^z})^{3/2}{}^{2/3}$	2.11	Continuity equation $AV = A_1V_1 + A_2V_2$ and empirically modified Manning's equation $V_i = \frac{1.49}{n_i}(\frac{A_i}{P_i^2})^{0.5+r} S^{1/2}$	$V_1=V_2=V$ and $A=A_1+A_2$ $z = (n_2/n_1)^{1/6}$ Correction for hydraulic radius

TABLE 2.1 (cont'd.)

	Dimensionless Equation of Composite Roughness	Equation Number	Basic Equation(s)	Assumption and Remarks
Krishna Murthy and Christensen (1972)	$\frac{n}{n_1} = (\frac{n_2}{n_1})^{1/}(1+\frac{P_1}{P_2}(\frac{Y_1}{Y_2})^{3/2})$	2.12(a)	$(\frac{u(y)}{V_*})_i = 8.48 + 2.5\,Ln(\frac{Y}{k})_i$ at $y = 0.368\ Y_i$,	Equation [2.12b] is obtained by assuming wide channel, where $a = P_1/P_2 = 1$
	$\frac{n}{n_1} = (\frac{n_2}{n_1})^{1/(1+\frac{Y_1}{Y_2})^{3/2}}$	2.12(b)	$u(y)_i = V_i$ Combined Manning-Strickler equation $n = 0.0342\ k^{1/6}$	
Chee and Haggag (1976)	$\frac{n}{n_1} = \frac{(\alpha+(1-\alpha)\lambda)^{5/3}}{\alpha+\frac{n_1}{n_2}(1-\alpha)\lambda^{5/3}}$ where, $\alpha = P_1/P$ and $\lambda = R_2/R_1$ and the division surface can be determined from: $\frac{3\kappa}{2}\frac{R^{1/6}}{n_1 g^{1/2}} = \frac{\lambda^{1/2}-1}{1-\frac{n_1}{n_2}\lambda^{2/3}}(\alpha+(1-\alpha)\lambda)^{1/6}$	2.13	General Reynolds form of Naviar-Stokes equation together with Prandtl-Von Karman mixing length theory: $u_i = V_i - \frac{V_{*i}}{\kappa}F_2(\epsilon_i)$ when $F_2(\epsilon_i) = 2[\ln\frac{\epsilon_i^{1/2}}{1-(1-\epsilon_i)^{1\,2}} -(1-\epsilon_i)^{1/2}-1/3]$ and i = 1,2; the continuity equation, $AV = A_1V_1 + A_2V_2$	Manning's equation is valid for both sub-section flows

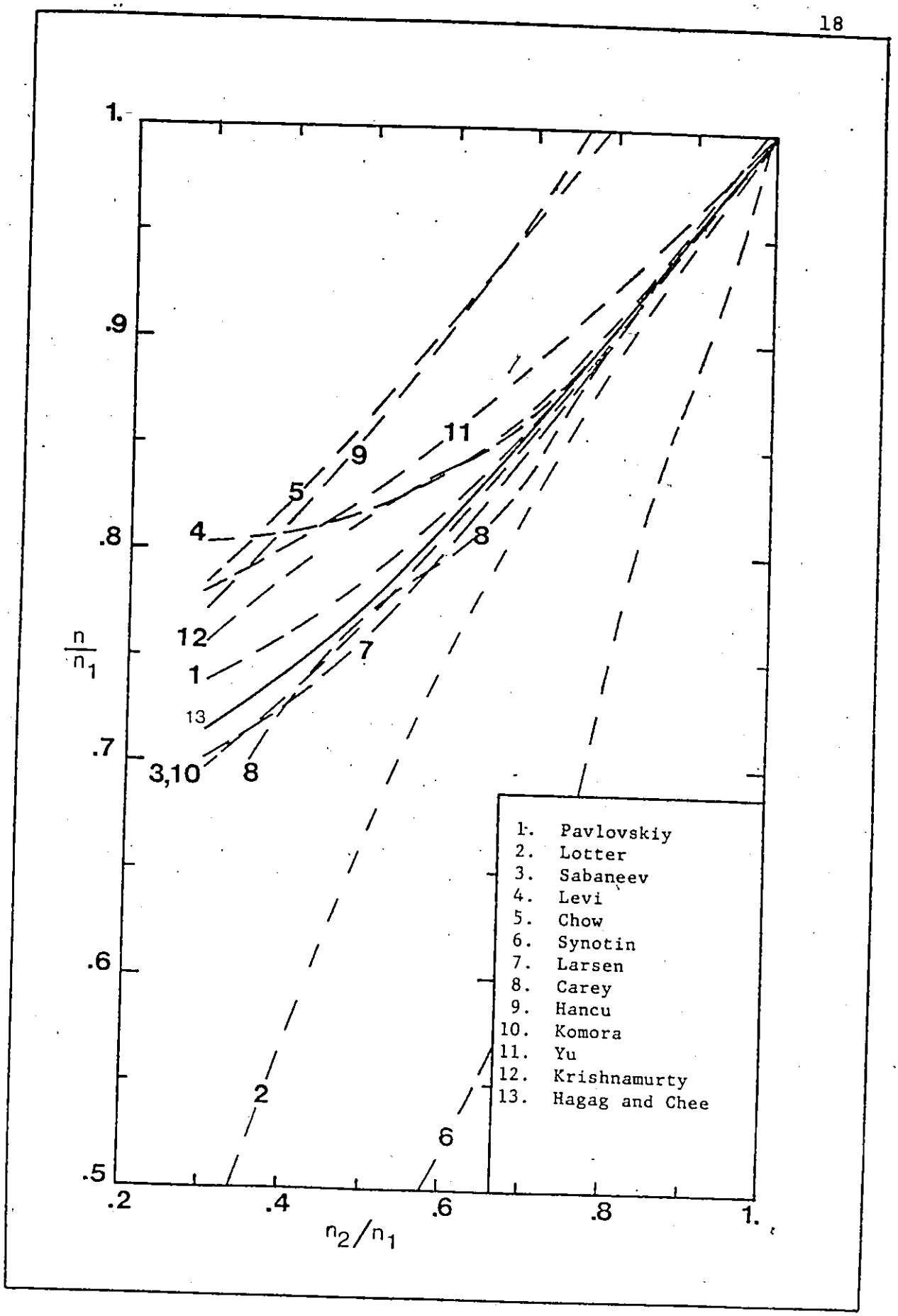

Fig. 2.2. Composite Roughness Comparison of Past Works of most of the Investigators as listed in Table 2.1 [Reference (30)].

roughnesses. Also, these can be applied only for the free-surface flow or it can be applied for both free-surface and covered surface flow. The three equations can be described as:

$$n = \left(\frac{\sum_{i=1}^{N} P_i n_i^{3/2}}{P}\right)^{2/3} \qquad 2.14$$

$$n = \left(\frac{\sum_{i=1}^{N} P_i n_i^{2}}{P}\right)^{1/2} \qquad 2.15$$

$$n = \left(\frac{PR^{5/3}}{\sum_{i=1}^{N} \frac{P_i R_i^{5/3}}{n_i}}\right) \qquad 2.16$$

The assumption made in developing equation 2.14 is that the mean velocity of each subsection is the same and equal to that of the entire channel cross-section. The other assumption is that the energy slope (S_i) of each subsection is constant and equal to that of the channel cross-section.

The basic equation is:

$$A = A_1 + A_2 + A_3 \ldots = \sum_{i=1}^{N} A_n.$$

In the second equation 2.15, the assumptions are made:

i) $V_1 = V_2 = \ldots = V$

ii) $R_1 = R_2 = \ldots = R$

iii) energy slope of each subsecion flow is discrete and not equal to the bed slope of the entire channel, and

iv) Mannings' equation is valid for each sub-section.

From the above assumption it can be shown that the energy slope of any sub-section is directly proportionate to the square of its boundary roughness (i.e., $S_i \alpha n_i^2$).

The basic equation is considered, in this case, that the total tractive force of the entire channel flow is equal to the summation of tractive forces of all the subsection flows, i.e.,

$$\gamma RPS = \sum_{i=1}^{N} \gamma R_i P_i S_i$$

The basic equation used in developing the equation 2.16 is the continuity equation with the assumptions that the Mannings equation is equally valid for sub-section flows and energy slopes are constant.

In 1972 Krishnamurthy and Christensen (44) developed a generalized equation by assuming the channel as very wide so that the side wall effect can be neglected. The channel is subdivided into finite strips as shown in Figure 2.3. He used a logarithmic velocity distribution $u(y)_i$, at any distance, y from the bed and the roughness expressed in terms of the hydraulic roughness, k, is

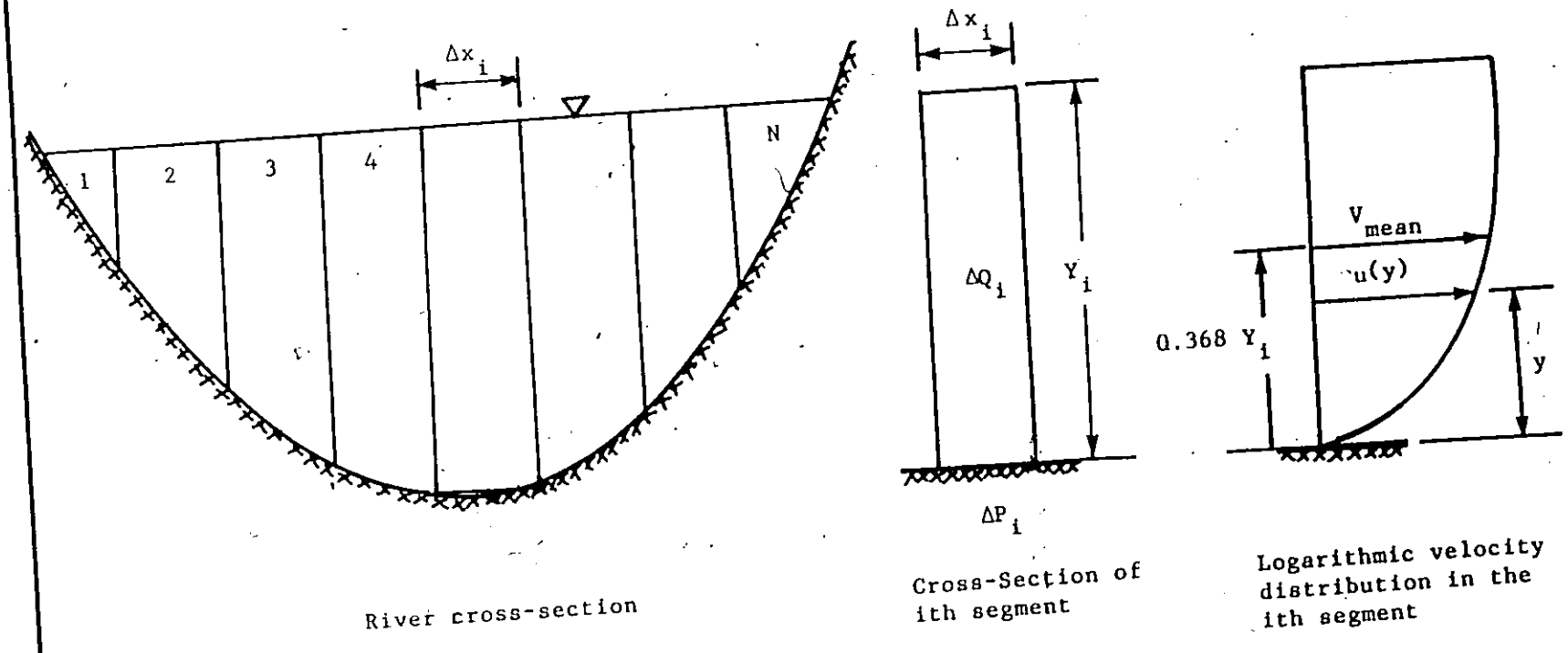

Fig. 2.3. Schematic River Cross-section used by Krishnamurthy and Christerson [44].

$$\left(\frac{u(y)}{V_*}\right)_i = 8.48 + 2.5 \ln \left(\frac{Y}{k}\right)i, \quad i=1, 2, 3 \ldots N$$

By using Strickler form of Manning's equation, $k = \left(\frac{n}{0.0342}\right)^6$ and the assumption that the mean velocity of any strip occurs at a distance of $0.368\ Y_i$ from the bed, the equivalent roughness expression was obtained from the continuity equation $Q = \sum_{i=1}^{N} Q_i$, and is:

$$n = \exp\left[\frac{\sum_{i=1}^{N} P_i Y_i^{3/2} \text{Ln } n_i}{\sum_{i=1}^{N} P_i Y_i^{3/2}}\right] \qquad 2.17$$

It can also be observed that the first two equations 2.14 and 2.15 are independent of the hydraulic radii, or flow depth and hence, these can be used for both free-surface and covered surface flow. The remaining two equations, 2.16 and 2.17, can only be used for free-surface flow.

2.3 COMPOUND CHANNEL

2.3.1 General

The most important of all the analyses of a compound channel is the determination of flood discharges that is in overbanks flows. In the past, many researchers had tried to establish more improved methods with better explanations and reasonings. Almost all of these works are developed and used for a free-surface flow condition.

From the past studies, three major approaches can be identified with the problem.

1. Conventional approach; it does not consider the momentum transfer (MT) effects.
2. Methods based on experimentally-derived correction factors to account for MT effects.
3. Methods based on development of a model considering momentum transfer and the effect of apparent shear stress at the vertical intersection of main channel and overbank.

2.3.2 Conventional Method

This method is further subdivided into:

1. 'Single Channel' method.
2. "Separate Channels' method

2.3.2.1 'Single-Channel' Method

In this method the compound section is considered as a single channel, and, therefore, the total discharge is calculated by means of a uniform flow formula (e.g., Manning) as follows:

$$Q = \frac{1}{n} A R^{2/3} S^{1/2}$$

where

Q = total discharge;

n = roughness coefficient (composite) for compound section,

A = total cross-sectional areas,

R = hydraulic radius of compound section.

This method has several limitations:

1. It employs a single (composite) roughness coefficient for the entire compound section including flood plain(s). Therefore, the composite roughness has to be calculated by using any one of the generalized relations described in the previous section, 2.2.2. The accuracy of the result is dubious while the accuracy of those relations are in question.
2. The relative depth of flood plain flow compared to the overall depth of flow (which is, in fact, the depth of the main channel flow) is very small. Hence, there is usually a very large increase in wetted perimeter compared to the corresponding increase in flow area. Thus it results in a decrease in hydraulic radius which would imply a corresponding decrease in discharge.

   Hence, it leads to an underestimation of system discharge, in the case of a known flow depth and an overestimation of the flow depth, in the case of a known discharge, specially when there exists a substantial difference in the roughness of flood plains in relation to that of the main channel.
3. This method has no provision for the determination of flood plain discharge and main channel discharge separately.

4. The use of a single energy slope equal to that of bed slope of the main channel is highly questionable.

2.3.2.2 'Separate Channels' Method

To overcome some of the problems associated with the 'Single Channel' method, many researchers had attempted this "Separate-Channel' method, which treats the channel and flood plain zones as separate entities. A major advantage of this method is that it provides a convenient way to account for different boundary roughnesses between the main channel and flood plain zones.

There are mainly three different approaches to this method.

Method 1

In the first approach, the total discharge is calculated by summing the discharges of the various subsections which are defined by imaginary vertical interface planes passing through the junctions between adjacent deep and shallow sections, as shown in Figure 2.5(a), and assuming no interaction between the various subareas gives

$$Q = \sum_{i=1}^{L} Q_i = S^{1/2} \sum_{i=1}^{L} \frac{A_i^{5/3}}{P_i^{2/3} n_i}$$

$$= \left[\frac{A_1 R_1^{2/3}}{n_1} + \frac{A_2 R_2^{2/3}}{n_2} + \frac{A_3 R_3^{2/3}}{n_3}\right] S^{1/2} \qquad 2.18$$

It should be noted that each subarea is considered as a separate and individual channel flow taking the wetted perimeter P of each section comprised of its physical boundary without including the imaginary interfaces.

Knight and Demetriou (38) in their early works (1983) have indicated that the choice of subareas in this method is inappropriate, on account of the significant lateral momentum transfer between the flood plains and the main channel. Hence, this approach of the 'Separate Channel' method tends to overestimate total discharge, the intensity of which depends on the relative ratio (h_{fp}/H) as well as the relative width ratio of flood plain and main channel.

Method 2

An alternative subdivision of the cross-section, as shown in Figure 2.4 (b), is suggested by many researchers, including Knight and Hamed (41), to overcome the inadequacy of Method 1. In this case vertical interfaces are again considered but with the length of the interface added into the wetted perimeter of each subarea in which it is considered that the vertical interface has the same boundary roughness equal to that of their respective bed roughness.

Knight and Hamed (41) indicated that this method overestimates the discharge at very low flow depth over the flood plains and underestimates the discharge at comparatively higher flow depth over the flood plains.

Method 3

Because of the defects as mentioned in Method 1 and Method 2, many researchers had attempted to correct the hydraulic radii of such subsections by arranging the imaginary plains in various alternative ways, including inclined and horizontal ones; these attempts were made to incorporate the effects of momentum transfer at the vertical interfaces in an indirect way.

Knight, et al. (41) had drawn the interfaces from the corner junctions between the flood plains and the main channel to the center-line position of the free-surface as shown in Figure 2.5(c). The angle of inclination of each interface thus increases from zero at $h_{fp}=0$ (without flood plains flow) to $\Pi/2$ at $h_{fp} = H$ (with flood plain flow depth equal to the depth of main channel flow). The authors indicated that their results give the closest agreement with a limited amount of experimental data within a limitation of $0 < h_f/H < 0.5$.

The authors did not indicate, however, clearly that what will be the inclination of imaginary interfaces in case of an asymmetrical compound channel or in case of a compound channel with one flood plain only.

In case of a comparatively small relative depth of overbank flow, it is observed that a horizontal interface plain produces results that are superior to those provided by other methods.

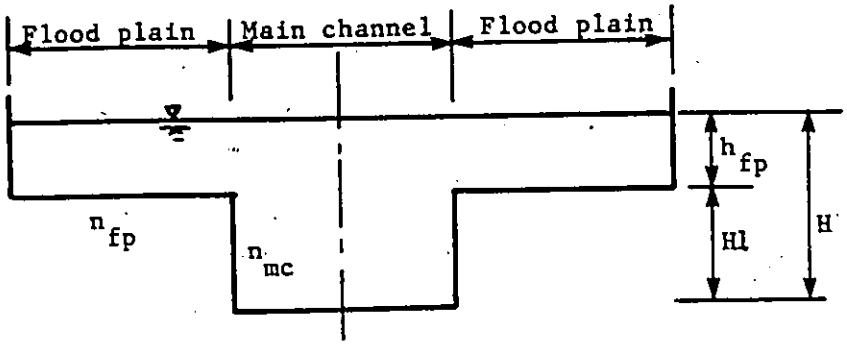

Fig. 2.4. Definition Channel

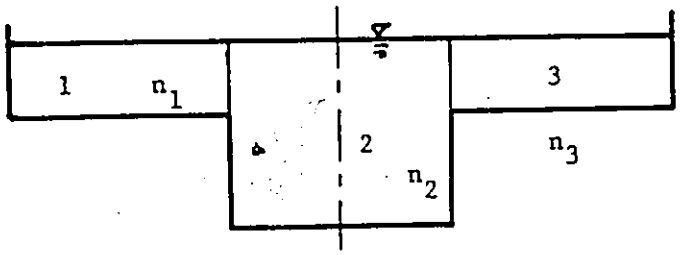

(a) Method 1

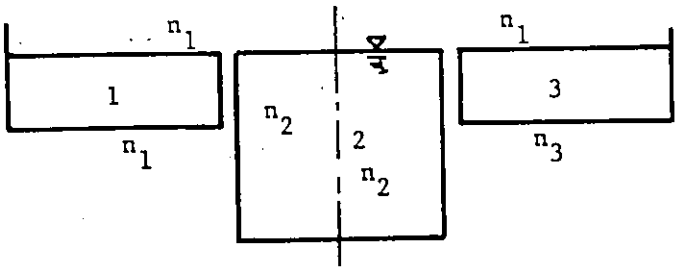

(b) Method 2

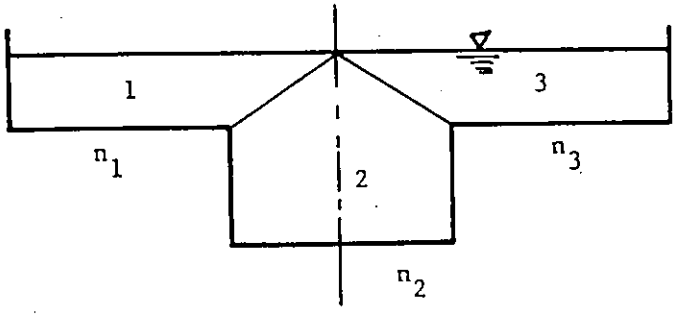

(c) Method 3

Fig. 2.5 Subdivision of Cross-section by Separate Channel Methods.

2.3.2.3 Significant Researches

A summary of some significant works in the area of 'Separate Channel' method is given below.

Rice (71) and Posey (61) divided the cross-section into hydraulically homogeneous zones using vertical, horizontal, diagonal imaginary interface planes. They assumed no shear acting on the imaginary planes and hence the latter were not included in the wetted perimeter calculations. In some cases, they also assumed that apparent shear stress and main channel boundary shear stress were approximately equal and hence the interface was included in the main channel wetted perimeter only.

Delleur, et al. (19) studied uniform flow in prismatic flood plain channels that had a variety of surface roughnesses. They had examined with different methods of subdividing the compound cross-section and compared formulae for evaluating the equivalent Manning's coefficient.

Wormleaton, et al. (85) used an apparent shear stress ratio as a criterion in deciding inclusion of a particular interface plane in the wetted perimeter calculation. For a ratio less than 0.2 the interface plane was neglected, where as for a ratio greater than 0.2, the plane was suggested to be included in the main channel wetted perimeter only. They also observed that a horizontal interface

plane produced the best results.

Wright and Carstens (87) suggested to include the interface plane in the wetted perimeter calculation for the main channel only, while Yen and Overton (88) proposed not to include such interface plane in the wetted perimeter calculation at all.

2.3.3 Experimental Method

Because of the difficulties in incorporating the effects of MT in developing a theoretical equation, many researchers had tried to find out a simple correction factor in the uniform flow calculation from laboratory investigation method.

James and Brown (33) in their 'modified single-channel' method introduced a simple correction factor for Manning's equation in the form of:

$$A = K\frac{1}{n}AR^{2/3}S^{1/2} \qquad 2.19$$

where, the correction factor, K was obtained from a curve-fitting technique which was applied to plots of n/n_b versus relative width for various relative depths.

Another approach was to find out the correction factor for each subsection of a compound channel while treating it as a 'Separate Channel' method. The form of the equation can be expressed as:

$$Q = S_i^{1/2} \sum_{i=1}^{I} K_i \frac{1}{n_i} A_i R_i^{2/3} \qquad 2.20$$

where, K_i = correction factor for the ith subarea.

Two pioneer researchers are Le Van Kiyen (47) and Karasev (34). Le Van Kiyen used five empirical relationships including the parameters, such as, relative depth of flow, relative roughness, degree of asymmetry, and shape of cross-section, to determine the correction factors. Kiyen's method is tedious and its application does not provide any significant improvements over other methods.

Karasev used the momentum equation to obtain expressions with two empirical parameters only. The correction factors were derived from approximately 300 experiments and hence, it can be considered quite significant from a statistical viewpoint.

2.3.4 Methods Considering the Effects of MT

In this approach, most of the researchers believed that an apparent shear stress that exists at the main channel and flood plain interface due to the interaction between the generally slower moving water on the flood plains and the faster moving water in the main channel, affects the flow structure in a number of ways and, hence, the effects of this apparent shear stress should have to be

incorporated in the analysis to obtain better results.

The main concept explains that the velocity difference and the differential boundary conditions between the main channel and flood plain are the causes of setting up an additional amount of turbulent shear (which is defined by recent researchers as an 'apparent shear') and a continuous momentum transfer diffusion from channel to flood plain.

In other words, in a discretized form it can be stated that with this momentum drain the equilibrium condition for the main channel can be obtained by an overall decrease in boundary shear, or conversely, the equilibrium state, in case of flood plain, can be achieved by an increase in boundary shear.

Mathematically, this can be stated as (see Figure 2.6) channel equilibrium,

$$\tau_{mc} P_{mc} = \rho g A_{mc} S_{mc} - \tau_a h_{fp} \qquad 2.21a$$

or

$$\tau_a h_{fp} = (\tau'_{mc} - \tau_{mc}) P_{mc} \qquad 2.21b$$

and flood plain equilibrium,

$$\tau_{fp} P_{fp} = \rho g A_{fp} S_{mc} + \tau_a h_{fp} \qquad 2.22a$$

or

$$\tau_a h_{fp} = (\tau_{fp} - \tau'_{fp}) P_{fp} \qquad 2.22b$$

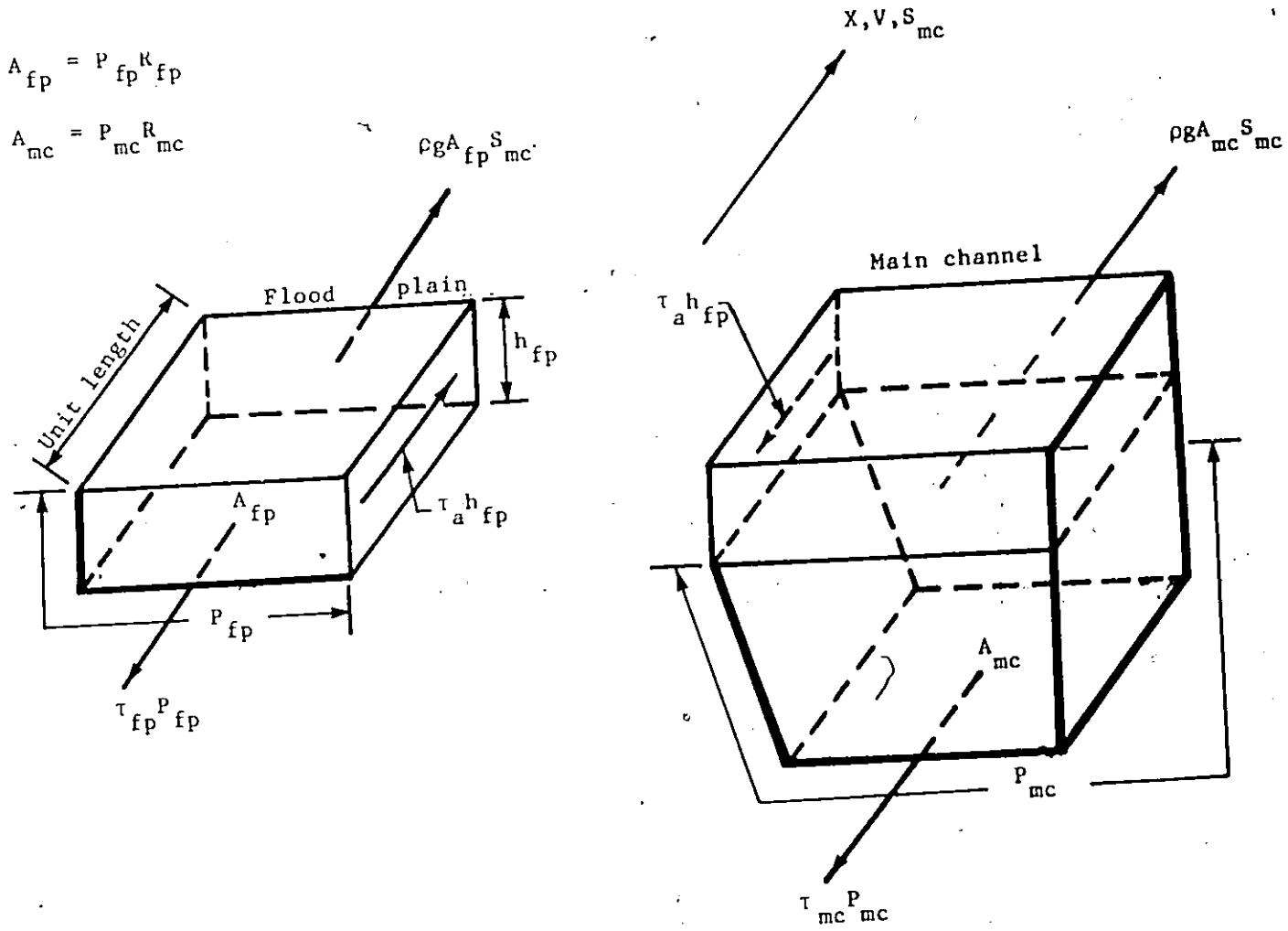

(N.B. Forces are per unit cross-sectional area)

Fig. 2.6. Equilibrium Configuration of Main Channel and Flood Plain with the Concept of Apparent Shear in a Compound Channel Flow with One Flood Plain.

where, τ_{mc} and τ_{fp} are average boundary shear stress of the main channel and flood plain, respectively, with correction for momentum, while τ'_{mc} and τ'_{fp} are without consideration of momentum and τ_a is the depth averaged apparent shear stress.

Boundary shear stress can be related with the corresponding mean velocity by the relation:

$$\tau_\phi \propto V^2 \qquad 2.23$$

Therefore, discharge of a compound channel can be determined by

$$Q = V_{mc}A_{mc} + V_{fp}A_{fp} \qquad 2.24$$

where, V_{mc} and V_{fp} is to be calculated from the corresponding boundary shear stress, τ_{mc} and τ_{fp} using the relation of equation 2.23.

While in the absence of proper mathematical relationship in generalized form for the determination of boundary shear stress, τ_{mc} and τ_{fp} researchers had attempted, in recent years, to establish proper relationship of apparent shear stress, τ_a, from equations 2.21b or 2.22b, using laboratory measured data of τ_{mc} and τ_{fp}, when τ'_{mc} and τ'_{fp} are known for a given slope, S_{mc}. The idea of obtaining such relationship of apparent shear stress is to calculate actual boundary shear stresses (τ_{mc} and τ_{fp}) and the discharge thereby (using equations 2.21 through 2.24) for a real value problem.

2.3.4.1 Determination of Apparent Shear Stress, τ_a from Laboratory Measured Data

Ervine and Baird (22) in 1982 established a linear relationship between the apparent shear stress and difference of velocities (ΔV) between the main channel and flood-plain from equation 2.21b using Rajaratnam and Ahmadi's (69) results; Rajaratnam and Ahmadi had produced graphs of the boundary shear stress (τ_{mc}) during interaction. The magnitude of the apparent shear stress was given by $50(\Delta V)^2$ in case of asymmetric channels and $25(\Delta V)^2$ in case of symmetric channels, where: $\Delta V = V'_{mc} - V'_{fp}$ can be determined by uniform flow equation using either Manning or Chezy. They used Prandtl's mixing length theory as the momentum equation. The relation for symmetrical channels was found from the test results (τ_{mc}) of Ghosh and Jena (28). They concluded the two results are practically the same considering the relation for symmetrical compound channel as:

$$2\tau_a h_{fp} = (\tau'_{mc} - \tau_{mc})P_{mc} \qquad 2.25$$

However, their results for apparent shear stress are valid for straight channels with smooth boundaries and the roughness of the flood plain equal to the main channel.

Prinos and Townsend (63) using the same discretized channel-flood plain concept (equations 2.22b and 2.25) extended their study in symmetrical compound channel with

two flood plains and with varying relative flood plain-main channel width, relative flow depth, and relative roughness to determine equation for apparent shear stress.

They evaluated the values of apparent shear stress (from equation 2.21b and 2.22b) by measuring local boundary shear stress (τ_{mc},τ_{fp}) using Preston-tube technique. Prinos (62) in his original works had established three relationships for apparent shear stress by multiple linear regression analysis of his experimental data. Later in the publication (63), Prinos and Townsend furnished the following relationship:

$$\tau_a = 0.874\ Y_r^{-1.129} B_r^{-0.514} \Delta V^{0.92} \qquad 2.26$$

where,

Y_r= relative flow depth

B_r= ratio of half width of the entire channel to the bottom half width of the main channel

and

$$\Delta V = V_{mc} - V_{fp}$$

The computed values of τ_a based on equation 2.26 were found to be in reasonably close agreement with their observed values for a wide range of flow conditions. The observed values were from the direct measurements of apparent shear stress at the vertical interface of the main channel-flood plain using

hot-film anemometer.

Hence, Prinos and Townsend found $\tau_a \alpha \Delta V$, while Ervine and Baird found $\tau_a \alpha \Delta V^2$. In his explanation Prinos (62) has indicated that apparent shear stress is not correlated to the actual differential velocity in the mixing region but to an 'imaginary' differential velocity for calculation purposes.

Later they expressed the relation of equation 2.23 in the form:

$$\tau_{mc} = \rho c_f V_{mc}^2 \qquad 2.27$$

where, c_f is a friction factor.

Using regression analysis of laboratory measured data of both boundary shear stress and velocities in the main channel and interacting flow condition, c_f was expressed as:

$$c_f = 0.015 - 0.003 \log (R_e) \qquad 2.28$$

in which R_e is the Reynolds number of the entire compound channel flow, calculated from single channel method.

2.3.4.2 From Numerical Model Technique

Another alternative method of determination of the depth-averaged apparent shear stress, τ_a is the numerical model technique, either finite element (FE) or finite difference solution of the equation of motion with the eddy-viscosity concept of Boussinesq's approximation.

Using the concept as mentioned earlier in section

2.3.4, the equation of motion was derived from the three-dimentional Navier-Stokes equation and it can be expressed in simplified form as:

$$\bar{u}\frac{\partial\bar{u}}{\partial x} + \bar{w}\frac{\partial\bar{u}}{\partial z} = \frac{\partial}{\partial z}(\bar{\nu}_t w\frac{\partial\bar{u}}{\partial z}) + gS_{mc} - g\frac{dH}{dx} - \frac{\bar{\tau}_b}{\rho H} \qquad 2.29$$

and for fully-developed flows, equation 2.29 can be simplified again to:

$$0 = \frac{d}{dz}(H\rho\nu_t\frac{d\bar{u}}{dz}) + \rho S_{mc}H - \bar{\tau}_b \qquad 2.30$$

where the apparent shear stress,

$$\tau_a = \rho\bar{\nu}_t\frac{d\bar{u}}{dz}$$

In fact, the discretized form of equations 2.21 and 2.22 was developed from the flow equation 2.30.

In the recent decade many researchers (64, 66, 67, 81, 82) had attempted to solve this equation by model technique with certain assumptions.

Among all the methods, it is reported (62) that depth averaged '$\bar{K} - \bar{\varepsilon}$' model of turbulence can be recommended for flow prediction in rivers with flood plains. The parameter, $\bar{K}$, is the turbulence kinetic energy while parameter, $\bar{\varepsilon}$ is the rate of dissipation of turbulence kinetic energy.

CHAPTER III

THEORETICAL INVESTIGATION

3.1 INTRODUCTION

A two-dimensional turbulent flow equation is developed from the basic equation of an elementary fluid in motion which is described by the Reynolds' form of Navier-Stokes equation in three-dimensional domain. The key concept is that each elementary fluid in motion within a channel cross-section possesses different energy slope to that of the overall channel or the bed slope of the main channel due to the existence of vertical and lateral momentum transfers. The flow equation is further reduced to one-dimensional form by discretizing the energy slope into two components to comply the equation with the Prandtl equation of mixing length theory. Combining the two equations, a one-dimensional velocity profile is developed by assuming that the one-dimensional component of energy slopes of all the elementary fluids in motion within the control volume of a finite strip of length equal to the local flow depth are equal to the average energy slope of that finite strip flow. This one-dimensional form of velocity profiles is assumed equally valid for the flow with two rigid boundaries provided the flow can be divided into two equivalent free-surface flows. The equations of the division surface and the composite

roughness of a strip flow with two rigid boundaries of unequal roughnesses are developed by satisfying the continuity and momentum equations of the strip flow. The horizontal strip of an open channel flow and the vertical strip of a covered-surface flow are assumed equivalent to the flow between the two rigid boundaries.

The resultant velocity of the discrete components of local velocity of each elementary fluid is described by an empirical equation in non-dimensional form which relates the discrete components of velocity with the mean velocity of the entire channel.

Two unknown coefficients are assumed to describe the velocity equation in its two-dimensional domain. The continuity and the momentum equations of the entire channel are required to be satisfied for the solution of the proposed equation. The solution of the velocity equation is the solution of the two-dimensional flow equation which was developed from the basic equation.

3.2 BASIC EQUATION OF TURBULENT FLOW

In hydrodynamics, basic equations of incompressible flow are given by physical principles of conservation of momentum and continuity.

For an incompressible and viscous flow, the conservation laws of momentum of turbulent flow can be described by the time-averaged Reynolds' form of the Navier-Stokes Equation in three-dimensional domain.

In the Cartesian coordinate system (Figure 3.1) the equations can be described for an elementary fluid in motion [50] as follows:

Momentum Equation, in the X-direction

$$\rho\left(\frac{\partial \bar{u}}{\partial t} + \bar{u}\frac{\partial \bar{u}}{\partial x} + \bar{v}\frac{\partial \bar{u}}{\partial y} + \bar{w}\frac{\partial \bar{u}}{\partial z}\right)$$

$$= -\frac{\partial}{\partial x}(\bar{p}+\rho g y) + \mu \nabla^2 \bar{u} - \rho\left(\frac{\partial \overline{u'^2}}{\partial x} + \frac{\partial \overline{u'v'}}{\partial y} + \frac{\partial \overline{u'w'}}{\partial z}\right) \qquad 3.1$$

Momentum Equation, in the Y-direction

$$\rho\left(\frac{\partial \bar{v}}{\partial t} + \bar{u}\frac{\partial \bar{v}}{\partial x} + \bar{v}\frac{\partial \bar{v}}{\partial y} + \bar{w}\frac{\partial \bar{v}}{\partial z}\right)$$

$$= -\frac{\partial}{\partial y}(\bar{p}+\rho g y) + \mu \nabla^2 \bar{v} - \rho\left(\frac{\partial \overline{u'v'}}{\partial x} + \frac{\partial \overline{v'^2}}{\partial y} + \frac{\partial \overline{v'w'}}{\partial z}\right) \qquad 3.2$$

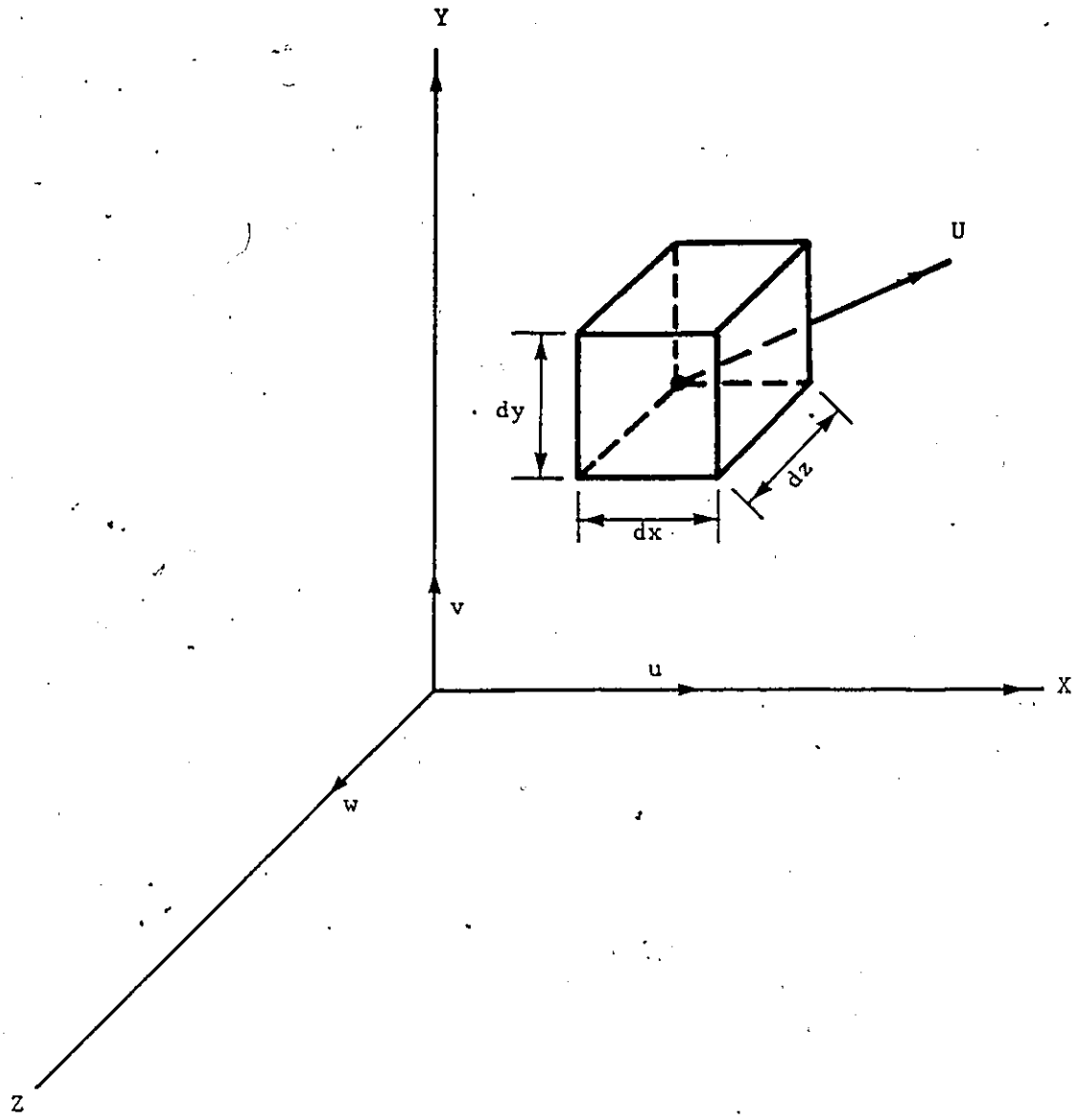

Fig. 3.1. Cartesian Coordinate System.

Momentum Equation, in the Z-direction

$$\rho\left(\frac{\partial \bar{w}}{\partial t} + \bar{u}\frac{\partial \bar{w}}{\partial x} + \bar{v}\frac{\partial \bar{w}}{\partial y} + \bar{w}\frac{\partial \bar{w}}{\partial z}\right)$$

$$= -\left(\frac{\partial}{\partial z}\bar{p} + \rho g y\right) + \mu\nabla^2\bar{w} - \rho\left(\frac{\partial \overline{u'w'}}{\partial x} + \frac{\partial \overline{u'w'}}{\partial y} + \frac{\partial \overline{w'^2}}{\partial z}\right) \qquad 3.3$$

where, the operator,

$$\nabla^2 = \frac{\partial^2}{\partial x^2} + \frac{\partial^2}{\partial y^2} + \frac{\partial^2}{\partial z^2}$$

The continuity principle expresses the conservation of mass and is described as:

$$\frac{\partial \bar{u}}{\partial x} + \frac{\partial \bar{v}}{\partial y} + \frac{\partial \bar{w}}{\partial z} = 0 \qquad 3.4$$

Equations 3.1 to 3.4 can be expressed more concisely in tensorial notation as follows:

The momentum equation

$$\rho\left(\frac{\partial \bar{u}_i}{\partial t}\right) + \rho\left(\bar{u}_j\frac{\partial \bar{u}_i}{\partial x_j}\right)$$

$$= -\frac{\partial}{\partial x_i}(\bar{p} + \rho g y) + \frac{\partial}{\partial x_j}\left(\mu\frac{\partial \bar{u}_i}{\partial x_j}\right) - \frac{\partial}{\partial x_j}\left(\rho\,\overline{u_i'u_j'}\right) \qquad 3.5$$

and the continuity equation:

$$\frac{\partial \bar{u}_i}{\partial x_i} = 0 \qquad 3.6$$

In the left hand side of equation 3.5 the first term is the 'local inertia forces' and the second term is the 'convective inertia forces'. In the right hand side of the equation, the first term is the 'pressure and gravity forces', the second term is the 'viscous forces', and the third term is the 'turbulent fluctuation forces'.

3.3 EQUATIONS OF FREE SURFACE FLOW

An exact solution of the system of differential equations, given by the continuity and momentum principles, described in the previous section, 3.2, is yet to be established in an applied field.

In this section, the required flow equation will be developed by simplifying the basic equations with some practical assumptions.

3.3.1 Development of Flow Equations

In most channel flow problems, the prime flow is in the longitudinal direction, i.e., in the X-direction. Hence, the time averaged velocities in the Y- and Z-directions can sensibly be neglected; i.e., $\bar{v}=0$ and $\bar{w}=0$ and thereby their derivatives will also be zero. Therefore, the Y- and Z-momentum equations vanish completely and the remaining equations will be the X-momentum equation only. The continuity equation will also reduce to: $\frac{\partial \bar{u}}{\partial x} = 0$, which implies that the flow is conventionally uniform in the longitudinal direction.

Moreover, in most channel flow the inertia force can

be neglected and in that case it can be described as steady flow; that is the term, $\frac{\partial \bar{u}}{\partial t} = 0$.

In an inclined channel flow, under the conditions mentioned above, the pressure force will be zero (i.e, $\frac{\partial \bar{p}}{\partial x} = 0$) and the only gravity force is the component of body force in the X-direction, which can be denoted by F_e, say. Therefore, the X-momentum equation, in its three-dimensional domain, reduces to:

$$0 = F_e + \rho\left(\frac{\partial^2 \bar{u}}{\partial x^2} + \frac{\partial^2 \bar{u}}{\partial y^2} + \frac{\partial^2 \bar{u}}{\partial z^2}\right) - \left(\frac{\partial \bar{u}'^2}{\partial x} + \frac{\overline{\partial u'v'}}{\partial y}\right) + \frac{\overline{\partial u'w'}}{\partial z} \qquad 3.7$$

Again, as the flow is considered uniform, all the derivatives with respect to 'x' are zero; i.e., $\frac{\overline{\partial u'^2}}{\partial x} = 0$ and $\frac{\partial^2 \bar{u}}{\partial x^2} = 0$.

As stated earlier, [Chapter I], with the concept assumed for the energy slope of an elementary fluid in motion, the body force, F_e can be substituted by '$\rho g S_e$'; where S_e is the energy slope of any elementary fluid. Hence, the flow equation can be written by rearranging as:

$$\frac{\partial}{\partial y}\left(\mu\frac{\partial \bar{u}}{\partial y} - \rho\overline{u'v'}\right) + \frac{\partial}{\partial z}\left(\mu\frac{\partial \bar{u}}{\partial z} - \rho\overline{u'w'}\right) + \rho g S_e = 0 \qquad 3.8$$

Physically, the quantities $\mu\frac{\partial \bar{u}}{\partial y}$ and $\mu\frac{\partial \bar{u}}{\partial z}$ are called viscous shear stresses, acting in the X-direction on the

planes normal to Y- and Z-axes, respectively. In a fully developed turbulent flow, the viscous terms are significant only in the region very close to the boundary; this region is called a laminar sublayer, the thickness of which is negligible compared to the flow-depth. The viscous terms can be neglected outside this sublayer.

On the other hand, the terms, $-\rho\overline{u'v'}$ and $-\rho\overline{u'w'}$ are called turbulent shear stresses which are very significant within the flow depth outside the viscous sublayer. Physically, the quantity $-\rho\overline{u'v'}$ is the transport of X-momentum in the Y-direction, whereas the term $-\rho\overline{u'w'}$ is the transport of X-momentum in the Z-direction.

Hence, within the turbulent flow zone, equation 3.8 can further be reduced to:

$$\frac{\partial}{\partial y}(-\rho\overline{u'v'}) + \frac{\partial}{\partial z}(-\rho\overline{u'w'}) = -\rho g S_e \qquad 3.9$$

and by definition, which can be expressed as:

$$\frac{\partial}{\partial y}(\tau_{yx}) + \frac{\partial}{\partial z}(\tau_{zx}) = -\rho g S_e \qquad 3.10$$

where, τ_{yx} is the turbulent shear stress acting in the X-direction on the plane normal to the Y-axis and τ_{zx} is the turbulent shear stress acting in the X-direction on the plane normal to the Z-axis (see Figure 1.2).

Equation 3.10 can be considered as three-dimensional,

but it is better to be defined as two-dimensional in the Y- and Z-coordinates system because the variation of all the parameters in the X-direction are already considered constant.

At the present state of knowledge the better hypothesis describing shear stress-velocity relationship within the turbulent zone of flow is the K-ε family of models which are more complex in nature. However, in the present study Prandtl-mixing length theory will be used as a compatible momentum transfer equation with the flow equation derived from the basic principle.

By examining equation 3.10, it can rationally be assumed that the energy slope, S_e has two components while the quantities, ρ and g are constants. In the first hand, it can be assumed that the fluid element is infinite in the Z-direction, and thereby the lateral momentum transfer can be ignored; i.e., the term, 'τ_{zx}' will vanish. In that case, the only shear stress, τ_{yx}, will act opposite to the body force; the corresponding energy slope will be denoted as 'S_{yx}' and then the equation 3.10 can be expressed in one-dimensional form:

$$\frac{\partial}{\partial y}(\tau_{yx}) = -\rho g S_{yx} \qquad 3.11$$

On the other hand, if it can be assumed that the fluid element is infinite in the Y-direction, 'τ_{yx}' will vanish and similar to the expression 3.11, equation 3.10 can be

expressed as:

$$\frac{\partial}{\partial z}(\tau_{zx}) = -\rho g S_{zx} \qquad 3.12$$

where, the term 'S_{zx}' is the energy slope corresponding to the lateral momentum transfer.

A proper mathematical combination of the individual solutions of equations 3.11 and 3.12 will be the solution for equation 3.10. The procedure will be described in subsequent sections. A symbolic presentation of this solution is shown in Figure 3.2.

3.3.2 Concept of Flow Strips

In Equation 3.10 the energy slope, S_e is a variable parameter with the position of the elementary fluid within a cross-sectional flow system, and so are the terms, S_{yx} and S_{zx} in equation 3.11 and 3.12; this is a constraint in solving these equations 3.11 and 3.12.

To remove this constraint another practical assumption has to be made. At the present state of knowledge, an attempt to establish a relationship between the energy slope of an elementary fluid with reference to its location, will magnify the complexity of the problem. However, it can be a better, if not the best, estimate if the energy slope of a fluid element in its one-dimensional form is assumed to be equal to an average value corresponding to the mean

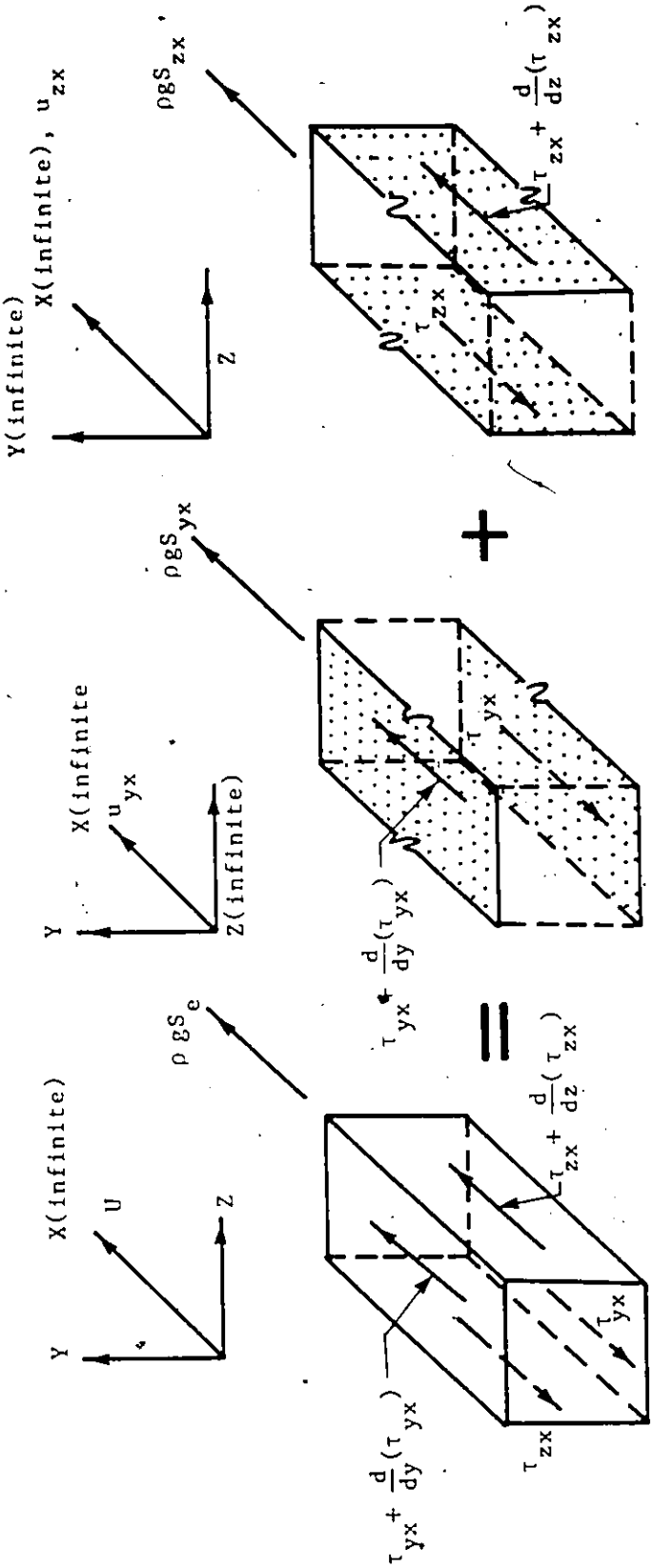

(N.B. Forces are per unit cross-sectional area).

Fig. 3.2. Symbolic Presentation of the Solution of the Flow Equation 3.10 (Elementary Fluid in Motion).

velocity of all the fluid elements in motion present within the control volume of a finite strip that can be drawn from the boundary to the free surface enclosing the elementary fluid in question.

In other words, it can be expressed that if the entire cross-sectional flow can be divided into a number of finite strips in one direction then the energy slope of each finite strip flow is equal to an average value corresponding to its mean velocity and thus, it can be considered as a constant value within the control volume of the strip in question. Hence, the assumption simplifies the concept of discrete energy slope of a fluid element to the discrete energy slope of a finite strip in one-dimensional flow system and, therefore, all the fluid elements within the control volume of a finite strip possess the energy slope equal to that of the finite strip flow.

3.3.2.1 Equation of Vertical Strip

Let a vertical strip of height equal to the local flow depth be drawn confining the fluid element and consider the strip is infinite in the Z-direction. The integration of equation 3.11 over the flow depth can be made possible with the assumption that has been indicated in Section 3.3.2. In that case, the term, S_{yx} can be replaced by the term, S_{vs}, the average energy slope of a vertical strip corresponding to the average velocity of the strip. Subscript 'vs'

denotes vertical strip (see Figure 3.3).

Hence, equation 3.11 can be written as:

$$\frac{\partial}{\partial y}(\tau_{yx}) = -\rho g S_{vs} \qquad 3.13$$

Integration of equation 3.13, with the boundary condition, $\tau_{yx} = 0$ at $y = Y_{vs}$, is:

$$\tau_{yx} = \rho g S_{vs}(Y_{vs} - y_{vs}) \qquad 3.14$$

3.3.2.2 Equation of Horizontal Strip

A horizontal strip, similar to a vertical strip, of length equal to the local flow width (say Z_{hs}) can also be drawn confining a fluid element and the strip is considered to be infinite in the Y-direction. Considering the same assumption as mentioned in previous section 3.3.2.1 the energy slope of a fluid element, S_{zx} can be expressed equal to the average slope of the horizontal strip, S_{hs} (see Figure 3.4). Equation 3.12 is expressed by

$$\frac{\partial}{\partial z}(\tau_{zx}) = -\rho g S_{hs} \qquad 3.15$$

Concept of Division Surfaces

Unlike a vertical strip, integration of equation 3.15 is not straightforward because of the absence of any

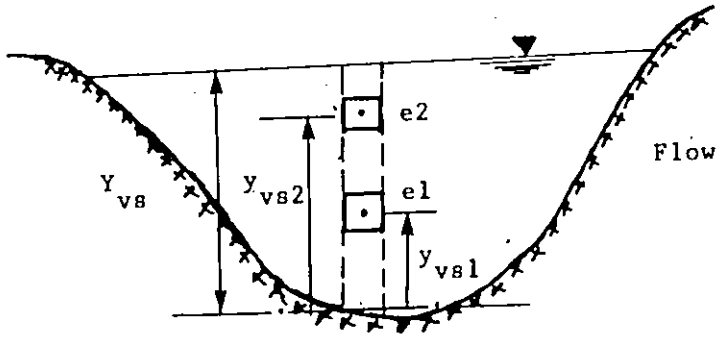

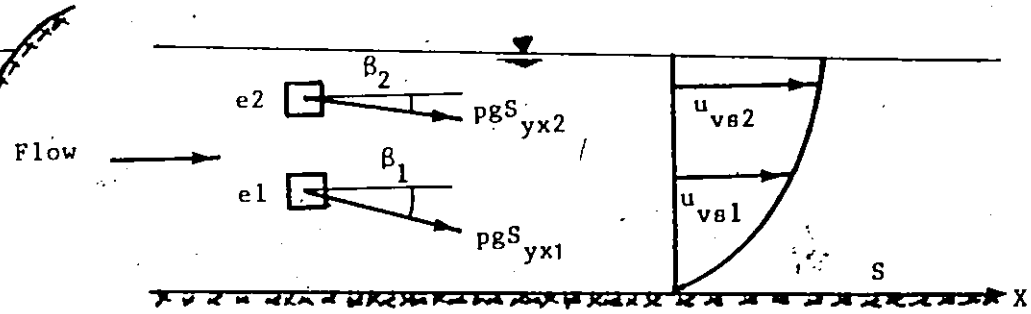

Concept of elementary fluid flow in one-dimensional system

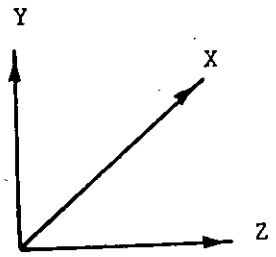

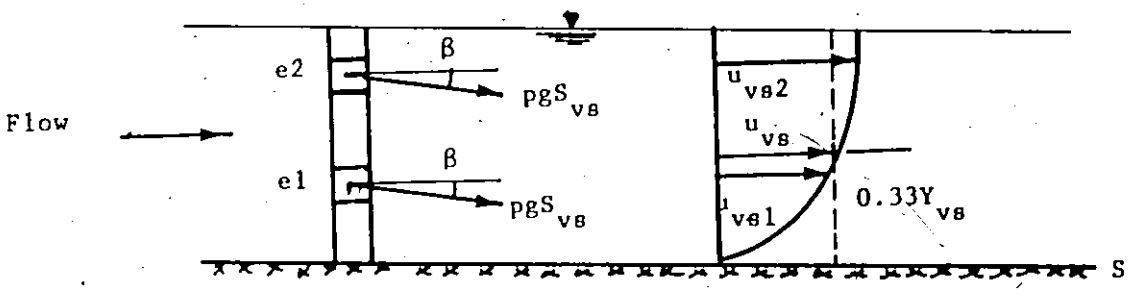

e1 - elementary fluid 1
e2 - elementary fluid 2

Concept of strip flow in one-dimensional system

Fig. 3.3. Concept of Vertical Strip in an Open Channel Flow.

free-surface in it. Similar to a flow between two parallel plates, an equivalent free-surface can be assumed to exist somewhere within the flow width, where the velocity of the strip flow will reach its maximum value and thus the shear stress will be zero at that location, which can be denoted by the term, 'division surface'. This division surface will divide a horizontal strip flow into two substrip flows and each substrip flow can be assumed independent from each other; this means each flow will be governed by its own local condition and is to be treated as a separate flow (see Figure 3.4).

Hence, equation 3.15 can be written for the two substrip flows as:

substrip 1 at the left hand side:

$$\frac{\partial}{\partial z}(\tau_{1zx}) = - \rho g S_{1hs} \qquad (3.16)$$

and substrip 2 at right hand side:

$$\frac{\partial}{\partial z}(\tau_{2zx}) = - \rho g S_{2hs} \qquad (3.17)$$

Assuming the energy slopes, S_{1hs} and S_{2hs} are the average values over their respective flow width, integration of each substrip flow equation can be made possible similar to that of vertical strip flow as described in the previous subsection 3.3.2.1.

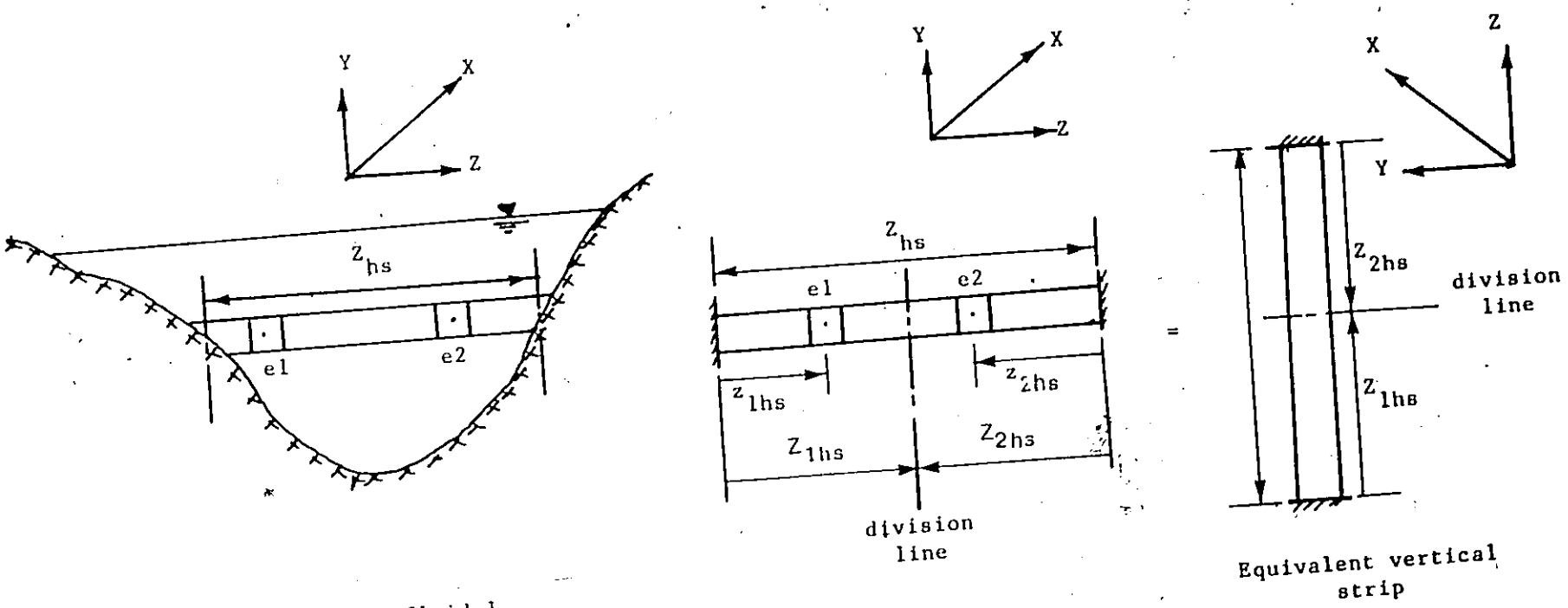

e1 - elementary fluid 1
e2 - elementary fluid 2

Fig. 3.4. Concept of Horizontal Strip and Substrips in an Open Channel Flow.

Now, depending on the location of the fluid element in question, either equation 3.16 or equation 3.17 can be used for the solution.

Considering the existence of the fluid element in substrip 1, the integration of equation 3.16 is written as:

$$\tau_{1zx} = \rho g S_{1hs}[Z_{1hs} - z_{1hs}] \qquad (3.18a)$$

and, similarly, if the fluid element is in the substrip 2, equation 3.17 is integrated as:

$$\tau_{2zx} = \rho g S_{2hs}[Z_{2hs} - z_{2hs}] \qquad (3.18b)$$

where, Z_{1hs} is the flow-width, from the left hand boundary to the division surface of substrip one (1) and, similarly, Z_{2hs} is that of the substrip two (2).

The equation of 'division surface' will be described later.

Denoting a general notation, m, for the subscript 1 and 2, equations 3.18a and 3.18b can be expressed by

$$\tau_{mzx} = \rho g S_{mhs}[Z_{mhs} - z_{mhs}] \qquad (3.19)$$

Equation 3.19 is the representative expression of a strip with two hydraulic boundary roughnesses.

It can be said, considering vertical strip division

only, that the free surface is the locus of maximum velocities and thus, the locus of zero shear for all the finite vertical strips. While the line joining the division surface of all the horizontal strips is the locus of maximum velocities and thus that of zero shears, considering this horizontal strip divisions only.

Combining both vertical and horizontal strip divisions the intersection of the two loci is the point of maximum velocity and zero shear of the entire channel (see Figure 3.5).

3.4 SHEAR STRESS-VELOCITY RELATION

The theoretical determination of shear stress-velocity relation in turbulent flow is very complex due to the undeterministic relations between the mean velocity components ($\bar{u}$, $\bar{v}$ and $\bar{w}$) and their respective fluctuation terms (u', v' and w').

However, at the present state of knowledge, the two most accepted concepts used in order to simplify the Reynolds equation are the 'Boussinesq Theory' of eddy viscosity and the 'Prandtl Theory for mixing length.

Despite a more complex mathematical form, the main advantage of Prandtl's theory over the Boussinesq theory is that it is easier to assume the value of the mixing length than the value of the eddy viscosity.

Hence, to establish the shear stress-velocity relation,

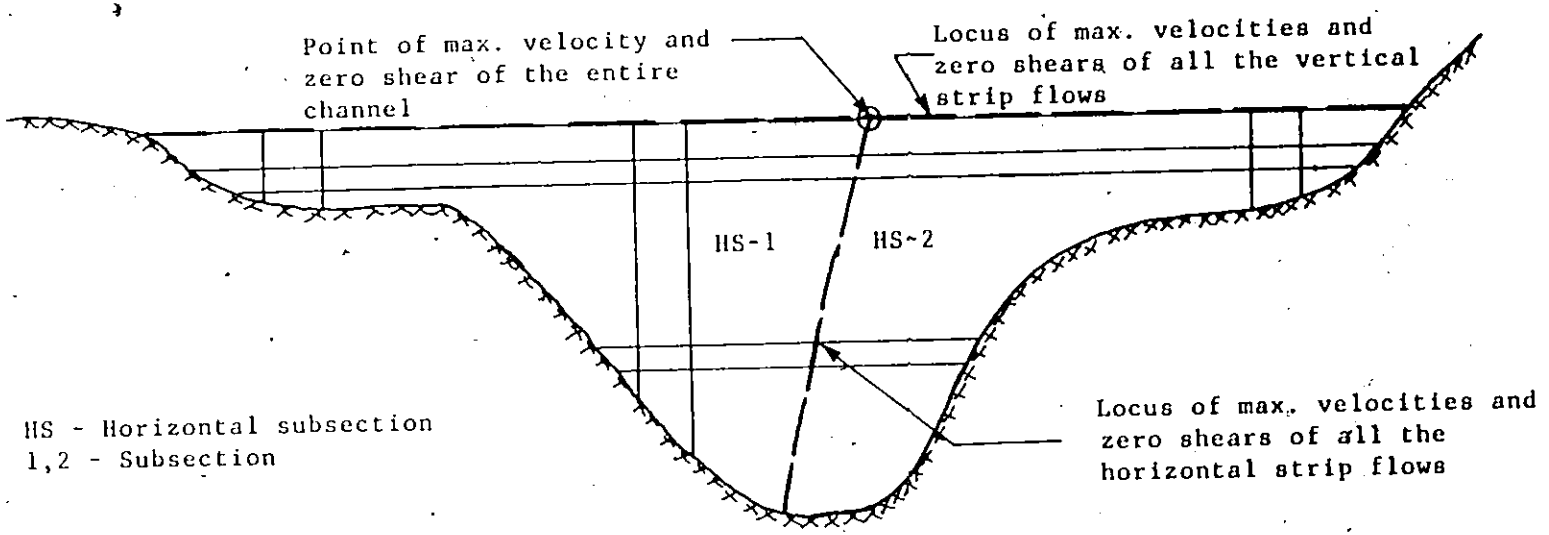

Fig. 3.5. Conception of Division Surfaces in Channel with Free-Surface Flow.

the Prandtl mixing length theory will be used.

Prandtl's mixing length theory is the momentum transfer theory in a one-dimensional domain and hence, it is fully compatible with the shear stress equations 3.14 and 3.19, which are developed in the previous section 3.3.

For a vertical strip, the Prandtl theory can be written as:

$$\tau_{yx} = -\rho\overline{u'v'} = \rho\kappa^2 y_{vs}^2 \frac{d\bar{u}_{vs}}{dy_{vs}}\left|\frac{d\bar{u}_{vs}}{dy_{vs}}\right| \qquad 3.20$$

Ignoring the sign convention and considering the time-average velocity component $\bar{u}_{vs} \equiv u_{vs}$), the equation 3.20 can be written as:

$$\tau_{yx} = \rho\kappa^2 y_{vs}^2 \left(\frac{du_{vs}}{dy_{vs}}\right)^2 \qquad 3.21$$

Like the relation (equation 3.21) established by Prandtl's Theory for the vertical momentum transfer, it can sensibly be assumed the Prandtl theory is equally valid for the horizontal momentum transfer. Hence, if the division surface for a horizontal strip flow can be determined, then the theory can be described in general form for a horizontal strip as:

$$\tau_{mzx} = \rho\kappa^2 z_{mhs}^2 \left(\frac{du_{mhs}}{dz_{mhs}}\right), \quad m = 1,2 \qquad 3.22$$

u_{vs} and u_{mhs} of equations 3.21 and 3.22, respectively, are the vertical and horizontal components of the actual velocity vector, U, of an elementary fluid flow. The direction of the velocity components are the same as that of their velocity vector; i.e., in the X-direction.

3.5 FREE-BOUYANT BOUNDARY FLOW

In the previous sections 3.3 and 3.4, the equations are developed for a free-surface flow. At this stage it is of great interest to observe the behavior of a channel flow under a free-bouyant cover condition like an ice-covered surface, and to establish the flow equations thereof.

The idea is to establish a set of global equations in the subsequent sections, so that a free-surface flow will be treated as a special case of a floating covered-surface flow.

3.5.1 Behavior of Flow Under a Floating Cover

Among all the types of floating cover in a natural stream flow, ice-cover is the most noticeable and important one to study from the hydraulic engineering point of view, especially in the cold regions like Canada, U.S.A., U.S.S.R. and other European countries.

Formation of ice-cover is a natural phenomenon due to the partial and total freezing of natural bodies of water

with the substantial drop of atmospheric temperature. In an open channel flow, at the beginning of ice formation the frazil ice accumulates, forming ice floes which travel downstream until they are stopped by natural or manmade obstacles and the formation of ice cover begins (see Figure 3.6). The hydraulic problems associated with the formation of ice cover are manifold and beyond the scope of present study.

However, one of the key problems is the change of flow pattern due to decreased carrying capacity of the natural river cross-section, and change of the friction factors of the entire channel cross-section due to the presence of ice-cover.

From the observations of the underside of ice-cover in natural streams, it was found that ice thickness varied considerably near the banks to the central part of the streams from several meters to several tenths of a meter or less and it may be extended to the streambed in some localities. In some cases frazil ice may accumulate immediately below the solid ice-cover and the amount of which depends on the thermal cycle with time.

As the conveyance capacity decreases, a natural stream with ice-cover and with alluvial soil bed has the tendency of erosion of bed in irregular dune form and the underside configuration of the ice-cover has a similar tendency to take

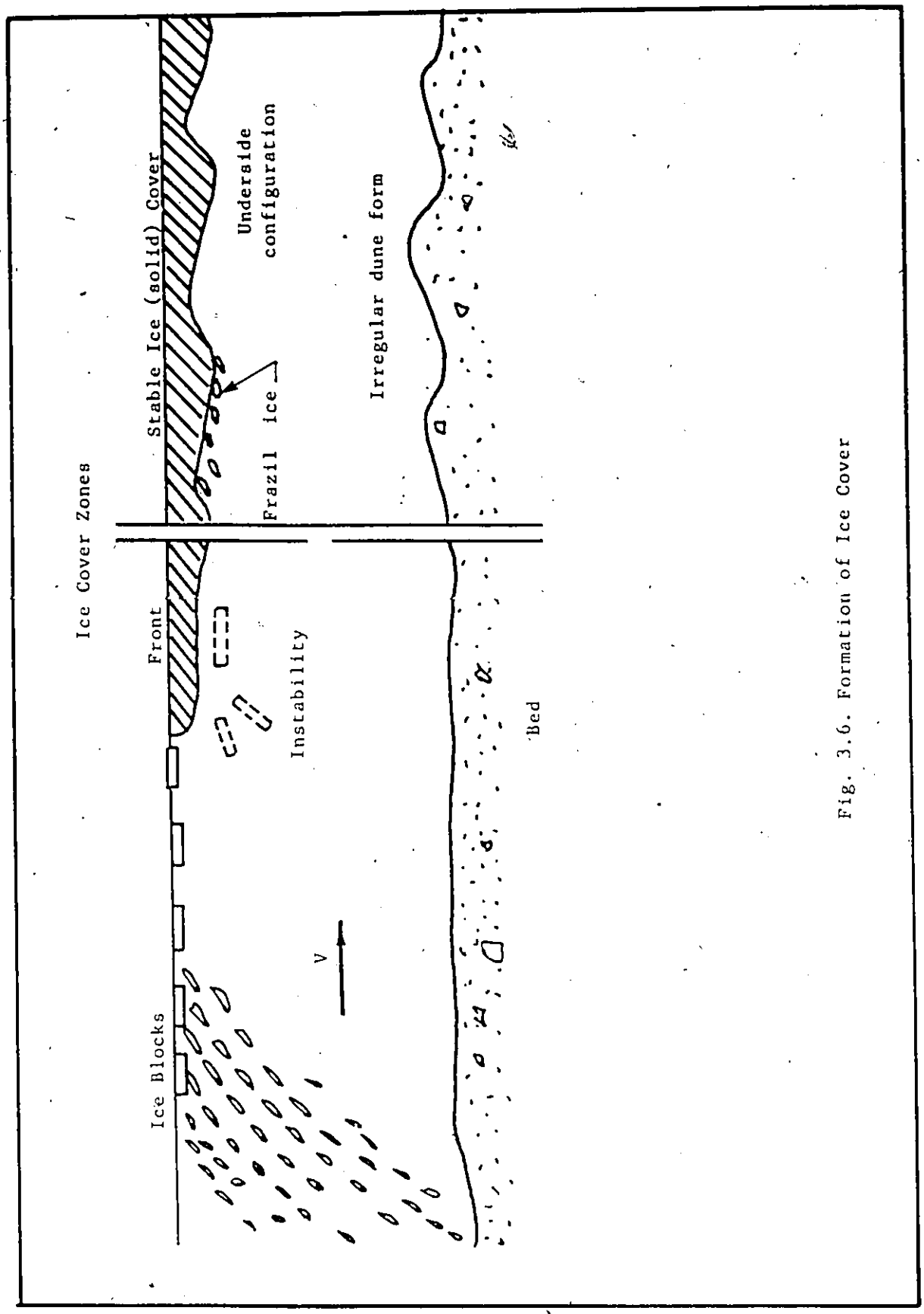

Fig. 3.6. Formation of Ice Cover

the shape of bed form.

All these factors are not in favor of predicting correctly the velocity profiles and boundary shear stress distributions and thus the flow rate of an ice-covered channel.

While direct field study has several limitations, many ice models have given unreliable and unproven results due to very poor knowledge of field conditions, including a lack of field data and thus the lack in the process of simulation in a model.

In the case of a model study in the area of flow pattern and in determination of composite roughness, the similitude was limited to representing the hydrodynamic conditions only considering the ice-cover as a rigid boundary, an unbreakable body.

The major variable in nature that cannot be simulated in a model is that of thermal exchange. However, except in the case of ice-cover formation where the thermal state of the ice varies quickly, the other thermal states during winter conditions or at breaking are constant for a long enough period so their variation could sensibly be eliminated in the model simulation.

In the present study, without going far along with the complexities of the factors mentioned in above, a simple theoretical solution has been looked for based on the present concept of the theory.

3.5.2 Equation for Free-Bouyant Boundary Flow

A channel flow under floating cover is a gravity flow and hence, an incompressible flow. For the application of the present theory in developing the flow equations of a floating ice-covered flow, some practical assumptions are to be made:

1. Ice cover itself can be considered a rigid, unbreakable body.
2. Channel bed is a rigid and undeformable boundary.
3. Flow is steady and conventionally uniform.
4. The prime flow is in longitudinal, i.e., in the X-direction, and hence, the flow is two-dimensional.

Hence, the flow equation 3.10 is also valid for any elementary fluid motion under a floating ice-covered flow.

Now, if the entire channel cross-section is divided into finite vertical and horizontal strips, each strip flow, either a vertical or a horizontal, can be considered as a flow under two parallel rigid boundaries.

In case of vertical strips alone, it can be assumed that an equivalent free-surface can be located for each vertical strip, where the maximum velocity of the concerned vertical strip will reach and this can be defined as a division surface similar to that of a horizontal strip of a channel under free surface flow. Therefore, the line joining all the division surface of vertical strips is the

locus of the maximum velocities or zero shear stresses in one dimensional domain (i.e., considering the strip flows are infinite in X- and Z- directions).

On the other hand, a horizontal strip flow of a floating covered channel is similar to that of an open channel flow, as observed earlier. Therefore, the locus of the division surfaces of vertical strip-flows and that of the horizontal strip-flows will divide the entire channel flow into four separate zones of equivalent free-surface flows. At this point the simplification of a complex flow under a floating covered surface is complete.

Figure 3.7 shows the schematic representation of above breakdown. The intersection of the two loci is the point of the maximum velocity of the entire channel flow.

Hence, the simplified flow equations of the Reynolds form of the Navier-Stokes equation and the Prandtl equations, which were developed in section 3.3 and 3.4, are equally applicable for covered channel flow.

Therefore, the flow equation 3.14 can be written for a vertical strip of a covered channel flow as:

$$\tau_{\ell yx} = \rho g S_{\ell v}(Y_{\ell vs} - y_{\ell vs}),$$

$$\ell = 1, 2 \qquad 3.23$$

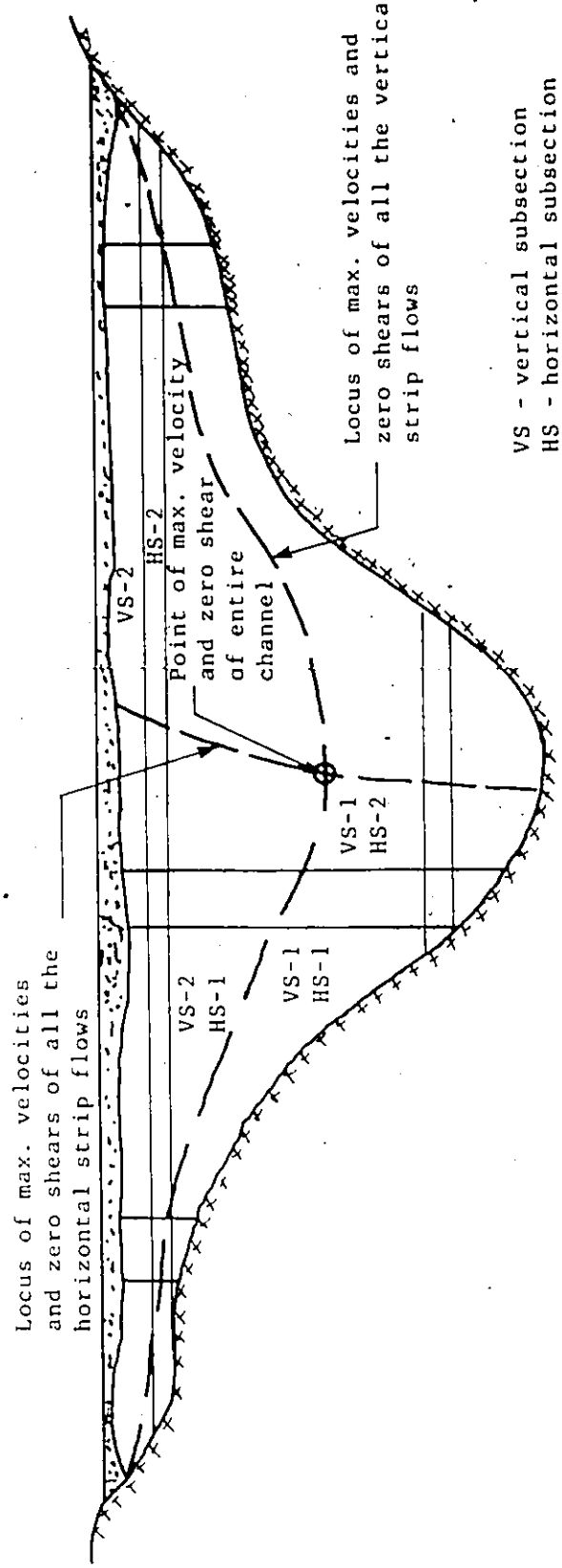

Fig. 3.7. Conception of Division Surface in Channels with Covered-Surface Flow.

and the Prandtl equation

$$\tau_{\ell yx} = \rho\kappa^2 y^2_{\ell vs} \left(\frac{du_{\ell vs}}{dy_{\ell vs}}\right)^2 \qquad 3.24$$

For horizontal strip flow, equations 3.19 and 3.22 will remain unchanged.

3.6 GENERALIZED STRIP ANALYSIS

It is understood, from the previous sections 3.3 through 3.5, that it needs to develop a velocity distribution equation for a strip-flow under free-surface condition only, because a strip-flow with two parallel boundary roughnesses are nothing but two independent and equivalent free-surface flow.

Also, the equation of a vertical strip-flow and that of a horizontal strip-flow are analogous.

Hence, in subsequent sub-sections, analysis for velocity distribution, division surface and other related relationships will be deduced in general terminology, so that it can be used for either strip with proper notations.

3.6.1 Velocity Distributions

Consider a strip as shown in Figure 3.8, where H_s, ds and A_s are the flow depth, the width and the area of the strip respectively. dA_s is the area of the elementary fluid of thickness, dh_s at a depth, h_s from the boundary. Subscript 's' denotes any strip.

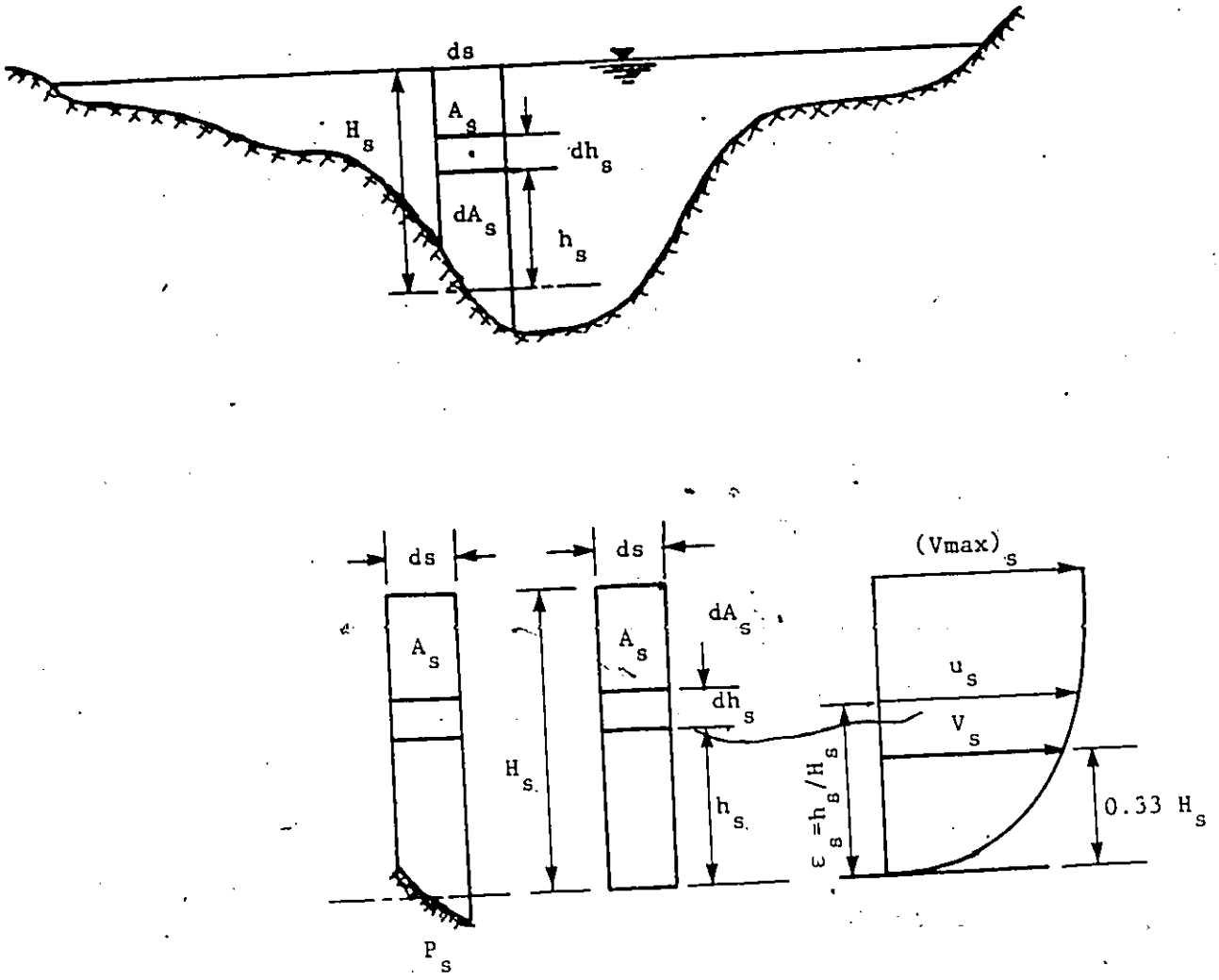

Fig. 3.8. Definition Sketch of a Generalized Strip in a Channel with Free-Surface Flow.

Hence, the general expression for the flow equation is:

$$\tau = \rho g S_s (H_s - h_s) \qquad 3.25$$

and for the Prandtl mixing length theory is:

$$\tau = \rho \kappa^2 h_s^2 \left(\frac{du_s}{dh_s}\right)^2 \qquad 3.26$$

Combining the equations 3.25 and 3.26 it can be obtained:

$$\frac{du_s}{dh_s} = \frac{(gS_s)^{1/2}}{\kappa} \frac{(H_s - h_s)^{1/2}}{h_s} \qquad 3.27$$

Denoting $\varepsilon_s = h_s/H_s$ and thereby $dh_s = H_s d\varepsilon_s$, the equation 3.27 can be rearranged,

$$\frac{du_s}{d\varepsilon_s} = \frac{(gH_s S_s)^{1/2}}{\kappa} \frac{(1-\varepsilon_s)^{1/2}}{\varepsilon_s} \qquad 3.28$$

From the definition of shear stress, $(gH_s S_s)^{1/2}$ can be substituted by the term V_{*s}, where H_s is to be assigned as a hydraulic radius of the strip.

Hence, the equation 3.28 can further be expressed as

$$\frac{du_s}{d\varepsilon_s} = \frac{V_{*s}}{\kappa} \frac{(1-\varepsilon_s)^{1/2}}{\varepsilon_s} \qquad 3.29$$

and integrating:

$$u_s = \frac{V_{*s}}{\kappa} \quad F_1(\varepsilon_s) + C_s \qquad 3.30$$

where

$$F_1(\varepsilon_s) = 2(1-\varepsilon_s)^{1/2} - \text{Ln}\frac{1+(1-\varepsilon_s)^{1/2}}{1-(1-\varepsilon_s)^{1/2}}$$

and C_s is the integration constant.

There are two conditions for which two sets of solution for C_s and that of u_s can be obtained:

The first condition is the continuity equation:

$$A_s \int u_s \, dA_s = A_s V_s \qquad 3.31a$$

where V_s is the mean velocity of the strip-flow.

From the above condition C_s can be solved for:

$$C_s = V_s + \frac{2}{3} \frac{V_{*s}}{\kappa} \qquad 3.31b$$

The details of the integration of equation 3.31a are given in Appendix A1.

Hence, the final form of the velocity distribution can be written as:

$$u_s = V_s - \frac{V_{*s}}{\kappa} F_2(\varepsilon_s) \qquad 3.32$$

where

$$F_2(\varepsilon_s) = -F_1(\varepsilon_s) - \frac{2}{3}$$

$$= 2\left[\mathrm{Ln}\frac{(\varepsilon_s)^{1/2}}{1-(1-\varepsilon_s)^{1/2}} - (1-\varepsilon_s)^{1/2} - 1/3\right]$$

The second condition is the boundary condition: that the strip velocity will attain its maximum value at the free-surface; that is, at $\varepsilon_s = 1$, $u_s = (V_{max})_s$.

Introducing this condition into equation 3.30,

$$C_s = (V_{max})_s \qquad 3.33$$

Substituting this value of C_s into equation 3.30, the second form of the velocity distribution is obtained:

$$u_s = (V_{max})_s + \frac{V_{*s}}{\kappa} F_1(\varepsilon_s) \qquad 3.34$$

Combining the two equations 3.31b and 3.33 of 'C_s', the following relation can be obtained:

$$V_s = (V_{max})_s - \frac{2}{3}\frac{V_{*s}}{\kappa} \qquad 3.35$$

3.6.1.1 Characteristics of Function $F_2(\varepsilon_s)$

Figure 3.9 shows the plot of dimensionless velocity function, $F_2(\varepsilon_s)$ against the relative depth ratio, ε_s. The following observation can be made from the plot:

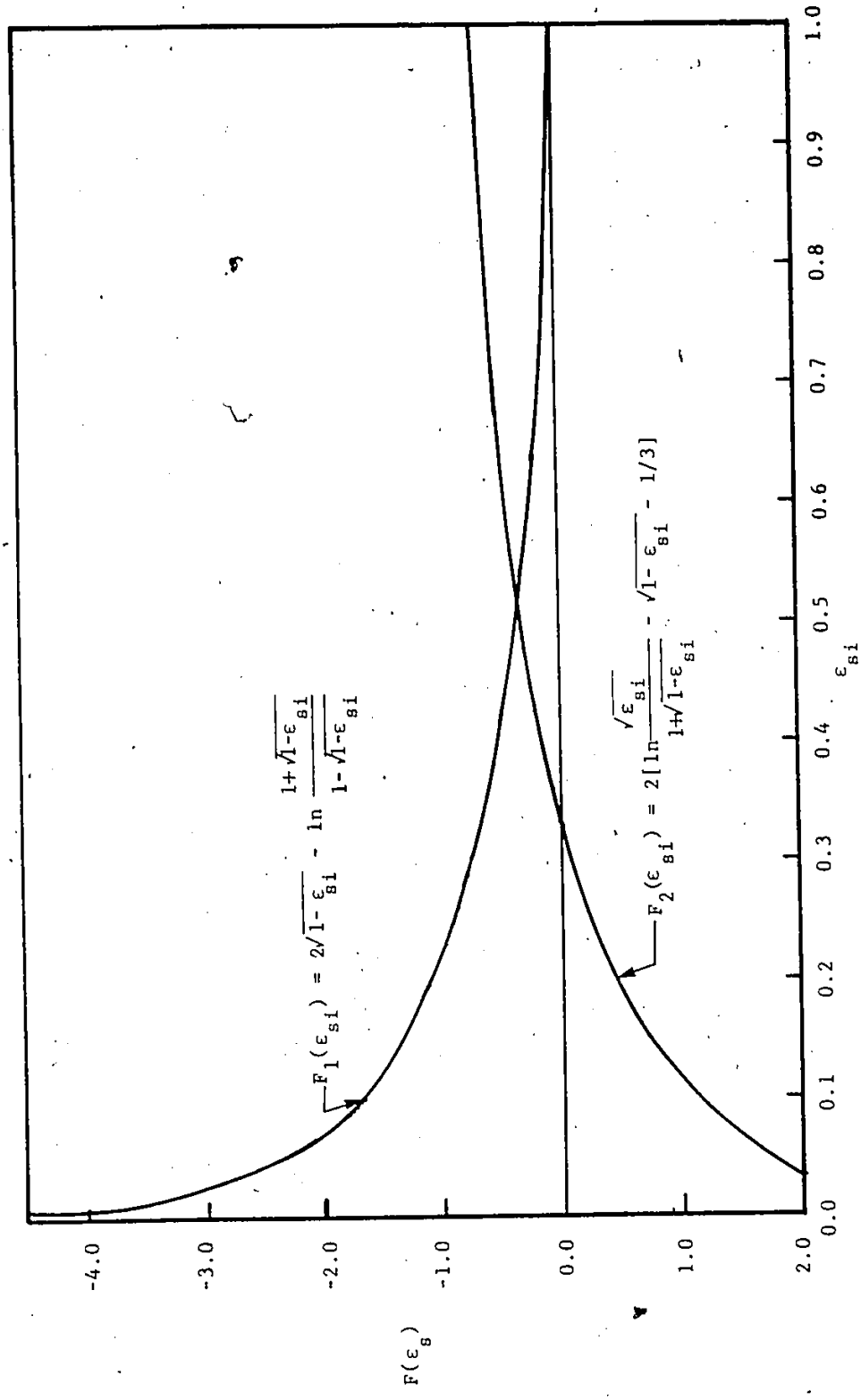

Fig. 3.9. Velocity Profile Functions.

1. Undefined Boundary

At the boundary, i.e., at $\varepsilon_s = 0$, the function is undefined and so is the velocity. This is sensible, because equation 3.32 is derived from the turbulent flow equation.

2. Shape of Velocity Profile

The shape of the velocity profile is solely defined by the function $F_2(\varepsilon_s)$, while other terms in the right hand side of equation 3.32 are constants. Hence, the shape of the profile is depth dependent only.

3. Location of Mean Velocity

It can also be observed from Figure 3.9 that with the increase of depth, i.e., increase of ε_s, the value of $F_2(\varepsilon_s)$ decreases with positive value and reaches zero at approximately $\varepsilon_s = 1/3$, and finally attained the minimum value of $-1/3$ at the free-surface, i.e., at $\varepsilon_s = 1$. Hence, the location of the mean velocity is approximately at one-third depth from the boundary of the flow (a more accurate value is 0.3304 of the flow depth, which can be obtained by solving $F_2(\varepsilon_s) = 0$).

3.6.1.2 Thickness of Zero Sublayer

As mentioned in observation (1) in subection 3.6.1.1, it is clear that the velocity will reach its zero value close to the boundary but not exactly at the boundary. The height of the location of this zero velocity from the boundary

can be defined as 'zero sublayer'.

Although, for all practical purposes, this thickness (which might be an approximate measure of the thickness of laminar sublayer) is negligible and can be ignored, the determination of its value is important as a check because the velocity will underestimate its value very close to the boundary.

The thickness can be determined by equating equation 3.32 to zero, i.e.,

$$V - \frac{2V_*}{\kappa} F_2(\varepsilon_s) = 0 \qquad 3.32a$$

An approximate solution of the equation can be obtained as

$$\varepsilon_{\phi s} = \left(\frac{2e^{C_{1s}}}{1+e^{2C_{1s}}}\right)^2 \qquad 3.32b$$

where 'e' denotes exponent and

$$C_{1s} = \frac{\kappa}{2} \frac{Y_s}{n_s \sqrt{g}} + 4/3$$

and $\varepsilon_{\phi s}$ is the thickness of zero sublayer relative to the flow depth.

The detailed analysis is shown in Appendix A3.

3.6.2 Division Surface

A strip-flow with two boundary roughnesses has its maximum velocity at the division surface and, therefore, the two substrip flows, separated by the division surface, will have the same maximum velocity of the strip $(V_{max})_s$. Hence, equation 3.35 can be written separately for the two substrip flows as: (refer to Fig. 3.10)

$$V_{1s} = (V_{max})_s - \frac{2}{3\kappa}V_{*1s} \qquad 3.36$$

and $$V_{2s} = (V_{max})_s - \frac{2}{3\kappa}V_{*2s} \qquad 3.37$$

Subtracting equation 3.37 from equation 3.36, the following relation is obtained:

$$V_{1s} - V_{2s} = \frac{2}{3\kappa}(V_{*2s} - V_{*1s}) \qquad 3.38$$

Considering that Manning's equation is valid for a strip flow, equation 3.38 can be written in non-dimensional form as given below:

$$\frac{3\kappa}{2}\frac{R_s^{1/6}}{n_{1s}g^{1/2}} = \frac{(\lambda_s^{1/2}\psi_s^{1/2} - 1)}{1 - \frac{n_{1s}}{n_{2s}}\lambda_s^{2/3}\psi_s^{1/2}}[\alpha_s + (1-\alpha_s)\lambda_s]^{1/6} \qquad 3.39$$

where

the hydraulic radius ratio, $\lambda_s = R_{2s}/R_{1s}$,

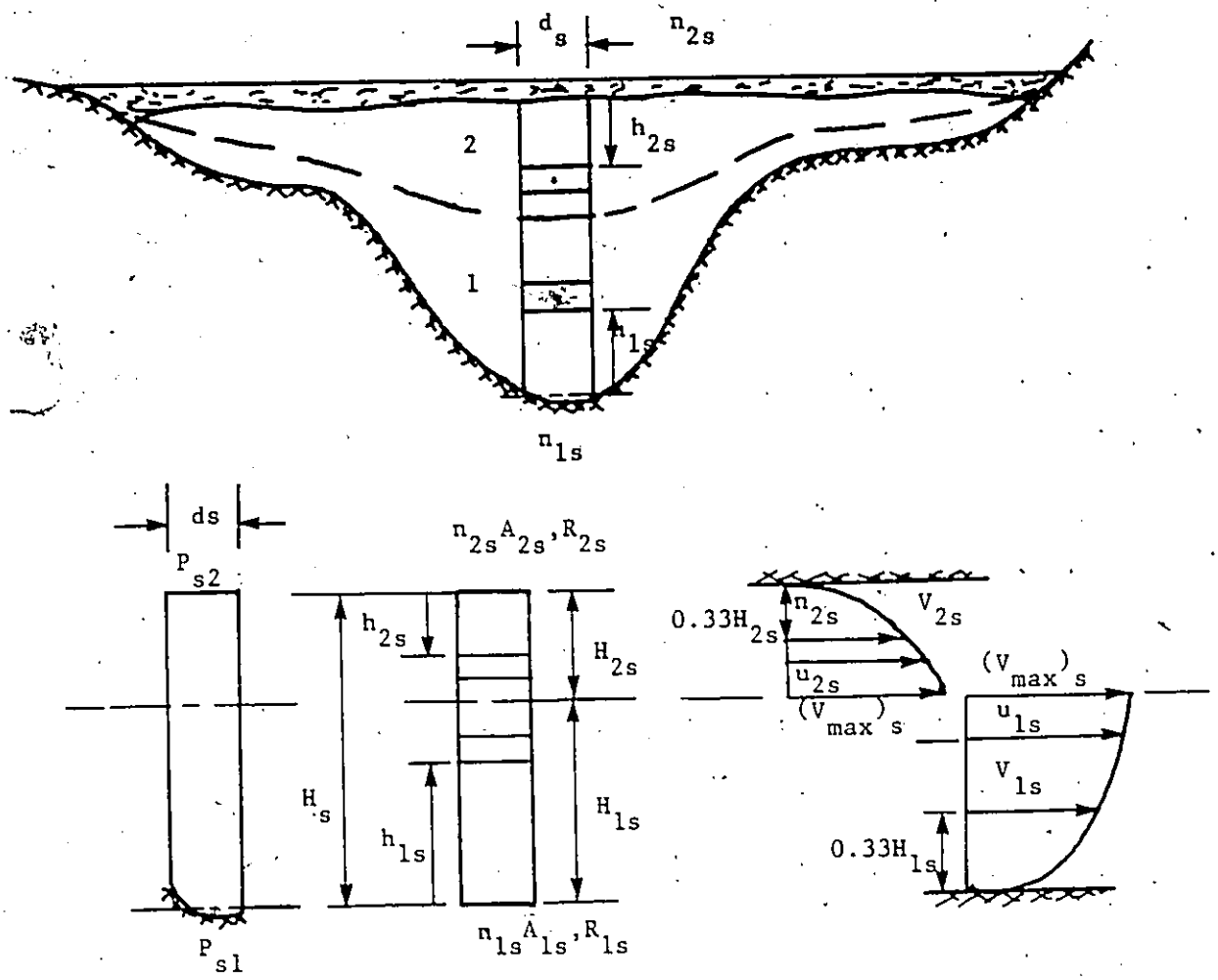

$$R_{1s} = \frac{A_{1s}}{P_{1s}} = H_{1s} \qquad R_{2s} = \frac{A_{2s}}{P_{2s}} = H_{2s}$$

Fig. 3.10. Definition Sketch of a Generalized Strip in a Channel Under Covered-Surface Flow.

the energy slope ratio, $\psi_s = S_{2s}/S_{1s}$,

and the hydraulic parameter ratio, $\alpha_s = P_{1s}/P_s$, also R, P, S, n are the hydraulic radius, hydraulic parameter, energy slope, and Manning's roughness , respectively, and subscripts s, 1s, 2s are applied for the strip, substrip one, and substrip two, respectively.

The detailed analysis is shown in Appendix 2.

The hydraulic radius ratio, λ_s is a measure of the division surface. Hence, equation 3.39 can be called an equation of the division surface.

3.6.3 Composite Roughness

In case of a strip-flow with two roughnesses, a relation can also be derived, for the determination of the composite roughness of the strip-flow from the continuity and momentum equations.

Continuity equation:

$$A_s V_s = A_{1s} V_{1s} + A_{2s} V_{2s} \qquad 3.40$$

and the momentum equation, per unit length of channel,

$$\gamma A_s S_s = \tau_{\phi 1s} P_{1s} + \tau_{\phi 2s} P_{2s} \qquad 3.41$$

where

$$\tau_{\phi 1s} = \gamma R_{1s} S_{1s} \qquad 3.42a$$

and

$$\tau_{\phi 2s} = \gamma R_{2s} S_{2s} \qquad 3.42b$$

Combining all these equations, 3.40 through 3.42b, with equations 3.36 and 3.37, and substituting the Manning equations for mean velocities, the relation for the composite roughness can be obtained as

$$\frac{n_s}{n_{1s}} = \left[\frac{\alpha_s + (1-\alpha_s)\lambda_s\psi_s}{\alpha_s + (1-\alpha_s)\lambda_s}\right]^{1/2}\left[\frac{(\alpha_s+(1-\alpha_s)\lambda_s)^{5/3}}{\alpha_s + \frac{n_{1s}}{n_{2s}}(1-\alpha_s)\lambda_s^{5/3}\psi_s^{1/2}}\right] \qquad 3.43$$

Equation 3.41 can be expressed in non-dimensional form for the energy slopes as:

$$\frac{S_s}{S_{1s}} = \frac{\alpha_s + (1-\alpha_s)\lambda_s\psi_s}{\alpha_s + (1-\alpha_s)\lambda_s} \qquad 3.44$$

The complete analysis of the equation 3.43 and 3.44 are shown in Appendix A2.

3.6.4 Supplementary Relationships Between Strip and Substrip Flow

Combining the sub-strip velocity equations 3.36 and 3.37 together with the continuity equation 3.40, the following relations can be obtained:

$$(V_{max})_s = \frac{1}{2}(V_{1s}+V_{2s}) + \frac{1}{3\kappa}(V_{*1s}+V_{*2s}) \qquad 3.45$$

and

$$V_s = \frac{1}{2}(V_{1s}+V_{2s}) - \frac{1}{3\kappa}(V_{*1s}-V_{*2s})\frac{(A_{1s}-A_{2s})}{A_s} \qquad 3.46$$

in which V_s and A_s denote the mean velocity and area of the entire strip, respectively.

The composite roughness equation 3.43 can also be derived from the equation 3.46.

3.7 CHANNEL-STRIP RELATIONSHIPS

3.7.1 General

In sections 3.3 through 3.6, a channel flow problem has been simplified from the complex three-dimensional relations to a one-dimensional discrete strip-flow relations, which are governed by the local conditions of the strip only. But each strip-flow is the integral part of a whole channel cross-sectional flow. Hence, the discrete relations of strip-flow should comply with the entire channel flow in all respect. In other words, the synthesis process in combining the channel-strip relationships should be such that for each elementary fluid flow characteristics like velocity, shear stress, etc., each should be of unique value.

In the absence of proper mathematical relationships,

an attempt has been made to establish an empirical expression, or model, combining the strip velocities with the channel velocities at any point within the control volume of the entire channel cross-section. The relationship is nothing but an expression of velocity profiles in two dimensional domain.

The model can be expressed in general form as:

$$\frac{U}{V} = E1[\ \Phi\ ]^{E2} \qquad 3.47$$

where, for any elementary fluid,

U = the actual velocity vector of the elementary fluid in two-dimensional form

V = the mean velocity of the entire channel

$\Phi = f(u_s/V_s)$, a function of dimensionless velocity of the elementary fluid that can be obtained from one-dimensional analyses of strips in which the elementary fluid belongs to.

E1 and E2 are the velocity coefficients. The coefficient, E1 is related with the total flow of a channel while the coefficient E2 relates to and affects the velocity gradient steepness.

Equation 3.47 is kept in generalized form because the same expression is valid for the case of both free-surface flow and floating covered surface flow. It is also valid in case of a wide channel as well (for both flows) where

the analysis with vertical strips, instead of both vertical and horizontal strips only, is of adequacy. Hence, the form of the function "Φ" will change with that of the condition of flow and the type of analysis.

For the solution of equation 3.47 it is required to satisfy the continuity equation and the momentum equation as well of the entire channel.

Continuity Equation of the Entire Channel

$$\int_A U \, dA = A \, V \qquad 3.48$$

Momentum Equation of the Entire Channel

$$P \int_{\tau_{\phi s}} P_s = \gamma A S \qquad 3.49$$

where,

dA = area of any elementary fluid

A = cross-sectional area of entire channel

$\tau_{\phi s}$ = boundary shear stress of any strip 's' in which the elementary fluid belongs to

P_s = hydraulic parameter of a strip, 's'

P = hydraulic parameter of entire channel

S = overall energy slope of the entire channel.

3.7.2 Boundary Shear Stress

In the absence of an exact mathematical relationship between the shear stress distribution within the turbulent

zone of the flow and the boundary shear stress in two-dimensional analysis, the boundary shear stress distribution will be determined indirectly in one-dimensional domain from the two-dimensional velocity distributions which are the results of the solution of equation 3.47.

Figure 3.11 shows the nature of the shear-stress distributions (laminar and turbulent) of a free-surface flow along a strip while Figure 3.12 shows those of a floating covered surface flow. The nature of combined distributions of laminar and turbulent shear stresses is of triangular form from free-surface or equivalent free-surface to the boundary in one dimensional domain. From the nature of the distributions it is observed that within the turbulent zone the contributions of laminar shear stresses can sensibly be ignored and in that case, the distribution of turbulent shear stresses can be well assumed as a triangular distribution. Therefore, the boundary shear stress of a strip can be determined by transposing the turbulent shear stress of any fluid element within the turbulent zone of the strip-flow by the similar triangle rule.

The procedure is the same for both vertical and horizontal strips. Hence, the turbulent shear stress of a fluid element is obtained from Prandtl's mixing length equation in conjunction with the two-dimensional velocity equation 3.47.

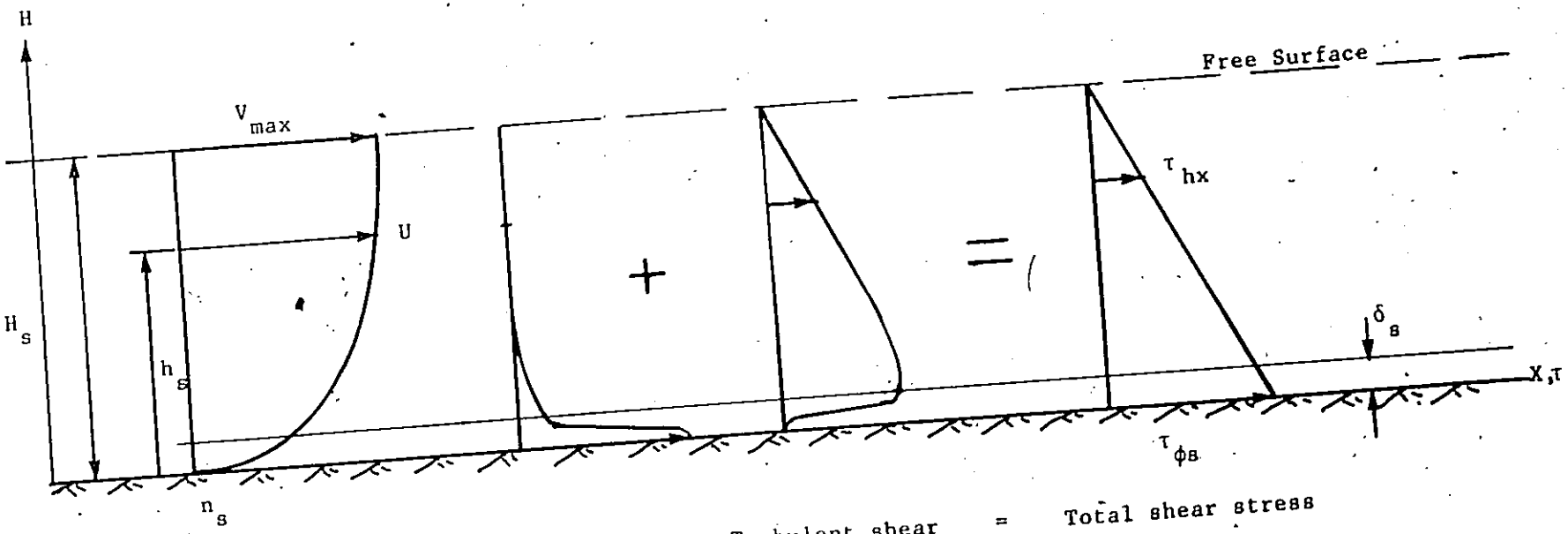

Fig. 3.11. Shear Stress Distribution of a Channel Strip with Single Boundary Roughness.

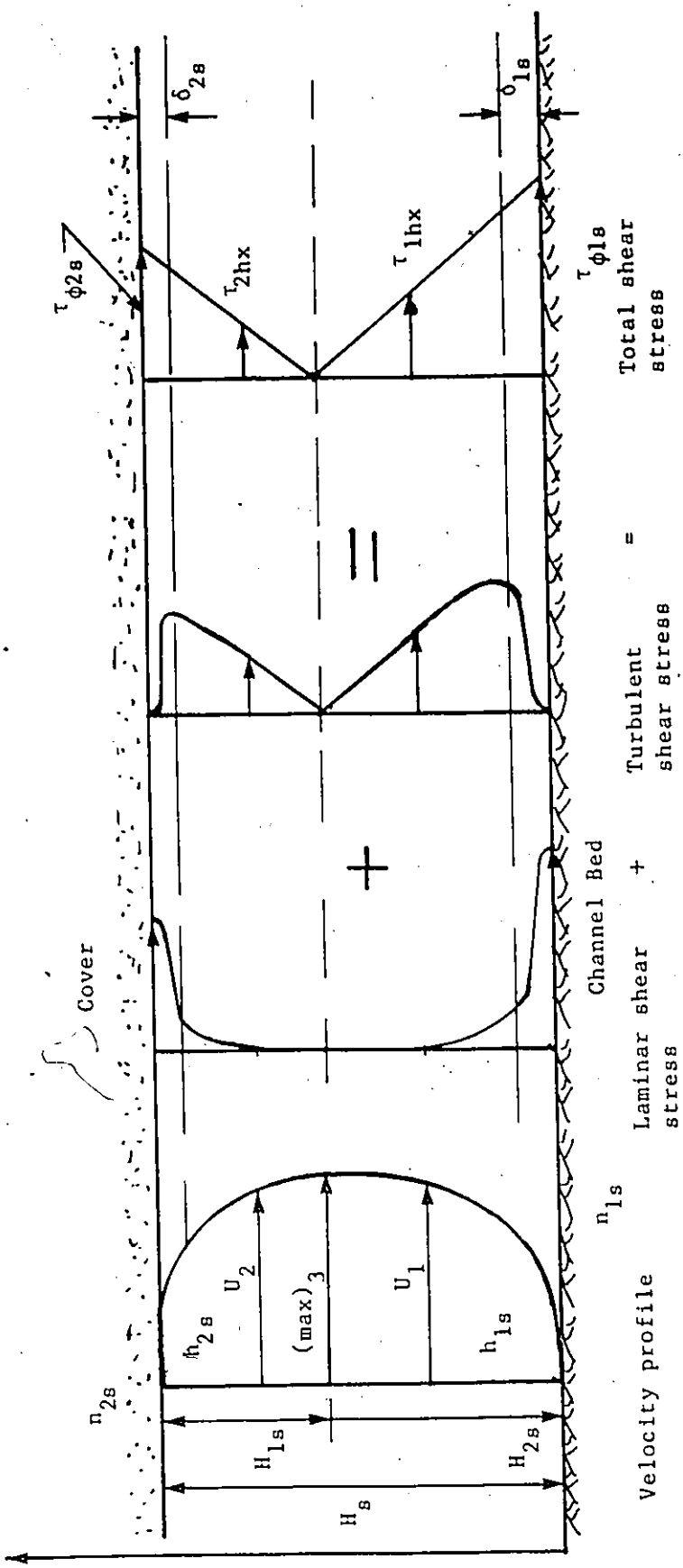

Fig. 3.12. Shear Stress Distribution of a Channel Strip with Two Roughness Boundaries.

Hence, the turbulent shear stress (in the X-direction) at any depth 'h' of a strip, 's' (Figure 3.8) is:

$$\tau_{hx} = \rho\kappa^2 h_s^2 \left(\frac{dU}{dh_s}\right)^2 \qquad 3.50$$

and the corresponding transposed boundary shear stress, $\tau_{\phi h}$ can be written as:

$$\tau_{\phi h} = \tau_{hx} \frac{H_s}{(H_s - h_s)} \qquad 3.51$$

Now, if more than one turbulent shear stresses are obtained at different flow depth of a strip-flow, 's', the average of all those transposed boundary shear stresses will be the boundary shear stress of the strip, and it can be expressed as:

$$\tau_{\phi s} = \frac{1}{N} \sum_{np=1}^{N} \left[\tau_{\phi h} \frac{H_s}{H_s - h_s}\right]_{np} \qquad 3.52$$

where, 'np' denotes at any nodal point.

From Figure 3.13, for a rectangular open channel flow, and Figure 3.14 for the covered channel flow, it can be observed that at any point within the flow there exists two components of shear-stress; one from the vertical momentum transfer and the other from the horizontal momentum transfer. The actual shear stress, must be the resultant of the two components (which is not known at

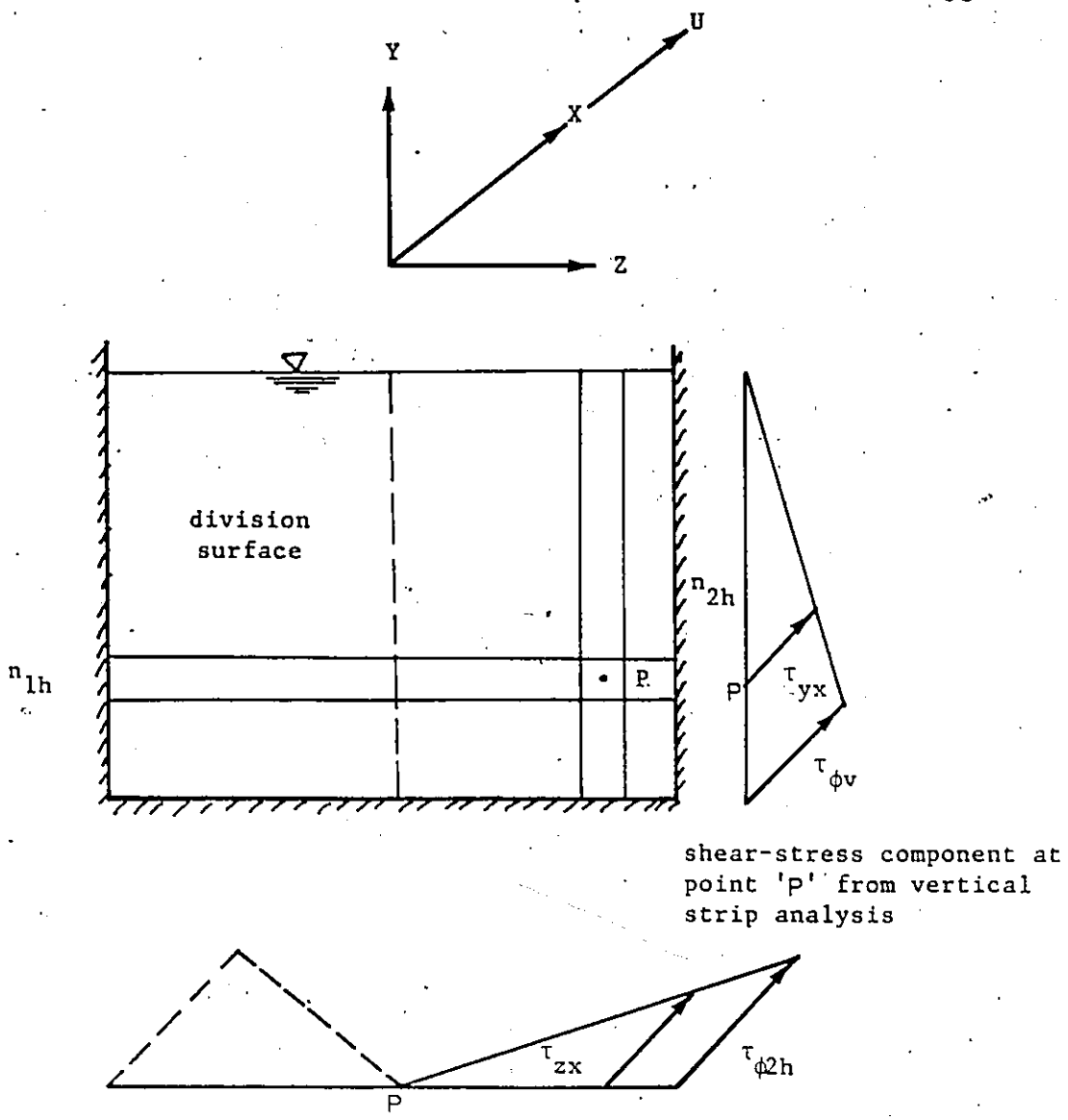

Fig. 3.13. Shear Stress Distributions Related with Two-Dimensional Velocity Distributions (U) - Free-Surface Flow.

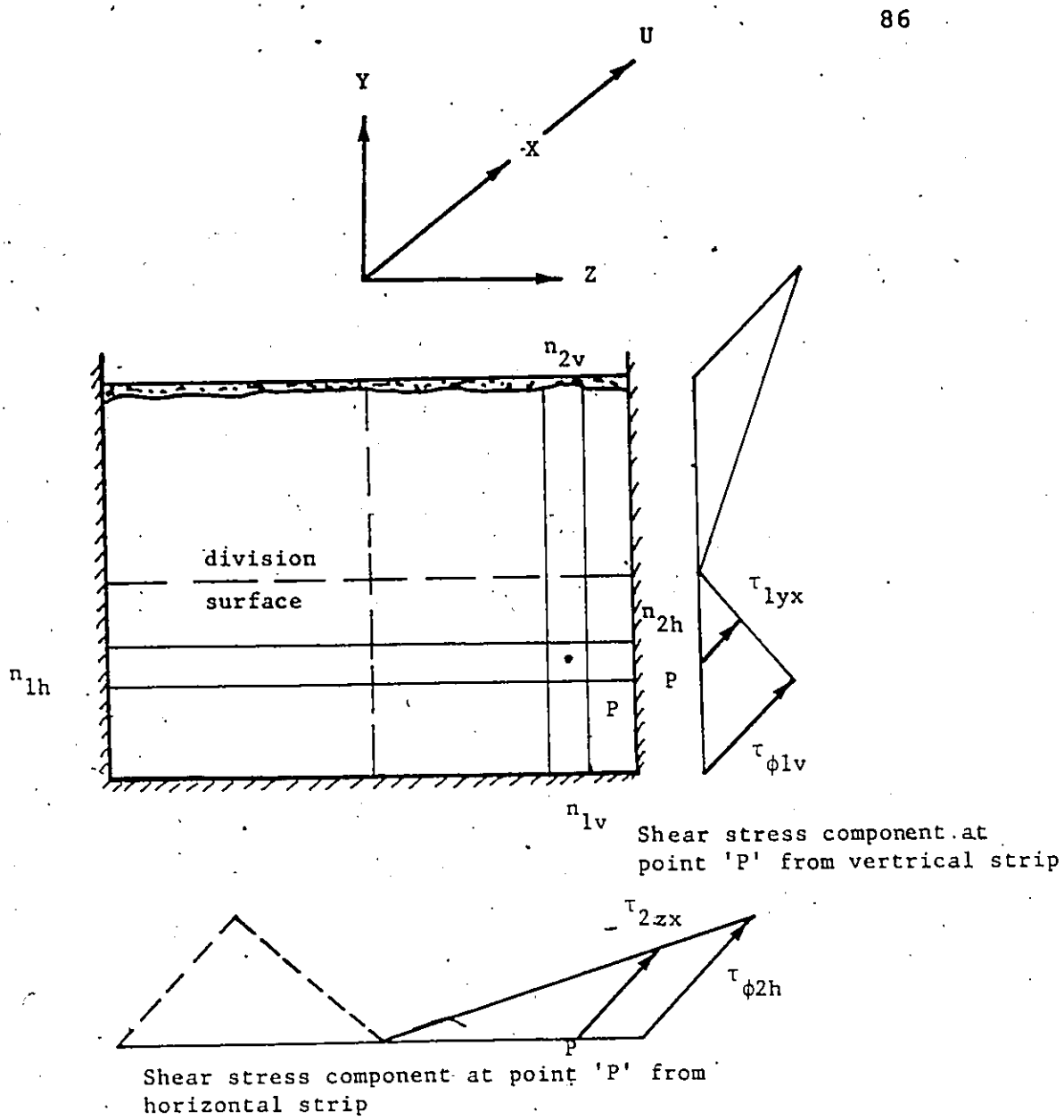

Fig. 3.14. Shear Stress Distributions Related with Two-Dimensional Velocity Distributions.

present, but this is not the interest of the present research and this does not affect obtaining the boundary shear stress at the bed).

In the synthesization process of channel-strip relationship in two-dimensional analysis, it can be observed from Figures 3.5 and 3.7 that although the shear stresses are assumed of zero values along the locus of the division surfaces or a free-surface in one-dimensional strip analysis as a first approximation, the resultant shear stresses on that surface are not zeros except at the point of intersection of the two loci of vertical strips and horizontal strips, respectively, where the channel velocity reaches its maximum value.

3.7.2.1 Boundary Shear Stresses on Inclined Boundaries

Unlike a horizontal bed or a vertical wall, a sloped bed or wall (such as: sides of a trapezoidal channel, bed of natural stream) has two components of boundary shear stresses; one is from the vertical strip and the other is from the horizontal strip. In this case the boundary shear stress at any point on the sloped surface (Figure 3.15) can be considered as an average of the two components; mathematically it can be stated as:

$$\tau_{\phi s} = \frac{1}{2}[\tau_{\phi vs} + \tau_{\phi hs}] \qquad 3.53$$

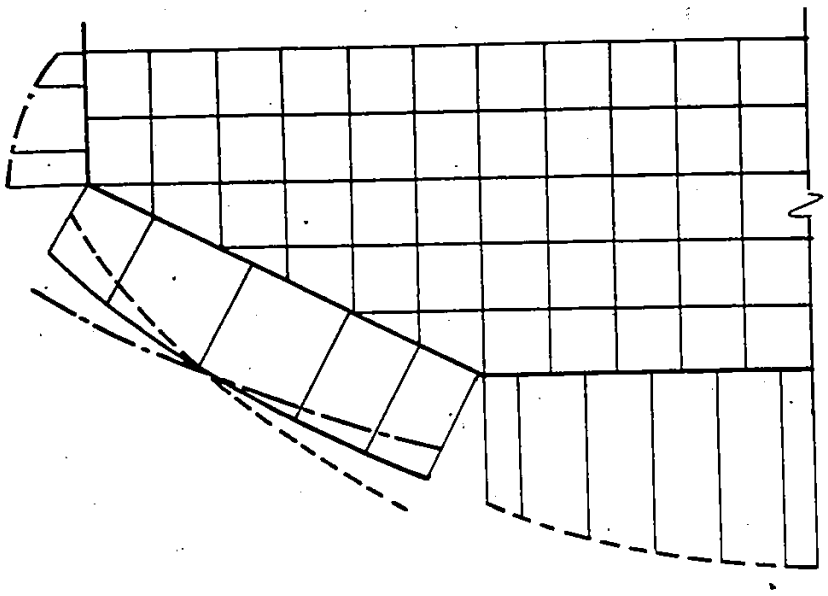

Legend

Boundary shear stress from vertical strip

Boundary shear stress for horizontal strip

Average boundary shear stress

Fig. 3.15. Boundary Shear Stress on an Inclined Plane.

3.8 THEORY OF ANALYSIS WITH VERTICAL STRIP METHOD

In nature many streams or rivers with or without flood plains can be considered as wide channels (when bottom width is ten times or more than the depth of flow). Hence, the effect of the lateral momentum transfer due to the prime flow in the longitudinal direction (X-direction) can sensibly be neglected. Therefore, the flow equation can be simplified for the vertical momentum transfer only,

$$\frac{\partial}{\partial y}(\tau_{yx}) = - \rho g S_e \qquad 3.54$$

and equation 3.54 can be integrated if the energy slope of an elementary fluid is assumed to be a constant over the local flow depth of a strip drawn confining the elementary fluid-boundary, as indicated earlier, and the integration can be expressed by equation 3.14, i.e.,

$$\tau_{yx} = \rho g S_{vs}(Y_{vs} - y_{vs}).$$

The velocity distribution equation can be established from the Prandtl mixing length theory, and the discrete velocity distributions of strips are to be synthesized within the entire channel cross-section in the similar way as were developed in the previous sections. Hence, the velocity equation 3.47 can also be used for this method.

The details of the equations for both the free-surface

flow and covered-surface flow and their solutions will be discussed in the next chapter.

3.9 GENERALIZED FORM OF MANNING'S EQUATION

Dimensional analysis shows that Manning's roughness coefficient, n, has the dimension $L^{-1/3}T$ in MLT-System (MLT - Mass, Length and Time).

Because of this dimensional form of Manning's roughness, the velocity expression is different in FPS-Unit system to that of in M.K.S.-Unit system. This creates problems in developing generalized monographs, equations, etc., which can be used in both unit systems.

In Appendix A.4, a generalized form of Manning's equation is derived from the dimensional analysis. The expression is valid for both unit systems as the Manning's roughness, n, is non-dimentionalized. The expression is:

$$V = \frac{0.061}{n}\left(\frac{g^5}{\nu}\right)^{1/9} R^{2/3} S^{1/2} \qquad \text{A.4.3}$$

CHAPTER IV

APPLICATION OF THEORY AND ITS SOLUTION

In this chapter the generalized equations, which were established in Chapter III, will be used to develop corresponding expressions for the special cases following their method of solutions categorically as below:

1. Ice Covered channel with both vertical and horizontal strips analyses.
2. Free-surface flow with both vertical and horizontal strips analyses.
3. Ice covered channel with vertical strip analysis.
4. Free-surface flow with vertical strip analysis.
5. Special considerations for compound channels.

4.1 ICE COVERED CHANNEL WITH VERTICAL AND HORIZONTAL STRIP ANALYSIS

4.1.1 Equations

In all the cases, factors related to the vertical strip will be denoted by the subscript, 'v' and those related to horizontal strip will be denoted by the subscript, 'h'.

The integral notation ($\int$) will be replaced by the summation (Σ) notation as the solution of the system is

based on numerical analysis.

I. STRIP

A. Velocity Distribution

Equation 3.32 will be used with the replacement of proper subscript notations.

Vertical Strip

$$u_{\ell v} = V_{\ell v} - \frac{V_{*\ell v}}{\kappa} F_2(\varepsilon_{\ell v}), \quad \ell = 1, 2 \qquad 4.1$$

when,

$$F_2(\varepsilon_{\ell v}) = 2\left[\mathrm{Ln}\frac{\varepsilon_{\ell v}^{1/2}}{1-(1-\varepsilon_{\ell v})^{1/2}} - (1-\varepsilon_{\ell v})^{1/2} - 1/3\right]$$

and

$$\varepsilon_{\ell v} = y_{\ell v}/Y_{\ell v}:$$

The dimensionless form of equation 4.1 can be obtained as

$$\frac{u_{\ell v}}{V_{\ell v}} = 1 - \frac{n_{\ell v} g^{1/2}}{\kappa Y_{\ell v}^{1/6}} F_2(\varepsilon_{\ell v}) \qquad 4.2$$

where, from the definition of Manning's equations

$$V_{\ell v} = \frac{1}{n_{\ell v}} Y_{\ell v}^{2/3} S_{\ell v}^{1/2}$$

and from the definition of shear velocity,

$$V_{*\ell v} = (gY_{\ell v}S_{\ell v})^{1/2}$$

have been substituted.

Horizontal Strip

Velocity distribution:

$$u_{mh} = V_{mh} - \frac{V_{*mh}}{\kappa}F_2(\epsilon_{mh}),\ m = 1,\ 2 \qquad 4.3$$

where

$$F_2(\epsilon_{mh}) = 2\left[\mathrm{Ln}\frac{\epsilon_{mh}^{1/2}}{1-(1-\epsilon_{mh})^{1/2}} - (1-\epsilon_{mh})^{1/2} - 1/3\right]$$

and

$$\epsilon_{mh} = z_{mh}/Z_{mh}$$

and the dimensionless form, after substituting for

$$V_{mh} = \frac{1}{n_{mh}} z_{mh}^{2/3} S_{mh}^{1/2}$$

and

$$V_{*mh} = (gZ_{mh}S_{mh})^{1/2}$$

is:

$$\frac{u_{mh}}{V_{mh}} = 1 - \frac{n_{mh} g^{1/2}}{\kappa Z_{mh}^{1/6}} F_2(\epsilon_{mh}) \qquad 4.4$$

B. Division Surface

Equation 3.39 will be used.

Vertical Strip

Considering the strip as a wide channel (i.e., infinite in the Z-direction) and replacing,

$$R_s = Y_v/2 \quad \text{and} \quad \alpha_s = \frac{P_{1v}}{P_v} = \frac{\Delta Z}{2\Delta Z} = 0.5,$$

the equation is:

$$\frac{3\kappa}{2} \frac{Y_v^{1/6}}{n_{1v} g^{1/2}} = \frac{\lambda_v^{1/2} \psi_v^{1/2} - 1}{1 - \frac{n_{1v}}{n_{2v}} \lambda_v^{2/3} \psi_v^{1/2}} (1+\lambda_v)^{1/6} \qquad 4.5$$

where

$$\lambda_v = Y_{2v}/Y_{1v}, \quad Y_v = Y_{2v}+Y_{1v}, \text{ and } \psi_v = S_{2v}/S_{1v}.$$

Horizontal Strip

Considering the strip as a deep channel (i.e., infinite in the Y-direction) and replacing

$$R_s = Z_h/2 \text{ and } \alpha_s = \frac{P_{1h}}{P_h} - \frac{\Delta Y}{2\Delta Y} = 0.5;$$

the equation is:

$$\frac{3\kappa}{2}\frac{Z_h^{1/6}}{n_{1h}g^{1/2}} = \frac{\lambda_h^{1/2}\psi_h^{1/2}-1}{1-\frac{n_{1h}}{n_{2h}}\lambda_h^{2/3}\psi_h^{1/2}}(1+\lambda_h)^{1/6} \qquad 4.6$$

where,

$$\lambda_h = Z_{2h}/Z_{1h}, \quad Z_h = Z_{1h}+Z_{2h}, \text{ and } \psi_h = S_{2h}/S_{1h}$$

C. Composite Roughness

Equation 3.43 will be used with $\alpha_s = 0.5$.

Vertical Strip

$$\frac{n_v}{n_{1v}} = [(0.5)^{2/3}\frac{(1+\lambda_v)^{5/3}}{1+\frac{n_{1v}}{n_{2v}}\lambda_v^{5/3}\psi_v^{1/2}}][(\frac{1+\lambda_v\psi_v}{1+\lambda_v})^{1/2}] \qquad 4.7$$

Horizontl Strip

$$\frac{n_h}{n_{1h}} = [(0.5)^{2/3}\frac{(1+\lambda_h)^{5/3}}{1+\frac{n_{1h}}{n_{2h}}\lambda_h^{5/3}\psi_h^{1/2}}][(\frac{1+\lambda_h\psi_h}{1+\lambda_h})^{1/2}] \qquad 4.8$$

D. Boundary Shear Stress

Equations 3.42a and 3.42b will be used.

Vertical Strip

$$\tau_{\phi \ell v} = \gamma Y_{\ell v} S_{\ell v} \qquad 4.9$$

Horizontal Strip

$$\tau_{\phi mh} = \gamma Z_{mh} S_{mh} \qquad 4.10$$

E. Momentum Equation

Equations 3.44 will be used; substituting $\alpha_s = 0.5$

Vertical Strip

$$\frac{S_v}{S_{lv}} = \frac{(1+\lambda_v \psi_v)}{1 + \lambda_v} \qquad 4.11$$

Horizontal Strip

$$\frac{S_h}{S_{lh}} = \frac{1 + \lambda_h \psi h}{1 + \lambda_h} \qquad 4.12$$

II. CHANNEL-STRIP COMBINED

A. Velocity Distribution

Equation 3.47 will be used, in this case,

$$\Phi = [(\frac{u_{\ell v}}{V_{\ell v}})(\frac{u_{mh}}{V_{mh}})]$$

Hence, the equation can be written as:

$$\frac{U}{V} = El\left[\left(\frac{u_{\ell v}}{V_{\ell v}}\right)\ \left(\frac{u_{mh}}{V_{mh}}\right)\right]^{E2} \qquad 4.13$$

B. Continuity Equation

Equation 3.48 can be written on substituting U from equation 4.13 and rearranging,

$$El\left\{\sum\left[\frac{u_{\ell v}}{V_{\ell v}}\ \ \frac{u_{mh}}{V_{mh}}\right]^{E2}\ \Delta A\right\}V = AV$$

and finally,

$$El\left\{\sum\left[\frac{u_{\ell v}}{V_{\ell v}}\ \ \frac{u_{mh}}{V_{mh}}\right]^{E2}\Delta A\right\} = A \qquad 4.14$$

C. Boundary Shear Stress

Equation 3.50 together with equations 3.51 and 3.52 will be used on substituting for U from equation 4.13.

Vertical Strip

At any nodal point of a vertical strip, the turbulent shear stress,

$$\tau_{\ell yx} = \rho\kappa^2 y_{\ell v}^2 \left(\frac{dU}{dy_{\ell v}}\right)^2 \qquad 4.15$$

where,

$$\frac{dU}{dy_{\ell v}} = \frac{d}{dy_{\ell v}}\left\{El\left[\frac{u_{\ell v}}{V_{\ell v}}\ \ \frac{u_{mh}}{V_{mh}}\right]^{E2}\ V\right\}$$

$$= (E1(\frac{u_{mh}}{V_{mh}})^{E2} \quad V)E2(\frac{u_{\ell v}}{V_{\ell v}})^{E2-1} \quad \frac{1}{V_{\ell v}} \frac{du_{\ell v}}{dy_{\ell v}}$$

$$= \{E1[\frac{u_{mh}}{V_{mh}} \quad \frac{u_{\ell v}}{V_{\ell v}}]^{E2} \quad V\}E2 \quad u_{\ell v}^{-1} \frac{du_{\ell v}}{dy_{\ell v}}$$

Referring to equation 4.13

$$E1[\frac{u_{\ell v}}{V_{\ell v}} \quad \frac{u_{mh}}{V_{mh}}]^{E2} \quad V = U$$

and from the equation 3.27 it can be written:

$$\frac{du_{\ell v}}{dy_{\ell v}} = \frac{(gS_{\ell v})^{1/2}}{\kappa} \frac{(Y_{\ell v}-y_{\ell v})^{1/2}}{y_{\ell v}}$$

Substituting, it can be obtained,

$$\frac{dU}{dy_{\ell v}} = \frac{U}{u_{\ell v}} \quad E2[\frac{(gS_{\ell v})^{1/2}}{\kappa} \quad \frac{(Y_{\ell v}-y_{\ell v})^{1/2}}{y_{\ell v}} \quad] \qquad 4.16$$

Combining equations 4.15 and 4.16, and rearranging, the shear stress at a depth of 'y' can be written as:

$$\tau_{\ell yx} = \rho g S_{\ell v}(E2\frac{U}{u_{\ell v}})^2(Y_{\ell v}-y_{\ell v}) \qquad 4.17$$

Hence, the corresponding boundary shear stress will be referring to equation 3.51,

$$\tau_{\phi \ell y} = \tau_{\ell yx} \quad \frac{Y_{\ell v}}{(Y_{\ell v}-y_{\ell v})}$$

or

$$\tau_{\phi \ell y} = \rho g S_{\ell v} (E2 \frac{U}{u_{\ell v}})^2 Y_{\ell v} \qquad 4.18$$

Hence, if the total 'N' number of nodal points within the sub-strip flow depth, $Y_{\ell v}$ are used for transposing the turbulent shear stresses at the boundary of that flow strip, then the average boundary shear stress for that strip can be obtained as:

$$\tau_{\phi \ell v} = \frac{1}{N} \sum [\rho g S_{\ell v} (E2 \frac{U}{u_{\ell v}})^2 Y_{\ell v}] \qquad 4.19$$

Horizontal Strip

Similar to the vertical strip, the boundary shear stress for a horizontal strip can be obtained as:

$$\tau_{\phi mh} = \frac{1}{M} \sum [\rho g S_{mh} (E2 \frac{U}{u_{mh}})^2 Z_{mh}] \qquad 4.20$$

where, M is the number of nodal points within the horizontal sub-strip.

D. Momentum Equation

Equation 3.49 will be used with notations:

$$\sum (\tau_{\phi \ell v} P_{\ell v}) + \sum (\tau_{mh} P_{mh}) = \gamma A S \qquad 4.21$$

E. Overall Channel Equation

Manning's equation for the entire channel can be written as:

$$V = \frac{1}{n} R^{2/3} S^{1/2} \qquad 4.22$$

4.1.2 Solution

4.1.2.1 General

By paying close attention to the construction of the equations right from the start with the velocity distribution of a strip to the end with the overall channel equation, it is clear that each equation is inter-dependent with the other equations and the solution is a cyclic process. As for an example: to obtain the energy slopes of a strip from equations 4.9 and/or 4.10, it has to wait till the steps reached by the equations 4.19 and/or 4.20 and to solve the equation 4.20 and/or 4.21; then, these have to return to the solution of the strips' velocity distributions equations 4.2 and/or 4.4. Hence, the solution is an iterative process.

In a real value problem of a channel flow with multiple boundary roughnesses, either the overall energy slope (or bed slope) or the overall discharge (i.e., mean velocity) is assumed to be a known parameter while the other one is to be determined. In this case another added parameter is

the composite or overall channel roughness which is to be determined as well. Hence, at this point it is better to examine how many equations are available against the number of unknowns which are to be solved for. It is given below in a tabular form, noting that the equations for the two substrips in both the vertical and horizontal directions are considered one equation for the convenience of observation.

TABLE 4.1

Comparison of Unknown Parameters with Number of Available Equations

Description	Unknown Parameter(s)	Equation(s)
Substrip velocity components	$u_{\ell v}$, $u_{\ell h}$	4.1, 4.3
Strip-hydraulic radius ratios	λ_v, λ_h	4.5, 4.6
Strip composite roughnesses	n_v, n_h	4.7, 4.8
Substrip slopes (energy)	$S_{\ell v}$, S_{mh}	4.9, 4.10
Strip energy slopes	S_v, S_h	4.11, 4.12
Channel's velocity distribution and coefficients of velocity	U, E1, E2	4.13, 4.14
Channel boundary shear stress	$\tau_{\phi \ell v}$, $\tau_{\phi mh}$	4.19, 4.20
Channel's overall slope	S	4.21
Channel's mean velocity on roughness (composite)	V, n	4.22
TOTAL	18	16

Although there are eighteen (18) unknown parameters, it should be actually seventeen (17) against sixteen available equations, if it is assumed that either the overall energy slope, S or the overall mean velocity, V is known. Hence, redundancy of the problem can be defined as of one degree.

It can be said that the actual unknown parameters are E1, E2, n, S, or V while the remaining unknowns are the results of the internal process of the entire system in the way of its solution. Hence, the solution of the problem at this stage is dependent on the external resources like laboratory or field data. While the discharge, flow depth (and, thereby, the velocity can be calculated), overall energy slope of a channel flow can be measured from the laboratory experiment, the set of equations can be solved for the coefficients E1 and E2. Once these coefficients are known, it can be used for the solution of real value problems.

4.1.2.2. 'Steps to Determine the Coefficients E1 and E2'

I. EXPERIMENTAL DATA

Obtain the following data from laboratory experiment:

a) Geometrical parameters of the experimental channel.

b) Boundary roughnesses.

c) Channel discharge.

d) Flow depth.

e) Ambient temperature

f) Energy slope of the flow or bed slope, S.

g) Velocity distributions (optional).

h) Boundary shear stresses (optional).

II. THEORETICAL SOLUTION

1. Divide the channel cross-section into finite vertical and horizontal strips of width ΔY and ΔZ, respectively.
2. Assign the boundary roughnesses for each vertical strip (n_{1v}, n_{2v}) and each horizontal strip (n_{1h}, n_{2h}).
3. Determine the coordinates of nodal points from Z- and Y-axes. Determine the overall length (physical boundary to boundary) of each vertical (Y_v) and horizontal strip (Z_h).
4. Using equation 4.5, determine the hydraulic radius ratio, λ_v for each vertical strip, assuming the energy slopes of each sub-strip and corresponding strip are equal to the overall channel's energy slope (i.e., $S_{1v} = S_{2v} = S_v = S$) and thus, $\psi_v = 1$ as a first approximation. Proceed in identical manner for each horizontal strip, using equation 4.6.
5. With a similar approximation to that of step 4, determine strip composite roughnesses (n_v,n_h) using equations 4.7 and 4.8.

6. Determine the transformed coordinates of the centre line point of each elementary fluid (can be defined as the cross-sectional area bounded by the intersection of each vertical and horizontal strip) from their respective boundaries.

   The details of the determination of coordinates of elementary fluids will be discussed later.

7. Determine the dimensionless velocity profiles for each vertical strip ($u_{\ell v}/V_{\ell v}$) and horizontal strip (u_{mh}/V_{mh}) by using equations 4.2 and 4.4.

8. Assuming an initial value for this coefficient E2 = 1, determine the other coefficient E1, from the equation 4.14,

$$E1 = \frac{\Delta A}{[\sum (\frac{u_{\ell v}}{V_{\ell v}} \quad \frac{u_{mh}}{V_{mh}})^{E2} \Delta A}$$

9. With the estimated value of E1 from Step 8 and E2=1.0, calculate the channel velocity profile from equation 4.13.

10. Obtain the boundary shear stress distribution ($\tau_{\phi \ell v}$, $\tau_{\phi mh}$) of the channel by using equations 4.19 and 4.20.

11. Determine the substrip and strip energy slopes ($S_{\ell v}$, $S_{\ell h}$, S_v and S_h) from equations 4.9, 4.10, 4.11 and 4.12.

12. Calculate the overall energy slops, S_c by using equation 4.21, where S_c is the calculated slope.

13. Check if the calculated slope, S_c is equal to the actual (experimental) overall energy slope, S.

14. If $S_c \neq S$, assign a modified value of E2 adjusting a small incremental or decremental value (i.e., $E2 = E2 \pm \Delta E2$, and with the calculated substrip slopes as obtained in step 11, repeat steps 4 to 13 till the energy slope, S_c comply with the experimental energy slope, S.

15. If $S_c = S$, obtain the final value of E1 and E2, and other parameters as desired.

The detailed flow chart of the above solution is shown in Figure FC.1 in Appendix D.

4.2 FREE-SURFACE FLOW WITH VERTICAL AND HORIZONTAL STRIP ANALYSIS

In this case, all the equations of horizontal strip, developed for covered flow, will remain unchanged and will not be repeated here except the equation numbers that were assigned. Only the equations of vertical strip will change or vanish due to the absence of the division surface. In mathematical terms it can be said that the division surface exists at the free-surface, hence, substrip two will vanish.

4.2.1 Equations

All the notations, used in the previous section 4.1 will remain unchanged.

I. STRIP RELATIONS

A. Velocity Distribution

Vertical Strip

$$u_v = V_v - \frac{V_{*v}}{\kappa} F_2(\epsilon_v) \qquad 4.23$$

where, $\epsilon_v = y_v/Y_v$

and the dimensionless form,

$$\frac{u_v}{V_v} = 1 - \frac{n_v g^{1/2}}{\kappa Y_v^{1/6}} F_2(\epsilon_v) \qquad 4.24$$

Manning's equation

$$V_v = \frac{1}{n_v} Y_v^{2/3} S_v^{1/2}$$

and shear velocity,

$$V_{*v} = (gy_v S_v)^{1/2}$$

Horizontal Strip

Use the same equations, 4.3 and 4.4

B. Division Surface

Vertical Strip

No equation is required, as $Y_{2v} = 0$; $\lambda_v = 0$.

Horizontal Strip

Use the same equation 4.6.

C. Composite Roughness

Vertical Strip

No equation is required; as $n_{2v} = 0$; $n_v = n_{1v}$.

Horizontal strip

Use the same equation 4.8.

D. Boundary Shear Stress

Vertical Strip

$$\tau_{\phi v} = \gamma Y_v S_v \qquad 4.25$$

Horizontal Strip

Use the same equation 4.10

E. Momentum Equation

Vertical Strip

No equation is required, as $S_{2v} = 0$; $S_{1v} = S$

Horizontal Strip

Use the same equation 4.12.

II. CHANNEL-STRIP COMBINED RELATIONSHIPS

A. Velocity Distribution

$$\frac{U}{V} = E1\left[\frac{u_v}{V_v} \quad \frac{u_{mh}}{V_{mh}}\right]E2 \qquad 4.26$$

B. Continuity Equation

$$E1\left\{\Sigma\left[\frac{u_v}{V_v} \quad \frac{u_{mh}}{V_{mh}}\right]E2 \ \Delta A\right\} = A \qquad 4.27$$

C. Boundary Shear Stress

Vertical Strip

$$\tau_{\phi v} = \frac{1}{N}\Sigma\left[\rho g S_v \left(E2 \ \frac{U}{u_v}\right)^2 Y_v\right] \qquad 4.28$$

Horizontal Strip

Use the same equation 4.20.

D. Momentum Equation

$$\Sigma(\tau_{\phi v} \ P_{\ell v}) + \Sigma(\tau_{\phi mh} \ P_{mh}) = \gamma AS \qquad 4.29$$

E. Overall Channel Equation

Use the same equation 4.22.

The detailed flow chart for the solution of the above equations is shown in Figure FC.2 in Appendix D.

4.3 VERTICAL STRIP ANALYSIS FOR COVERED CHANNEL FLOW

It is already mentioned earlier in case of a wide channel, the effects of the lateral momentum transfer can sensibly be ignored. Therefore, the analysis of a wide channel by the vertical strip method alone is adequate to accomplish the purpose. Hence, the equations which are required for the vertical strip analysis only will be described. Almost all the equations were already developed in Section 4.1.

I. STRIP RELATIONSHIP

A. Velocity Distributions

$$u_{\ell v} = V_{\ell v} - \frac{V_{*\ell v}}{\kappa} F_2(\varepsilon_{\ell v}) \qquad \ell = 1,2 \tag{4.1}$$

B. Division Surface

$$\frac{3\kappa}{2}\frac{n_{1v} g^{1/2}}{Y_v^{1/6}} = \frac{(\lambda_v^{1/2}\psi_v - 1)}{1 - \frac{n_{1v}}{n_{2v}}\lambda_v^{2/3}\psi_v^{1/2}}(1+\lambda_v)^{1/6} \tag{4.5}$$

C. Composite Roughness

$$\frac{n_v}{n_{1v}} = \left[(0.5)^{2/3}\frac{(1+\lambda_v)^{5/3}}{1+\frac{n_{1v}}{n_{2v}}\lambda_v^{5/3}\psi_v^{1/2}}\left(\frac{1+\lambda_u\psi_v}{+\lambda_v}\right)^{1/2}\right] \tag{4.7}$$

D. Boundary Shear Stress

$$\tau_{\phi\ell v} = \gamma Y_{\ell v} S_{\ell v} \tag{4.9}$$

E. Momentum Equation

$$\frac{S_v}{S_{1v}} = \frac{1+\lambda_v \psi_v}{1+\lambda_v} \qquad (4.11)$$

II. CHANNEL-STRIP RELATIONSHIPS

A. Velocity Distributions

$$\frac{U}{V} = E1\left[\frac{u_{\ell v}}{V_{\ell v}}\right)^{E2} \qquad (4.30)$$

B. Continuity Equation

$$E1\{\Sigma[\frac{u_{\ell v}}{V_{\ell v}}]^{E2}\}\ \Delta A = A \qquad (4.31)$$

C. Boundary Shear Stress

$$\tau_{\phi \ell v} = \frac{1}{N}\Sigma[\rho g S_{\ell v}(E2\frac{U}{u_{\ell v}})^2 Y_{\ell v}] \qquad (4.19)$$

D. Momentum Equation

$$\Sigma(\tau_{\phi \ell v} P_{\ell v}) = \gamma A s \qquad (4.32)$$

E. Overall Channel Equation

$$V = \frac{1}{n} R^{2/3} S^{1/2} \qquad (4.22)$$

where

$$R = Y_v/2$$

See detailed flow chart in Figure FC.3, Appendix D.

4.4. VERTICAL STRIP ANALYSIS FOR FREE SURFACE FLOW

The relationship as well as the method of analysis are exactly the same as described in section 4.3, except it does not require the analysis for division surfaces. Hence, the method is very straightforward and simple.

I. STRIP RELATIONSHIP

A. Velocity Distribution

$$u_v = V_v - \frac{V_{*v}}{\kappa} F_2(\varepsilon_v) \tag{4.23}$$

and the dimensionless form

$$\frac{u_v}{V_v} = 1 - \frac{n_v g^{1/2}}{\kappa Y_v^{1/6}} F_2(\varepsilon_v) \tag{4.24}$$

B. Boundary Shear Stress

$$\tau_{\phi v} = \gamma Y_v S_v \tag{4.25}$$

II. CHANNEL-STRIP RELATIONSHIPS

A. Velocity Distributions

$$\frac{U}{V} = E1\left[\frac{u_v}{V_v}\right]^{E2} \tag{4.33}$$

B. Continuity Equation

$$E1\left\{\Sigma \left[\frac{u_v}{V_v}\right]^{E2} \Delta A\right\} = A \tag{4.34}$$

C. Boundary Shear Stress

$$\tau_{\phi v} = \Sigma \frac{1}{N} [\rho g S_v (E2 \frac{U}{u_v})^2 \quad Y_v] \qquad (4.28)$$

D. Momentum Equation

$$\Sigma(\tau_{\phi v} \quad P_v) = \gamma A S \qquad (4.35)$$

E. Overall Channel Equation

$$V = \frac{1}{n} R^{2/3} S^{1/2} \qquad (4.22)$$

where $R = Y_v$.

See flow chart in Figure FC.4 in Appendix D.

4.5 COMMENTS ON THE SOLUTION PROCEDURES

The procedures which are described in sections 4.1 through 4.4 for different flow conditions and different method of analysis, are for the determination of the velocity coefficients E1 and E2 of the generalized equation 3.47 by theoretical analysis of experimental data. These procedures are equally valid for any channel cross-section including simple, complex, and compound channels irrespective of their shapes, sizes and boundary conditions.

Once the coefficient values for E1 and E2 are established the model can be solved for real value problems, while in nature the main channel bed slope, flow depth

and the properties of the stream cross-sections are known. The method of solution will be described in Chapter VII.

In the next section, the theoretical consideration for a compound channel will be described in determining flood plain and main channel discharges separately with composite roughnesses and energy slopes, as well.

4.6 COMPOUND CHANNEL

4.6.1 Theoretical Consideration

After a compound channel is solved by the generalized method following the procedures described in the previous sections, the compound channel is to be separated into main channel and flood plain cross-sections by dividing at their vertical interface planes to obtain the flow characteristics of respective cross-sections. The division procedure is shown in Figure 4.1 . This is identical to the type of division of the conventional separate channel method. But, unlike the conventional method, the Manning equation of uniform flow is corrected for energy slope of the cross-section in question. Hence, the continuity equation can be written as

$$Q = Q_{mc} + Q_{fp}$$

i.e.,

$$A\frac{1}{n}R^{2/3}S^{1/2} = A_{mc}\frac{1}{n_{mc}}R_{mc}^{2/3}S_{mc}^{1/2} + A_{fp}\frac{1}{n_{fp}}R_{fp}^{2/3}S_{fp}^{1/2} \qquad (4.36)$$

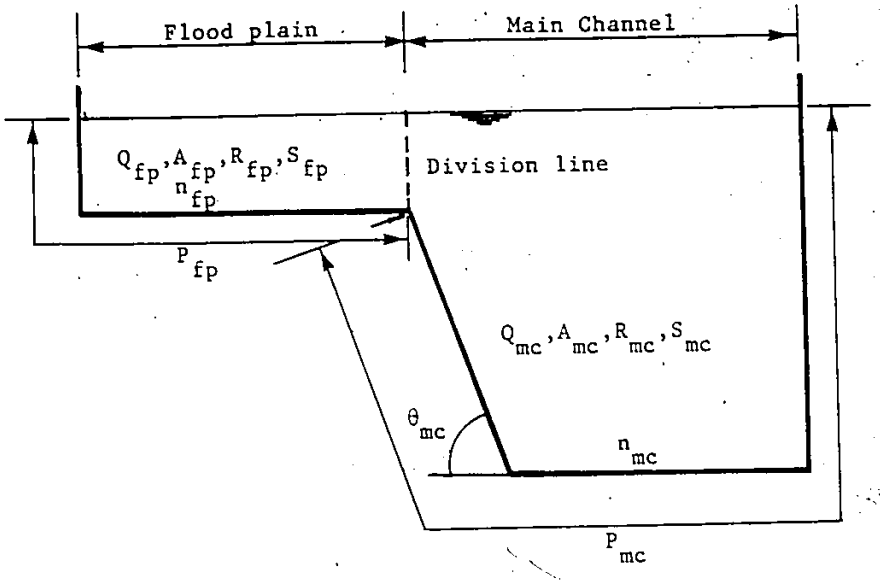

Fig. 4.1. Definition Sketch of Compound Channel Showing Division of Main Channel and Flood Plain.

where, subscripts 'mc' and 'fp' denote main channel and flood plain, respectively.

The energy slope of each cross-section is the result of the iterative solution of the model equation 3.47 in appropriate forms that are described in sections 4.1 through 4.4.

4.6.2 Hydraulic Perimeter

The hydraulic perimeter of each cross-section, main channel or flood plain, is equal to its solid hydraulic boundary only.

4.6.3 Discharge

The discharge of each cross-section can be obtained from the two-dimensional velocity distributions by numerical integration over the respective cross-section, i.e.,

$$Q_{mc} = \sum^{A_{mc}} U \, dA \qquad (4.37)$$

and

$$Q_{fp} = \sum^{A_{fp}} U \, dA \qquad (4.38)$$

4.6.4 Energy Slope

The energy slope of each cross-section can be determined from the boundary shear stress distributions and the average tractive force equation.

$$S_{mc} = \frac{\sum^{P_{mc}} \tau_{\phi s} \, P_s}{\gamma A_{mc}} \qquad (4.39)$$

and

$$S_{fp} = \frac{\sum^{P_{fp}} \tau_{\phi s} P_s}{\gamma A_{fp}} \qquad (4.40)$$

4.6.5 Composite Roughness

The composite roughnesses are to be determined from the Manning equation after correction for energy slopes determined in section 4.6.4

$$n_{mc} = \frac{A_{mc} R_{mc}^{2/3} S_{mc}^{1/2}}{Q_{mc}} \qquad (4.41)$$

and

$$n_{fp} = \frac{A_{fp} R_{fp}^{2/3} S_{fp}^{1/2}}{Q_{fp}} \qquad (4.42)$$

Figure FC.5 shows the flow chart describing the extension of analysis over that of a simple or complex channel. Figure FC.5 is enclosed in Appendix D.

CHAPTER V

EXPERIMENTAL PROCEDURES

5.1 INTRODUCTION

Laboratory experiments were conducted, mainly to determine the values of the velocity coefficients, El and E2 for compound channel sections with one flood plain under both free and covered surface flow conditions, and with the variation of shape, boundary roughnesses and discharge.

Theoretical analyses of experimental data were extended for simple and complex channel cross-sections under covered surface flow conditions only. The experimental data for this purpose were taken from the experimental investigation conducted by the previous researcher, Andrew Hok-Bun Lau (45). Laboratory experiments were performed on the same test flume following almost the same procedures that had been used by the author of the present research.

In both investigations, the present and the previous one, respectively, vertical as well as lateral velocity profiles were measured as a check on the accuracy of the analysis of the theoretical model.

In this chapter the following topics will be discussed:

1. Laboratory facilities and equipment.
2. Experimental channels.

3. Calibrations

4. Experimental procedures.

Theoretical analyses of experimental data and discussions will be furnished in the subsequent chapters.

5.2 LABORATORY FACILITIES AND EQUIPMENT

5.2.1 Test Flume

All the experiments were carried out with the same test flume in the hydraulics laboratory of the Civil Engineering Department at the University of Windsor.

The effective length of the test flume was 7.315 m (24 ft.) long with a rectangular cross-section of 0.4572 m (1.5 ft.) wide by 0.61 m (2.0 ft.) deep. The bed and one side of the flume were made of plywood and the other side was made of transparent plexiglass. In order to determine flow depths and energy slopes, as well, two clear plexiglass still water wells (tubes) were placed at one of the outside wall of the flume centrally at 3.66 m (12 ft.) apart.

The upstream of the flume was provided with a head tank of size 1.42 m by 1.18 m (4.25 ft. x 3.66 ft.) in plan and 1.22 m (4 ft.) in depth. A control gate was provided with the head tank at its intersection with the flume. Inside the tank a gauze screen was installed between the inlet water supply pipe and the outlet to the flume, in order to reduce entrained air bubbles within the water

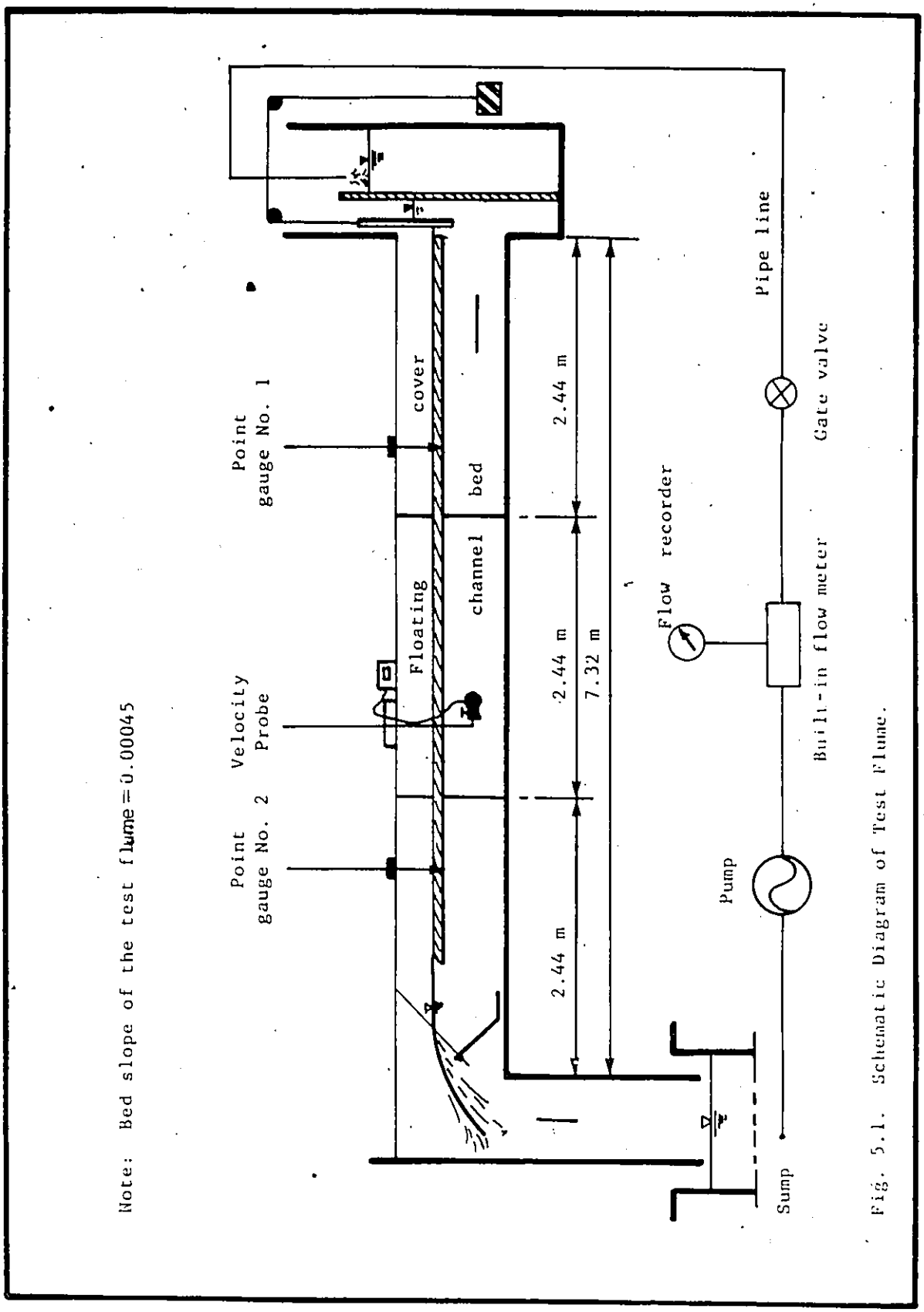

Note: Bed slope of the test flume = 0.00045

Fig. 5.1. Schematic Diagram of Test Flume.

and dampen surface waves, as well, caused by turbulence.

The downstream of the flume was provided with an inclined hinged gate (of plexiglass) with a view to control the flow depth by allowing the overflow of water on it and a closed conduit connecting the flume to an underground sump.

The flume was served by a constant speed centrifugal pump with a maximum supply capacity of 3500 USGPM (0.221 m^3/s). The flow was adjusted by a gate valve installed between the pump and the inlet pipe of the head tank.

The total discharges of the flume were measured by an electromagnetic flow meter, which was built into the pipe system between the pump ahd the gate valve. The reading facility was provided by a separately installed recording device with a circular disk scale calibrated to read directly to 10 USGPM (1 USGPM = $6.31 \times 10^{-5} m^3/s$).

The complete flow system of the test flume is shown by the schematic diagram in Figure 5.1,

5.2.2. Other Measuring Equipment

Measurement of Point Velocities

An electromagnetic water current meter, Digital Model 201D, of Marsh-McBirney, Inc., was used to measure most of the point velocities at a cross-section of turbulent flow. The range control allows selection of three velocity units

in ft/s, m/s, and knots with full scale provision of 20 ft/s, 6 m/s, and 12 knots in three units, respectively. A liquid crystal display presents the velocity with resolution of 0.01 ft/s, 1 cm/s, or 0.01 knot. As the sensitivity of the meter is more in foot-scale (0.01 ft/s = 0.3048 cm/s < 1 cm/s in meter scale) all the velocity measurements were taken in foot-scale and converted later into meter-scale. The diameter of the probe at its contact point is 3.7 cm (1.46 in).

A miniature current flow meter was also used to measure point velocities close to the boundaries because its probe size is smaller than that of the electromagnetic current meter. This probe is also less sensitive to the magnetic-materials (such as wire mesh). This is a flow meter with a propeller type probe, having vanes set on the horizontal axis and rotate by the direct action of the flow current and connected to a voltmeter. The velocity measured in volts can be read out in proper units (m/s or ft/s) from the calibration charts supplied with it. The meter, together with two separate probes (of high speed and low speed), could operate in four different ranges with a maximum reading of 4m/s (13.12 ft/s). The sensitivity of the meter is 0.4 cm/s ((0.0137 ft/s).

Beside the miniature current flow meter, a pitot tube with a manometer reading directly to 0.01 in (0.025 cm) was

also used in some cases.

Point gauges were used to measure water surface elevation at upstream and downstream still-water wells of the test flume. The point gauges were calibrated to read directly to a value of 0.01 in. (0.025 cm).

All this equipment is shown in Figures 5.2 to 5.5

5.3 EXPERIMENTAL CHANNELS

All the experimental channels were custom made with 19 mm and 12 mm thick plywood and constructed inside the test flume.

5.3.1 Compound Channels

A definition channel, as a representative of all the channel cross-sections that were constructed for experimental purpose, is shown in Figure 5.6.

The notations used in the definition sketch are described below:

H = Total or main channel flow depth.

$H1$ = Height of the flood plain bed above the main channel bed.

h_{fp} = $(H-H1)$ = Flood plain flow depth

BT = Top width of the entire channel.

BT_{mc} = Top width of main channel.

BT_{fp} = Top width of flood plain.

B_{mc} = Bottom (or bed) width of main channel.

B_{fp} = Bed width of flood plain.

θ_{mc} = Inclination of main channel's side wall with horizontal

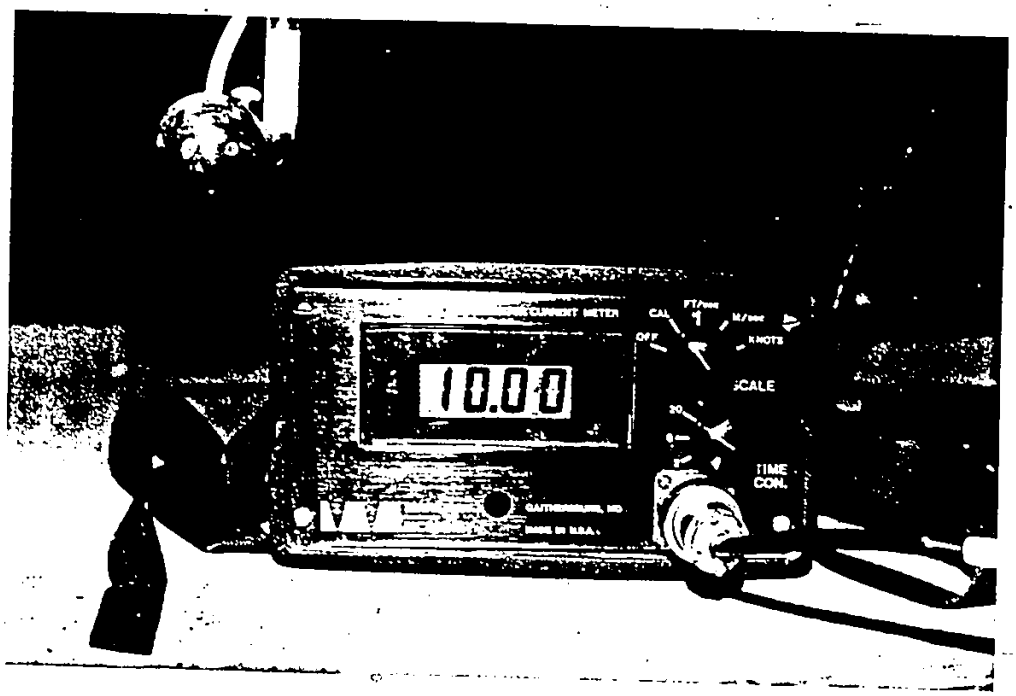

Fig. 52. Electronic Water Current Meter, Digital Model 201D, of Marsh-McBirney Inc.

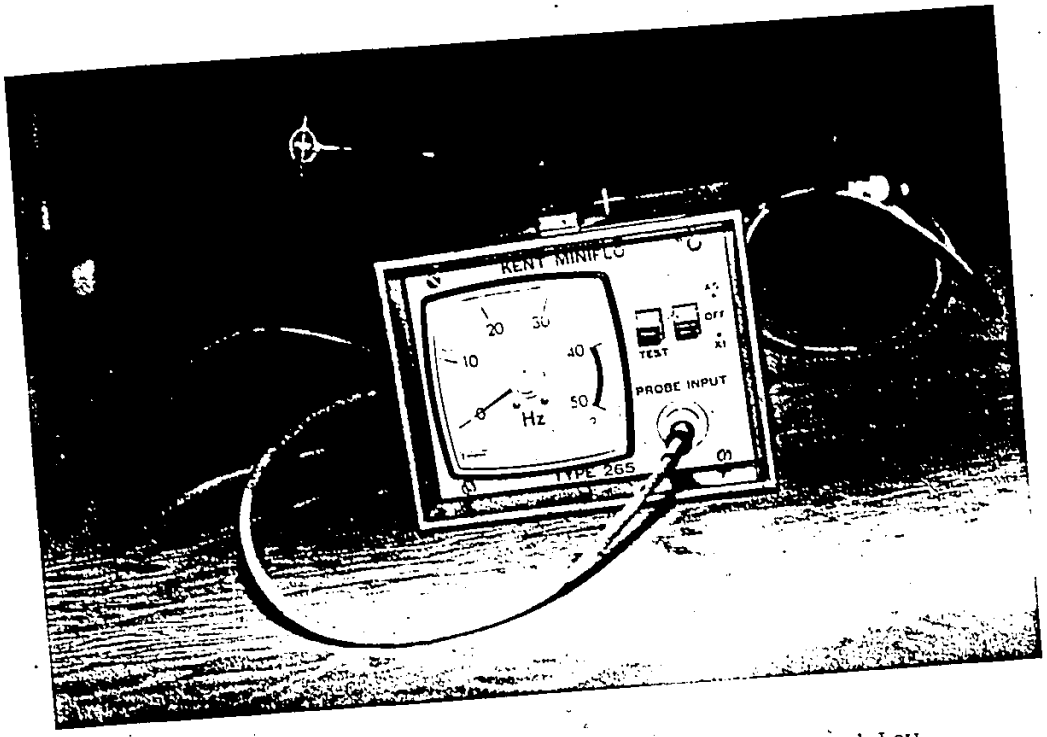

Fig. 5.3. Miniature Current Flow Meter with High and Low Speed Probes.

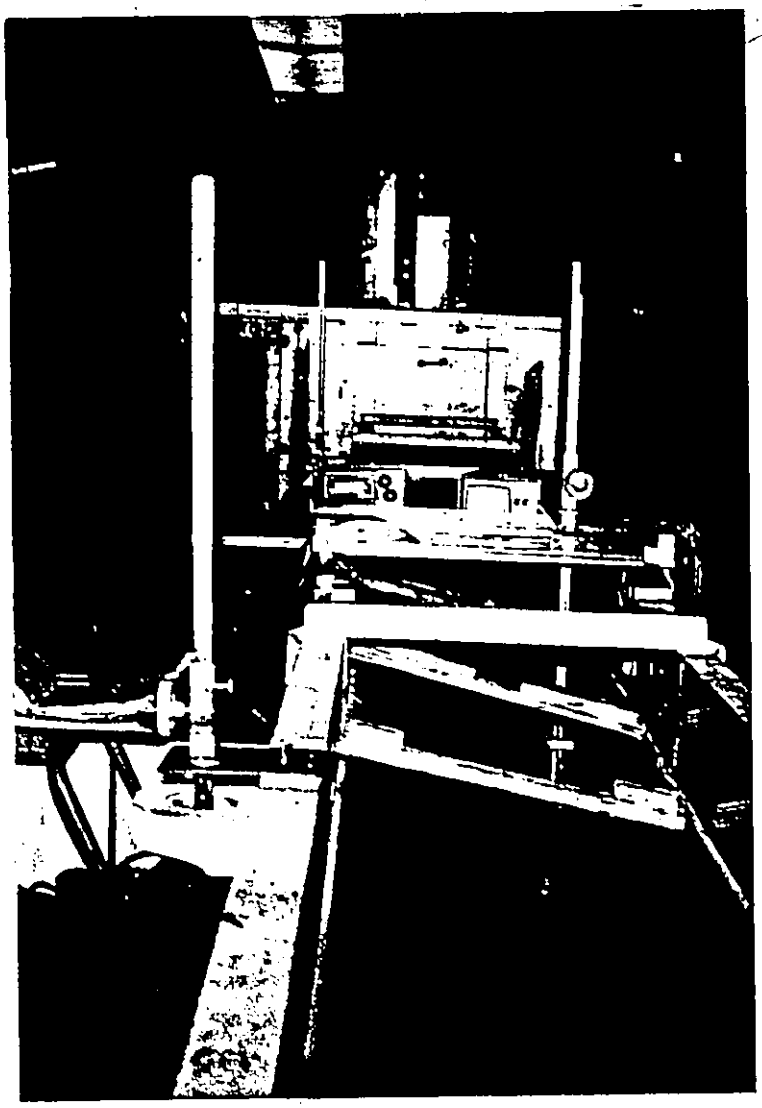

Fig. 5.4. A General View of the Test Flume with an Experimental Compound Channel and the Measuring Equipment.

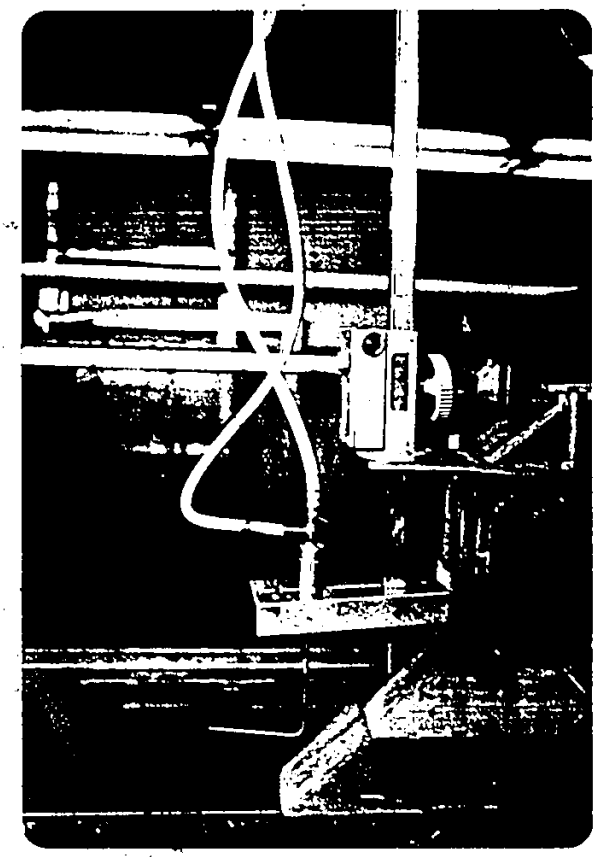

Fig. 5.5. Pitot Tube with Point Gauge.

θ_{fp} = Inclination of flood plain's side wall with horizontal.

Also, two dimensionless parameters are introduced and defined as:

the relative depth ratio, $\alpha_f = h_{fp}/H$,

and the relative width ratio, $\beta_f = BT_{fp}/BT_{mc}$.

A total of eleven channel cross-sections, as described in Table 5.1, were constructed for the experimental investigations under both free- and covered-surface flow conditions.

In all the cases, the height of the flood plain floors, Hl was kept constant at 203 mm (8 in) above the main channel bed. Also, as it can be seen from the definition sketch of the experimental compound channel in Figure 5.6, the right hand side wall of the main channel was kept vertical in all the cases.

Originally, it was planned in the test program to investigate the effects of the inclination of flood plain side wall, θ_{fp}. But at the time of the laboratory experiments difficulties were encountered in placing the floating cover on it. However, in one case with $\theta_{mc} = 60°$ and $\theta_{fp} = 22°$ flow observations for several flow depths were recorded under free-surface flow condition. But due to the insufficient data this is excluded from this thesis. Hence, in all the eleven channel cross-section, $\theta_f p$ was kept at 90°, i.e., vertical with the flood plain bed.

The bed slope of all the experimental channels was equal to 0.00045.

TABLE 5.1

Dimensions of Experimental Channel Cross-sections

β	θ_{fp} °	θ_{mc} °	BT mm	H1 mm	Bt_{mc} mm	BT_{fp} mm	B_{mc} (mm)	B_{fp} mm	Actual β	Channel Cross-Section No.
0.5	90	90	432	203	287	145	287	145	0.505	1
0.5	90	75	432	203	287	145	233	145	0.505	2
0.5	90	60	432	203	287	145	170	145	0.505	3
0.5	90	45	432	203	287	145	84	145	0.505	4
1.0	90	90	432	203	216	216	216	216	1.0	5
1.0	90	75	432	203	216	216	161	216	1.0	6
1.0	90	60	432	203	216	216	99	216	1.0	7
1.0	90	45	432	203	216	216	13	216	1.0	8
2.0	90	90	432	203	140	292	140	292	2.09	9
2.0	90	75	432	203	140	292	85	292	2.09	10
2.0	90	60	432	203	140	292	22	292	2.09	11

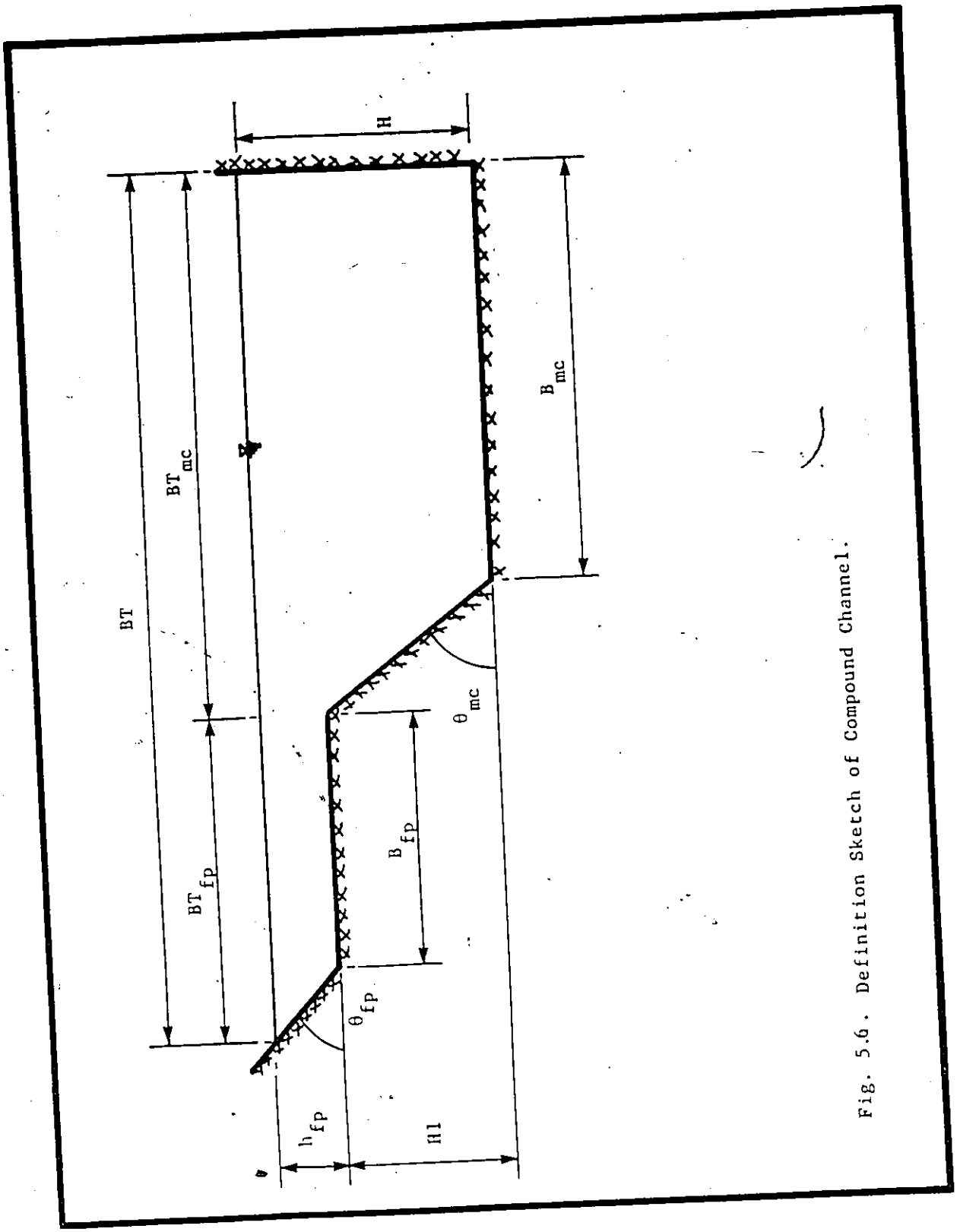

Fig. 5.6. Definition Sketch of Compound Channel.

A detailed drawing with specifications of a typical experimental compound channel cross-section is shown in Figure 5.7 , which is self explanatory. Figure 5.8 is the photograph of a typical experimental compound channel.

5.3.2 Simple and Complex Channel

Experiments were conducted on seven different channel cross-sections, viz, rectangular, trapezoidal, triangular, semi-circular, and three combined variations of the last three shapes with rectangular one. From the construction point of view it can be said that altogether four (4) channels were actually built into the test flume. The same 19 mm thick plywood was used for all the channels.

The schematic details and dimensions of these channel cross-sections are shown in Figure 5.9, together with a photograph of a typical channel cross-section as shown in Figure 5.10.

5.3.3 Simulated Covers

The floating covers for an ice-covered surface flow were made out of plywood and used with or without roughness materials on it. For the convenience of handling, the size of the covers were made 42 cm square by 38 mm thick (see Figure 5.11.

They were held floating freely on a flow surface by tying the last block at the downstream end of the channel

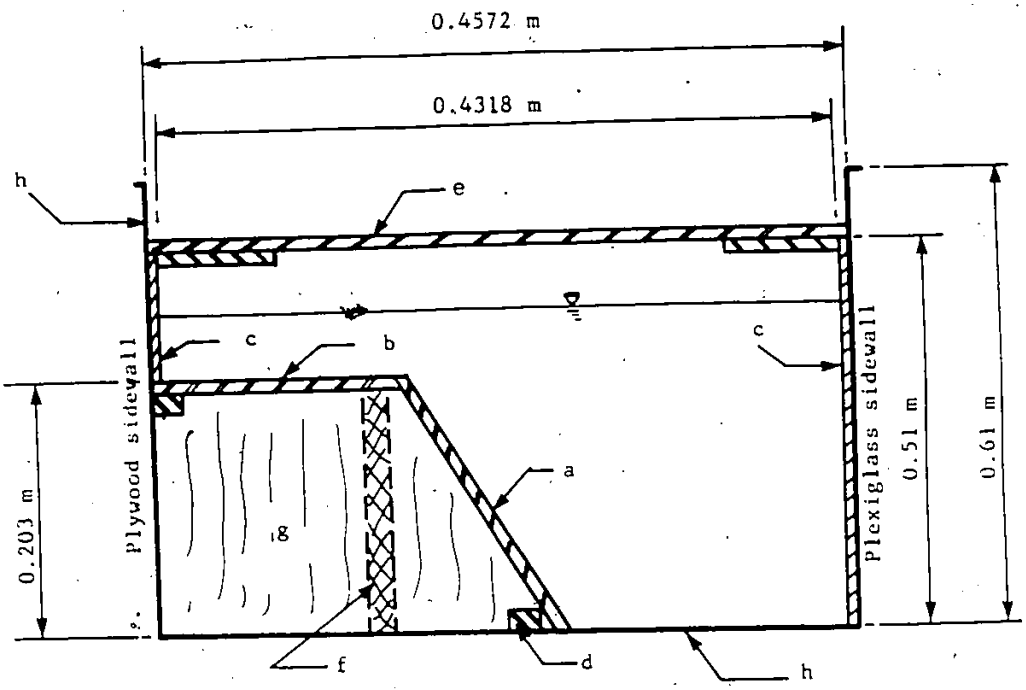

a & b = 19 mm Thick Plywood Board
c = 12.5 mm Thick Side Walls (plywood)
d = 19 mm x 25 mm Supporting Guide Raile (plywood)
e = 19 mm x 50 mm x 432 mm Supporting Struts; 1 m c/c
f = 50 mm x 50 mm x 184 mm Props; 1 m c/c
g = Partition Blocks
h = Inner Line of the Test Flume

(Marked dimensions are constant; remaining dimensions are variable according to the shape of channel)

Fig. 5.7. Construction of a Typical Experimental Channel.

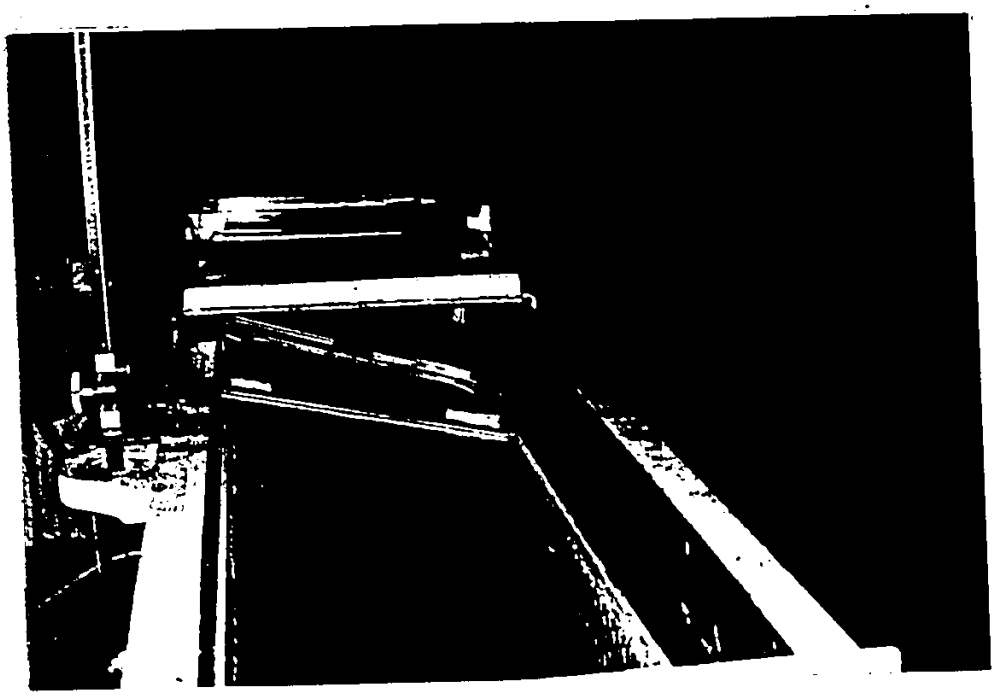

Fig. 5.8. An Experimental Compound Channel with Flood Plain (Main Channel Ratio, $\alpha_f = 2.0$ and $\theta_{mc} = 90°$, $\theta_{fp} = 90°$.

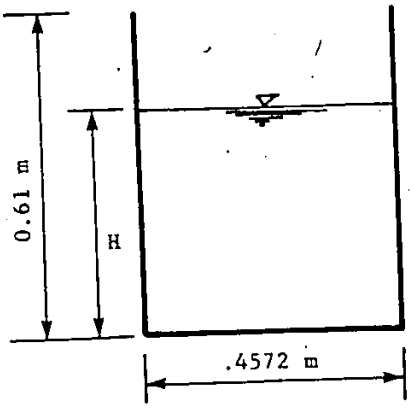

Rectangular channel

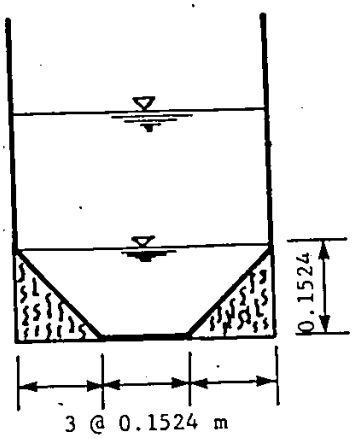

Trapezoidal and complex trapezoidal channel

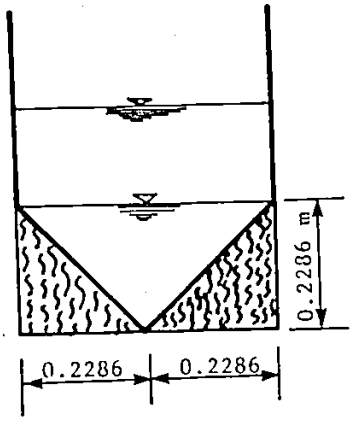

Triangular and complex triangular channel

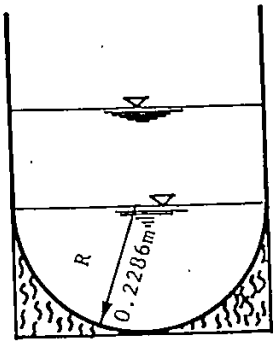

Semi-circular and complex semi-circular channel

Fig. 5.9. Experimental Channels - Simple and Complex Cross-Sections.

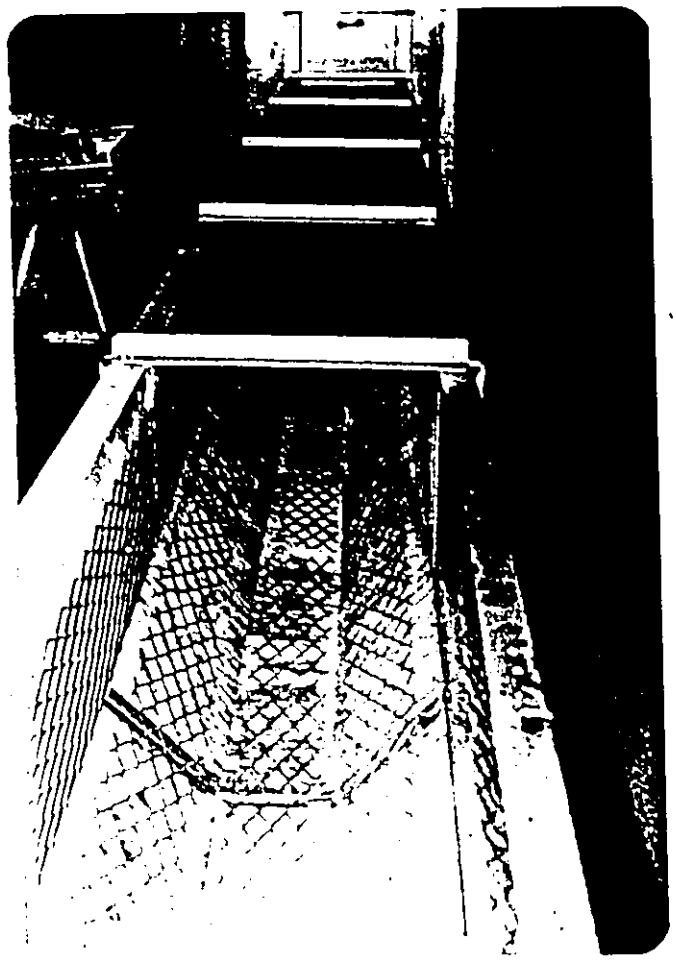

5.10. An Experimental Simple and Complex Channel (Trapezoidal Cross-Section).

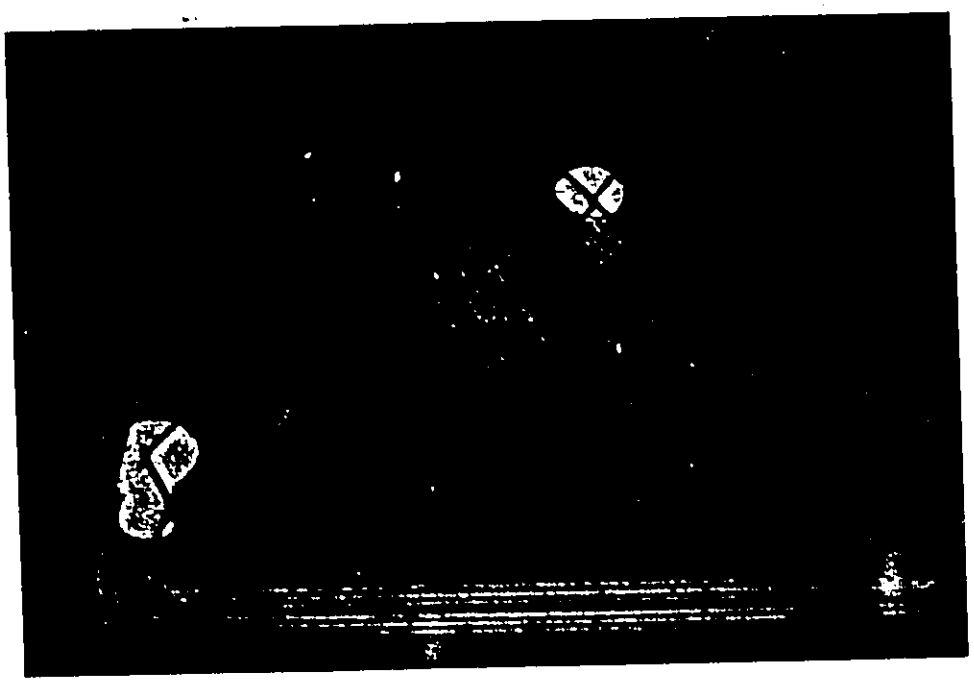

Fig. 5.11. Plywood Block with Wire Mesh used as a Floating Cover.

to the channel frame.

5.4 ROUGHNESS MATERIALS

To increase the roughness of the channel bed, walls and covers, two different kinds of wire mesh, with diamond shape patterns of sizes as shown in the definition sketch (Figure 5.13), for a diamond, were used. These wire meshes were imbedded to the plywood surface by nails to give the roughness of the channel beds and walls. In case of simple and complex channels plain plywood also was used as a roughness material.

The wire meshes are shown in Figure 5.12. The symbols, n_C, n_F, and n_p will be used to denote for the coarse mesh (64 mm x 31 mm x 5.8 mm), fine mesh (41 mm x 21 x 5.8 mm) and plywood, respectively.

5.5 EXPERIMENTAL PROCEDURES

5.5.1 Calibration of Material Roughnesses

Three methods were followed to determine the material roughnesses. In all the cases the rectangular channel was chosen as the standard shape for comparison. The methods are described below:

Method 1. By Strip Flow

In this method the entire bed of the test flume was lined with the desired material (wire mesh) of one kind at a time (see Figure 5.14(a)). The plywood side wall of the flume was painted to reduce its roughness, and the

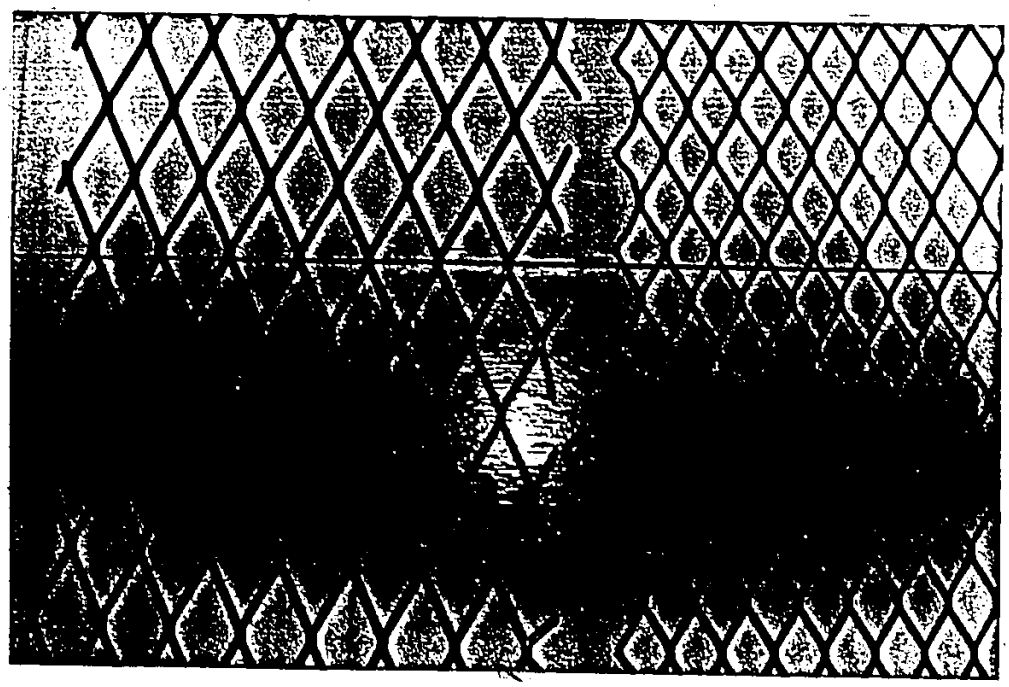

Fig. 5.12. Roughness Materials (Wire Mesh).

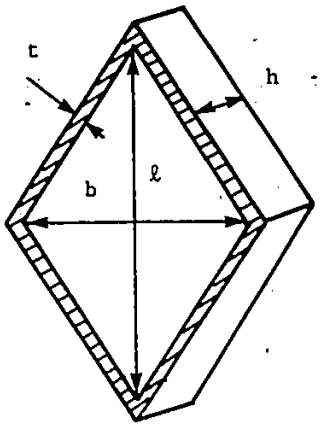

Materials	ℓ	b	t	h
Coarse mesh	64	31	1.8	6.0
Fine mesh	41	21	2.5	5.8

(all are in mm)

Fig. 13. Specification of Diamond of Wire Mesh Gratings.

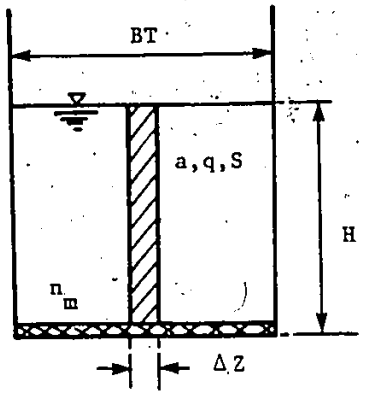

$$n_m = \frac{a}{q} H^{2/3} S^{1/2}$$

where, a = ΔZ.H, q = strip flow

(a) Method 1

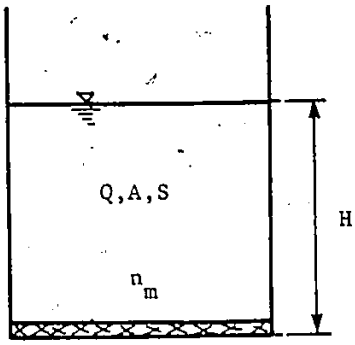

$$n_m = \frac{A}{Q} R^{2/3} S^{1/2}$$

where, A = BT*H, Q = channel flow

(b) Method 2

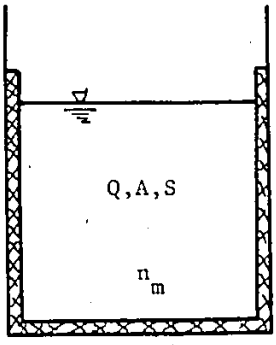

$$n_m = \frac{A}{Q} R^{2/3} S^{1/2}$$

(c) Method 3

Fig. 5.14. Calibration of Roughness Materials.

other side wall of plexiglass was kept as it was. Thus, the effect of side walls at the centre line flow was minimized. A strip flow of width, ΔZ is considered at the centre line of any cross-sectional flow. The strip discharge, q, is determined by integrating measured point velocities along the centre line of the vertical strip over the entire flow depth. The energy slope was determined from the surface elevation at stations 1 and 2. Considering the strip flow as a wide channel flow, the roughness coefficient was determined by applying Mannings equation:

$$n_m = \frac{a}{q} H^{2/3} S^{1/2}$$

where, n_m = roughness coefficient of any material.

Method 2. By Total Flow with Bed Roughness Only

Similar to Method 1, the test flume was lined with the desired material at the entire bed only leaving the side walls as it were (Figure 5.14(b)). Total discharge, Q and energy slop, S, were recorded. The roughness coefficient of material was estimated by Mannings equation:

$$n_m = \frac{A}{Q} R^{2/3} S^{1/2}$$

where, hydraulic radius of the flow, R = A/P, is the total hydraulic perimeter.

Method 3. By Total Discharge with Entire Channel Roughness

Unlike the above two methods the entire test flume, including the side walls, were lined with the desired material as shown in Figure 5.14(c). The roughness coefficient of the material was determined by Mannings equation:

$$n_m = \frac{A}{Q} R^{2/3} S^{1/2}$$

Following the above three methods the roughness coefficients of fine wire mesh, n_F, coarse wire mesh, n_C, and the plywood, n_p were determined by six different setups and tabulated in Appendix B.

The calibration curves obtained for the three materials by the three different methods are shown in Figures, 5.15, 5.16 and 5.17.

The calibrated values of the roughness materials from Method 3 were taken into account for analysis purpose.

In Method 1, consideration of strip flow as a wide channel was not true because the ratio of the flow depth to the width of the flume is, by definition, a narrow channel. Hence, the side wall effects exist at any point of the cross-sectional flow. Thus, the roughness of the materials were overestimated.

In Method 2, while the hydraulic radius was determined for the total channel flow, the value of roughness coeffi-

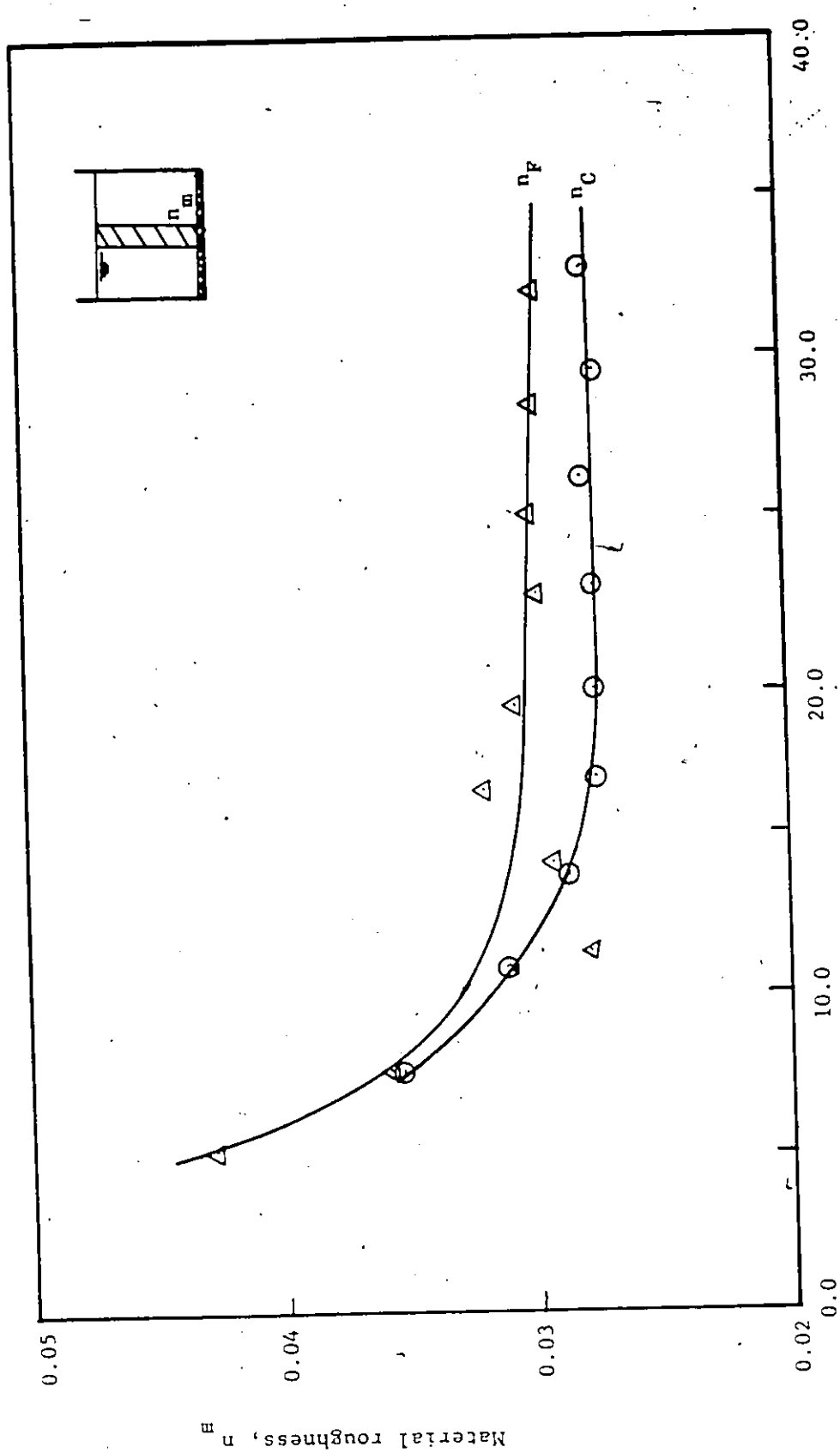

Fig. 5.15. Calibration of Roughness Material by Vertical Strip Method. (Method 1).

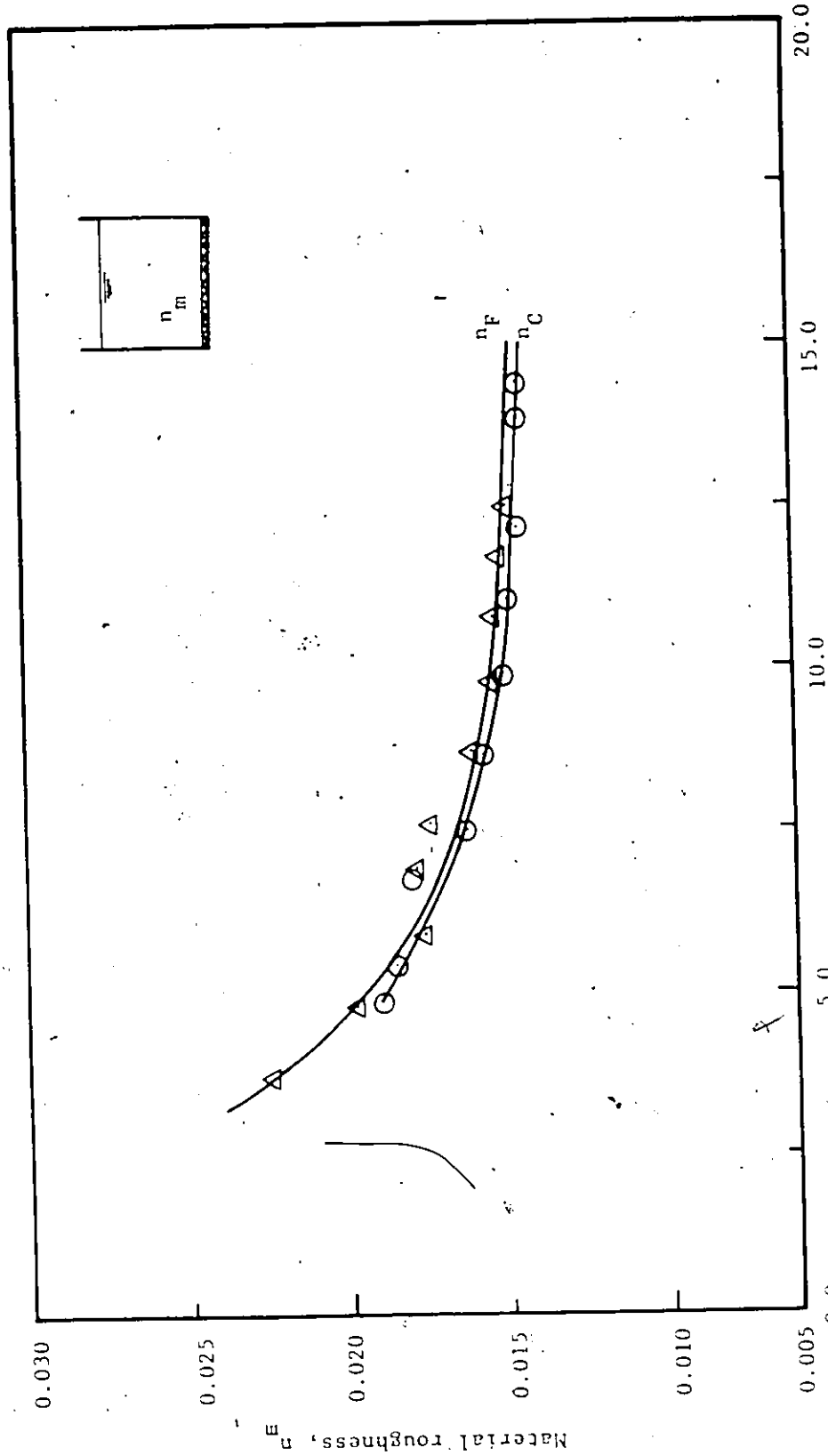

Fig. 5.16. Calibration of Roughness Materials by Total Flow Method. (Method 2).

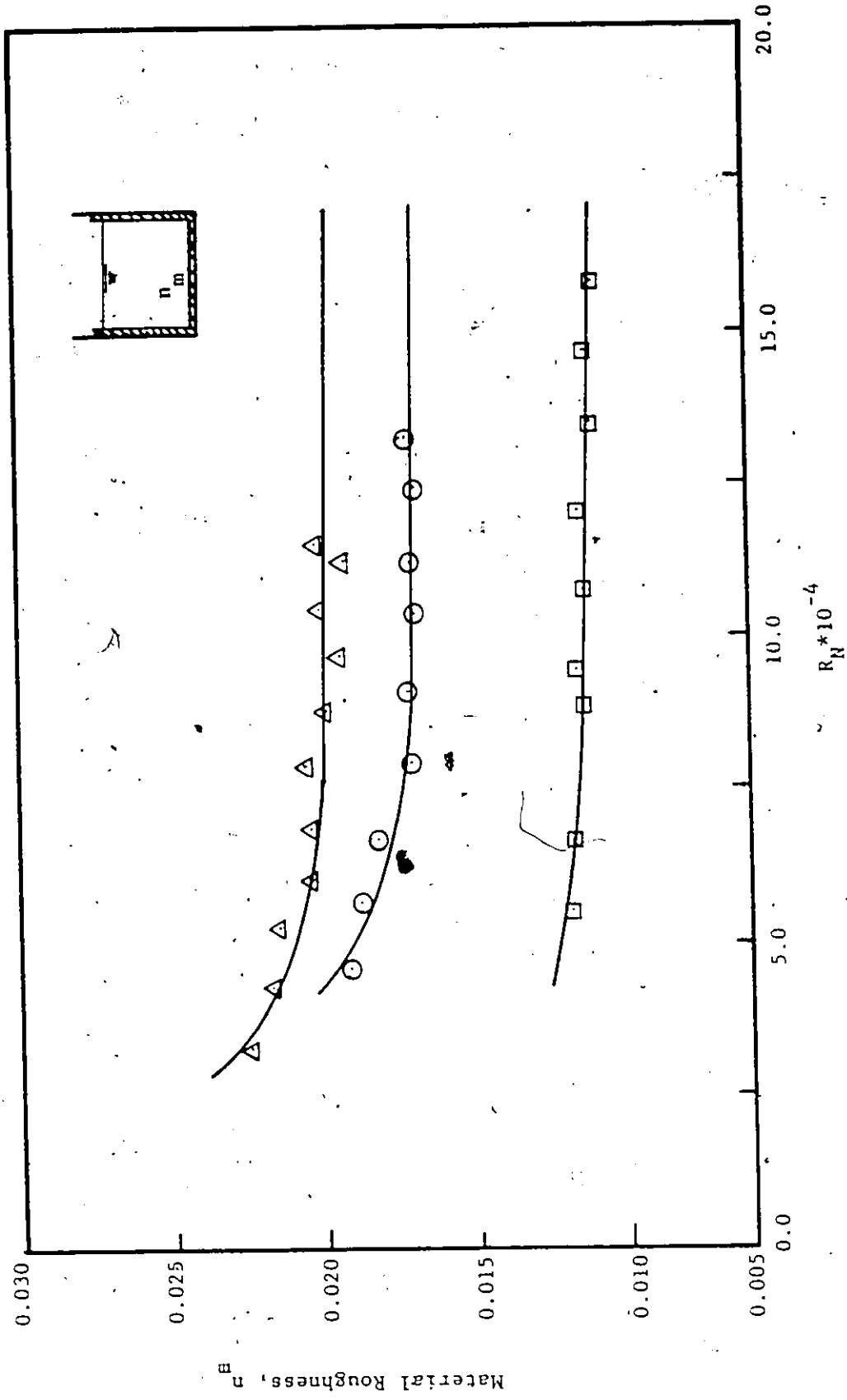

Fig. 5.17. Calibration of Roughness Materials by Total Flow Method. (Method 3).

cient of the bed material will be underestimated by the resistance, no matter how small it was, of the smooth walls.

Hence, logically, the results of Method 3 are more acceptable.

The values are observed (from Figures 5.15, 5.16 and 5.17) fairly constant at higher Reynolds number. Hence, from the calibration curve in Figure 5.15, the roughness (Manning's) values, 0.020, 0.017 and 0.0115 were recorded as average roughness coefficients for n_p, n_c and n_p, respectively.

5.5.2 Experimental Programme

5.5.2.1 For Compound Channels

All the eleven compound channel cross-sections were investigated for both free-surface flow and covered surface flow conditions.

Each channel cross-section under each flow condition was run for several flow depths within the approximate h_{hp}/H (or α_f) ratio ranges from 0.15 to 0.4.

The objective of the experimental work was to measure slope energy and velocity distributions along a cross-section corresponding to each flow depth so that the following purposes can be servedi.

1. to determine the experimental overall roughness of the channel from the measured energy slope and discharge,

2. to determine analytically the velocity coefficients E1 and E2 for the proposed velocity model from the observed energy slopes and discharges,
3. to obtain the experimental values of overbank flow and main channel flow fractions of the total flow from the measured velocity distributions and to verify these vales to those of analytically obtained values in the process of solving the model equation 3.47 for coefficients E1 and E2.

At least 3 observations were made to measure velocity distributions and energy slope for each set of channel cross-section within the above mentioned flow depth range (h_{fp}/H ratios of 0.15 to 0.40). Another 3 to 6 additional observations (within the above flow depth range) were made to obtain energy slope and discharge rate with a view to determine statistically more accurate values of the coefficients E1 and E2.

In all the cases the boundary roughnesses of the main channel, the flood plain and covers (in case of covered surface flow) were kept the same by using fine wire mesh over plywood board. The purpose is to observe the effects of shape of the channel on the overall roughness.

To obtain the effects of multiple boundary roughnesses over the overall channel roughness and other parameters, several observations were recorded by changing the roughnesses of flood plain and cover block with coarse wire mesh.

Velocities were recorded at 10 positions across the channel: 5 positions within the flood plain and 5 positions within the main channel; and at approximately 25 mm to 50 mm intervals within each vertical of the main channel and at approximately 12 mm to 25 mm intervals for the flood plain as shown in Figure 5.18(a).

The details of measured data excluding velocity distributions for each set of channel cross-section and its boundary conditions are tabulated in Tables C1 to C6.

The station for measuring flow depth and velocity distributions were established 4.27 m (14.0") downstream from the entrance section of water to the channel from the tank. The location was chosen so as to ensure that fully developed turbulent flow would be obtained for any flow depth and discharge, given the relatively large length to depth ratios.

5.5.2.2 For Simple and Complex Channels

In case of simple and complex channel cross-sections velocity profiles were recorded at 7 horizontal positions and at certain interval of elevation as a ratio to the maximum flow depth within each vertical. The coordinate system is shown in Figure 5.18(b).

To give the multiple boundary roughness effects to the channel cross-section both fine and coarse wire meshes together with plain plywood were used in the channel bed, side walls, and floating cover surface by rotation. A

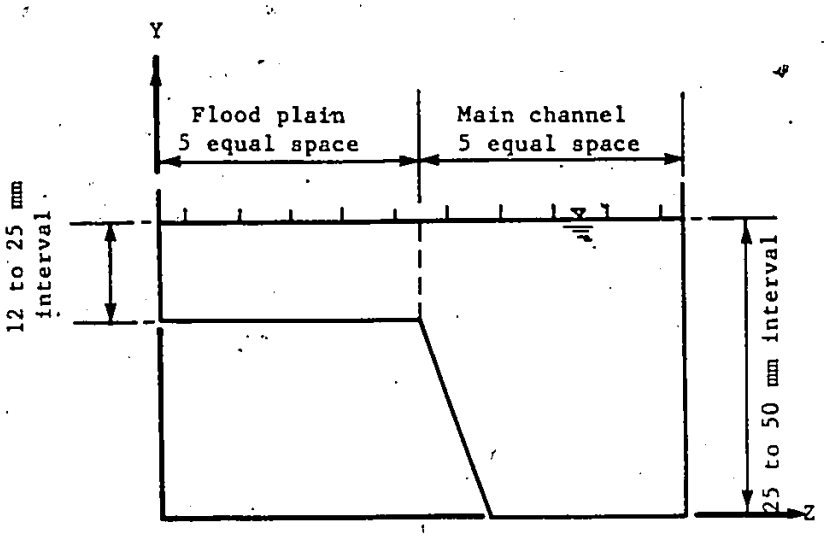

(a) Compound Channel

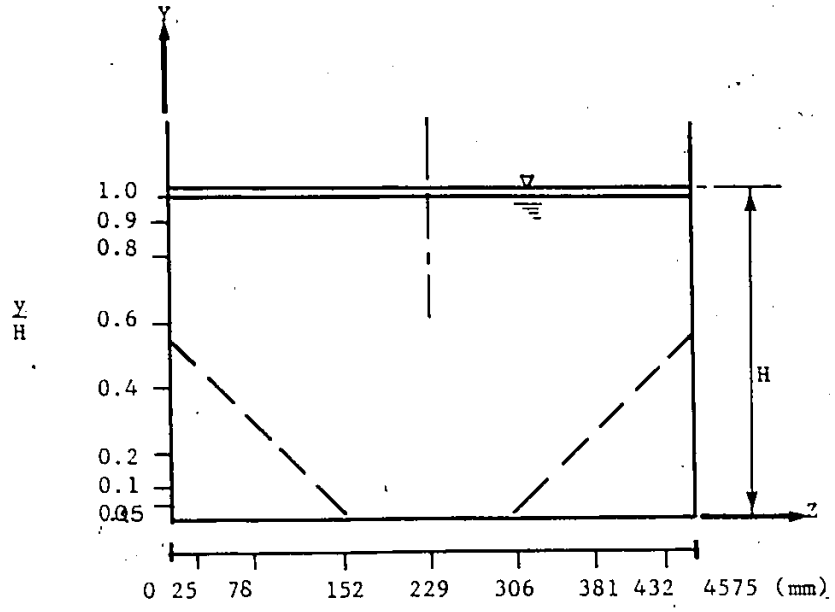

(b) Simple or Complex Channel

Fig. 5.18. Coordinate System for Observed Velocity Profiles.

list of experimental data for these channel cross-sectional flows are furnished in Table C7.

CHAPTER VI

DISCUSSION OF RESULTS

6.1 INTRODUCTION

In this chapter the results of the velocity coefficients E1 and E2 of the proposed two-dimensional velocity distribution model (Equation 3.47) for different channel cross-sections as indicated in Chapter V are furnished. The results are the analytical solution of the model based on the experimentally measured data.

Two sets of design curves each for the compound channels under free-surface and covered-surface flows are proposed on the basis of the statistical analysis of the experimental results.

The validity of the proposed curves are verified and compared by two different ways. Firstly, the observed discharge of each channel flow is verified with the calculated discharge using the readout data of the design curves. This will be discussed in this chapter. Secondly, several workout examples are solved using the design curves and the results are compared with other methods, viz., single channel method, conventional separate channel method, and Knight's method (40). This will be discussed in Chapter VII separately.

The discussion will be concentrated mainly on the values of the velocity coefficients E1 and E2 which is the main goal of the present study.

The other flow characteristics, viz., overall roughness, velocity distributions, shear stress distribution, main channel-flood plain discharges, energy slopes, are the computational results of the numerical solution of Equation 3.47.for the velocity coefficient E1 and E2. Hence, the discussion will be followed by brief overviews of such characteristics.

For the present computational analysis Von-Karman's constant κ is taken as equal to 0.4.

6.2 VELOCITY COEFFICIENTS E1 AND E2

6.2.1. General

All the experimental flows were of such magnitudes that the channel width to maximum flow depth ratios of main channel cross-section were well below ten (a conventional condition of a wide channel) and hence, the computational analyses were done with vertical and horizontal strip method to incorporate the effects of momentum transfers in both directions. The solution steps as indicated in Sections 4.1 and 4.2 were used for the computation of channel section under free-surface flows and covered-surface flows, respectively.

As mentioned earlier in Chapter V that altogether eleven compound channel cross-sections with varying shape and sizes

(Table 5.1) were experimentally investigated for each flow condition (free-surface and covered-surface). According to the computational requirements for the determination of the velocity coefficients E1 and E2 of Equation 3.47, laboratory data in respect of total discharge, Q, flow depth, H, relative flow depth, $\alpha_f(h_{fp}/H)$, water temperature, T boundary roughness ($n_1, n_2, \ldots$), and overall energy slope, S of each channel flow were recorded. The overall discharge of each flow was cross-checked by taking direct reading of built-in current meter recorder and by measuring velocity traverses at a cross-section in both horizontal and vertical direction by a portable current meter as indicated in Chapter V.

The total discharge computed from the velocity traverse by numerical integration over the channel width and flow depth. In most of the cases the discrepancies between the two values (recorded and computed) were noticed within ±7%. Allowing the errors involved in numerical computation and the instrumental error of the built-in current meter, the average of the two values was accepted as an experimental data.

Experimental data of compound channel under free-surface flows are furnished in Tables C.1 through C.3 and those of compound channel under covered-surface flows are furnished in Tables C.4 through C.6. A total of 97 obser-

vations for eleven channel cross-sections with at least six observations for any one cross-section were investigated in case of free-surface flows. The relative flow depth (α_f) range was of 0.15 to 0.40. In the case of floating covered-surface, a total of 98 observations were made. Experimental data of simple rectangular, simple and complex triangular and trapezoidal covered-sections are listed in Table 7. A total of 14, 7 and 9 observations for rectangular, triangular and trapezoidal channel sections were considered for the computational purpose.

The computed values of the velocity coefficients E1 and E2 are furnished in Tables C.8 to C.10 for compound channels under free-flow conditions. Tables C.11 to C.13 provide results of compound channels under buoyant flows, and Table C.14 for simple and/or complex channels under floating covered-surface flows.

6.2.2. Velocity Coeffient E2 for Compound Channels

In both flow conditions it is observed that the velocity coefficient, E2, varies considerably with the change of shape of channel cross-section. Hence, to compare the trend of variations, E2-values are plotted against the Reynolds numbers for each cross-section and best fitting curves are drawn separately for each cross-section. In both flow conditions, the E2-curves are drawn in two sets.

In the first set of curves the relative top width

(ratio of flood plain/main channel), β_f was kept constant while the angle of inclination of one of the main channel side slope, θ_{mc}, was taken as a variable factor. The purpose of this set of curves is to observe the shape effects of main channel cross-section on the coefficient E2. In the second set of curves the shape of the main channel cross-section, i.e., the factor θ_{mc} was kept constant while the relative top width, β_f was taken as a variable factor. The purpose of the second set of curves is to observe the effects of the relative size of flood plain to main channel on the values of coefficient E2. A third parameter, the relative flow depth of flood plain to main channel flow depth or maximum flow depth, $\alpha_f(h_{fp}/H)$, was also made variable by changing the discharge rate for each channel cross-section. This factor (α_f) is included in the Reynolds number.

The two sets of E2-curves for compound channels under free-flows are shown in Figures 6.1 through 6.7 while those for compound channels under buoyant flows are drawn in Figures 6.8 through 6.14.

In both flow conditions the range of θ_{mc} was 90° to 45° at an interval of 15° and that range of θ_{mc} was observed for each of three relative top widths, β_f of values 0.5, 1.0 and 2.0.

In the case of free-surface flows each experimental

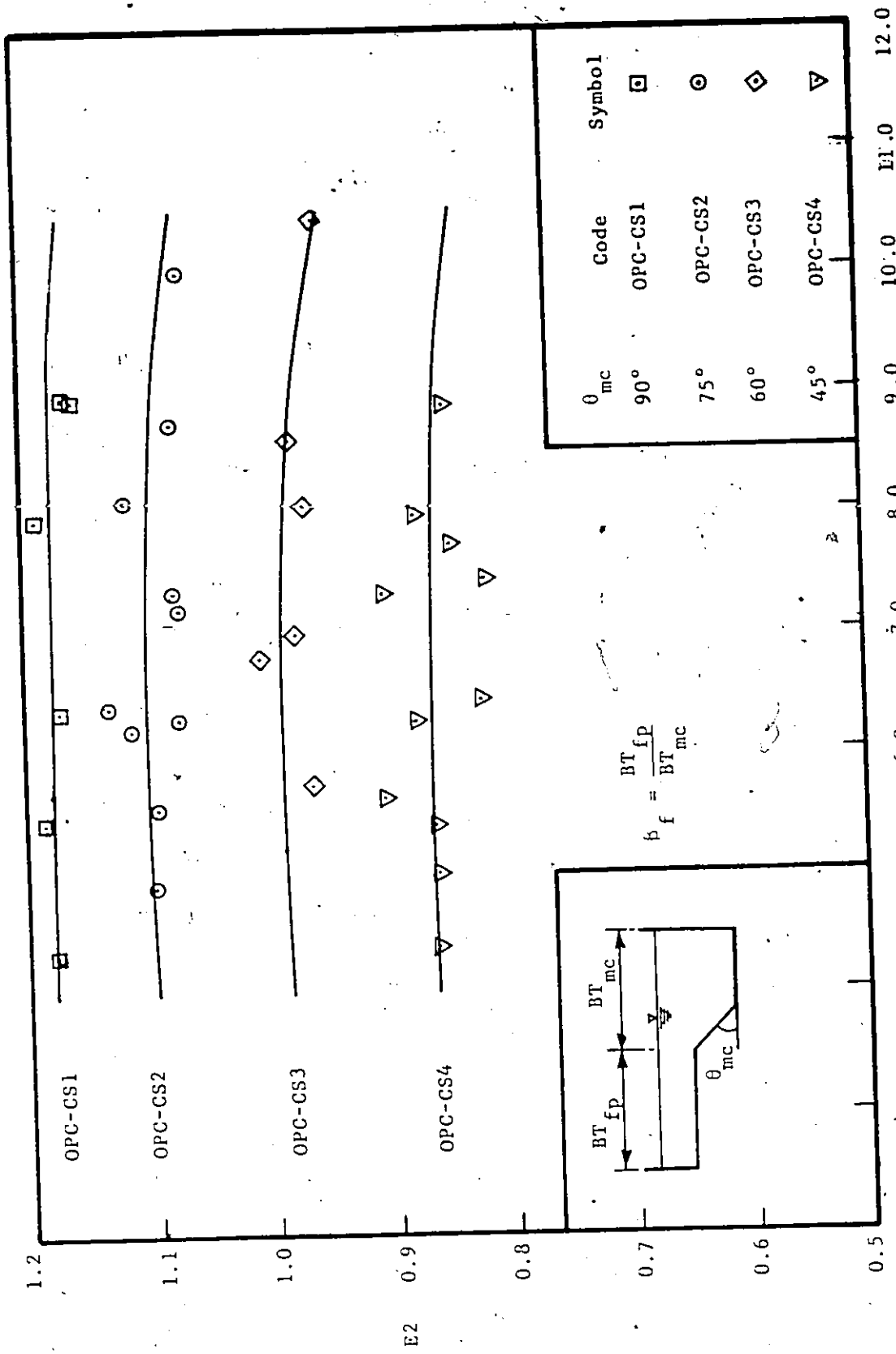

Fig. 6.1 E2-curves for Compound Channels under Free-Surface Flows with $\beta_f = 0.5$

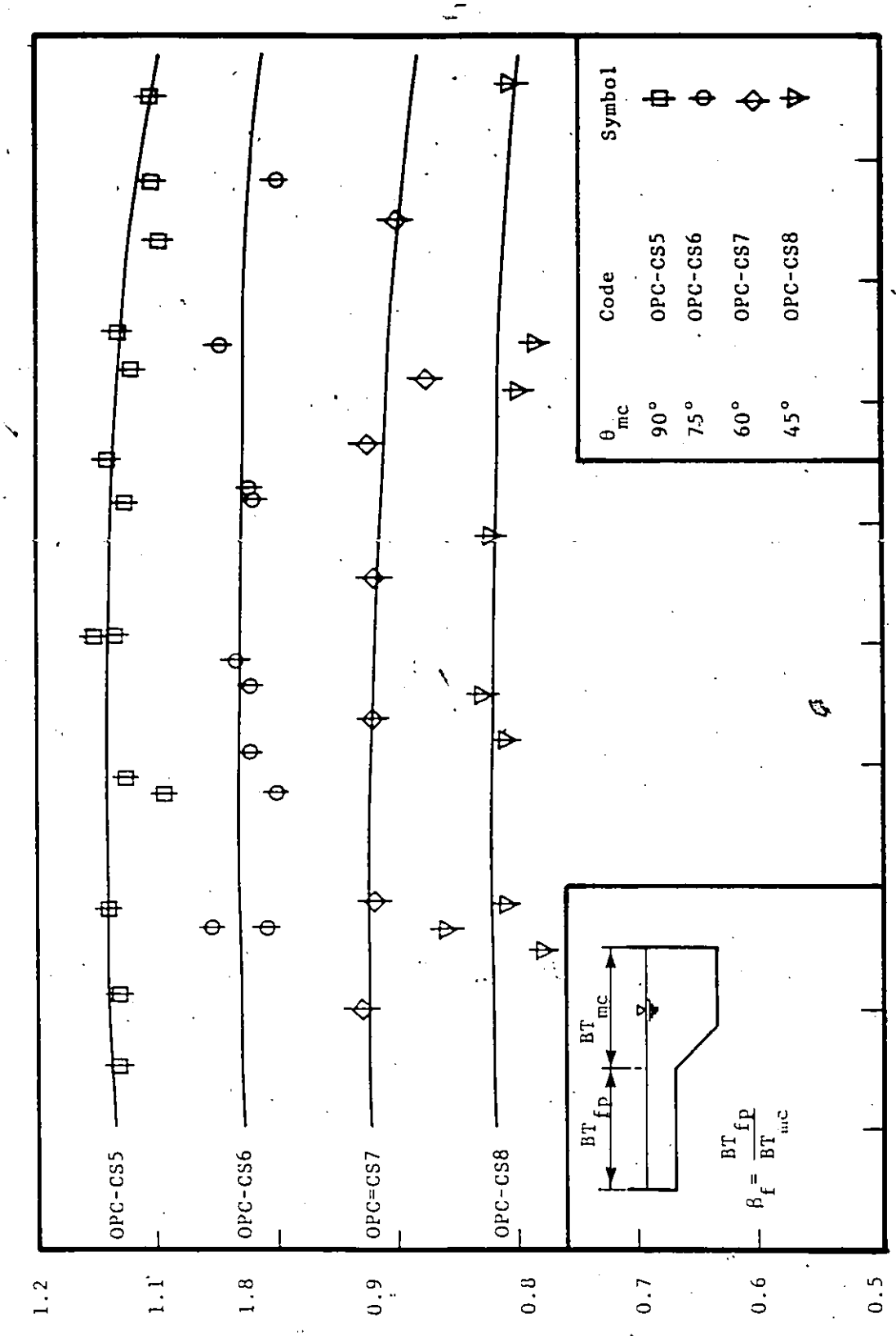

Fig. 6.2. E2-Curves for Compound Channels under Free-Surface Flows with $\beta_f = 1.0$.

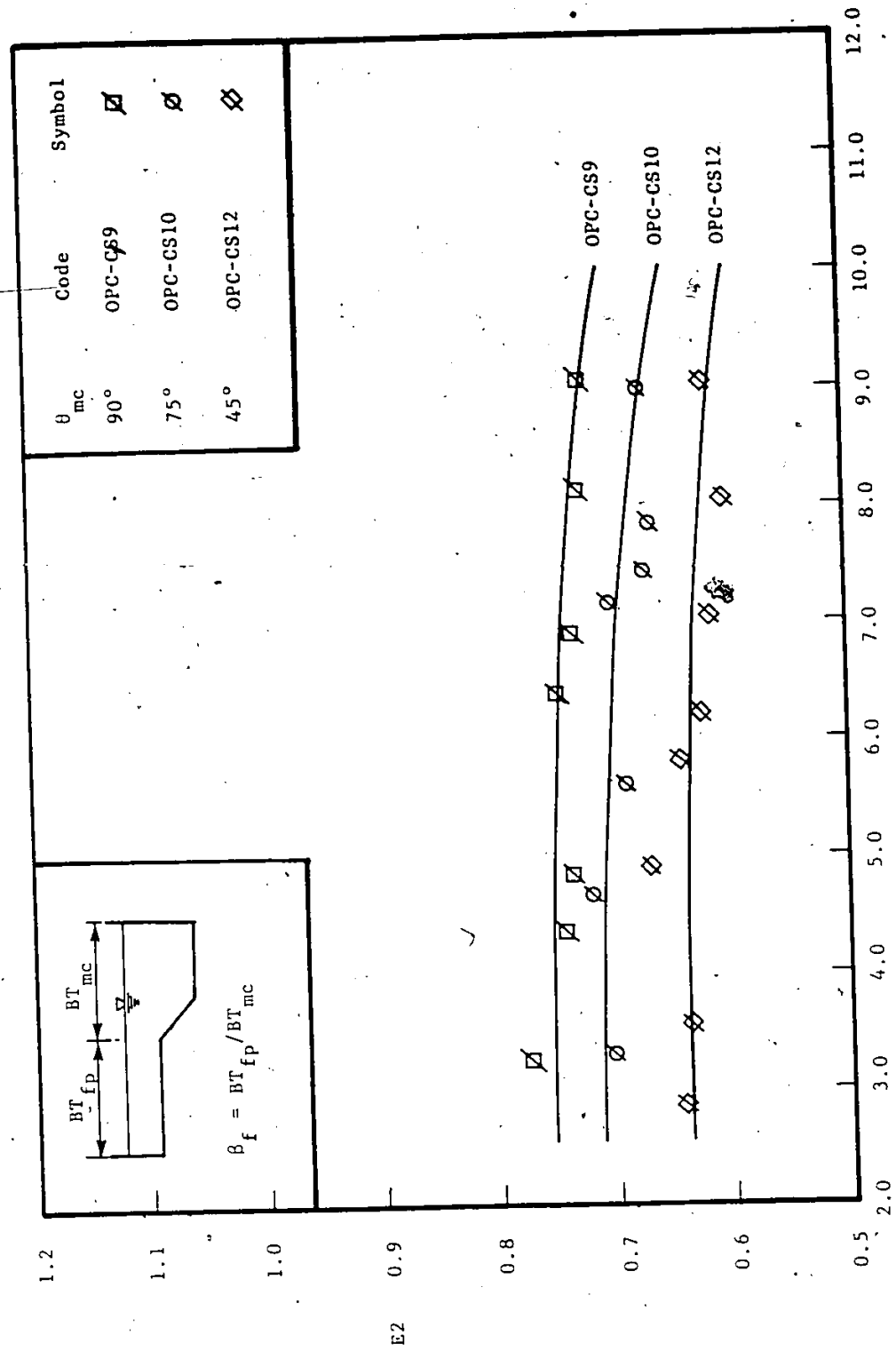

Fig. 6.3. E2-Curves for Compound Channels under Free-Surface Flows with $\beta_f = 2.0$

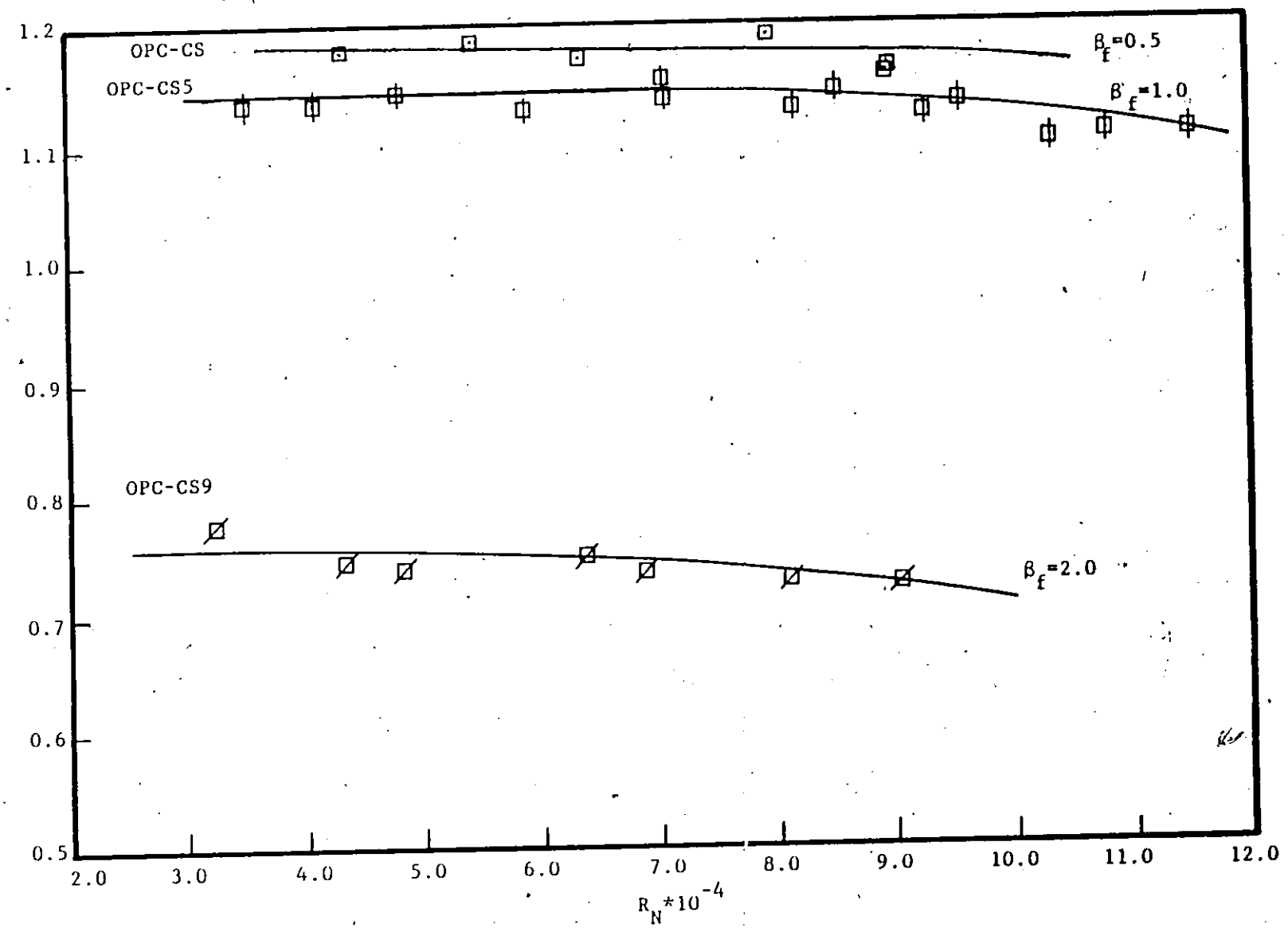

Fig. 6.4. Comparison of E2-Curves for Compound Channels Under Free-Surface Flows with θ_{mc}=90°, θ_{fp}=90° and Varying Relative top Width, β_f.

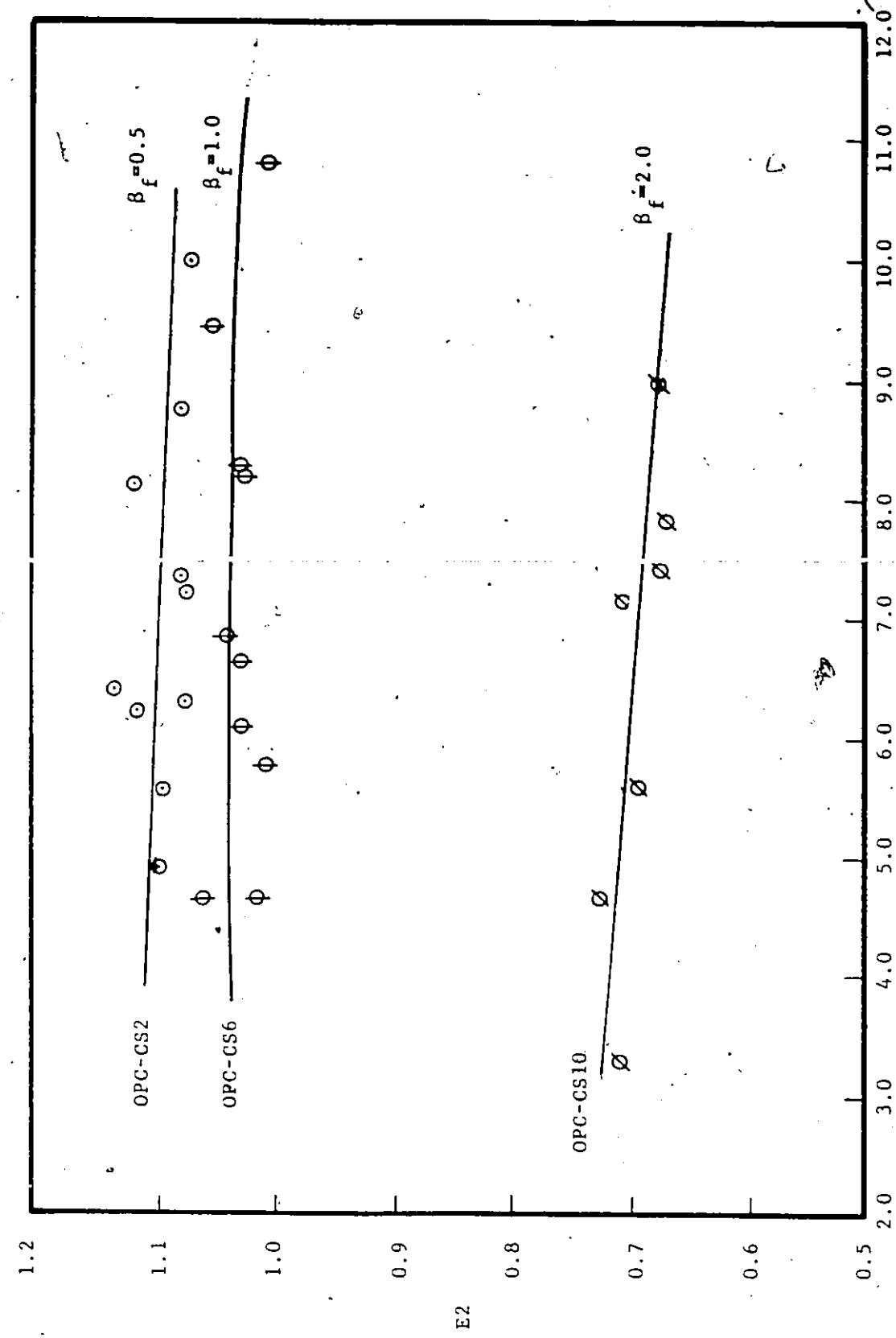

Fig. 6.5. Comparison of E2-Curves for Compound Channels Under Free-Flows with θ_{mc}=75°, θ_{fp}=90° and Varying β_f.

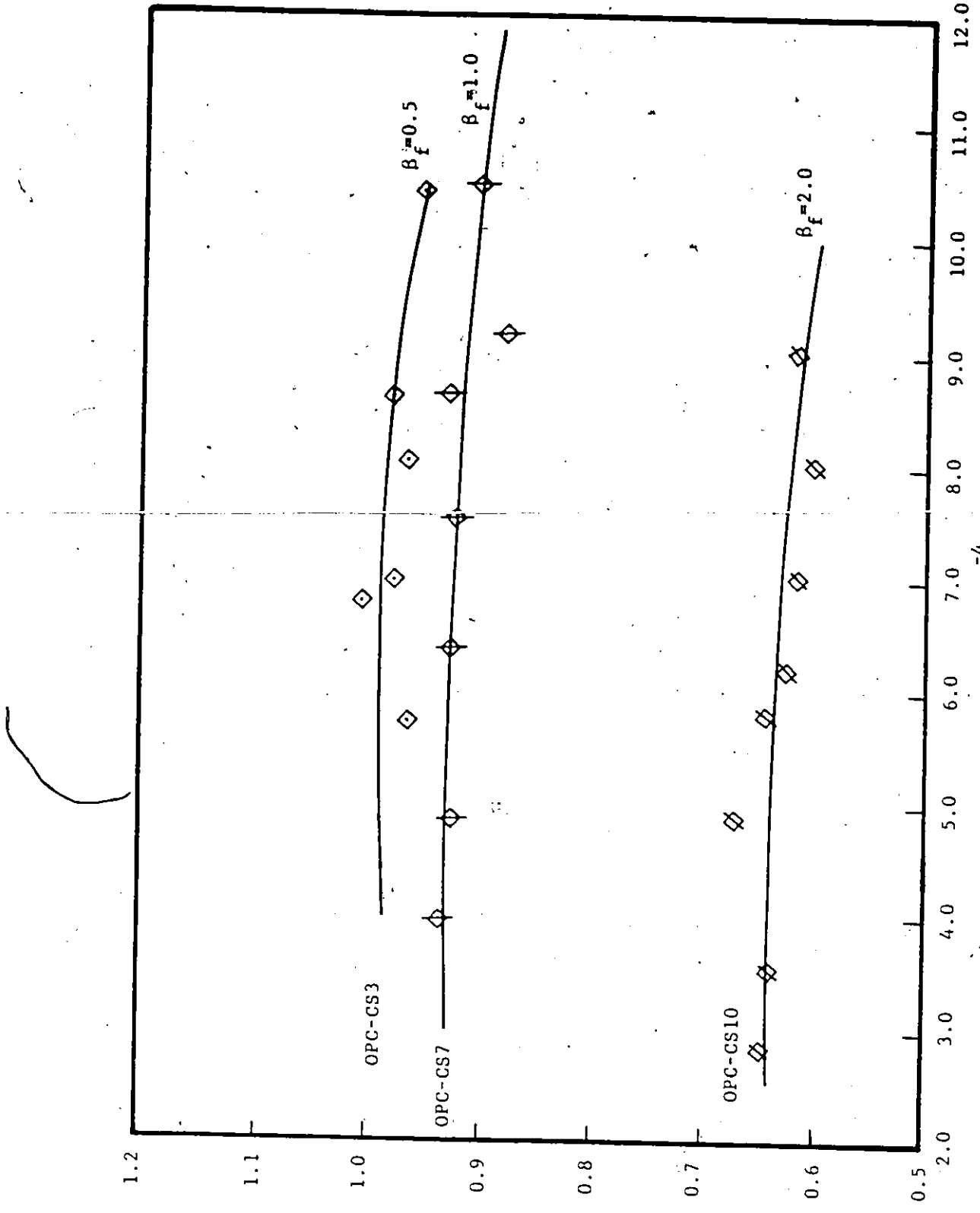

Fig. 6.6. Comparison of E2-Curves for Compound Channels Under Free-Flows with θ_{mc}=60°, θ_{fp}=90° and Varying β_f.

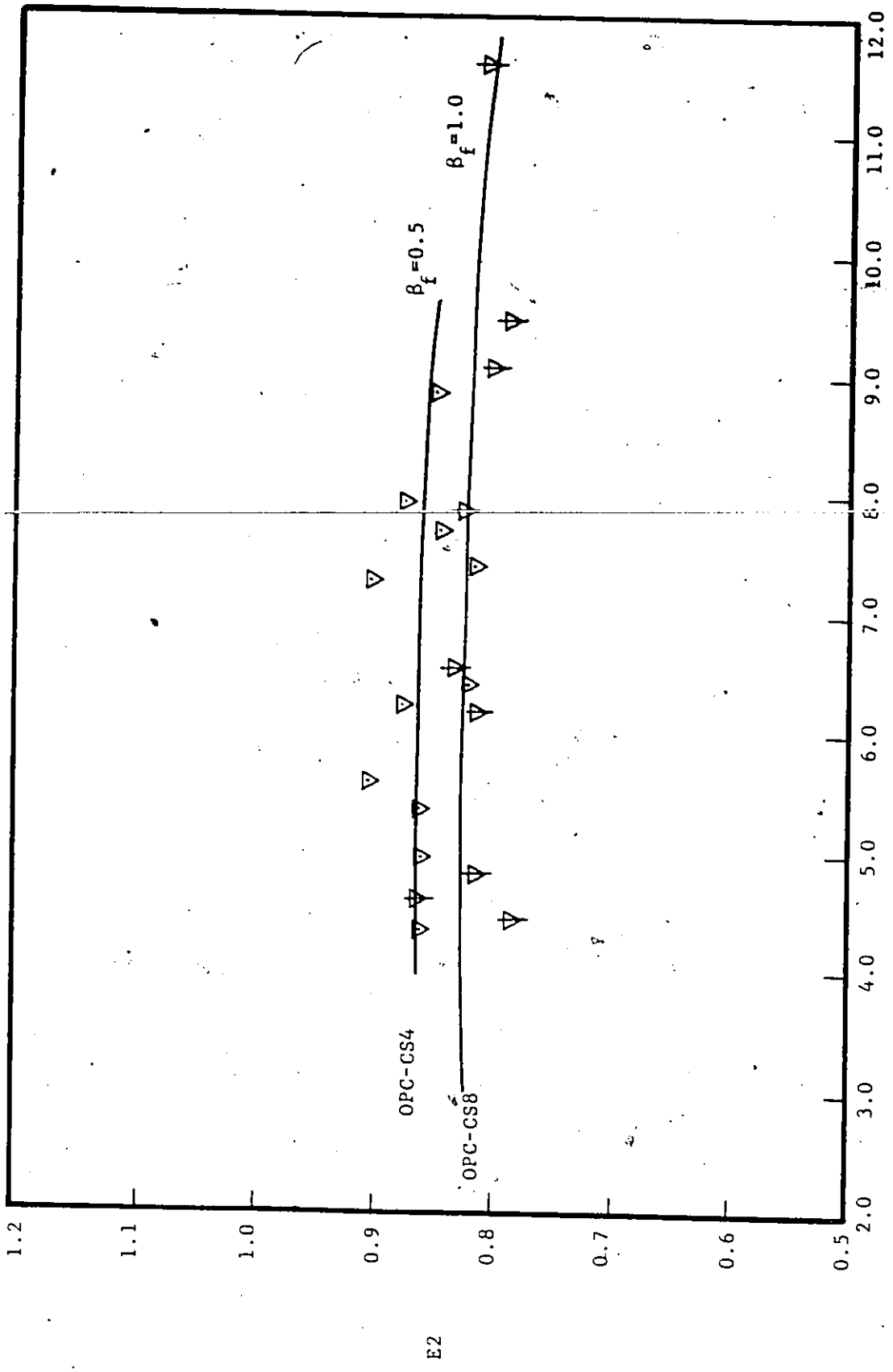

Fig. 6.7. Comparison of E2-Curves for Compound Channels Under Free-Flow with θ_{mc}=45°, θ_{fp}=90° and Varying β_f.

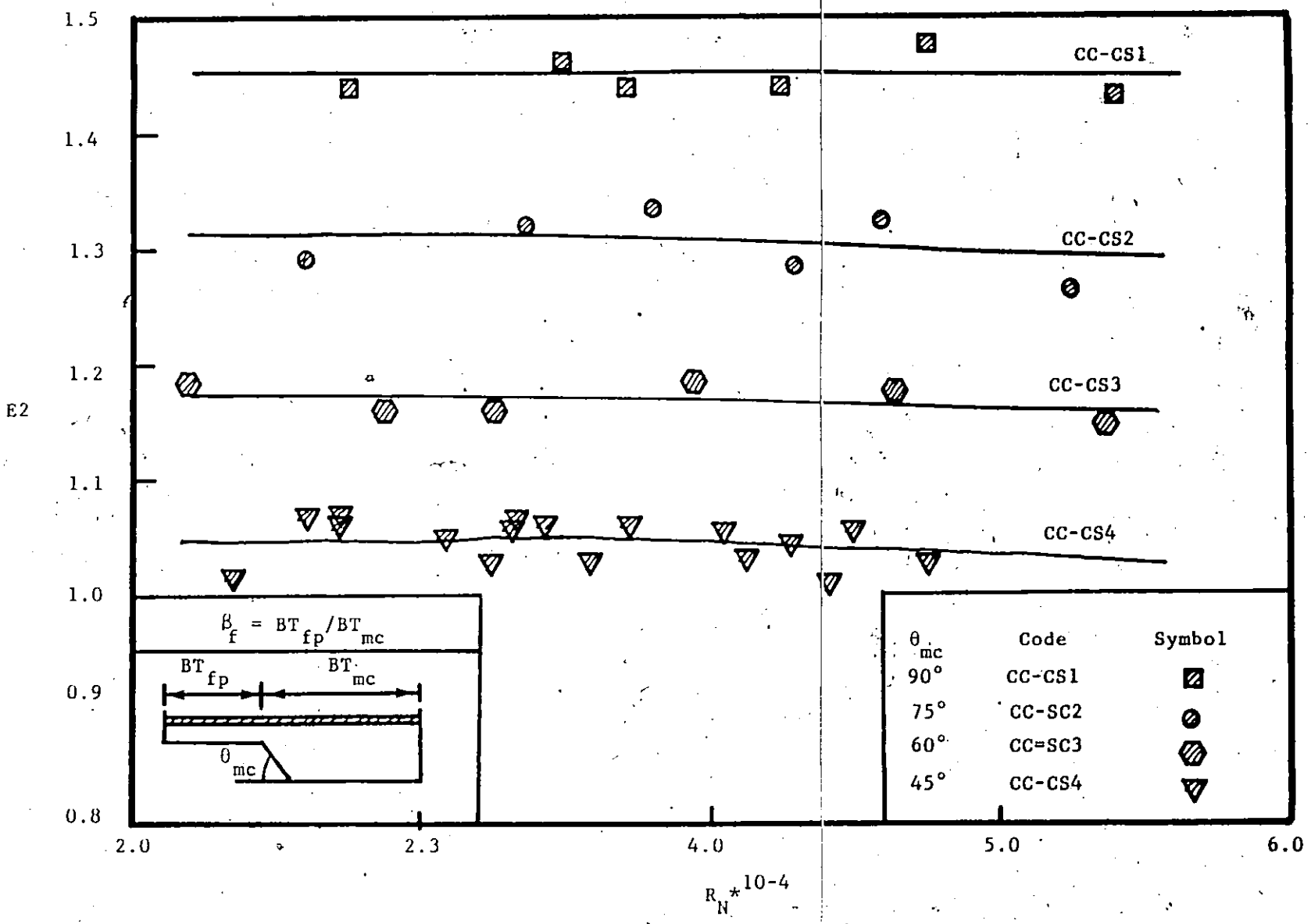

Fig. 6.8. E2-Curves for Compound Channels under Covered Surface Flows with $\beta_f = 0.5$.

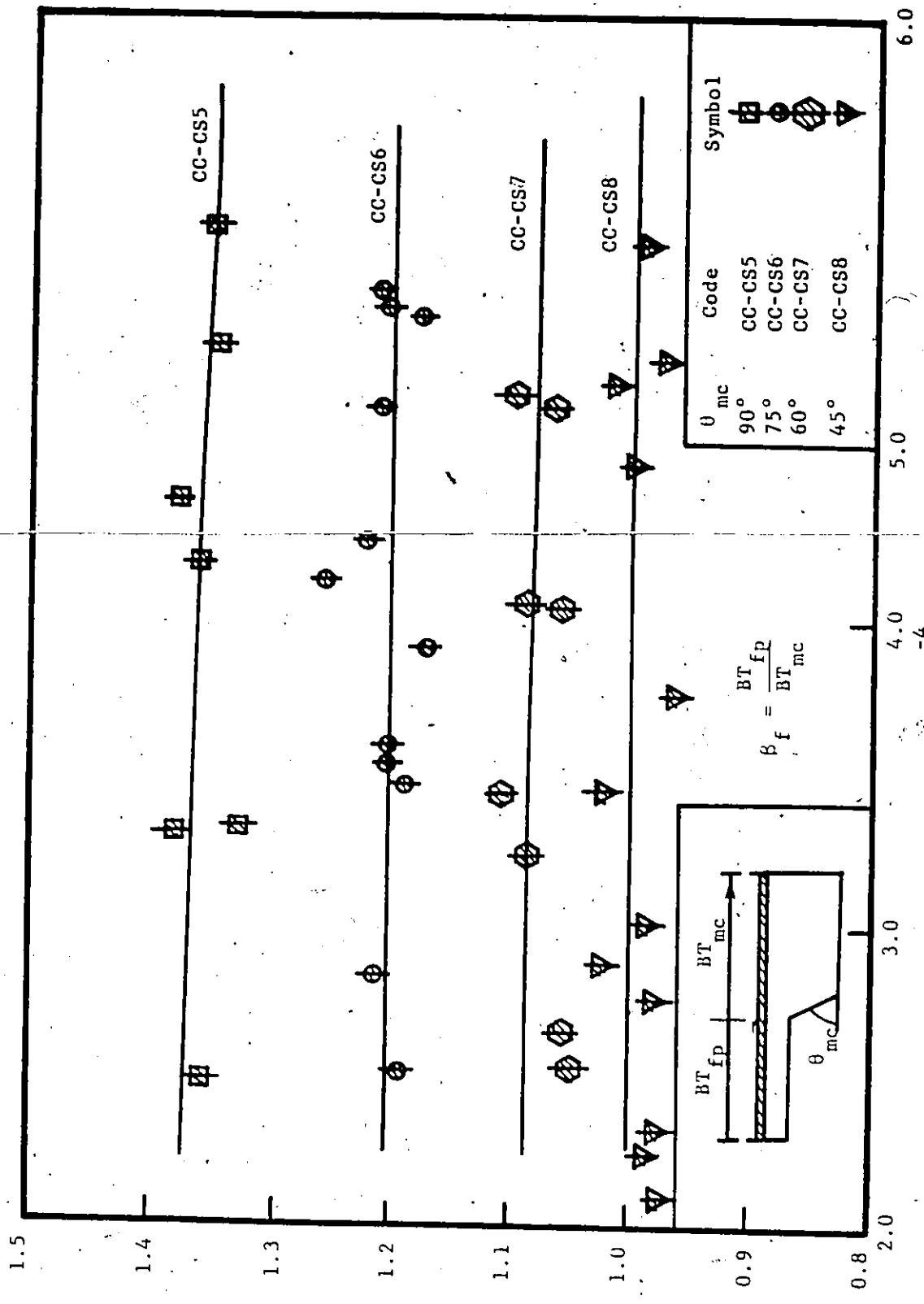

Fig. 6.9. E2-Curves for Compound Channels under Covered Surface Flows with $\beta_f = 1.0$.

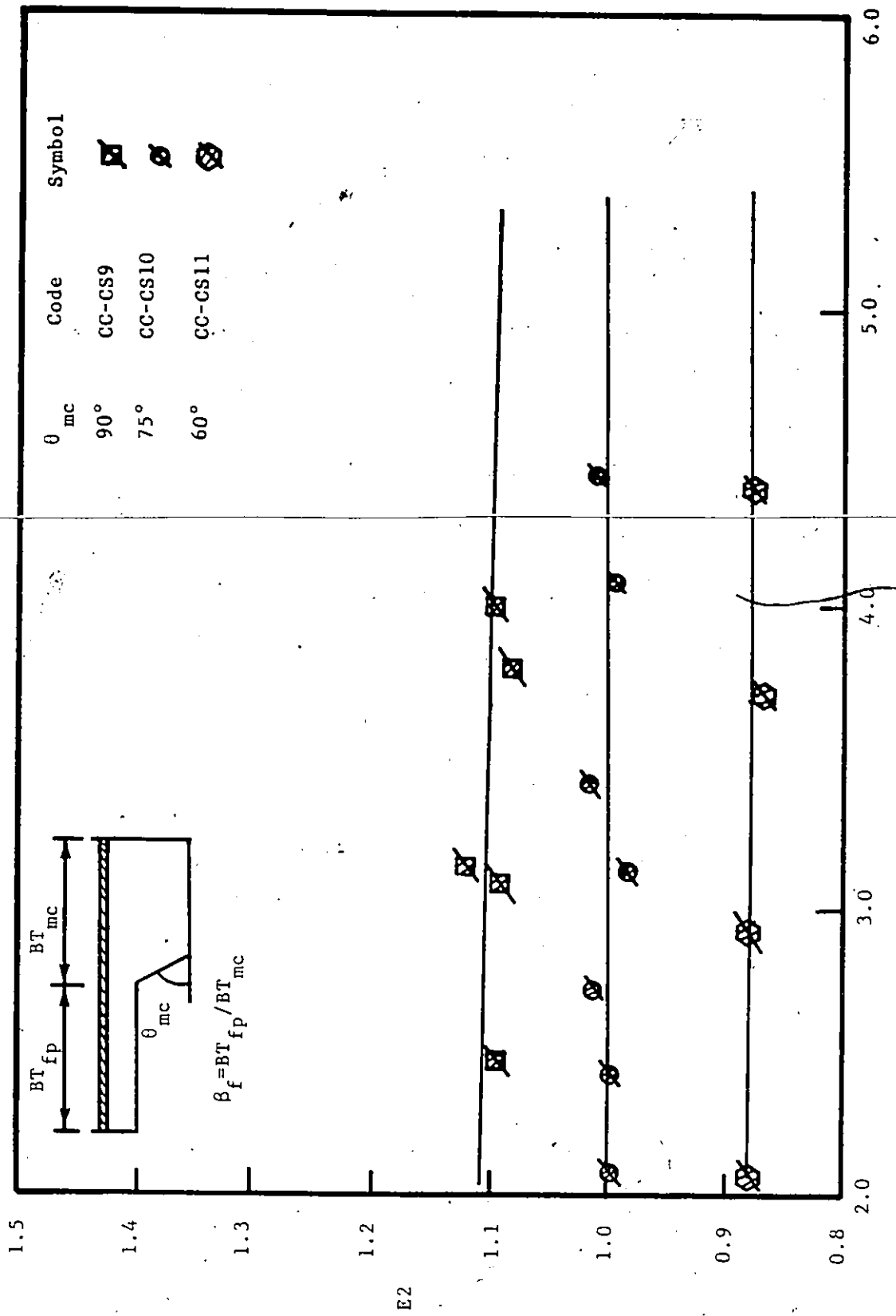

Fig. 6.10. E2-Curves for Compound Channels under Curved Surface Flows with $\beta_f = 2.0$.

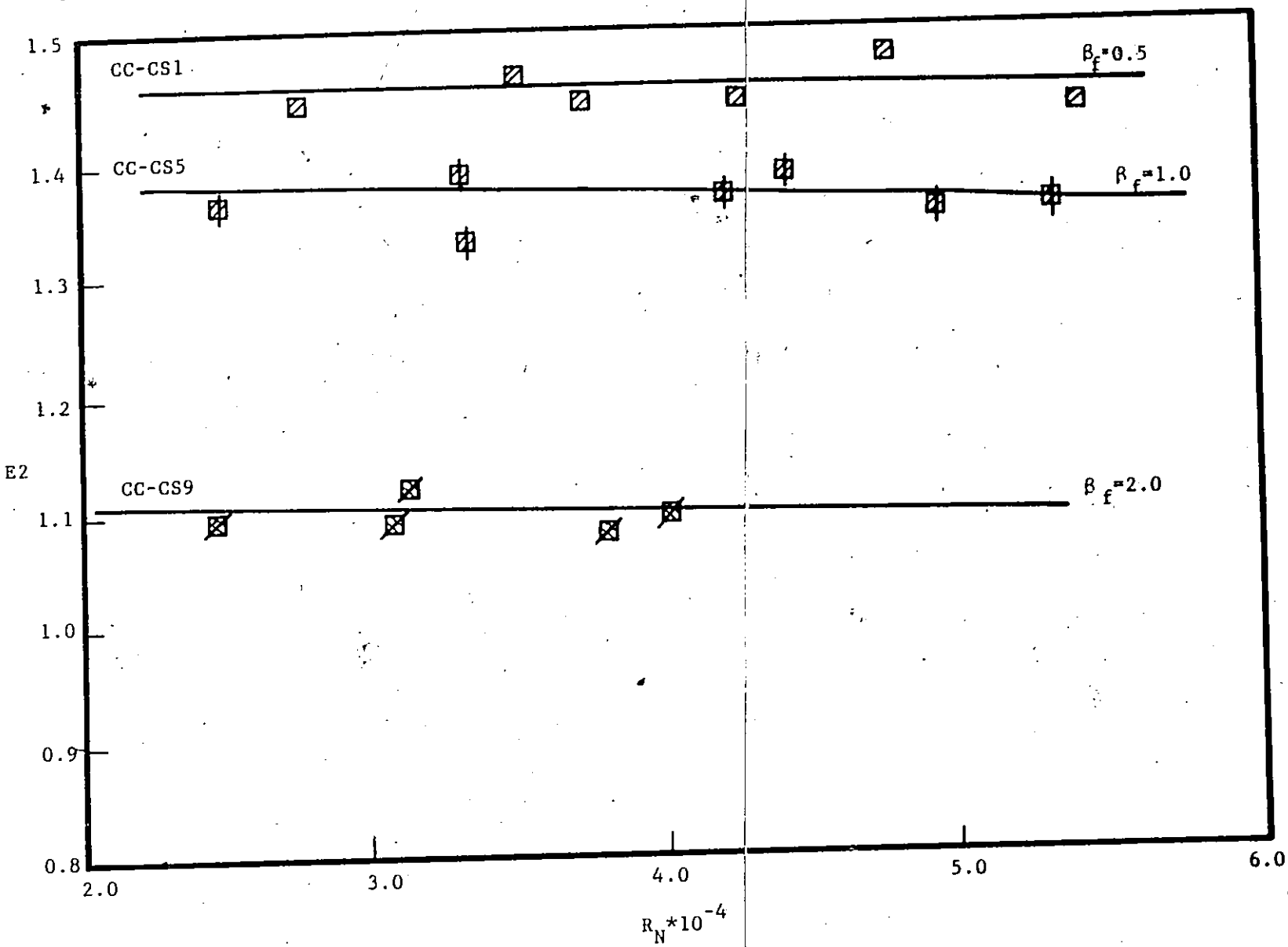

Fig. 6.11. Comparison of E2-Curves for Compound Channels under Covered-Surface Flows with $\theta_{mf}=90°$, $\theta_{fp}=90°$ and Varying β_f.

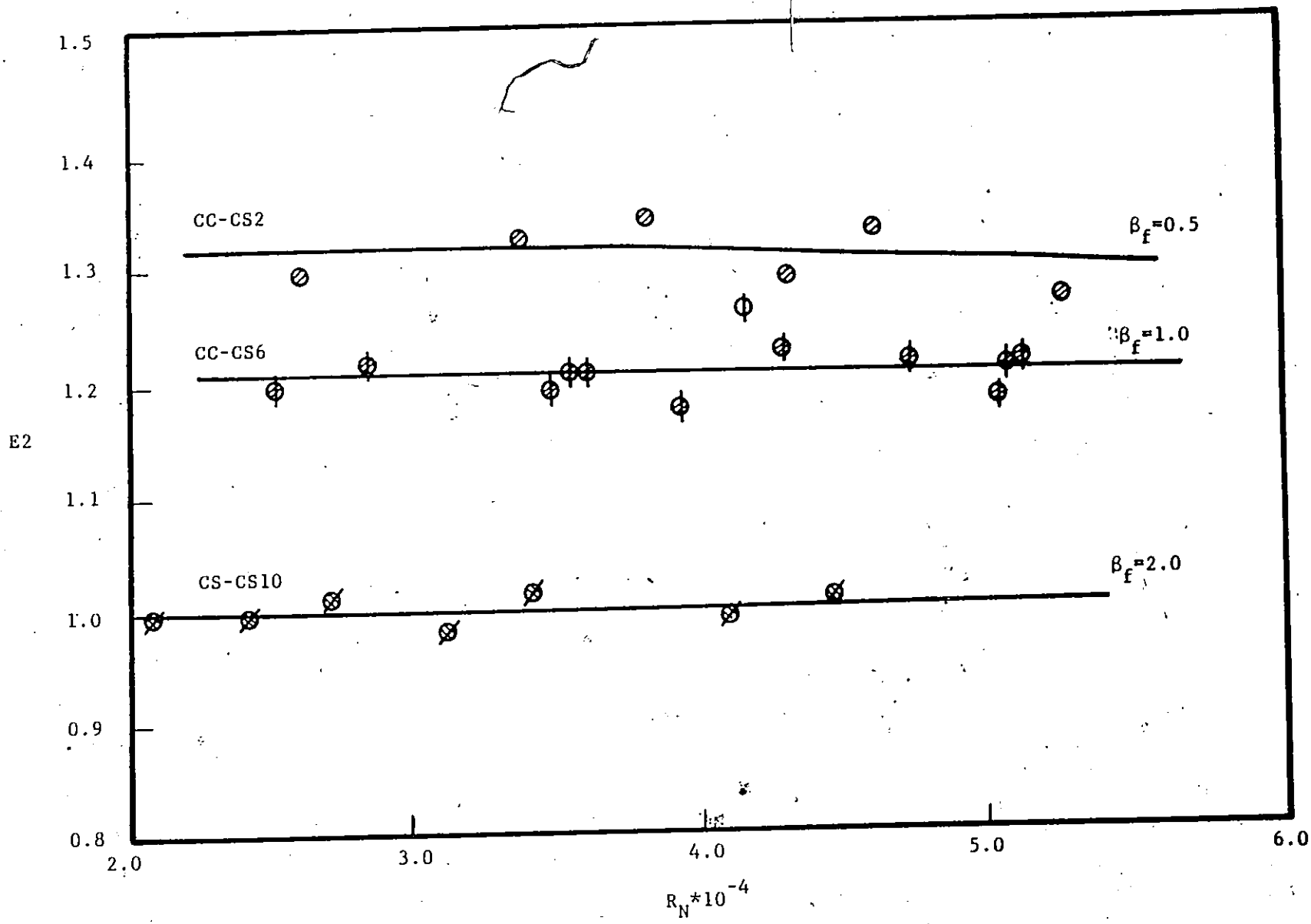

Fig. 6.12. Comparison of E2-Curves Under Covered-Surface Flows with θ_{mc}=95°, θ_{fp}=90° and Varying β_f.

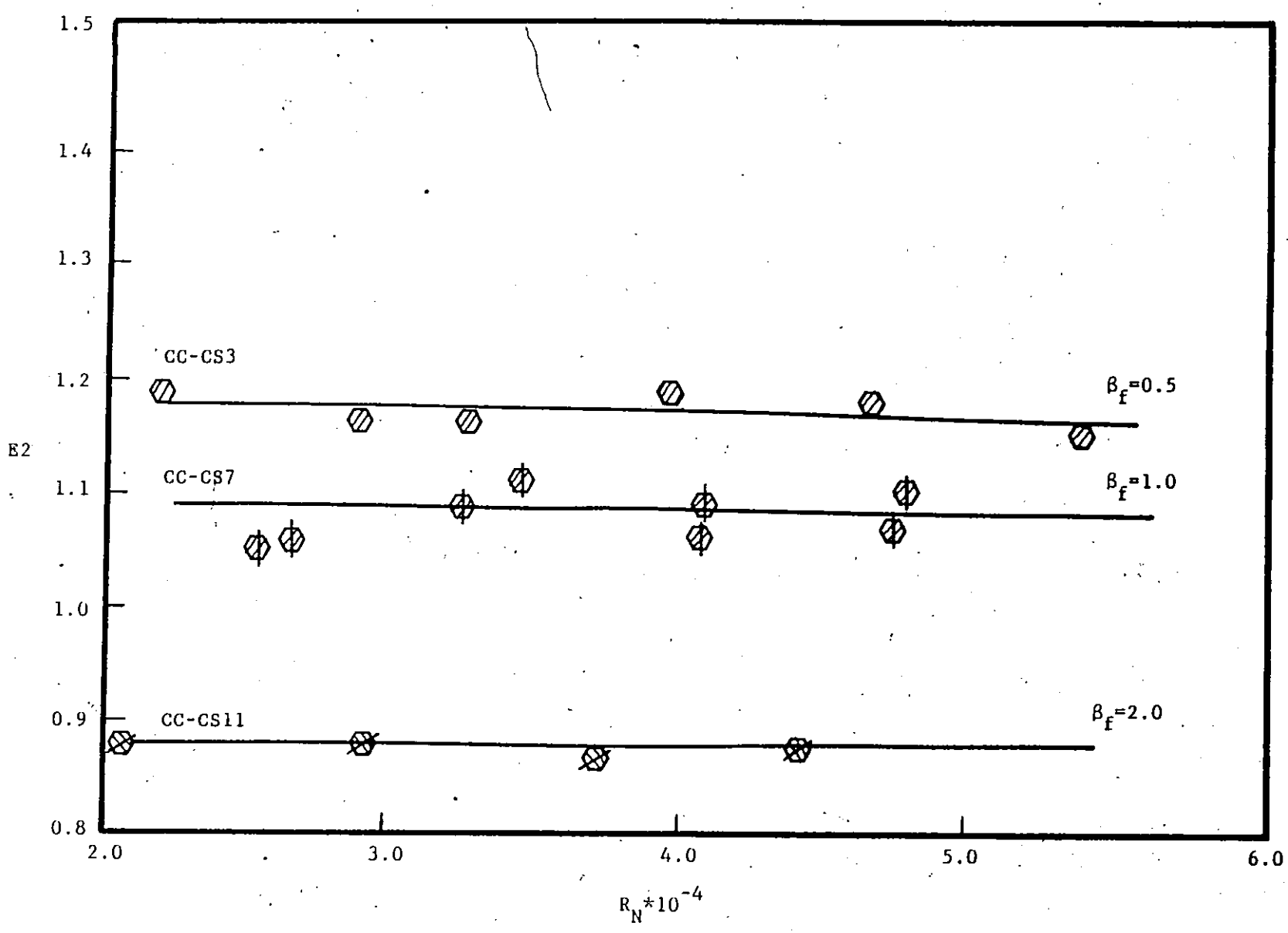

Fig. 6.13. Comparison of E2-Curves of Compound Channels Under Covered-Surface Flows with θ_{mc}=60°, θ_{fp}=90° and Varying β_f.

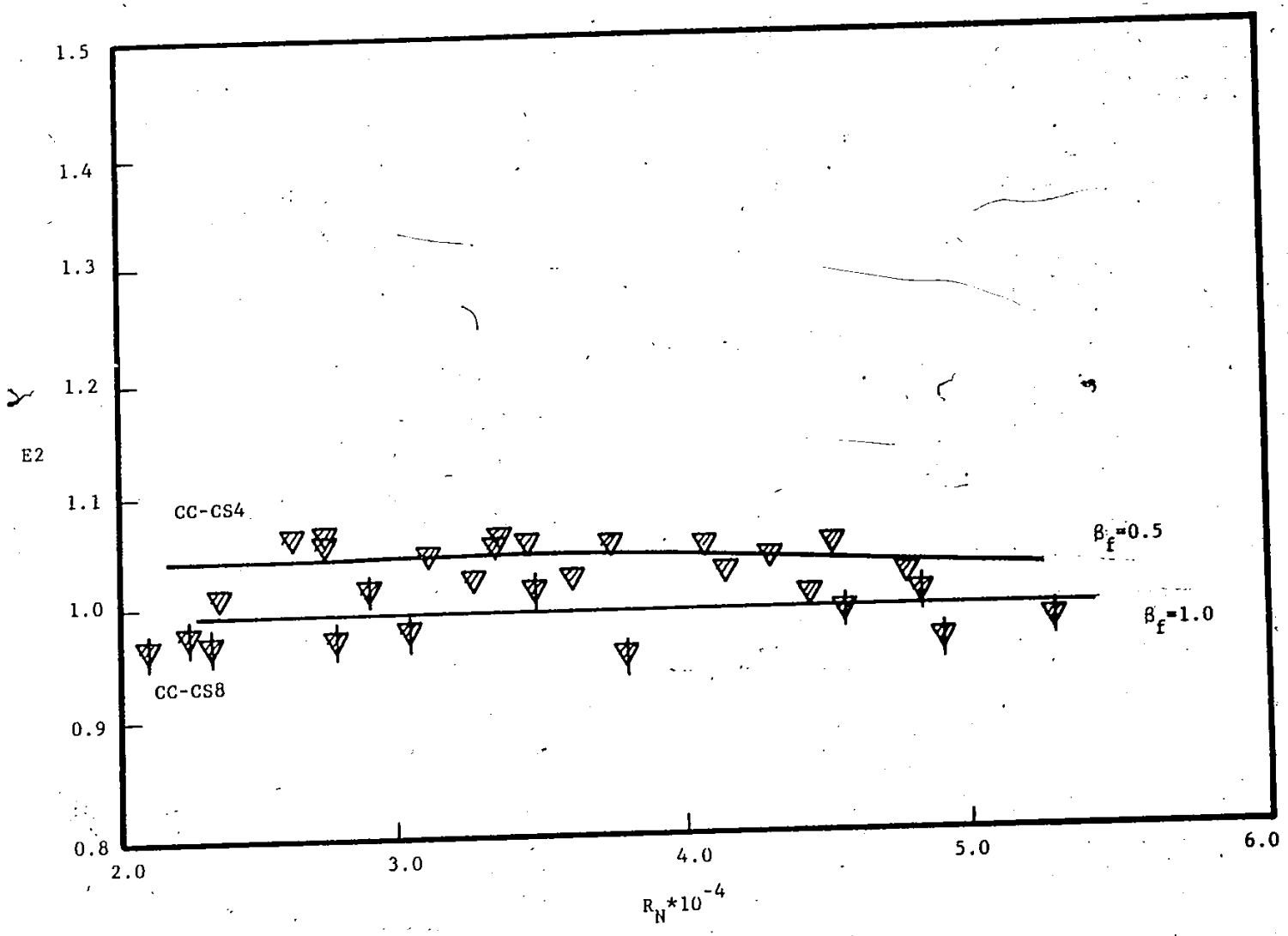

Fig. 6.14. Comparison of E2-Curves of Compound Channels Under Covered-Surface Flows with θ_{mc}=45°, θ_{fp}=90° and Varying β_f.

channel cross-section was observed for α_f within the range of 0.15 to 0.4, while the corresponding range of Reynolds numbers was $3*10^4$ to $11*10^4$.

In the case of floating covered-surface flow each channel cross-section was observed for the range of α_f equal to 0.20 to 0.36 with corresponding Reynolds number of $2.0*10^4$ to $5.5\ 10^4$. Below the lower limit of α_f (i.e., less than 0.20) difficulties were observed in measuring velocity distributions with available instrumentations. Beyond the upper limit of α_f (i.e., greater than 0.36), breaking up of the floating covered blocks were observed for the same set-up of the tailgate.

Within the specified limit of the relative flow depth, α_f the E2-values are found fairly constant if the shape and the size of a channel cross-section remain constant, in other words it can be said that for a particular shape and size of a compound channel cross-section, the E2-values are independent of the effects of Reynolds number. The values are within ±5% from the mean value of E2 for any particular shape of channel cross-section.

On the other hand, the E2-values are found very sensitive with the change of the main channel shape and the relative top width (β_f) of channel cross-sections. The value decreases with the decrease in inclination of the side wall, θ_{mc}, i.e., the decrease in overall hydraulic perimeter or hydraulic radius for same depth of channel flow when the

relative top width, β_f is kept constant. The value also decreases with the increase of relative top width, β_f when the shape of a channel cross-section remains unchanged, i.e., the overall perimeter for same depth of channel flow is kept constant, but with the decrease of overall hydraulic radius for the same depth of flow.

In fact, in both cases the E2-value decreases with the decrease of overall hydraulic radius of a channel flow depth, or in other words, it can be said that the E2-values decreases with the increase of relative hydraulic radius of flood plain to the main channel (R_{fp}/R_{mc}) for the same flow depth of a channel cross-section.

Hence, within the specified limit of relative flow depth (α_f), the E2-values are a function of the overall hydraulic radii and overall flow depths of channel cross-sections. Therefore, a relation between the overall hydraulic radius to the flow depth of a channel cross-section can be described as a 'shape factor'. The relationships of the E2-values with the shape factor will be described later.

6.2.3 Velocity Coefficient E1 of Compound Channel

From the observations of the computational results of the velocity coefficient E1 for each cross-section as furnished in Tables C.8 through C.13 of both free-surface flow and covered-surface flow conditions, it is found that unlike the velocity exponent E2, the velocity coefficient E1 is

insensitive with the change of shape, size, discharge rate, and type of flow and found fairly constant.

Hence, El-values are plotted against experimental run for all the cross-sections in a group separately for each flow condition (free-surface and covered-surface). Figure 6.15 shows the El-values for compound channels under free-surface flows while Fig. 6.16 is that of compound channels under covered-surface flows. Although for any particular channel cross-section El-values are fairly constant, the trend in change of value with the change of cross-sectional shape of channel cross-section has no regular pattern. Of course, the values range from 1.0 to 1.1 with an average range of 1.0 to 1.07 with a range of standard deviation of 0.0016 to 0.058.

6.2.4 Velocity Coefficients El and E2 for Simple and Complex Channels

Solution steps as indicated in section 4.2 for the floating covered-surface flow are used for the computation of the El and E2-values. The results are furnished in Table C.14.

Velocity Coefficient E2

The E2-values are plotted against the Reynolds numbers in Figure 6.17. The range of the Reynolds numbers is found between $1*10^4$ and $5.5*10^4$. Three linear best fitting curves, each for simple rectangular, complex triangular and complex

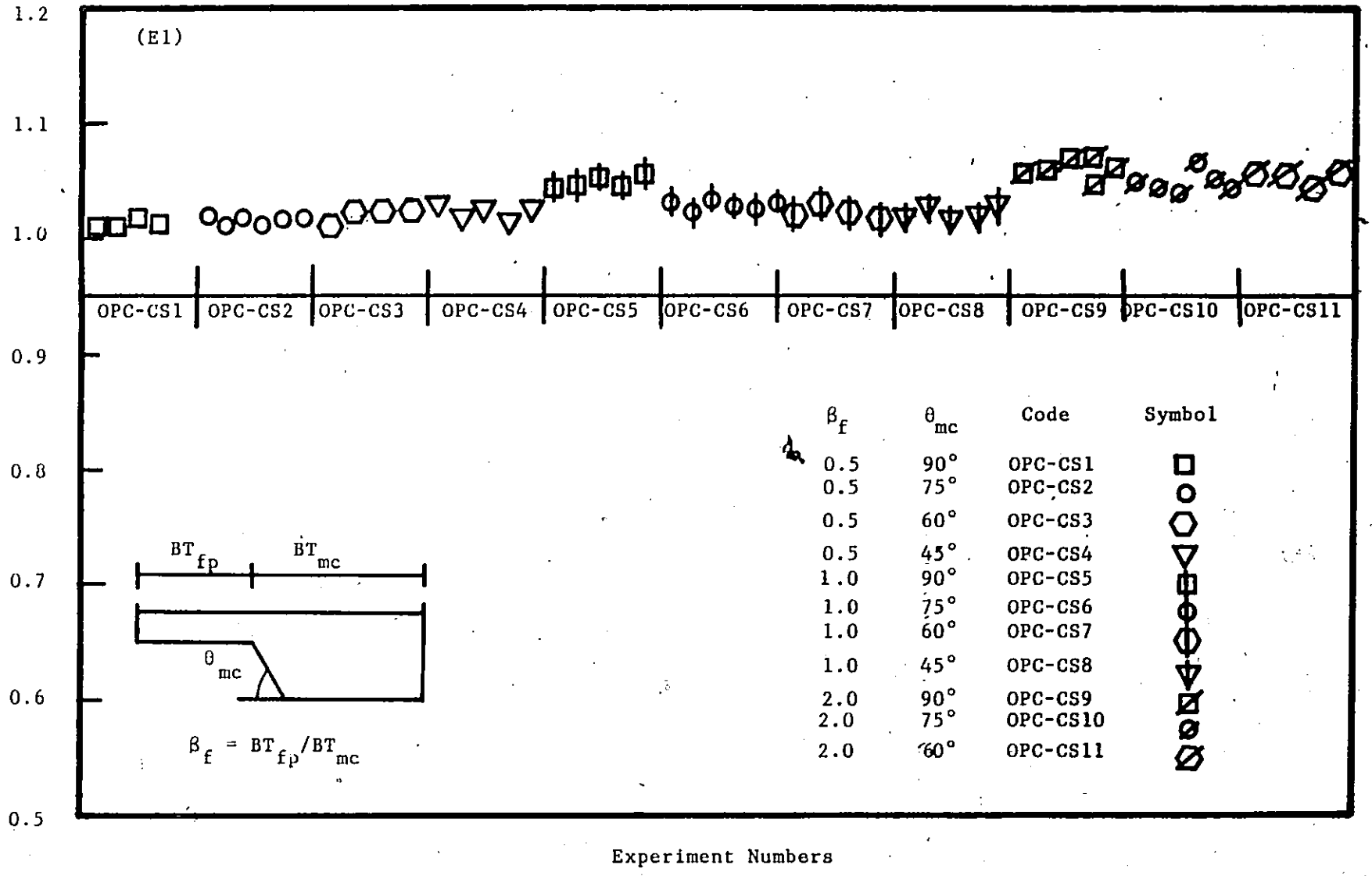

Fig. 6.15. Velocity Coefficient E1 of Compound Channels under Free-Surface Flows.

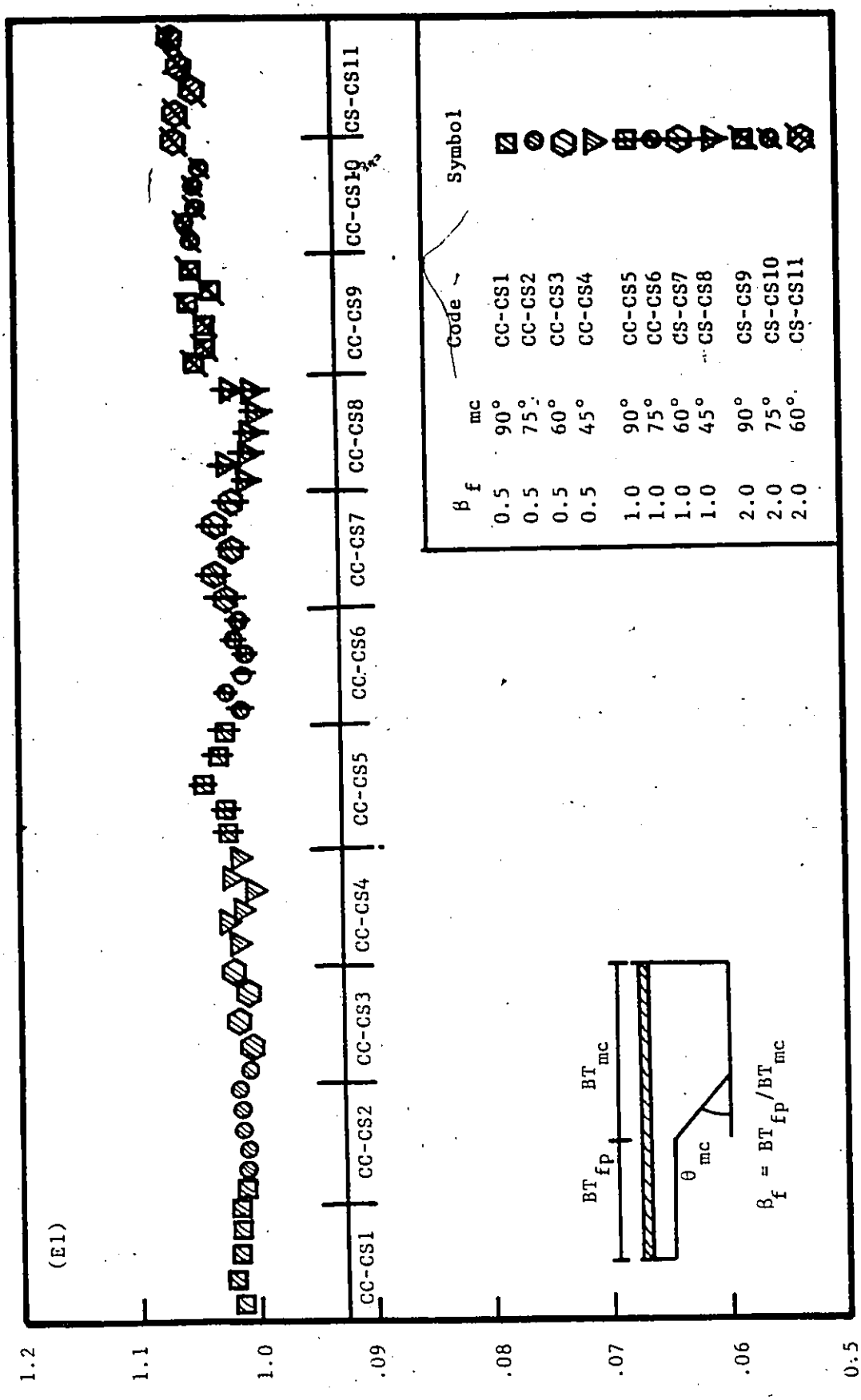

Fig. 6.16. Velocity Coefficients of Compound Channels Under Covered-Surface Flows.

trapezoidal cross-section are drawn. Significant difference in values between the rectangular cross-section and the trapezoidal or triangular cross-section is noticed. While the difference in values between the complex trapezoidal and complex triangular cross-section are negligible. In fact, a single curve would have been drawn for two cross-sections. The mean E2-values of 1.015, 0.714 and 0.702 are found for rectangular, triangular and trapezoidal channel cross-section, respectively. The corresponding standard deviations are 0.076, 0.0186 and 0.0667.

Velocity Coefficient E1

The E1-values for all three types of channel cross-sections are found fairly constant and are within the range of 1.02 to 1.06. Like compound channels the E1-values are plotted against experimental runs and shown in Fig. 6.18.

6.2.5 Choice of Velocity Coefficients E1 and E2 in Design Problems

It has been already discussed in Chapter III that to solve the velocity model (Equation 3.47) for real value problems, either of the two coefficients, E1 and E2, has to be known.

From the previous discussion it is clear that E1 is not at all sensitive to the channel cross-sectional shape, size, flow rate or the type of flow condition. On the other hand, the velocity exponent E2 is very sensitive to

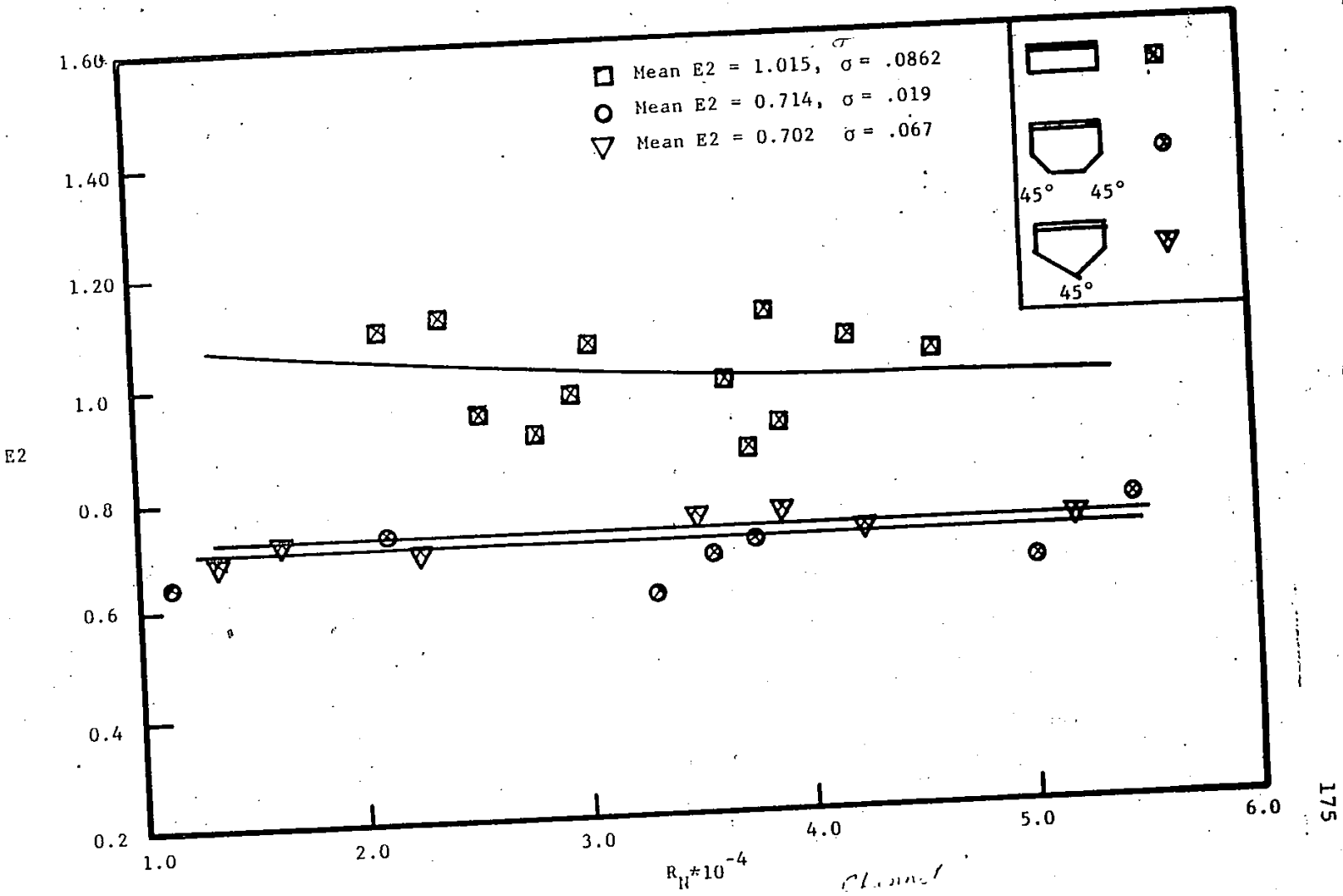

Fig. 6.17. E2 $V_{\div}^{s}$ Reynold's Number for Simple and Complex Channel.

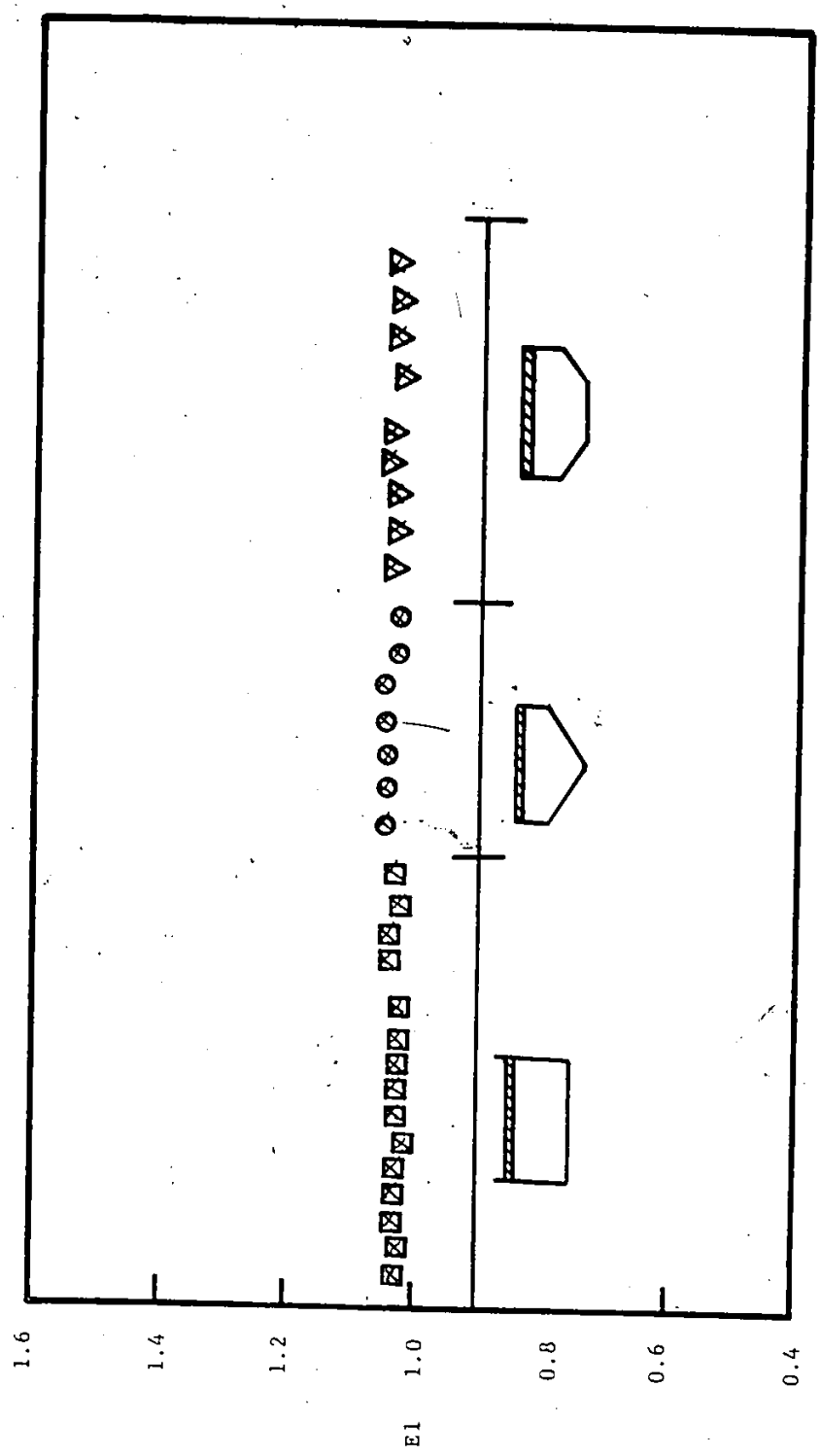

Fig. 6.18. Velocity Coefficients, E1, for Simple and Complex Channels Under Covered-Surface Flows.

all those factors except the flow rate within the specified limit of relative flow depth and the Reynolds numbers. Hence, for the solution of a problem, the correct value of the velocity exponent, E2, has to be known.

Therefore, from the present investigation it is quite clear that for a particular type of flow condition (free-surface or covered-surface) the E2-values are solely dependent on some shape factors of a channel flow. In the next section, investigation will be made to search appropriate shape factors to relate it with the E2-values.

6.2.6 Relationships of E2 with Shape Factor

6.2.6.1 Shape Factor

A shape factor is defined in various ways by many researchers. Also the term 'aspect ratio' sometimes replaces the term 'shape factor'.

For many decades it was assumed that the hydraulic radius alone could effectively measure the hydraulic efficiency of a channel cross-section irrespective of its size and shape. But from the experimental evidence, many researchers, in recent decades, have come to the conclusion that the shape of a channel cross-section has tremendous effects on the channel's overall resistance and thereby in the computation of channel discharge. The present study also confirms this statement while the velocity coefficient, E2, can be said as an indirect measure of discharge.

Nalluri and Adepoju (56), in their recent studies found the geometric parameter, H/P as a suitable shape factor in case of smooth channels of circular cross-section for the range of flow depths $0<H<0.85D$, where D is the diameter of the circular cross-section. They reached this conclusion after reviewing the past works of Jayaraman (Ref. 4 of Nalluri and Adepoju) and Kazemipour and Apelt (36).

Jayaraman indicated two non-dimensional parameters, BT/P and H/P as shape factors in case of smooth channels of both rectangular and circular cross-section.

Kazemipour and Apelt defined shape factor, ϕ, in case of semi-circular channels (i.e., for flow depth $H<D/2$) as a ratio of two other shape factors, ϕ_1 and ϕ_2.

where

$$\phi_1 = (P/D)^{1/2}$$

and

$$\phi_2 = f(D^2/A)$$

and

$$\phi = \phi_1/\phi_2$$

Hey (32) defined the shape factor by the parameter R/y_p for any channel cross-section, in which y_p is the perpendicular distance from the perimeter to the point of

maximum velocity. This is normally the maximum flow depth unless the channel is very narrow and deep.

Knight, et al., (40) denoted the shape factor as an aspect ratio and defined it as $\phi = B_{mc}/H$ in case of compound channels of rectangular shape.

The shape factors defined by Nalluri, Jayaraman and Kazemipour are related to the channel shapes of circular or semi-circular cross-section and hence, they are not considered in the present investigation.

The difficulty in applying Knight's definition of the aspect ratio is the proper measurement of the bottom width in case of a cross-section other than a rectantular one.

On the other hand, the shape factor, as defined by Hey, is more generalized because the perpendicular distance of the point of maximum velocity of a channel cross-section is usually the maxmimum flow depth, unless the flow width/depth ratios are very small. But the problem arises in determining the point of maximum velocity in case of more complex cross-sections, such as compound channels, with or without multiple boundary roughnesses, unless the velocity profiles of such sections are known beforehand. The problem, however, becomes more difficult in case of a floating covered-surface flow.

6.2.6.2 Velocity Coeffient E2-Shape Factor Relationship

In the present study it is well observed that although the E2-values for any particular shape of compound channel is fairly constant for the same type of flow condition (free-surface or covered-surface) within the specified range of relative flow depth, α_f, the variation are of considerable amount with the change of any kind of shape of the cross-section.

Three factors are found to be responsible for this change in the E2-values: the overall shape of the compound section, relative top width, β_f and the shape of the main channel cross-section.

The overall shape can be defined by the ratio of overall hydraulic radius to overall flow depth (R/H) of any compound cross-section and is denoted by ϕ_1. For any particular cross-section ϕ_1 is a dependent factor of the relative flow depth, α_f.

The second factor, β_f is constant for any channel shape and independent of flow depth.

The third factor can be defined by the ratio of average width of the main channel to the depth of lower main channel (β'_{mc}/H1). This is also independent of flow depth and constant for any channel shape.

As E2 is almost constant for any channel cross-section, it is required to define the channel shape by a constant or

fairly constant shape factor. Among the three factors as described in above, the factor, ϕ_1(=R/H) varies with the flow depth. In Table C.15 the change of ϕ_1 is examined for the free-surface flow with the change of α_f within its range of 0.15 to 0.40. Although the percentage difference between maximum to minimum values is very low (below 10%) for the channel cross-section with smaller relative top width, the difference is very high (33%) for the higher relative top width. Similarly, in the case of covered-surface flow, it is as high as 43%. But this difference is found very low (below 5%) for the exponent of factor ϕ_1 and can be considered as constant. The exponent values of the corresponding ϕ_1 are listed in the same Tables C.15 and C.16. Hence, the combined shape factor can be described as below

$$\phi = \frac{\phi_2 \beta_f}{\exp(\phi_1)}$$

$$= \frac{(B'_{mc}/H1)\beta_f}{\exp(R/H)}$$

Hence, the shape factor, ϕ, can be considered constant for any shape of compound channel cross-section.

In Table C.17, the values of shape factor ϕ and the corresponding mean values of the velocity coefficient E2 are furnished for all the experimental channel cross-sections under free-surface flows. Similarly, the values for covered

surface flows are furnished in Table 6.18. To minimize the error in the values of shape factor, ϕ, the values of ϕ are taken corresponding to the mean of the range of $\alpha_f(0.275)$. Figures 6.19 and 6.20 are the graphical representation of the E2-values with the corresponding values of ϕ of Tables C.17 and C.18, respectively.

The trend of the E2-curves in both flow conditions shows a good uniformity with the shape factor, ϕ. These curves of Figs. 6.19 and 6.20 can be considered as design curves for the determination of E2-values for a given channel cross-sections, within the specific ranges of the relative flow depth, α_f and the Reynolds numbers.

6.2.6.3 Verification of the Proposed Design Curves

The validity of the proposed design curves of Figs. 6.19 and 6.20 are justified by computing theoretically the discharge for each experimental channel flow corresponding to its readout E2-value from the appropriate proposed curves of Figs. 6.19 and 6.20 and compared the value with the experimentally measured total flow. The observed discharges are plotted with its corresponding theoretically computed values in Figs. 6.21 through 6.26. In all the cases it is found a very closed relation between the experimental value and the theoretically determined value. The maximum differences between the two values are well within ±10% and the range of correlation coefficients are found

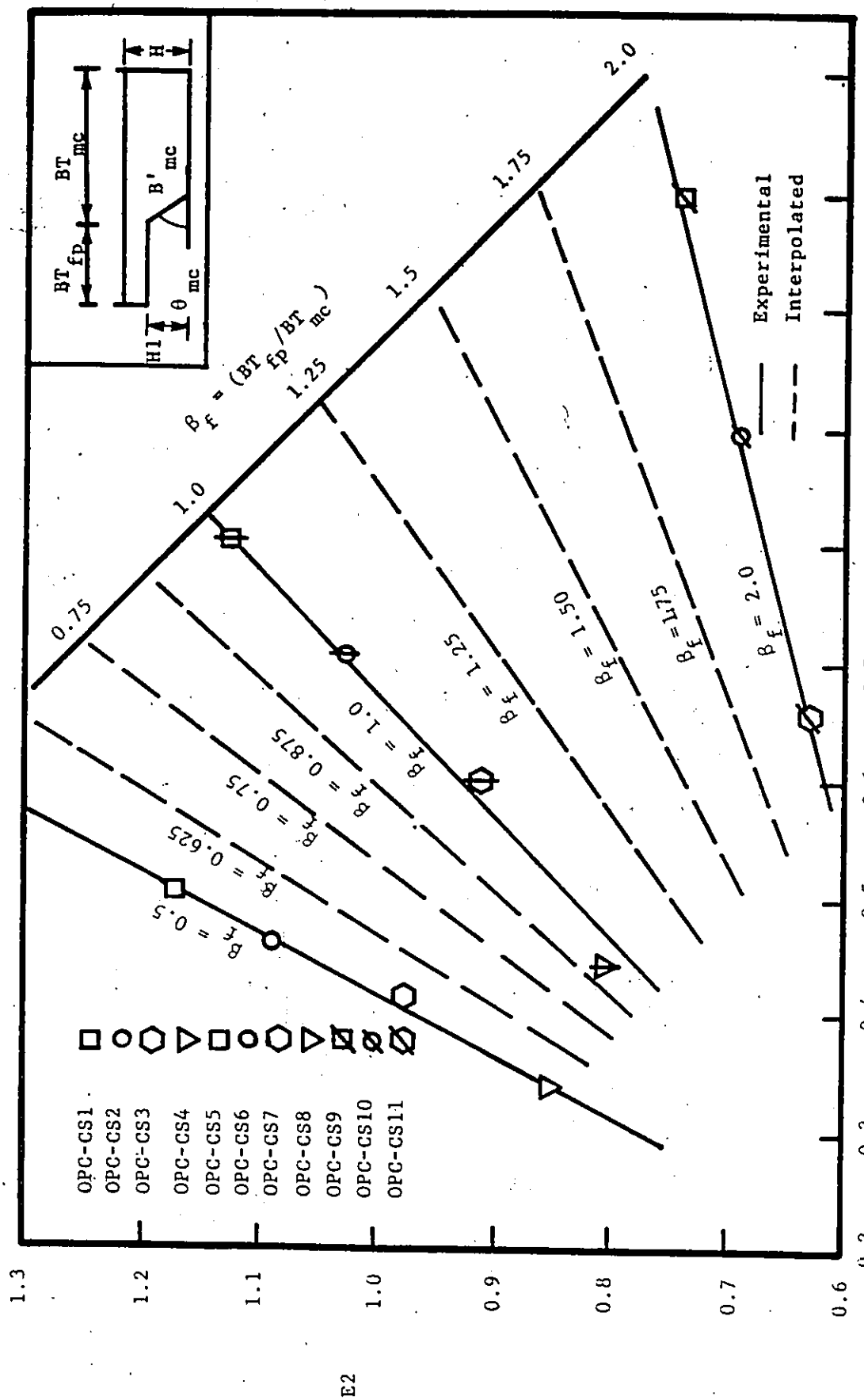

Fig. 6.19. Design Curves of the Coefficient, E2, for Compound Channels under Free-Surface Flows.

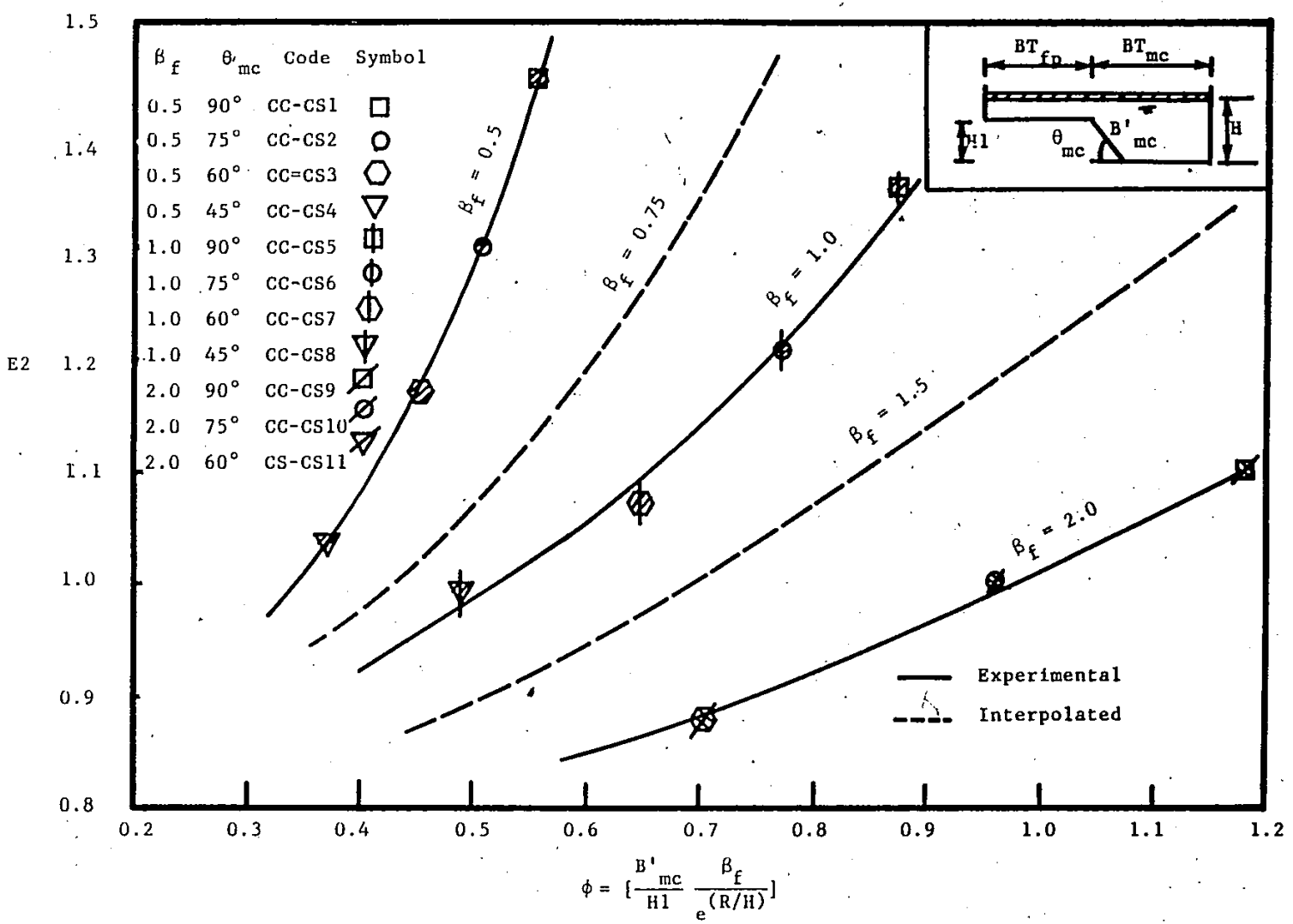

Fig. 6.20. Design Curves of the Coefficient, E2 for Compound Channels under Floating Cover Surface Flows.

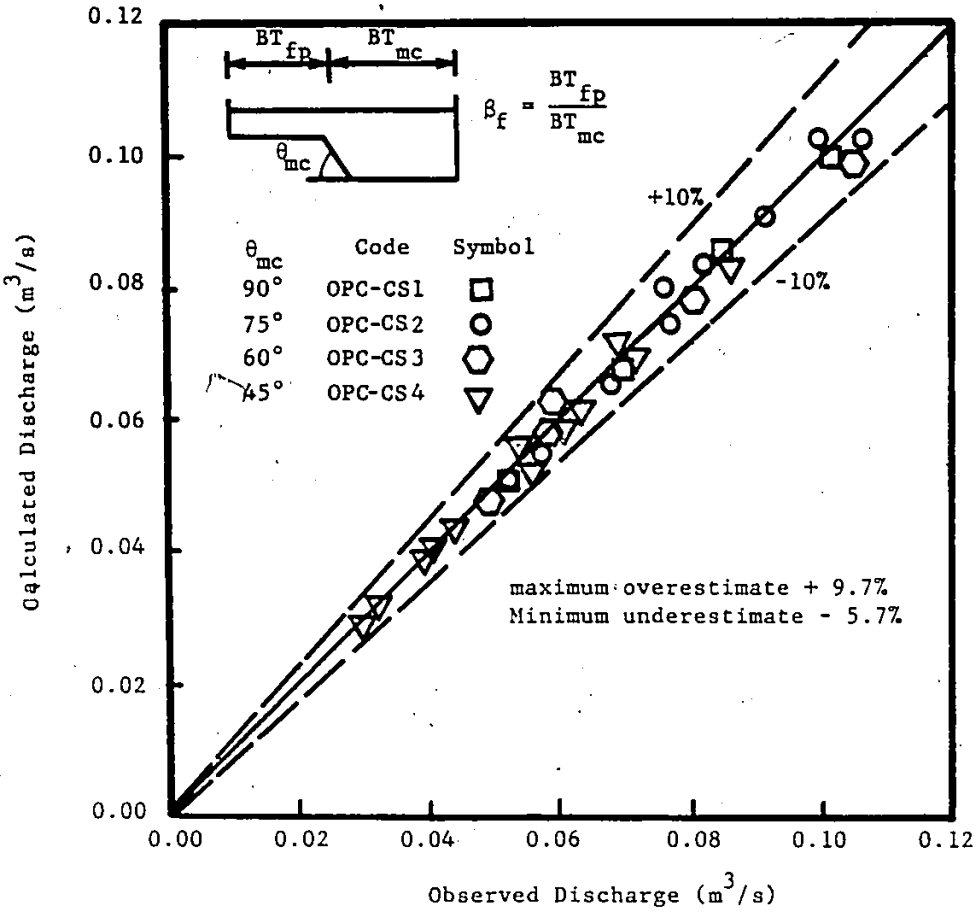

Fig. 6.21. Verification of Design Curves (Fig. 6.19) of 'E2' for Computation of Discharge of Compound Channels under Free-Surface Flows with β_f=0.5.

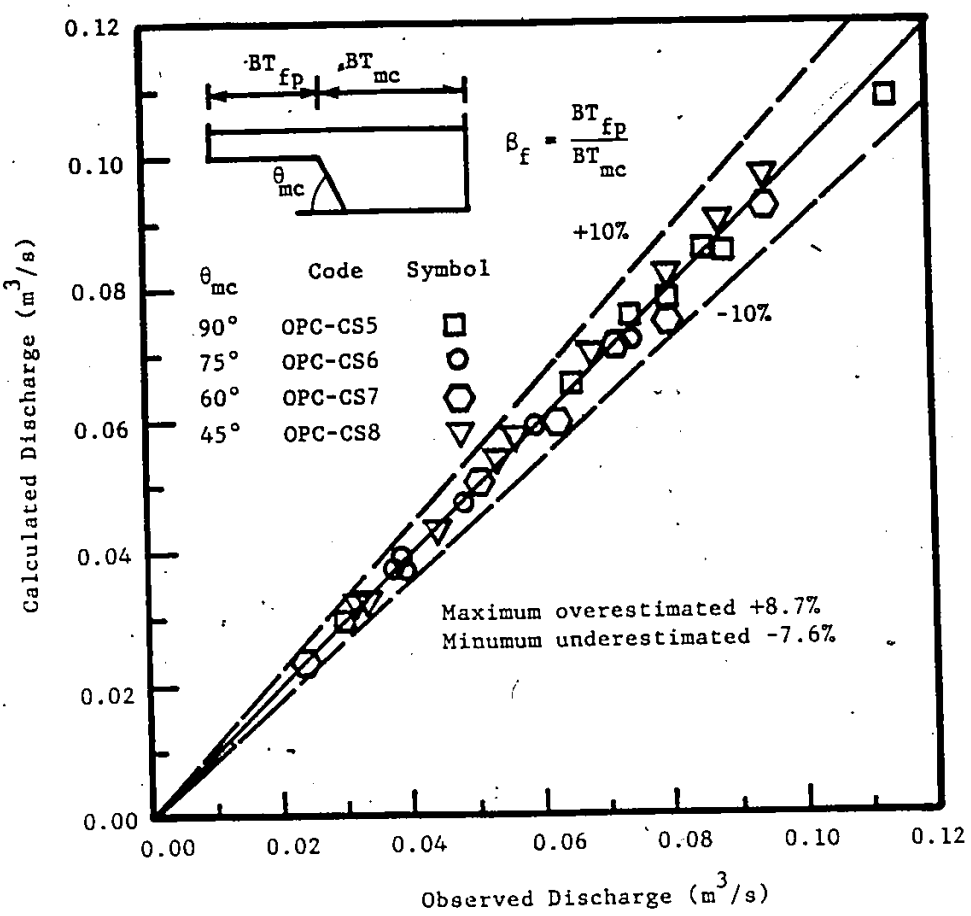

Fig. 6.22. Verification of Design Curve (Fig. 6.19) of E2 for Computation of Discharge of Compound Channels under Free-Surface Flows with β_f = 1.0.

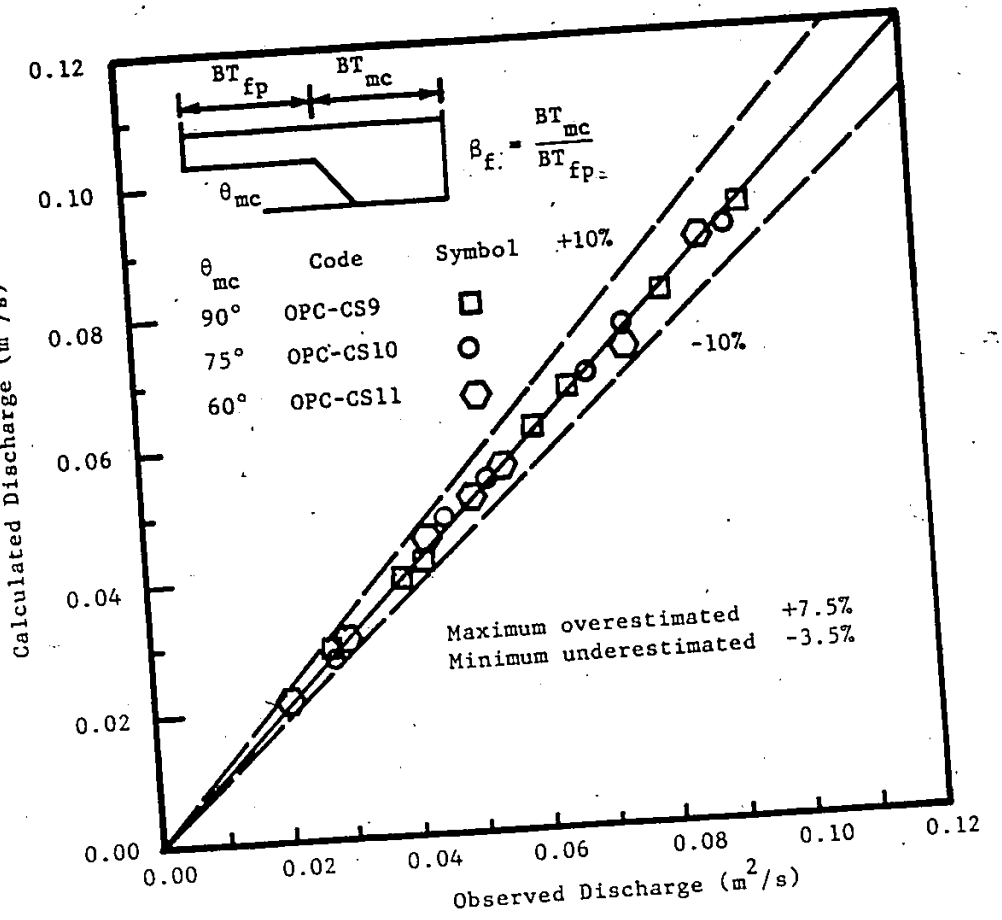

Fig. 6.23. Verification of Design Curve (Fig. 6.19) of 'E2' for Computation of Discharge of Compound Channels under Free Surface Flows with $\beta_f = 2.0$.

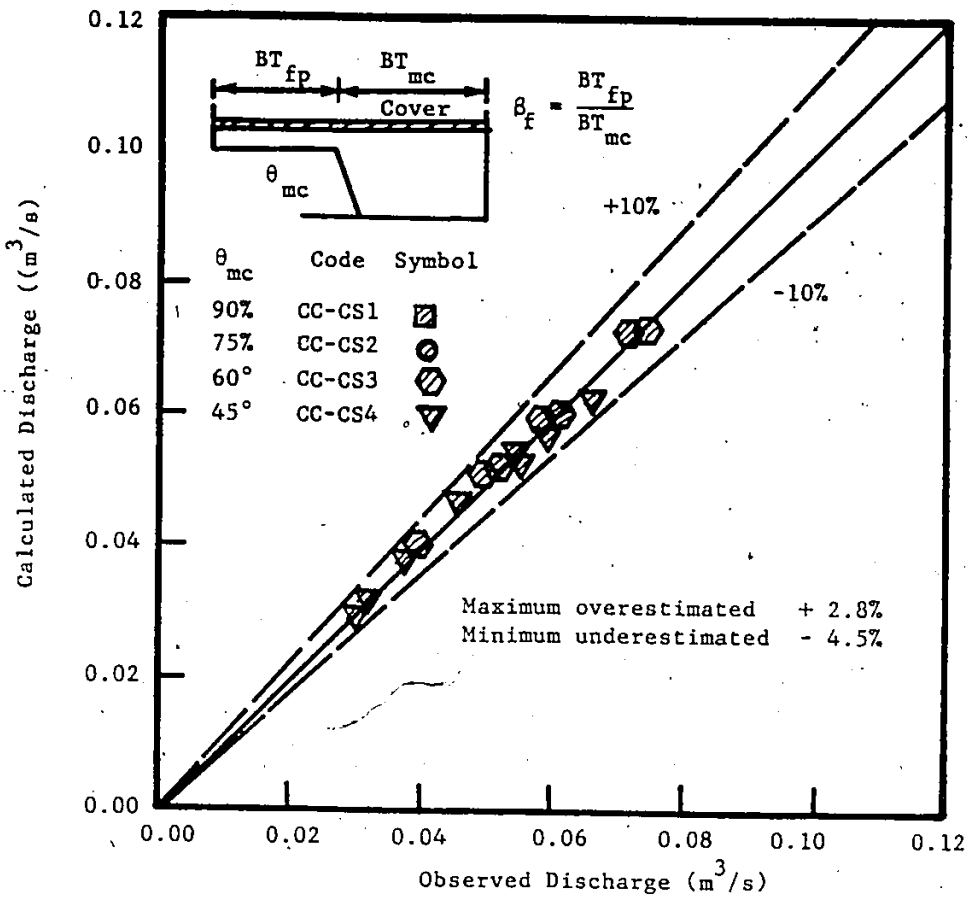

Fig. 6.24. Verification of Design Curve (Fig. 6.20) of 'E2' for Computation of Discharge of Compound Channels under Curved-Surface Flows with $\beta_f = 0.5$.

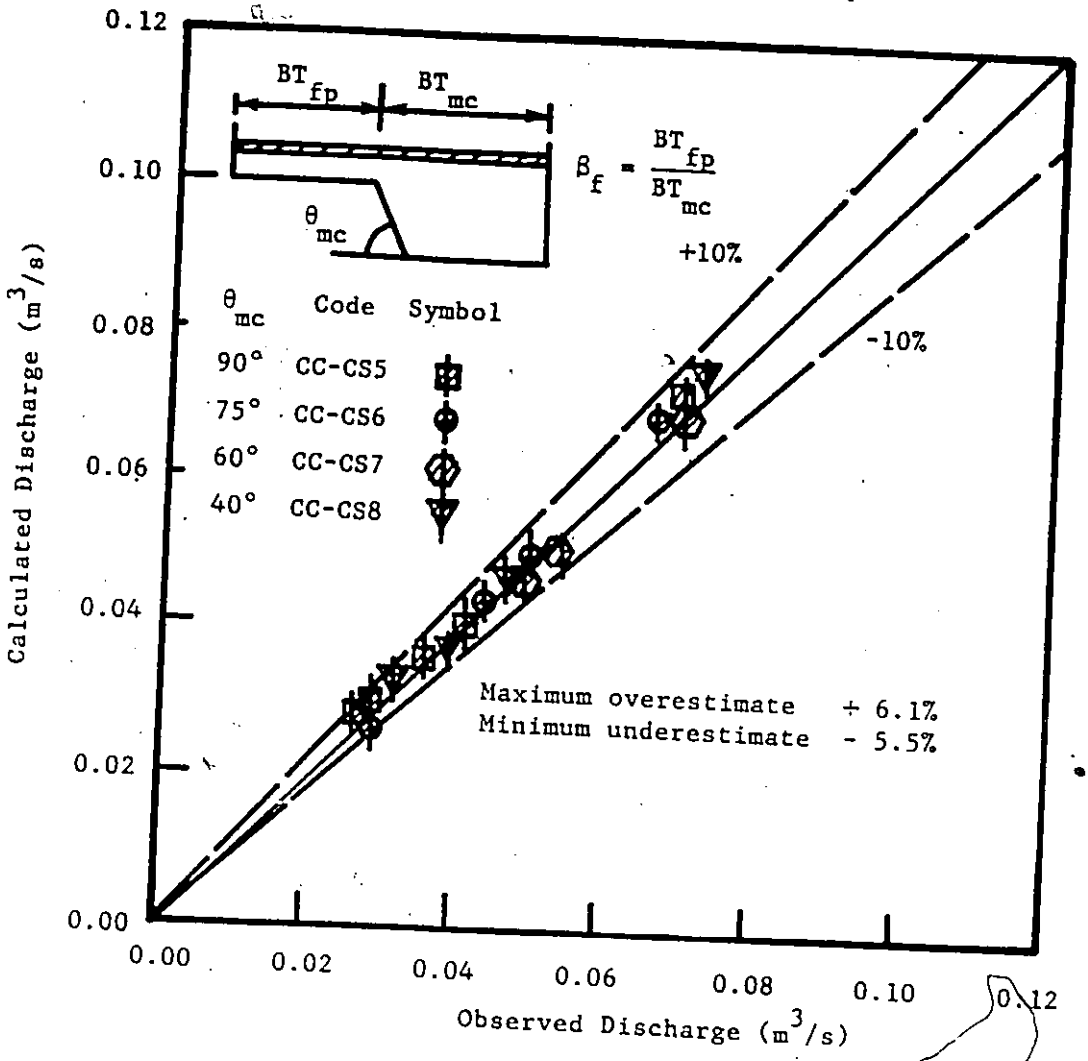

Fig. 6.25. Verification of Design Curve (Fig. 6.20) of 'E2' for Computation of Discharge of Compound Channels under Covered Surface Flows with $\beta_f = 1.0$.

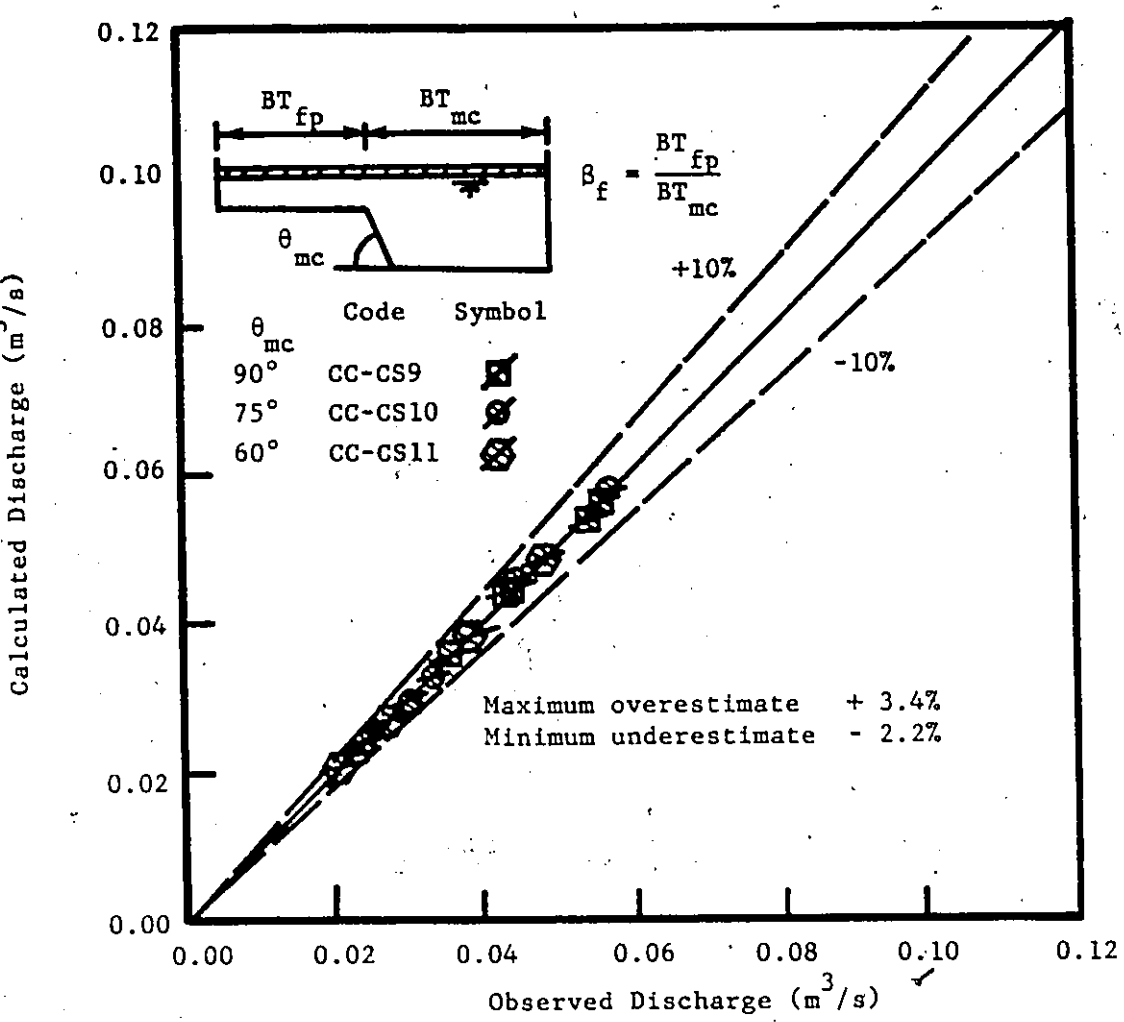

Fig. 6.26. Verification of Design Curve (Fig. 6.20) of 'E2' for Computation of Discharge of Compound Channels under Covered Surface Flows with $\beta_f = 2.0$.

between 0.965 to 0.995.

The values of shape factors ϕ_1, ϕ_2 and ϕ for each experimental channel flow are tabulated in Tables C.8 through C.13.

6.3 SHAPE EFFECT ON CHANNEL OVERALL RESISTANCE

Overall roughness, n, of an experimental channel was computed from the experimental discharge and corresponding energy slope of the entire channel by using Manning's equation. The computed roughnesses are furnished in Tables C1 to C3 for compound open channel flows; Tables C4 to C6 for compound covered-surface flows; and Table C7 for simple and/or complex 'cross-sectional' flows under covered-surface.

The shape effects on the overall channel roughness can be well observed if a single boundary roughness material is maintained for an entire channel cross-section. As such all the channel cross-sections with single boundary roughness materials are considered. Within the observed range of relative flow depth, like E2-values, composite roughnesses are also found fairly constant for the same shape and size of a channel cross-section. To verify the statement, the overall roughnesses are plotted against the Reynolds numbers in Figs. 6.27 to 6.29 for the compound channel with free-surface flows. The overall roughness is plotted in the form of the ratio of the overal roughness

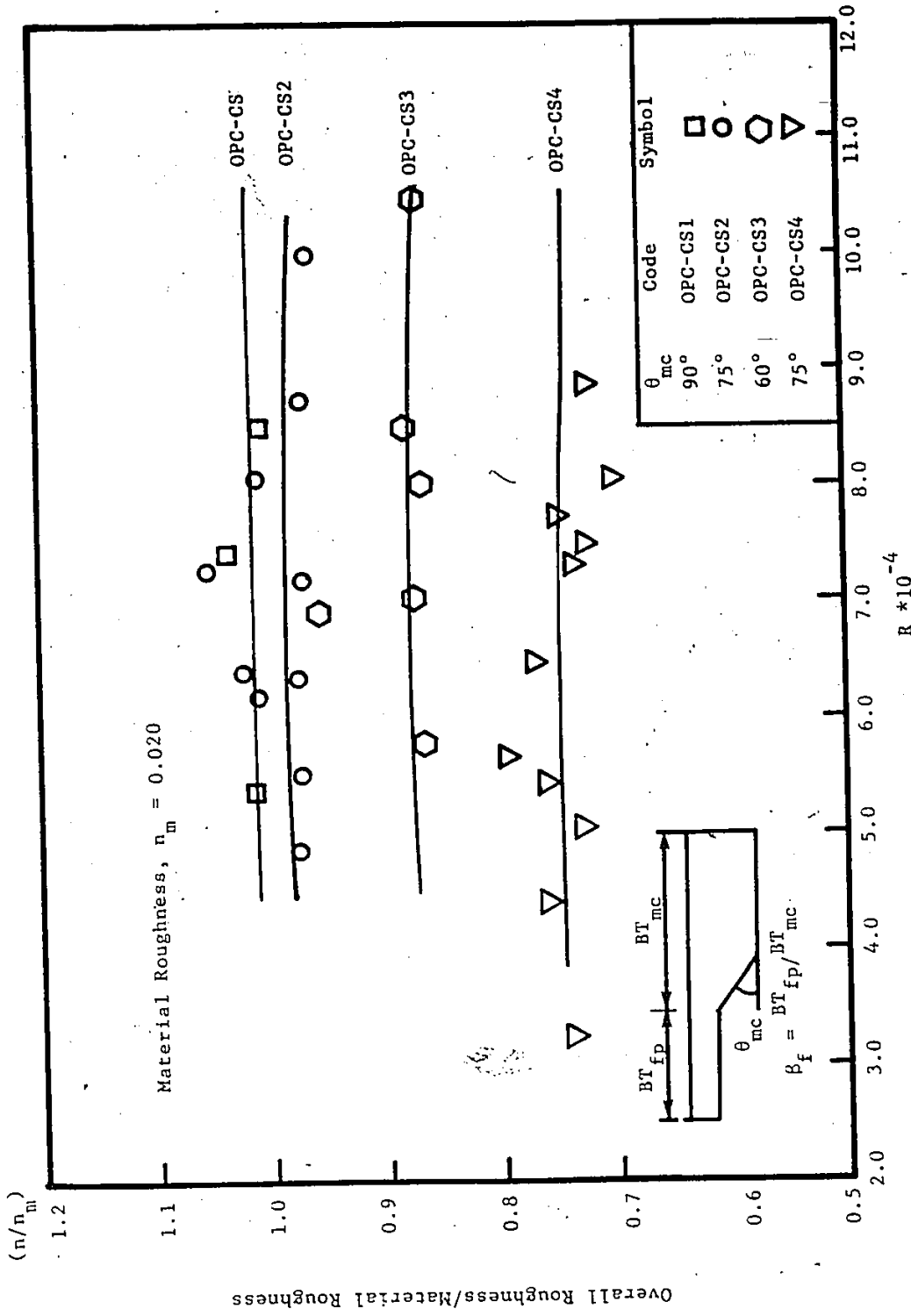

Fig. 6.27. Shape Effects on Overall Roughness, of Compound Channels Under Free-Surface Flows with β_f = 0.5 and Same Material Roughness.

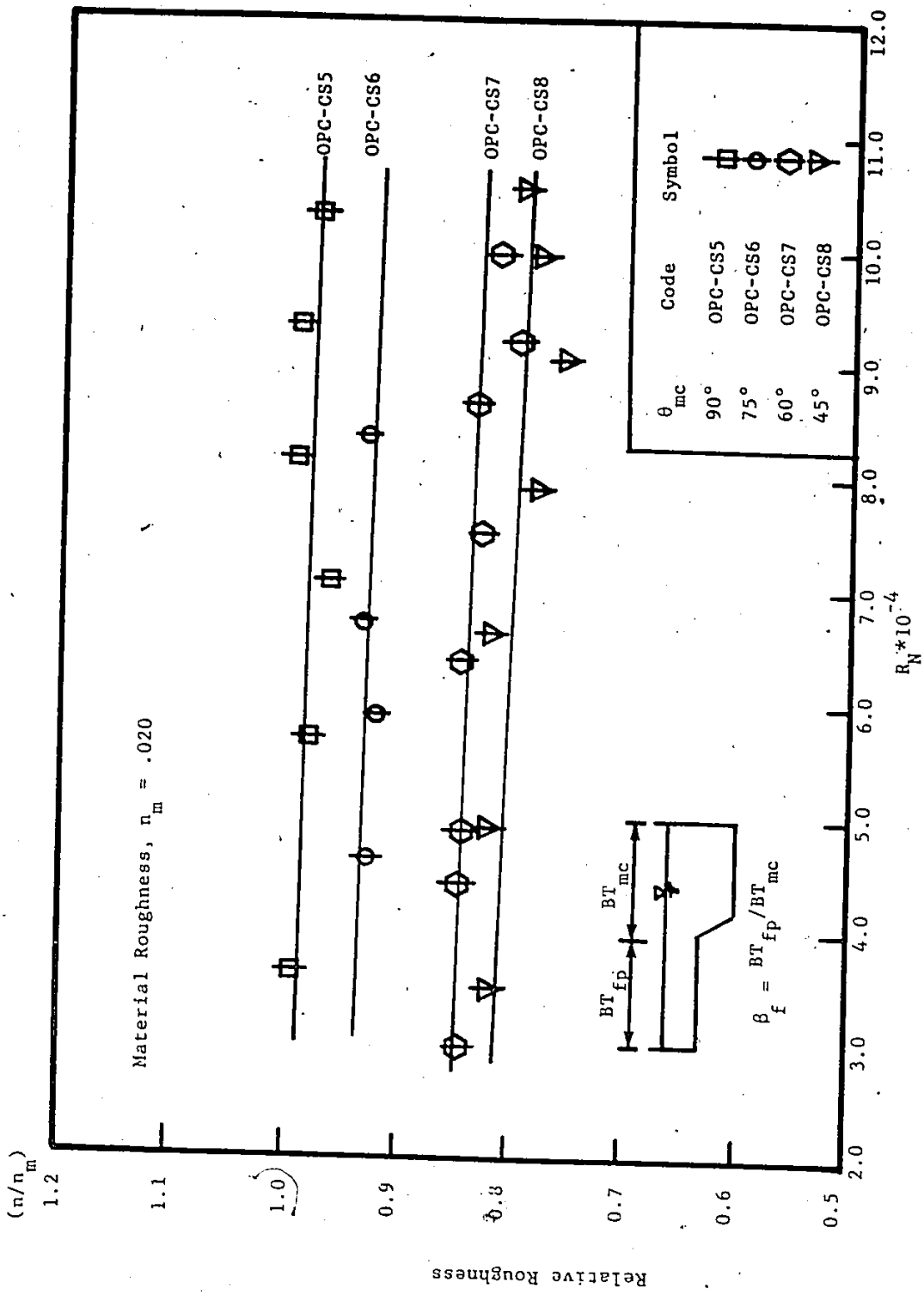

Fig. 6.28. Shape Effects on Overall Roughness of Compound Channels Under Free-Surface Flows with β_f = 1.0 and with Same Material Roughness.

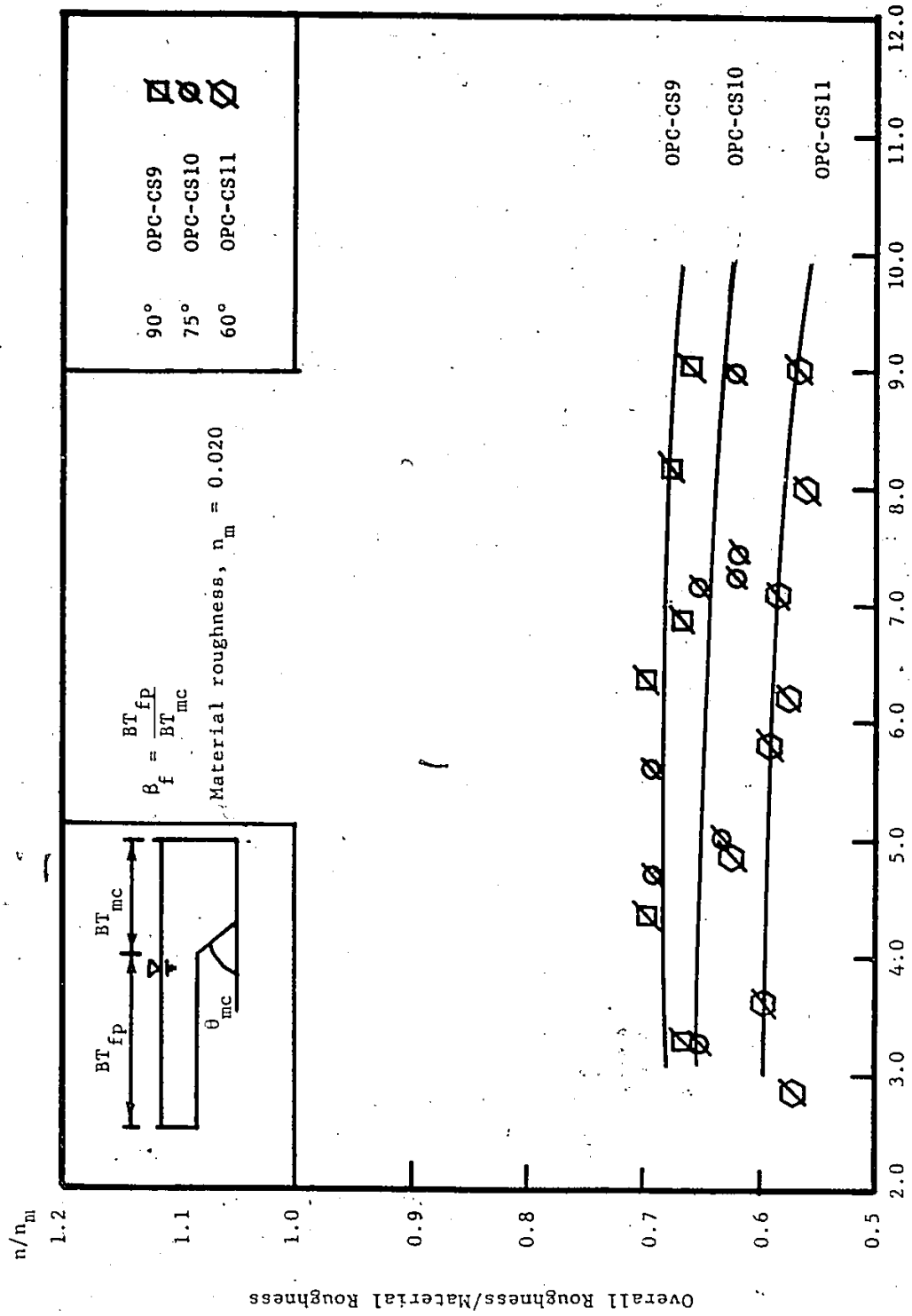

Fig. 6.29. Shape Effects on Overall Roughness by Compound Channels Under Free-Surface Flows with β_f=2.0 and with same Material Roughness.

to the material roughness, n_m.

It can be observed from the figures 6.27 to 6.29 that the compound channel of rectangular cross-section with the smaller relative top width attains maximum value of overall roughness and the ratio, n/n_m, is slightly over 1.0. The value is justified because the calibration value of the material roughness was determined from the simple rectangular channel flows. The trend of the shape of the roughness curves of the remaining cross-sections are very similar to those of E2-curves. At this point it can be said that the velocity coefficient, E2 is directly proportional to the overall roughness of the channel section.

Figure 6.30 shows the relation of the mean value of roughnesses in the form of ratio (n/n_m) of each channel cross-section with its corresponding shape factor, ϕ. Hence, if the channel cross-section and the relative top width of the flood plain are known, the overall roughness can be directly read out from the curves of Fig. 6.30, provided the boundary roughness of the entire channel cross-section remain the same.

Similar results are observed from Tables C4 to C6 in case of compound channels under covered-surface flows and, hence, the final results of the mean value of roughnesses in the form of ratio (n/nm) of each channel cross-section with its corresponding shape factor, ϕ, are presented in Fig. 6.31.

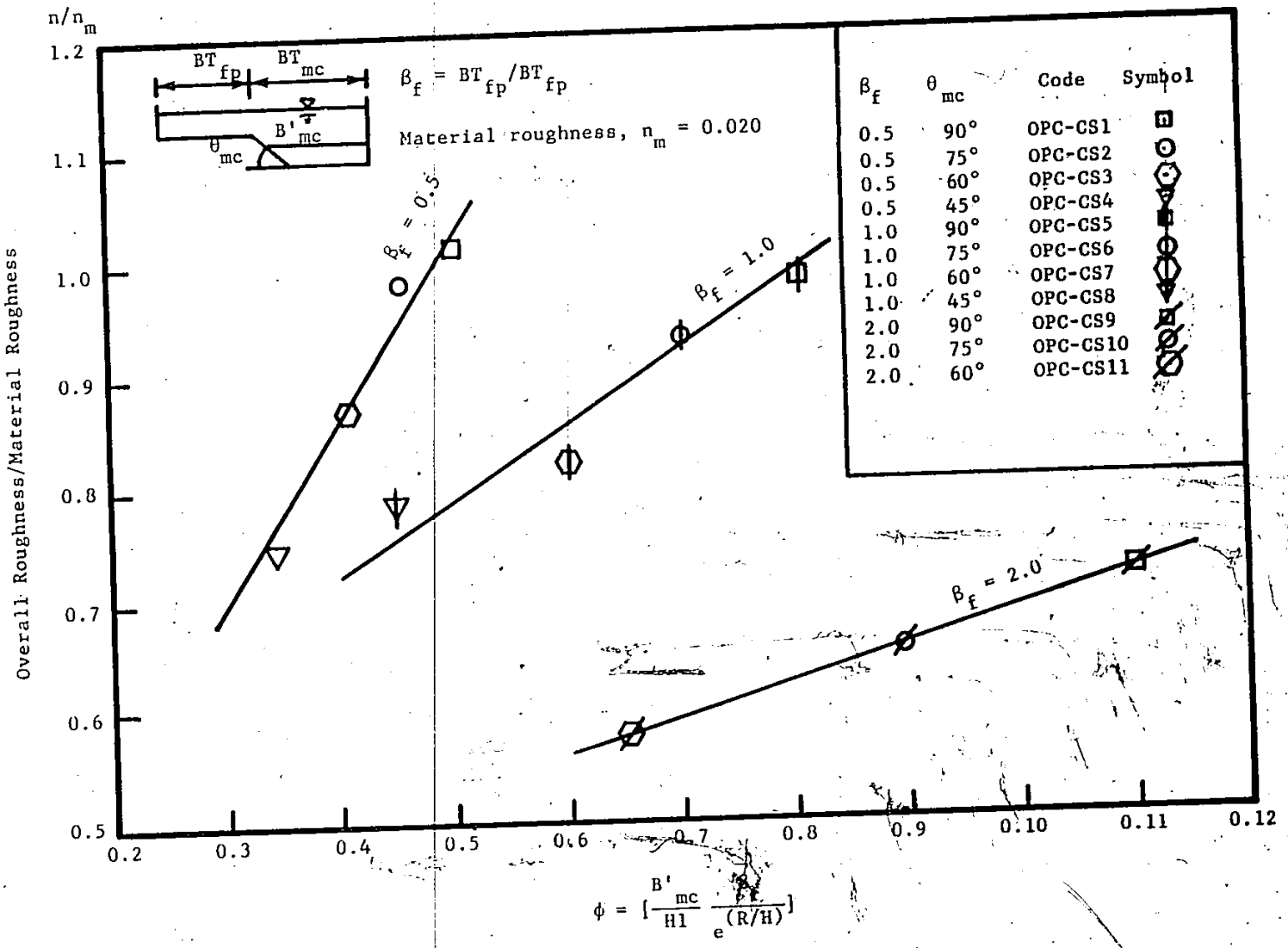

Fig. 6.30. Relationship Between Overall Roughness of Compound Channels under Free-Surface Flow and Shape Factor.

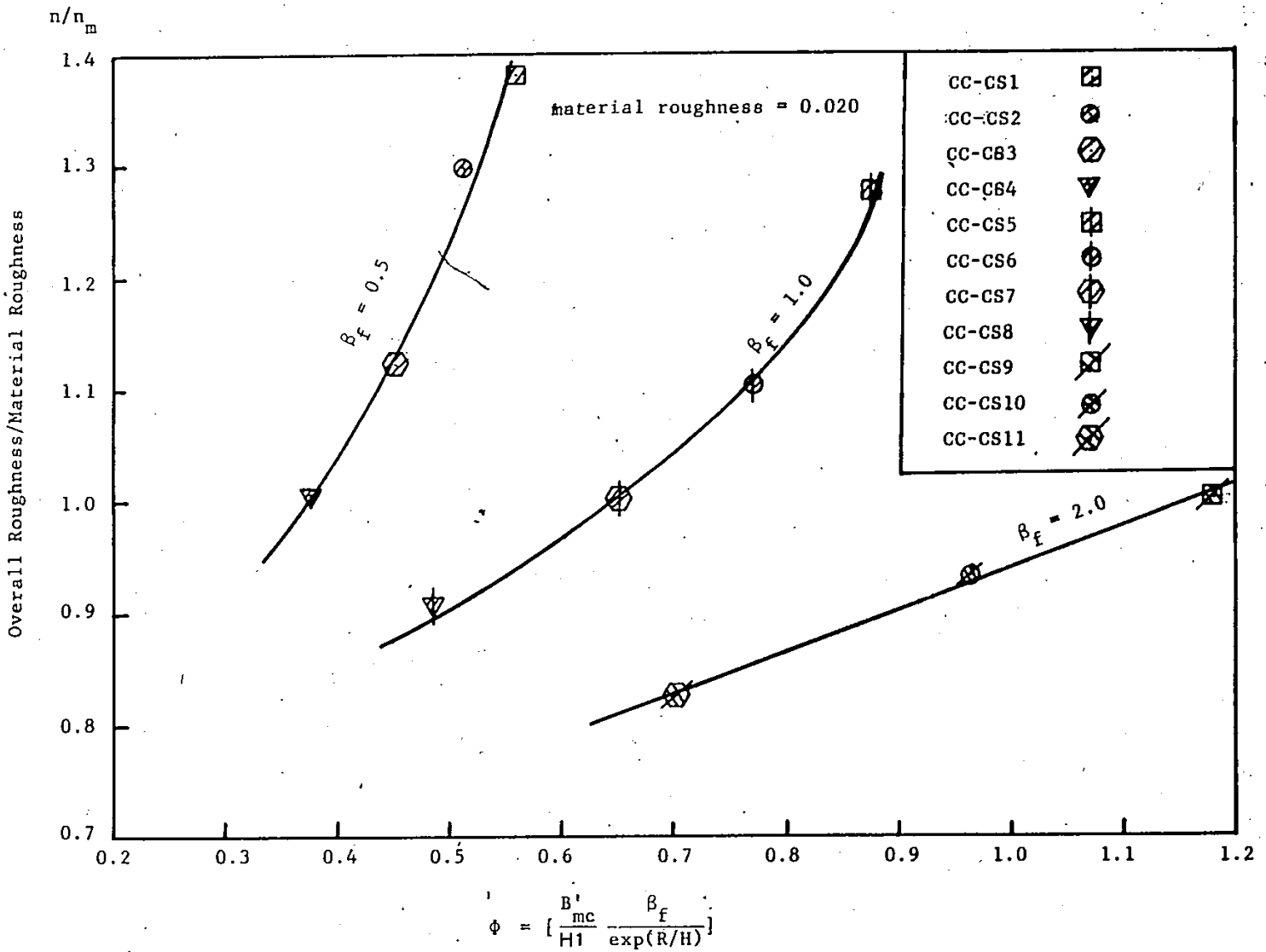

Fig. 6.31. Relationship Between Overall Roughness of Compound Channels Under Covered-Surface Flow and Shape Factors.

Hence, it can be concluded that both the channels' geometrical shape and the relative size of the flood plain to the main channel have tremendous effects on the determination of the overall or composite roughness of a compound channel cross-sections.

CHAPTER VII

APPLICATION OF THE METHOD AND COMPARISON WITH OTHER METHODS

7.1 INTRODUCTION

In case of natural stream flow in a compound channel cross-section, it is a frequently encountered problem in nature that the main channel bed slope is known and the properties of the stream cross-section are also available. Hence, for a given water elevation it is to be solved for the total discharge as well as flood plain discharge and main channel discharge rates.

In this chapter attempts have been made to solve this problem of the compound channel cross-sections under free-surface flows through several worked out examples by applying the proposed method. The results are compared with other methods, viz. 'Single Channel Method', 'Separate Channel Method (Conventional)', and 'Knight's Separate Channel Method (40)'.

As the E2-values are established for non-wide channels with one flood plain, examples are set up accordingly. However, in one case an attempt has been made to solve a problem of compound channel cross-section with two flood plains. For the determination of the velocity

coefficient E2 of a given channel cross-section, the proposed design curves of Figure 6.19 will be used.

7.2 SOLUTION OF THE PROPOSED MODEL

The solution steps of the proposed model, when the velocity coefficient E2 and the main channel bed slope are known, are almost alike to those which are described in Chapter IV for the determination of the velocity coefficients E1 and E2 for different flow conditions and for different types of analysis. Here, in the case where main channel bed slope and velocity coefficient E2 are available, the iterative process proceeds with an approximate value of the overall channel mean velocity and corrects it till the mean velocity satisfies the main channel bed slope. The first approximate value of the overall channel mean velocity can be determined from the summation of the initial strip flows using Manning's equation and assuming strip slopes are equal to that of given main channel bed slope. A generalized flow chart for the solution of the proposed model is shown in Figure 7.1. A generalized computer programme following the steps described in the flow chart (Fig. 7.1) is developed for a generalized prismatic channel cross-section and enclosed in Appendix E2. The programme can be used for both vertical and horizontal strip analysis as well as for only vertical strip analysis under both free-surface and covered surface flows. The generalized pris-

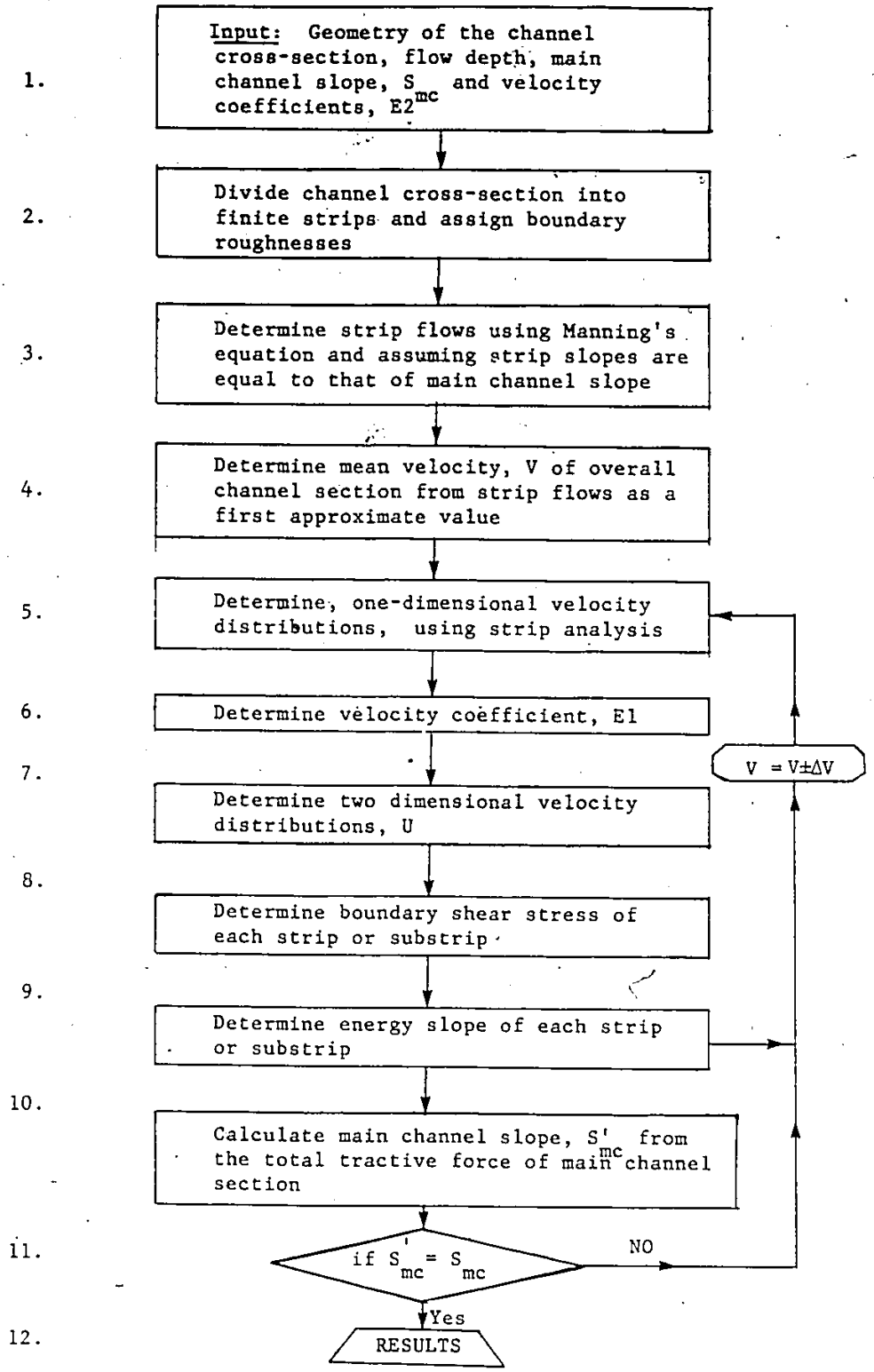

Fig. 7.1. Flow Chart for the Solution of the Proposed Method.

matic channel cross-section is shown in Figure 7.2.

7.3 EQUATIONS OF DISCHARGE FOR DIFFERENT METHODS

The equations for the determination of discharge of compound channel cross-sections by 'Single Channel' method, 'Conventional Separate Channel' method and Knight's Separate Channel' method are already described in Section 2.3.2 of Chapter 2. However, the equations which will be used for different methods, including the proposed method, are once again summarized below.

Proposed Method

Refer to Figure 7.3a.

$$Q = A_{mc} \frac{1}{n_{mc}} R_{mc}^{2/3} S_{mc}^{1/2} + A_{fp} \frac{1}{n_{fp}} R_{fp}^{2/3} S_{fp}^{1/2}$$

where

Q = total discharge

A = cross-sectional area

n = composite roughness

R = hydraulic radius

S = energy slope or bed slope.

Subscript 'mc' denotes main channel and 'fp' denotes flood plain. Notations without subscript are related with the overall channel cross-section.

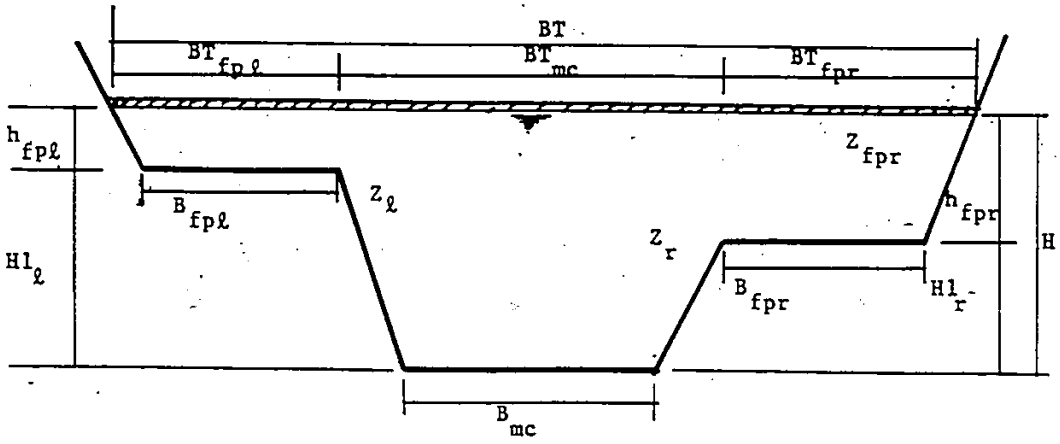

Fig. 7.2 Definition Sketch.

Given: $BT, B_{fp\ell}, B_{fpr}, H, Hl_\ell, Hl_r, Z_\ell, Z_r, Z_{fp\ell}, Z_{fpr}$.

Computation: $h_{fp\ell} = H-Hl_\ell$, $h_{fpr} = H-Hl_r$, $BT_{fp\ell} = B_{fp\ell}+Z_{fp\ell}h_{fp\ell}$,

$BT_{fpr} = B_{fp\ell}+Z_{fpr}h_{fpr}$, $BT_{mc} = BT-BT_{fp\ell}-BT_{fpr}$,

Areas: $A_{fp\ell} = (BT_{fp\ell}-0.5Z_{fp\ell}h_{fp\ell})h_{fp\ell}$,

$A_{fpr} = (BT_{fpr}-0.5Z_{fpr}h_{fpr})h_{fpr}$, $A_{mc} = BT_{mc}H-0.5(Z_\ell Hl_\ell^2+ Z\ Hl_r^2)$,

$A = A_{fp\ell} + A_{fpr} + A_{mc}$

Parameters: Covered-Surface:

$$P_{fp\ell} = BT_{fp\ell} + B_{fp\ell} + h_{fp\ell}(1 + Z_{fp\ell}^2)^{1/2}$$

$$P_{fpr} = BT_{fpr} + B_{fpr} + h_{fpr}(1 + Z_{fpr}^2)^{1/2}$$

$$P_{mc} = BT_{mc} + B_{mc} + Hl_\ell(1+Z_\ell^2)^{1/2} + Hl_r(HZ_r^2)^{1/2}$$

Free-Surface

$$P_{fp\ell} = P_{fp\ell}\ (\text{Cover}) - BT_{fp\ell}$$

$$P_{fpr} = P_{fpr}\ (\text{Cover}) - BT_{fpr}$$

$$P_{mc} = P_{mc}\ (\text{Cover}) - BT_{mc}$$

$$P = P_{fp\ell} + P_{fpr} + P_{mc}$$

Hydraulic Radius

$R_{fp\ell} = A_{fp\ell}/P_{fp\ell}$, $R_{fpr} = A_{fpr}/P_{fpr}$

$R_{mc} = A_{mc}/P_{mc}$, $R = A/P$

Special Cases

i) Compound channel with one flood plain (left) and rectangular section:

$B_{fpr} = 0.0$, $H_{lr} = H$, $Z_{\ell} = 0.0$, $Z_{r} = 0.0$, $Z_{fp\ell} = 0.0$,

$Z_{fpr} = 0.0$

Substituting these in the above equations, necessary equations of geometrical parameters can be determined.

ii) Simple Rectangular Cross-Section

$B_{fp} = 0.0$, $B_{fpr} = 0.0$, $Hl_{\ell} = H$, $Hl_{r} = H$, $Z_{\ell} = 0.0$,

$Z_{r} = 0.0$, $Z_{fpr} = 0.0$, $Z_{fp\ell} = 0.0$

Fig. 7.2 (Cont'd.)

Single Channel Method

Refer to Figure 7.3b,

$$Q = A\frac{1}{n}R^{2/3}S_{mc}^{1/2}$$

Conventional Separate Channel Method

Refer to Fig. 7.3c

$$Q = A_{mc}\frac{1}{n_{mc}}R_{mc}^{2/3}S_{mc}^{1/2} + A_{fp}\frac{1}{n_{fp}}R_{fp}^{2/3}S_{mc}^{1/2}$$

Knight's Separate Channel Method

Knight described his method in separating the flood plain zone from the main channel zone for the symmetrical compound channel of rectangular cross-section with two flood plains. Hence, his method of zonal separations in case of the compound channel cross-section other than the rectangular one and with one flood plain will be modified as shown in Figure 7.3d. The vertical centre line of the main channel will be determined by drawing a perpendicular to bisect the average width of the main channel.

The equation of discharge is the same as that of Conventional Separate Channel method with modifications for the areas of main channel and flood plain and the hydraulic radii thereof while the hydraulic perimeters remain unchanged.

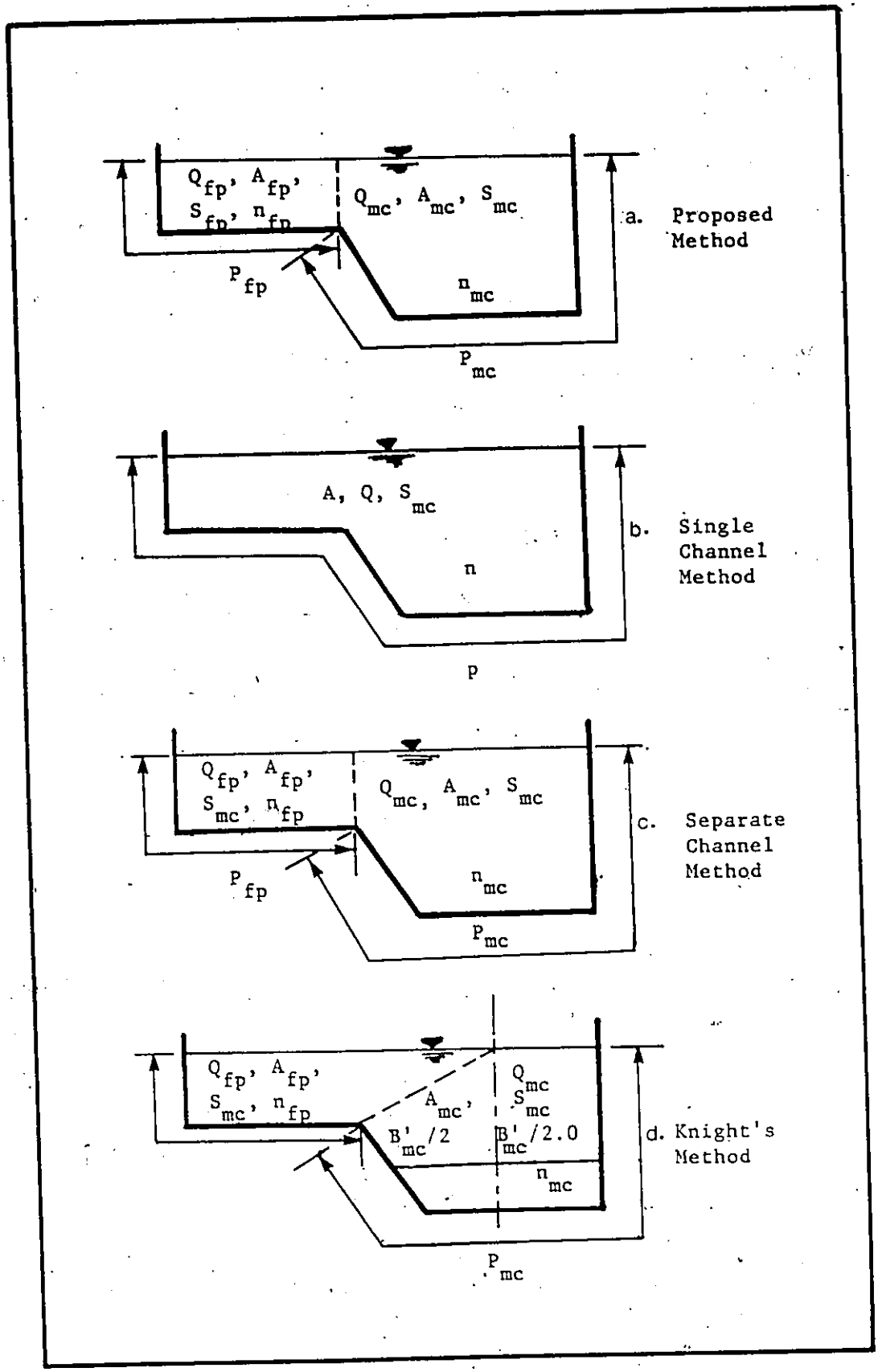

Fig. 7.3 Definition Sketch.

Composite Roughness

In all the cases except the proposed method, the composite roughness of the overall channel or the part of the channel will be calculated by the equations 2.14 and 2.15 as indicated in Chapter 2. The equations are:

$$n = \left(\frac{\sum_{i=1}^{N} P_i n_i^{3/2}}{P}\right)^{2/3} \qquad 2.14$$

and

$$n = \left(\frac{\sum_{i=1}^{N} P_i n_i^{2}}{P}\right)^{1/2} \qquad 2.15$$

7.4 WORKED OUT EXAMPLES

In all the worked out examples, the factors to be determined are described below:

(1) Overall channel discharge, friction slope and composite roughness.

(2) Main channel discharge, friction slope, and composite roughness.

(3) Flood plain discharge, slope, and composite roughness.

In all the cases overall channel will be denoted by 'OC', main channel by 'MC' and flood plain by 'FP'.

Problem No. 1

The compound channel cross-section is shown in Figure 7.4 and the main channel bed slope is 0.0009.

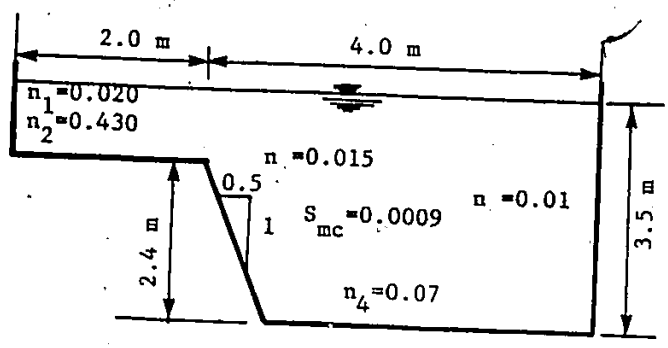

Fig. 7.4. Problem No. 1

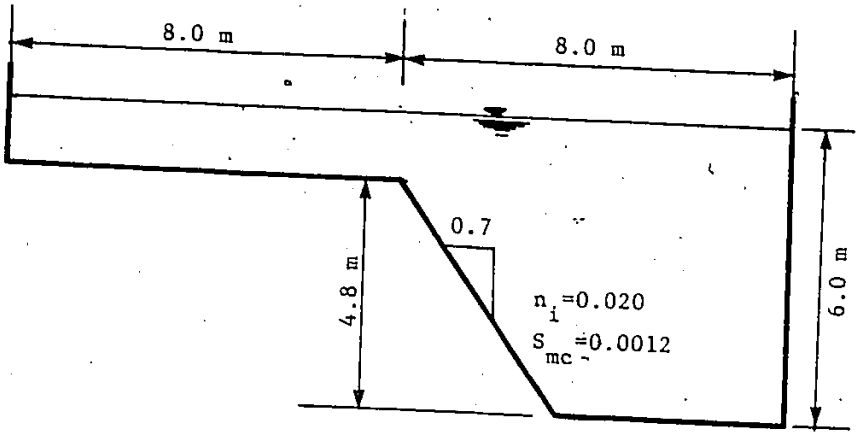

Fig. 7.5 Problem No. 2.

Solution

Geometrical properties of the channel, valid for all the methods except Knight's method, are:

Description	OC	MC	FP
Area, m^2	14.76	12.56	2.20
Perimeter, m	12.08	8.98	3.10
Hyd. Radius, m	1.2215	1.3982	0.71

A. Results of Proposed Method

Determination of the Velocity Coefficient, E2

$$\phi_1 = R/H = \frac{1.2215}{3.5} = 0.349$$

$$\phi_2 = \frac{\beta'_{mc}}{H1} = \frac{3.4}{2.4} = 1.4167$$

$$\beta_f = BT_{fp}/BT_{mc} = 0.5$$

therefore,

$$\phi = \phi_2 \beta_f / e^{\phi_1} = 0.5$$

$$\alpha_f = h_{fp}/H = 0.314$$

Hence, from the curve $\beta_f = 0.5$ of Figure 6.19,

E2 = 1.165

Results

Description	OC	MC	FP
Flow, m^3/s	29.63	26.48	3.15
Roughness, n	0.02217	0.0178	0.0282
Slope, S	0.00152	0.0009	0.00504

B. Results of Single Channel Method

Composite Roughness of Overall Channel

from equation 2.14, n = 0.0183
from equation 2.15, n = 0.0189

therefore,

average n = 0.0186

$$\text{overall discharge } Q = 14.76\frac{(1.2215)^{2/3}(.0009)^{1/2}}{.0186}$$

$$= 27.20 \ m^3/s.$$

C. Results of Separate Channel Method

Description	OC	MC	FP
Flow m^3/s	33.35	31.31	2.04
Comp. Roughness	0.0152	0.01505	0.0258
Slope	0.0009	0.0009	0.0009

D. Knight's Method

Geometrical Properties

Area m^2	14.76	11.295	3.465
Perimeter, m	12.08	8.98	3.10
Hyd. Radius, m	1.2215	1.0742	1.1177

Results

Description	OC	MC	FP
Flow, m^3s	27.95	23.61	4.34
Comp. roughness	0.0182	.01505	0.0258
Slope	0.0009	.0009	0.0009

E. Comparison of Method

i) Discharge (m^3/s)

	Proposed Method	Single Channel	Separate Channel	Knight's Method
Main channel	26.48	-	31.31(+18.24)	23.61(-10.8)
Flood plain	3.15	-	2.04(-35.24)	4.34(+37.77)
Overall channel	29.63	27.20(-8.42)	33.35(+12.55)	27.95(- 5.67)

ii) Composite Roughness

	Proposed Method	Single Channel	Separate Channel	Knight's Method
Main channel	0.0178	-	.01505(-15.45)	.01505(-15.45)
Flood plain	0.0282	-	.0258(-8.51)	.0258(-8.51)
Overall channel	0.02217	.0186(-16.1)	.0152(-31.44)	.0182(-17.91)

iii) Energy Slope

In all the methods, except the Proposed Method, energy slope is the same for flood plain, main channel and overall channel and is equal to the main channel bed slope.

(N.B. Figures in parenthesis are percentage differences with the Proposed Method).

Problem No. 2

The compound channel cross-section with flood plain/main channel ratio (β_f):1, and main channel bed slope of 0.0012 is shown in Figure 7.5. The roughnesses of main channel boundary and flood plain boundary are same and equal to 0.020.

Solution

Geometrical properties for all the methods except for Knight's method.

Description	OC	MC	FP
Area, m^2	49.536	39.936	9.60
Perimeter, m	25.70	16.50	9.20
Hyd. Radius, m	1.928	2.42	1.043
Knight's Method			
Area, m^2	49.536	37.036	12.50
Perimeter, m	25.70	16.50	9.20
Hyd. Radius, m	1.928	2.245	1.359

Determination of E2-value for the Proposed Method

$$\phi_1 = R/h = .3213$$

$$\phi_2 = \frac{B'_{mc}}{H1} = \frac{6.32}{4.8} = 1.317$$

$$\beta_f = 1.0$$

$$\phi = \phi_2 \beta_f / e^{\phi_1} = .725$$

From β_f= 1.0 curve of Figure 6.19,

E2 = 1.05

From the solution, the velocity coefficient, E1 = 1.0124.

The comparison of results of the different methods are described below:

Comparison of Results

i) Discharge

	Proposed Method	Single Channel	Separate Channel	Knight's Method
Main channel	124.55	-	124.66(0.0)	109.98(-11.7)
Flood plain	28.00	-	17.11(-38.9)	26.57(-5.1)
Overall channel	152.55	132.89(-12.9)	141.76(-7.2)	136.55(-10.5)

ii) Composite Roughness

	Proposed Method	Single Channel	Separate Channel	Knight's Method
Main channel	0.01968	-	0.02(+1.6)	0.02(+1.6)
Flood plain	0.0199	-	0.02	0.02
Overall channel	0.02067	0.02(-32.4)	-	-

iii) Energy Slope

	Proposed Method	Single Channel	Separate Channel	Knight's Method
Main channel	0.0012	-	0.0012	0.0012
Flood plain	0.00372	-	0.0012	0.0012
Overall channel	0.00169	0.0012	0.0012	0.0012

(N.B. Figures are within parenthesis are percentage difference with Proposed Method).

Problem No. 3

This is an example of compound channel with two flood plains. The channel section is shown in Figure 7.6. The main channel bed slope is equal to 0.0002.

Solution

Geometrical properties for all the methods except for Knight's method.

Description	OC	MC	FP(L)	FP(R)
Area, m^2	58.8	42.0	8.4	8.4
Perimeter, m	32.0	17.20	7.4	7.4
Hyd. Radius, m	1.838	2.412	1.135	1.135
Knight's Method				
Area, m^2	58.8	37.8	10.5	10.5
Perimeter, m	32.0	17.20	7.4	7.4
Hyd. Radius, m	1.838	2.198	1.42	1.42

FP(L) - left hand side flood plain
FP(R) - right hand side flood plain

Determination of E2-Value for the Proposed Method

In this case the equivalent flood plain width is considered equal to the average width of the two flood plains. This is a symmetrical channel. Hence, the equilvalent one-flood plain channel is shown in Figure 7.6a.for the calculation of shape factors. Therefore, $\beta_f = 6/6 = 1.0$, $A = 50.4m^2$, $P = 24.6$ m

$$\phi_1 = R/H = 2.0488/5.6 = .3659$$

$$\phi_2 = \frac{\beta'_{mc}}{H1} = 6.0/5.6 = 1.6714$$

therefore,

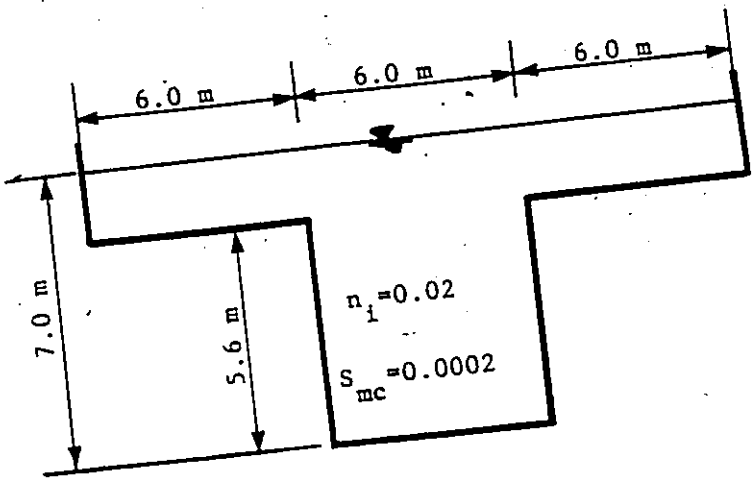

Fig. 7.6 Problem No. 3.

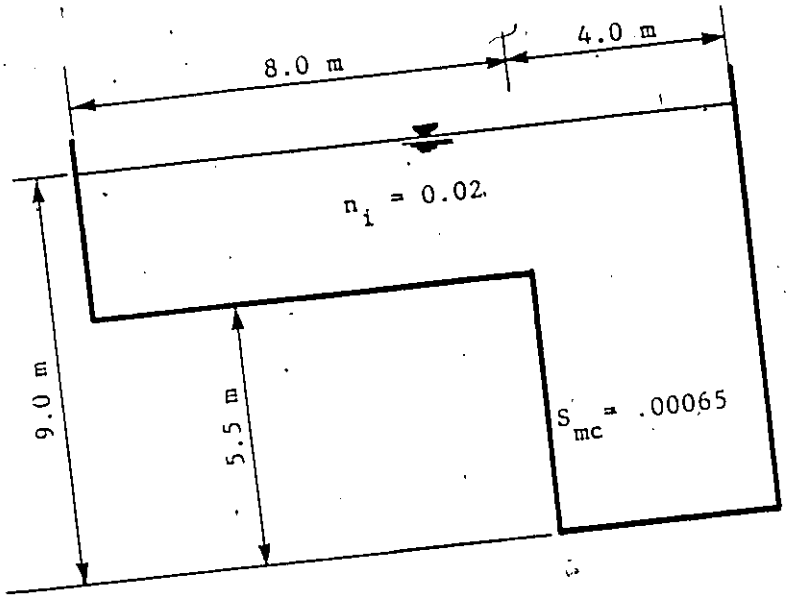

Fig. 7.7. Problem No. 4.

$$\phi = \phi_2 \beta_f / e^{\phi_1} = .743$$

From the $\beta_f = 1.0$ curve of Figure 6.19, E2 = 1.07

The comparison of results are described below:

Comparison of Results

i) Discharge

	Proposed Method	Single Channel	Separate Channel	Knight's Method
Main channel	56.08	-	53.41(-4.8)	45.19(-19.4)
Flood plain (2)	7.62	-	6.46(-15.2)	9.38(+16.2)
Overall channel	71.33	62.38(-12.5)	66.33(-7.0)	63.95(-10.4)

ii) Composite Roughness

	Proposed Method	Single Channel	Separate Channel	Knight's Method
Main channel	0.0182	-	0.02	0.02
Flood plain (2)	0.0199	-	0.02	0.02
Overall channel	0.02125	0.02(-5.9)	-	-

(iii) Energy Slope

	Proposed Method	Single Channel	Separate Channel	Knight's Method
Main channel	0.00022	-	0.0002	0.0002
Flood plain (2)	0.00055	-	0.0002	0.0002
Overall channel	0.0003	0.0002	0.0002	0.0002

Problem No. 4

The compound channel cross-section with flood plain/main channel ratio (β_f):2, and main channel bed slope of 0.00065 is shown in Figure 7.7. The roughnesses of main channel boundary and flood plain boundary are same and equal to 0.020.

Solution

Geometrical properties for all the methods except for Knight's method.

Description	OC	MC	FP
Area, m^2	64.0	36.0	28.0
Perimeter, m	30.0	18.50	11.50
Hyd. Radius, m	2.133	1.95	2.43

Knight's Method

Area, m^2	64.0	31.50	32.50
Perimeter, m	30.0	18.50	11.50
Hyd. Radius, m	2.133	1.703	2.826

Determination of E2-Value for the Proposed Method

$\alpha_f = 0.389$

$\beta_f = 2.0$

$\phi_1 = 2.13/9 = 0.237$

$\phi_2 = 4/5.5 = 0.727$

$\phi = 1.148$

From the $\beta_f = 2.0$ curve of Figure 6.19, E2 = 0.76.

The comparison of results are described below:

Comparison of Results

(i) Discharge

	Proposed Method	Single Channel	Separate Channel	Knight's Method
Main channel	101.25	-	71.53(-29.4)	57.20(-43.5)
Flood plain	76.91	-	64.6(-16.0)	82.80(+7.6)
Overall channel	178.16	135.18(-24)	136.13(-23.6)	140.80(-21.0)

(ii) Composite Roughness

	Proposed Method	Single Channel	Separate Channel	Knight's Method
Main channel	0.0137	-	0.02	0.02
Flood plain	0.1405	-	0.02	0.02
Overall channel	0.1435	0.02	-	-

(iii) Energy Slope

	Proposed Method	Single Channel	Separate Channel	Knight's Method
Main channel	0.00065	-	0.00065	0.00065
Flood plain	0.00049	-	0.00065	0.00065
Overall channel	0.00058	0.00065	0.00065	0.00065

7.5 DISCUSSION OF RESULTS

From the workout examples of the previous section, the following observations can be made:

1. In all the cases the relative flow depth of the flood plains, α_f, is above 0.2.

2. With smaller relative top width, β_f(=0.5), the estimated total discharge by proposed method is well within that estimated by the single channel method and separate channel method and close to Knight's method. The single channel and Knight's method underestimates, while the separate channel method overestimates the value. The percentage difference is below ±15%. But the difference is as high as ±38% in case of estimation of flood plain or main channel discharge.

3. In the case of equal flood plain and main channel top width (β_f=1) all the methods underestimate the total discharge by -15%, while the difference is as high as ±38% in estimation of flood plain or main channel discharge.

4. As the relative top width is getting larger in width β_f=2.0 the underestimation by the other methods is as high as 25% and the differences in estimation of main channel or flood plain discharge is as high as 43%.

5. Estimation by Knight's method is always within

that of single channel and separate channel methods. Many researchers, including Knight, concluded that separate channel method overestimates and single channel method underestimates the total discharge.

6. The statement in observation 5 is not always true. Ervine and Baired (23) compared their experimental results of asymmetrical channel with one flood plain (β_f=1.0) with single channel method, separate channel method and other methods (Fig. 7 of Ref. 23). It can be observed that both the methods underestimate when the relative flow depth is above 0.1. The difference increases with the increase of relative flow depth, α_f. The statement of observation 5 is only true for α_f below 0.1.

7. The author compared his experimental results for a rectangular (θ_{mc}=90°, θ_{fp}=90°), and asymmetrical channel with both single channel method and separate channel method in Fig. 7.8. From the figure it is clear that in all the cases both the methods underestimate the total discharge. The percentage difference is very high (35%) in case of β_f=2.0 while it is below 15% in case of β_f=0.5 and β_f=1.0

8. The result for β_f=0.5 of observation 7, contradicts the statement of observation 2. The discrepancies are quite possible because one is derived from the design curve and the other one is from the experimental results. But the discrepancies are in the border line.

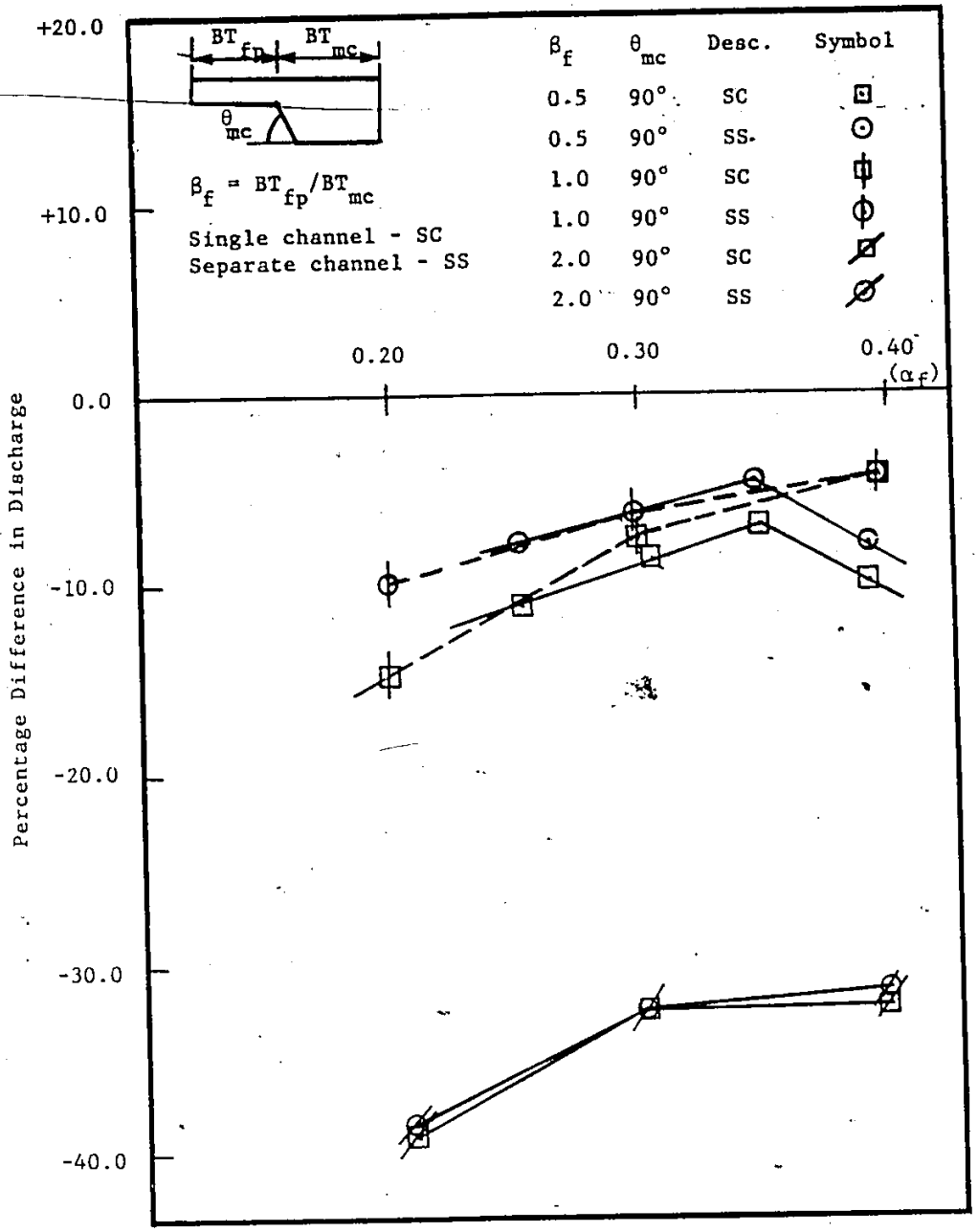

Fig. 7.8. Comparison of Experimental Discharge with that of Single Channel Method and Separate Channel Method.

CHAPTER VIII

CONCLUSIONS AND RECOMMENDATIONS FOR FUTURE RESEARCH

8.1 GENERAL

The central idea of the present study was to predict flood discharge of a compound channel cross-section by an improved method, where Manning's equation can be used after due correction for the momentum transfer phenomenon.

In the present theoretical investigation the parameter "energy slope" was conceptually considered as a correction factor to Manning's equation for the computation of flood discharge of a compound channel. The reason behind this concept is that, due to the existence of differential boundary conditions such as comparatively higher roughness and smaller flow depth in flood plain of a compound channel cross-section with rigid boundary, the flow is in "quasi-uniform" state and not strictly conforming to the "classical uniform" flow concept. For the simplification of the complexities of the solution of Reynolds' form of Navier Stokes equation in its three-dimensional domain the flow equation is first developed in one-dimensional form. The two-dimensional velocity equation for any elementary fluid

within the turbulent zone of flow was proposed on the basis of the concept that the flow is in a quasi-uniform state. It was also found that the composite roughness or the overall roughness of any part of the entire channel cross-section changes from one section to another due to their change of energy slopes within the same cross-section.

In the present method of computation the prediction of discharge is not the direct application of Manning's equation with the correction of energy slope. The application of Manning's equation is an indirect process whereas discharge is computed directly by integrating the local velocities of all the elementary fluid flows over the desired cross-section. In the course of developing the velocity profiles, the energy slope is the result of the equality of boundary shear force over the wetted perimeter of the desired cross-section with the total tractive force of the said cross-section. While the boundary shear stress distributions are the indirect solution of the two-dimensional velocity profile, the composite roughness of the concerned channel cross-section is computed from the direct application of Manning's equation.

From the above discussion it is clear that the whole process of predicting discharge is dependent on the development of the correct velocity distributions. Therefore, in the theoretical investigation a two-dimensional velocity

profile equation was proposed and the main goal of the present study was to establish this equation by computing the two unknown velocity coefficients, E1 and E2.

The analytical solution for two velocity components was carried out using the experimental data. Extensive laboratory investigations were executed with a wider range of channel shapes, sizes and flow rates under both free-surface and free-buoyant surface conditions.

8.2 CONCLUSION

From the observations of the result furnished in Chapter VI and Chapter VII, it can be concluded that:

1. The present theory and the computational method is applicable for the flow in "quasi-uniform" state only and not strictly conforming to "classical uniform" flow.

2. It has already been mentioned that only one out of the two unknown velocity coefficients (E1 or E2) is to be known for the solution of the proposed velocity profile equation. The coefficient E1 is found insensitive to the change of shape, size or flow rate of a channel cross-section. On the other hand, the coefficient, E2, is very sensitive to the change of shape (θ_{mc}), relative size of the flood plain (β_f)

3. Although the method of computation is an iterative one, the advancement of micro-computer technology greatly facilitates its solution.

4. The present method can be considered to be a general one and can be applied to a wider range of channel cross-sections. Also the method provides information on the flow characteristics such as velocity profiles, boundary shear stress distributions and composite roughness.

8.3 RECOMMENDATIONS FOR FUTURE RESEARCH

The application of the proposed theory in the area of compound channel alone is manifold. A few of them can be mentioned as below:

1. Experiments should be conducted on a wider range of compound sections with two or more flood plains.

2. The effects of higher roughness values on the flood discharge and the effects of multiple roughness should also be examined.

3. The experiments should be conducted in larger laboratory models.

4. The application of the method should be examined from very wide channel to very deep channel as well.

5. The laboratory investigation should be compared with a field study, especially in the case of ice-covered streams in nature.

APPENDIX A

Continuity Equation of Strip Flow

APPENDIX A1

Continuity Equation of Strip Flow

Integration of equation 3.31a in Chapter III

$$\int_{A_s} u_s dA_s = A_s V_s$$

Refer to Figure 3.8.

Substituting $A_s = ds.H_s$ and $dA_s = dsdh_s$ and rearranging equation 3.31a can be written as:

$$\frac{1}{H_s} \int_0^{H_s} U_s dh_s = V_s \qquad \text{A1.1}$$

denoting $\epsilon_s = h_s/H_s$ and thereby $H_s d\epsilon_s = dh_s$, equation A1.1 is reduced to:

$$\int_0^1 u_s d\epsilon_s = V_s \qquad \text{A1.2}$$

as at $h_s=0$, $\epsilon_s=0$ and at $h_s=H_s$, $\epsilon_s=1$.

From equation 3.30 u_s can be substituted in equation A1.2 and by rearranging left hand side of equation A1.2 can be written as,

$$\int_0^1 u_s d\epsilon_s$$

$$= \underbrace{\left[2 \int_0^1 (1-\epsilon_s)^{1/2} d\epsilon_s\right.}_{I} - \underbrace{\left.\int_0^1 \mathrm{Ln}\frac{(1+\epsilon_s)}{1-(1-\epsilon_s)^{1/2}} d\epsilon_s\right]}_{II}$$

$$+ \underbrace{\int_0^1 d\epsilon_s}_{III} \qquad \text{A1.3}$$

Integration of term I

$$2\int_0^1 (1-\epsilon_s)^{1/2} d\epsilon_s$$

$$= 2[-\frac{(1-\epsilon_s)^{3/2}}{3/2}]_0^1$$

$$= 2 * \frac{2}{3}$$

$$= 4/3$$

Integration of term II

$$\int_0^1 \text{Ln} \frac{1+(1-\epsilon_s)^{1/2}}{1-(1-\epsilon_s)^{1/2}} d\epsilon_s$$

$$= \int_0^1 \text{Ln}[\frac{1+(1-\epsilon_s)^{1/2}}{\epsilon_s}] d\epsilon_s$$

$$= 2\int_0^1 \underbrace{\text{Ln}[1+(1-\epsilon_s)^{1/2}] d\epsilon_s}_{\text{IIa}} - \int_0^1 \underbrace{\frac{\text{Ln}\epsilon_s \, d\epsilon_s}{\text{IIb}}}$$

Integration of term IIa

$$2\int_0^1 \text{Ln}[1+(1-\epsilon_s)] d\epsilon_s$$

denoting $x^2 = 1-\epsilon_s$ and thereby $2xdx = -d\epsilon_s$

the term IIa can be written as:

$$-4\int_1^0 [\text{Ln}(1+x)](x)dx$$

as at $\varepsilon_s=0$; $x=1$ and $\varepsilon_s=1$; $x=0$

which can further be written,

$$4\int_0^1 [Ln(1+x)xdx$$

$$= [(Ln(1+x)\ \frac{x^2}{2})^1 - \int_0^1 \frac{x^2}{2}\ \frac{1}{1+x}dx]$$

by applying the integration rule, $\int uvdx$

$$= u\int vdx - \int(\int vdx)u'dx)$$

$$= \frac{4}{2}[(x^2Ln(1+x))^1 - \int_0^1 \frac{(x^2-1)+1}{x+1}dx]$$

$$= 2[Ln2 - \int_0^1 (x-1) + \frac{1}{x+1}\ dx]$$

$$= 2[Ln2 - \{\frac{x^2}{2} - x+Ln(x+1)\}_0^1]$$

$$= 2[Ln2 + \frac{1}{2} - Ln2]$$

$$= 1$$

Integration of term IIb

$$\int_0^1 Ln\varepsilon_s d\varepsilon_s$$

$$= [\varepsilon_s Ln\varepsilon_s - \varepsilon_s]_0^1$$

$$= [-1 - (\lim_{\varepsilon_s \to 0} \frac{Ln\varepsilon_s}{1/\varepsilon_s} - 0)]$$

$$= -1 - \lim_{\varepsilon_s \to 0} \frac{1/\varepsilon_s}{1/\varepsilon_s^2}$$

$$= 1 - \lim_{\varepsilon_s \to 0} (-\varepsilon_s)$$

$$= -1$$

Therefore, the solution of term II is:

$$\int_0^1 \text{Ln} \frac{1+(1-\varepsilon_s)^{1/2}}{1-(1-\varepsilon_s)^{1/2}} d\varepsilon_s$$

$$= 1 - (-1)$$

$$= 2$$

Integration of term III is

$$C_s \int_0^1 d\varepsilon_s = C_s$$

Substituting the solutions for the term I, II and III in equation A1.3 it can be written as:

$$\int_0^1 u_s d\varepsilon_s = -\frac{2}{3} \frac{V_{*s}}{\kappa} + C_s$$

Substituting the above into equation A1.2, the integration constant C_s can be obtained:

$$C_s = V_s + \frac{2}{3} \frac{V_{*s}}{\kappa} \qquad \text{A1.4}$$

APPENDIX A2

Equations of Division Surface and Composite Roughness

A2.1 Division Surface

Solution of equation 3.38

$$V_{1s} - V_{2s} = \frac{2}{3\kappa}(V_{*2s} - V_{*1s}) \qquad \text{A2.1}$$

Refer to Figure

From Manning's equation:

$$V_{1s} = \frac{1}{n_{1s}} R_{1s}^{2/3} S_{1s}^{1/2}$$

and

$$V_{2s} = \frac{1}{n_{2s}} R_{2s}^{2/3} S_{2s}^{1/2}$$

From the definition of shear velocity:

$$V_{*1s} = (gR_{1s}S_{1s})^{1/2}$$

and

$$V_{*2s} = (gR_{2s}S_{2s})^{1/2}$$

Subtituting in equation A2.1 and rearranging, it can be obtained

$$\frac{1}{n_{1s}} R_{1s}^{2/3} S_{1s}^{1/2}\left[1 - \frac{n_{1s}}{n_{2s}}\left(\frac{R_{2s}}{R_{1s}}\right)^{2/3}\left(\frac{S_{2s}}{S_{1s}}\right)^{1/2}\right]$$

$$= \frac{2}{3\kappa}(gR_{1s}S_{1s})^{1/2}\left[\left(\frac{R_{2s}}{R_{1s}}\right)^{1/2}\left(\frac{R_{2s}}{R_{1s}}\right)^{1/2}\left(\frac{S_{2s}}{S_{1s}}\right)^{1/2} - 1\right.$$

denoting $\lambda_s = R_{2s}/R_{1s}$ and $\psi_s = \frac{S_{2s}}{S_{1s}}$, which can be rearranged to:

$$\frac{3\kappa}{2}\frac{R_{1s}^{1/6}}{n_{1s}g^{1/2}} = \frac{(\lambda_s^{1/2}\psi_s^{1/2}-1)}{1-\frac{n_{1s}}{n_{2s}}\lambda_s^{2/3}\psi_s^{1/2}} \qquad \text{A2.2}$$

From the geometry;

$$A_s = A_{1s} + A_{2s} \text{ and } P_s = P_{1s} + P_{2s}$$

combining, it can be obtained

$$\frac{R_{1s}}{R_s} = \frac{1}{\alpha_s+(1-\alpha_s)\lambda_s} \qquad \text{A2.3}$$

where

$$\alpha_s = P_{1s}/P_s$$

Substituting equation A2.3 into equation A2.2 and rearranging it is obtained:

$$1.5\kappa\frac{R_s^{1/6}}{n_{1s}g^{1/2}} = \frac{(\lambda_s^{1/2}\psi_s^{1/2}-1)}{1-\frac{n_{1s}}{n_{2s}}\lambda_s^{2/3}\psi_s^{1/2}}[\alpha_s+(1-\alpha_s)\lambda_s]^{1/6} \qquad \text{A2.4}$$

A2.2 Composite Roughness

Solution of the equation 3.40.

The continuity equation,

$$A_s V_s = A_{1s}$$

can be rearranged as:

$$V_s = \frac{A_{1s}}{A_s} V_{1s} + \frac{A_{2s}}{A_s} V_{2s} \qquad \text{A2.5}$$

From the geometry:

$$\frac{A_{1s}}{A_s} = \frac{R_{1s}}{R_s} \frac{P_{1s}}{P_s}$$

$$= \frac{\alpha_s}{\alpha_s + (1-\alpha_s)\lambda_s}$$

and

$$\frac{A_{2s}}{A_s} = \frac{R_{2s}}{R_s} \frac{P_{2s}}{P_s}$$

$$= \frac{\lambda_s R_{1s}}{R_s} \left(\frac{P_s - P_{1s}}{P_s}\right)$$

$$= \frac{\lambda_s}{\alpha_s + (1-\alpha_s)\lambda_s} (1-\alpha_s)$$

$$= \frac{(1-\alpha_s)\lambda_s}{\alpha_s + (1-\alpha_s)\lambda_s}$$

Substituting the values for A_{1s}/A_s and A_{2s}/A_s in equation A2.5 and the Manning's equations for the mean

velocities, it can be written as

$$\frac{1}{n_s}R_s^{2/3}S_s^{1/2} = \frac{\alpha_s}{\alpha_s+(1-\alpha_s)\lambda_s}\frac{1}{n_{1s}}R_{1s}^{2/3}S_{1s}^{1/2} + \frac{(1-\alpha_s)\lambda_s}{\alpha_s+(1-\alpha_s)\lambda_s}\frac{1}{n_{2s}}R_{2s}^{2/3}S_{2s}^{1/2}$$

by rearranging:

$$\frac{1}{n_s} = \frac{1}{n_{1s}}\left(\frac{S_{1s}}{S_s}\right)^{1/2}\frac{\alpha_s+\frac{n_{1s}}{n_{2s}}(1-\alpha_s)\lambda_s^{5/3}\psi_s^{1/2}}{(\alpha_s-(1-\alpha_s)\lambda_s)^{5/3}}$$

OR

$$\frac{n_s}{n_{1s}} = \left(\frac{S_s}{S_{1s}}\right)^{1/2}\frac{(\alpha_s-(1-\alpha_s)\lambda_s)^{5/3}}{\alpha_s+\frac{n_{1s}}{n_{2s}}(1-\alpha_s)\lambda_s^{5/3}\psi_s^{1/2}} \qquad \text{A2.6}$$

Now, from the momentum equation of a unit length of a channel flow,

$$\gamma A_s S_s = \tau_{\phi 1s}P_{1s} + \tau_{\phi 2s}P_{2s} \qquad \text{A2.7}$$

where,

$$\tau_{\phi 1s} = \gamma R_{1s}S_{1s} \text{ and } \tau_{\phi 2s} = \gamma R_{2s}S_{2s}$$

Hence, equation A2.7 can be rearranged to

$$S_s = \frac{R_{1s}P_{1s}}{R_sP_s}S_{1s} + \frac{R_{2s}P_{2s}}{R_sP_s}S_{2s}$$

$$= \frac{\alpha_s}{\alpha_s+(1-\alpha_s)\lambda_s}S_{1s} + \frac{(1-\alpha_s)\lambda_s}{\alpha_s+(1-\alpha_s)\lambda_s}S_{2s}$$

$$= S_{1s}\left[\frac{\alpha_s+(1-\alpha_s)\lambda_s\psi_s}{\alpha_s+(1-\alpha_s)\lambda_s}\right]$$

therefore,

$$\frac{S_s}{S_{1s}} = \frac{\alpha_s+(1-\alpha_s)\lambda_s\psi_s}{\alpha_s+(1-\alpha_s)\lambda_s} \qquad \text{A2.8}$$

Substituting the relation A2.8 into equation A2.6, the final form of the composite roughness relation is obtained;

$$\frac{n_s}{n_{1s}} = \left[\frac{\alpha_s+(1-\alpha_s)\lambda_s\psi_s}{\alpha_s+(1-\alpha_s)\lambda_s}\right]^{1/2}\left[\frac{(\alpha_s-(1-\alpha_s)\lambda_s)^{5/3}}{\alpha_s+\frac{n_{1s}}{n_{2s}}(1-\alpha_s)\lambda_s^{5/3}\psi_s^{1/2}}\right]$$

A2.9

A2.3 Special Case

In the case of a conventional uniform flow, where energy slopes of strips are assumed equal to the energy slope of the entire channel, i.e., $S_{1s}=S_{2s}=S_s=S$, $\psi_s=1$ and equation A2.4 of division surface and equation A2.9 of composite roughness, can be reduced to:

Division Surface

$$1.5\kappa \frac{R_s^{1/6}}{n_{1s}+g^{1/2}} = \frac{(\lambda_s^{1/2}-1)}{1-\frac{n_{1s}}{n_{2s}}\lambda_s^{2/3}}[\alpha_s+(1-\alpha_s)\lambda_s]^{1/6} \qquad \text{A.10}$$

Composite Roughness

$$\frac{n_s}{n_{1s}} = \frac{(\alpha_s-(1-\alpha_s)\lambda_s)^{5/3}}{\alpha_s+\frac{n_{1s}}{n_{2s}}(1-\alpha_s)\lambda_s^{5/3}} \qquad \text{A.11}$$

APPENDIX A3

Determination of Thickness of Zero Sub-layer

Let at

$$\epsilon_s = \epsilon_{\phi s} \quad , \quad u(\epsilon_s) = 0$$

then the equation 3.32a is:

$$0 = V_s - \frac{2V_{*s}}{\kappa} F_2(\epsilon_{\phi s})$$

$$F_2(\epsilon_{\phi s}) = \frac{\kappa}{2} \frac{V_s}{V_{*s}} \qquad \text{A3.1}$$

Substituting $V_s = \frac{1}{n_s} Y_s^{2/3} S_s^{1/2}$ and $V_{*s} = (gY_s S_s)^{1/2}$, equation A3.1 can be written as:

$$F_2(\epsilon_{\phi s}) = \frac{\kappa}{2} \frac{Y_s^{1/6}}{n_s \sqrt{g}} \qquad \text{A3.2}$$

Again,

$$F_2(\epsilon_{\phi s}) = \text{Ln} \frac{\epsilon_{\phi s}^{1/2}}{1-(1-\epsilon_{\phi s})^{1/2}} - (1- \quad _s)^{1/2} - 1/3$$

As $\epsilon_{\phi s}$ is very small $(1-\epsilon_{\phi s})^{1/2} \cong 1$, hence, equation A3.2 can be rearranged as:

$$\text{Ln} \frac{\epsilon_{\phi s}^{1/2}}{1-(1-\epsilon_{\phi s})^{1/2}} = \frac{\kappa}{2} \frac{Y_s^{1/6}}{n_s \sqrt{g}} + \frac{4}{3} \qquad \text{A3.3}$$

denoting

$$c = \frac{\kappa}{2} \frac{Y_s^{1/6}}{n_s \sqrt{g}} + \frac{4}{3} ;$$

Equation A3.3 can be written as

$$\frac{\varepsilon_{\phi s}^{1/2}}{1-(1-\varepsilon_{\phi s})^{1/2}} = e^{c_1}$$

by squaring and rearringing, which can be written

$$\varepsilon_{\phi s} = 2e^{2c_1}(1-\sqrt{1-\varepsilon_{\phi s}}) - \varepsilon_{\phi s} e^{2c_1}$$

which can be written as:

$$\varepsilon_{\phi s}(1+e^{2c_1}) = 2e^{c_1}[e^{c_1}(1-\sqrt{1-\varepsilon_{\phi s}})] \qquad \text{A3.4}$$

But $e^{c_1}(1-\sqrt{1-\varepsilon_{\phi s}}) = \varepsilon_{\phi s}^{1/2}$; substituting this in equation A3.4, it can be obtained:

$$\varepsilon_{\phi s}(1+e^{2c_1}) = 2e^{c_1}\varepsilon_{\phi s}^{1/2}$$

rearranging,

$$\varepsilon_{\phi s} = [\frac{2e^{c_1}}{1+e^{2c_1}}]^2 \qquad \text{A3.5}$$

where,

$$c_1 = \frac{\kappa}{2} \frac{Y_s^{1/6}}{n_s \sqrt{g}} + 4/3$$

APPENDIX A4

Modification of Manning's Equation

At the first place Manning's equation was developed in Metric Unit system and the equation was expressed as:

$$V = \frac{1}{n} R^{2/3} S^{1/2}$$

Later, with the conversion factor, the equation was established in FPS-system as:

$$V = \frac{1.486}{n} R^{2/3} S^{1/2}$$

Dimensional analysis shows that Manning's roughness coefficient, n, has the dimension $L^{-1/3}T$ in MLT-system [MLT = Mass, Length and Time).

Because of these two different expressions of the Manning's equation, problem sometime arises to establish a generalized model, monograms, etc., which could be accepted in both unit systems.

An attempt has been made, hereby, to establish a generalized expression of the Manning's equation.

Considering Manning's roughness, n, as a non-dimensional parameter, a coefficient parameter, c, is introduced to express Manning's equation to a generalized expression in both units:

$$V = \frac{c}{n} R^{2/3} S^{1/2} \qquad \text{A4.1}$$

Then, 'c' has the dimension, $L^{1/3}T^{-1}$, and is equal to 1 in metric unit, and is equal to 1.486 in FPS unit.

Another multification factor, c' is introduced to make 'c' as a non-dimensional parameter. Hence, the equation A4.1 is:

$$V = \frac{cc'}{n} \frac{1}{c'} R^{2/3} S^{1/2}$$

denoting $C_1 = cc'$ and $C_2 = \frac{1}{c'}$, the above expression can be written as

$$V = \frac{C_1}{n} C_2 R_2^{2/3} S^{1/2} \qquad A4.2$$

Dimensional analysis of factor, c:

Let $c = f(g, \mu, \rho)$

i.e., $f'(c, g, \mu, \rho) = 0$

In MLT system, therefore, only one (4-3) dimensionless parameter exists:

Symbol	M	L	T
c	0	1/3	-1
g	0	1	-2
μ	1	-1	-1
ρ	1	-3	0

	c	g	μ	ρ	
M	-	-	x_3	x_4	= 0
L	$x_1/3$	x_2	$-x_3$	$-3x_4$	= 0
T	$-x_1$	$-2x_2$	$-x_3$	-	= 0

therefore,

$$x_3 + x_4 = 0,$$

$$x_1/3 + x_2 - x_3 - 3x_4 = 0,$$

and

$$-x_1 + 2x_2 - x_3 = 0.$$

Solving it can be written:

$$x_2 = -\frac{5}{9}x_1$$

$$x_3 = \frac{x_1}{9}$$

and $x_4 = -\frac{x_1}{9}$

Putting $x_1 = 1$, $x_2 = -5/9$, $x_3 = 1/9$, and $x_4 = -1/9$

Hence, the non-dimensional parameter, i.e.,

$$\pi_1 = \frac{c\mu^{1/9}}{g^{5/9}\rho^{1/9}} = c\left(\frac{\nu}{g^5}\right)^{1/9}$$

where,

$$\nu = \mu/\rho$$

Therefore c can be non-dimensionalized multiplying it by $\left(\frac{\nu}{g^5}\right)^{1/}$

Hence, $c' = \left(\frac{\nu}{g^5}\right)^{1/9}$

It is observed that the value of c' varies with the ambient (water) temperature. Although, it is not clear that at what temperatures the documented values of Manning's n of different materials were calculated, it can sensibly be assumed of an average temperature of 20°C or 68°F, equal to an average ideal laboratory temperature. Therefore, the numerical value of C_1 can be calculated:

in metric unit

$$C_1 = cc', \text{ and } c = 1$$

$$= c' = \left(\frac{\nu_{20°C}}{g^5}\right)^{1/9}$$

$$= \left(\frac{1.002 \times 10^{-6}}{(9.806)^5}\right)^{1/9}$$

$$= 0.061$$

and in the FPS system:

$$C_1 = cc', \quad c = 1.486$$

$$= 1.486\left(\frac{\nu_{68°F}}{g^5}\right)^{1/9}$$

$$= 1.486\left(\frac{1.0906 \times 10^{-5}}{(32.17)^5}\right)^{1/9}$$

$$= 0.061$$

and

$$C_2 = 1/c' = (g^5/\nu)^{1/9}$$

Hence, the generalized expression of Manning's equation is:

$$V = \frac{0.061}{n} \left(\frac{g^5}{\nu}\right)^{1/9} R^{2/3} S^{1/2} \qquad \text{A4.3}$$

where, the parameter, n, is dimensionless.

In my opinion, the modified expression is better than the original form of Manning's equation because of three reasons:

1. The roughness coefficient, n, is made dimensionless,
2. the expression is a generalized one and can be used in both MKS and FPS system,
3. although the apparent change in discharge or velocity with the change of temperature is unnoticable and is ignored in conventional design, it is sensible and logical argument that with the increase of temperature, viscosity of fluid (water) will decrease, thus, the frictional resistance in fluid motion will decrease and, therefore, it is obvious that the velocity will increase with the increase of temperature, or vice-versa, if the other parameters (n, R and S) are kept unchanged. Hence, velocity or the discharge, can be said, is directly proportional to the temperature of fluid.

APPENDIX B

Experimental Data for the Calibration of Roughness Materials

TABLE B.1

Calibration of Roughness Materials by Vertical Strip Method (Method 1)

Fine Mesh

Total Flow Q (m^3/s)	Measured Strip Velocity, V_s (m/s)	S $*10^2$	R_N $*10^{-4}$	n_F
0.1318	0.726	0.165	31.98	0.0295
0.1186	0.688	0.166	28.31	0.0295
0.1066	0.642	0.156	25.40	0.0298
0.0940	0.597	0.139	22.57	0.0297
0.0814	0.532	0.128	19.04	0.0308
0.0688	0.484	0.124	16.38	0.0321
0.0549	0.506	0.147	13.78	0.0288
0.0454	0.448	0.117	11.37	0.0278
0.0360	0.323	0.113	7.65	0.0361
0.0265	0.243	0.101	5.21	0.0427

Coarse Mesh

Total Flow Q (m^3/s)	Measured Strip Velocity, V_s (m/s)	S $*10^2$	R_N $*10^{-4}$	n_C
0.1318	0.861	0.268	32.73	0.0277
0.1192	0.812	0.243	29.57	0.0272
0.1066	0.754	0.219	26.21	0.0279
0.0940	0.688	0.201	22.81	0.0274
0.0814	0.627	0.182	19.60	0.0276
0.0688	0.574	0.167	16.80	0.0276
0.0552	0.521	0.165	14.20	0.0293
0.0454	0.427	0.136	10.92	0.0311
0.0360	0.326	0.119	7.69	0.0356

TABLE B.2

Calibration of Roughness Materials by Total Flow Method (Method 2)

Fine Mesh

Total Flow Q (m^3/s)	Channel Mean Velocity, V (m/s)	S $*10^2$	R_N $*10^{-4}$	n_F
0.1318	0.755	0.165	12.47	0.0147
0.1186	0.727	0.166	11.69	0.0150
0.1066	0.681	0.156	10.78	0.0154
0.0940	0.628	0.139	9.76	0.0156
0.0814	0.575	0.128	8.73	0.0161
0.0688	0.513	0.124	7.61	0.0174
0.0549	0.509	0.147	6.83	0.0178
0.0454	0.452	0.117	5.85	0.1760
0.0360	0.383	0.113	4.79	0.0198
0.0260	0.312	0.101	3.69	0.0223

Coarse Mesh

Total Flow Q (m^3/s)	Channel Mean Velocity, V (m/s)	S $*10^2$	R_N $*10^{-4}$	n_C
0.1318	0.920	0.268	14.33	0.0146
0.1192	0.868	0.243	13.89	0.0146
0.1066	0.813	0.219	12.20	0.0146
0.0940	0.752	0.201	11.05	0.0149
0.0814	0.690	0.182	9.87	0.0151
0.0688	0.622	0.167	8.64	0.0158
0.0552	0.525	0.165	6.80	0.0182
0.0454	0.460	0.136	5.38	0.0186
0.0360	0.404	0.119	4.91	0.0190

TABLE B.3

Calibration of Roughness Materials by Total Flow Method (Method 3)

Fine Mesh

Total Flow Q (m^3/s)	Channel Mean Velocity, V (m/s)	S $*10^2$	R_N $*10^{-4}$	n_F
0.1318	0.695	0.228	11.22	0.0192
0.1186	0.665	0.236	10.52	0.0201
0.1066	0.627	0.203	9.70	0.0195
0.0940	0.575	0.179	8.78	0.0198
0.0814	0.530	0.165	7.86	0.0208
0.0688	0.478	0.144	6.86	0.0206
0.0549	0.463	0.148	6.15	0.0204
0.0454	0.420	0.145	5.26	0.0216
0.0360	0.356	0.147	4.31	0.0218
0.0260	0.293	0.137	3.32	0.0225

Coarse Mesh

Total Flow Q (m^3/s)	Channel Mean Velocity, V (m/s)	S $*10^2$	R_N $*10^{-4}$	n_C
0.1318	0.860	0.313	13.30	0.0172
0.1192	0.802	0.267	12.35	0.0169
0.1066	0.750	0.245	11.25	0.0171
0.0940	0.712	0.225	10.36	0.0169
0.0814	0.642	0.194	9.13	0.0172
0.0688	0.573	0.156	7.95	0.0170
0.0552	0.505	0.148	6.72	0.0182
0.0454	0.445	0.128	5.69	0.0188
0.0360	0.378	0.101	4.62	0.0192

TABLE B.3 - (cont'd.)

Plywood

Total Flow Q (m^3/s)	Channel Mean Velocity, V (m/s)	S $*10^2$	R_N $*10^{-4}$	n_p
0.1318	1.012	0.181	15.76	0.0110
0.1192	0.952	0.186	14.73	0.0113
0.1066	0.889	0.163	13.45	0.0112
0.0940	0.826	0.156	12.12	0.0116
0.0814	0.758	0.134	10.82	0.0115
0.0688	0.682	0.117	9.48	0.0117
0.0552	0.589	0.091	7.85	0.0115
0.0454	0.515	0.076	6.73	0.0119
0.0360	0.443	0.060	5.52	0.0119

APPENDIX C

Tables of Main Results

TABLE C.1

Experimental Data of Compound Channel with β_f=0.5 under Free-Surface Flows

Channel Cross-Section No. OPC-CS1 with θ_{mc}=90° and θ_{fp}=90°

Run No.	Q (m^3/s)	H (m)	α_f	T °C	Boundary Roughness MC	Boundary Roughness FP	S $*10^2$	n
1	2	3	4	5	6	7	8	9
1	0.1029	0.3343	0.392	18.5	0.020	0.020	0.665	0.0202
2	0.0846	0.3115	0.348	20.0	0.020	0.020	0.595	0.0206
3	0.0679	0.2924	0.305	18.5	0.020	0.020	0.451	0.0206
4	0.0543	0.2715	0.252	20.0	0.020	0.020	0.364	0.0196
5	0.0410	0.2546	0.202	20.0	0.020	0.020	0.295	0.0208
6	0.0964	0.3231	0.371	20.0	0.020	0.020	0.642	0.0200

Channel Cross-Section No. OPC-CS2 with θ_{mc}=75° and θ_{fp}=90°

Run No.	Q (m^3/s)	H (m)	α_f	T °C	Boundary Roughness MC	Boundary Roughness FP	S $*10^2$	n
1	2	3	4	5	6	7	8	9
7	0.0820	0.3129	0.351	10.0	0.020	0.020	0.597	0.0202
8	0.0669	0.2913	0.302	12.0	0.020	0.020	0.487	0.0195
9	0.0537	0.2709	0.250	14.0	0.020	0.020	0.419	0.0195
10	0.1009	0.3330	0.390	14.0	0.020	0.020	0.729	0.0203
11	0.0752	0.2537	0.199	17.0	0.020	0.020	0.814	0.0205
12	0.0920	0.2896	0.298	17.0	0.020	0.020	0.940	0.0194
13	0.0753	0.2709	0.250	17.0	0.020	0.020	0.894	0.0212
14	0.0580	0.2381	0.147	18.0	0.020	0.020	0.823	0.0195
15	0.0681	0.2540	0.200	18.0	0.020	0.020	0.851	0.0194
16	0.1058	0.3047	0.333	18.0	0.020	0.020	1.020	0.0193

TABLE C.1 - cont'd.

Channel Cross-Section No. OPC-CS3 with $\theta_{mc}=60°$, $\theta_{fp}=90°$

Run No.	Q (m^3/s)	H (m)	α_f	T °C	Boundary Roughness MC	Boundary Roughness FP	S $*10^2$	n
1	2	3	4	5	6	7	9	9
17	0.0602	0.2540	.200	20.0	0.020	0.020	0.706	0.0175
18	0.0801	0.2930	.306	20.0	0.020	0.020	0.678	0.0176
19	0.1039	0.3388	.400	21.5	0.020	0.020	0.630	0.0174
20	0.0684	0.2905	.300	24.0	0.020	0.020	0.485	0.0173
21	0.0454	0.2548	.203	24.0	0.020	0.020	0.377	0.0173

Channel Cross-Section No. OPC-CS4 with $\theta_{mc}=45°$, $\theta_{fp}=90°$

Run No.	Q (m^3/s)	H (m)	α_f	T °C	Boundary Roughness MC	Boundary Roughness FP	S $*10^2$	n
1	2	3	4	5	6	7	8	9
22	0.0690	0.2899	.300	22.2	0.020	0.020	0.452	0.0141
23	0.0451	0.2539	.200	21.5	0.020	0.020	0.486	0.0159
24	0.0343	0.2395	.152	21.0	0.020	0.020	0.356	0.0152
25	0.0443	0.2576	.211	21.0	0.020	0.020	0.399	0.0152
26	0.0644	0.2863	.290	21.0	0.020	0.020	0.446	0.0144
27	0.0699	0.2990	.320	21.0	0.020	0.020	0.456	0.0149
28	0.0573	0.2920	.304	21.0	0.020	0.017	0.304	0.0140
29	0.0665	0.2883	.295	21.0	0.020	0.017	0.407	0.0154
30	0.0548	0.2678	.241	21.0	0.020	0.017	0.326	0.0147
31	0.0420	0.2435	.166	21.0	0.020	0.017	0.270	0.0146
32	0.0240	0.2263	.103	21.0	0.020	0.017	0.205	0.0148
33	0.0745	0.3325	.389	21.0	0.020	0.017	0.413	0.0142

TABLE C.2

Experimental Data of Compound Channel with β_f=1.0 under Free-surface Flows

Channel Cross-Section No. OPC-CS5 with θ_{mc}=90° and θ_{fp}=90°

Run No.	Q (m^3/s)	H (m)	α_f	T °C	Boundary Roughness MC	Boundary Roughness FP	S $*10^2$	n
1	2	3	4	5	6	7	8	9
34	0.1002	0.3376	0.398	26.1	0.020	0.020	0.888	0.0195
35	0.0880	0.3256	0.376	26.1	0.020	0.020	0.818	0.0199
36	0.0752	0.3101	0.345	26.1	0.020	0.020	0.734	0.0199
37	0.0849	0.2941	0.309	26.1	0.020	0.020	0.648	0.0193
38	0.0492	0.2731	0.256	26.1	0.020	0.020	0.513	0.0197
39	0.0331	0.2450	0.170	25.6	0.020	0.020	0.406	0.0180
40	0.1061	0.3375	0.398	25.6	0.020	0.017	0.898	0.0186
41	0.0639	0.2908	0.301	25.6	0.020	0.017	0.624	0.0188
42	0.0398	0.2538	0.199	25.6	0.020	0.017	0.443	0.0185
43	0.1146	0.3445	0.410	25.6	0.020	0.017	0.954	0.0184
44	0.0914	0.3239	0.373	25.6	0.020	0.017	0.794	0.0186
45	0.0796	0.3094	0.343	25.6	0.020	0.017	0.730	0.0187
46	0.0510	0.2714	0.251	25.6	0.020	0.017	0.534	0.0188
47	0.0279	0.2339	0.130	25.6	0.020	0.017	0.356	0.0194

Channel Cross-Section No. OPC-CS6 with θ_{mc}=75°, θ_{fp}=90°

Run No.	Q ($m^3/3$)	H (m)	α_f	T °C	Boundary Roughness MC	Boundary Roughness FP	S $*10^2$	n
1	2	3	4	5	6	7	8	9
48	0.0587	0.2907	0.301	24.5	0.020	0.020	0.620	0.0187
49	0.0375	0.2553	0.204	25.0	0.020	0.020	0.474	0.0186
50	0.0609	0.2913	0.302	23.9	0.020	0.017	0.591	0.0178
51	0.0375	0.2552	0.204	24.5	0.020	0.017	0.467	0.0185
52	0.1044	0.3380	0.399	24.5	0.020	0.017	0.842	0.0172
53	0.0893	0.3256	0.376	24.5	0.020	0.017	0.760	0.0176
54	0.0751	0.3106	0.346	24.5	0.020	0.017	0.677	0.0179
55	0.0524	0.2788	0.271	24.5	0.020	0.017	0.565	0.0182
56	0.0751	0.3118	0.348	25.0	0.020	0.020	0.734	0.0187
57	0.0495	0.2776	0.268	25.0	0.020	0.020	0.530	0.0184
58	0.0280	0.2350	0.135	25.0	0.020	0.020	0.470	0.0196

Table C.2 - cont'd.

Channel Cross-Section No. OPC-CS7 with $\theta_{mc}=60°$, $\theta_{fp}=90°$

Run No.	Q (m^3/s)	H (m)	α_f	T °C	Boundary Roughness MC	Boundary Roughness FP	S $*10^2$	n
1	2	3	4	5	6	7	8	9
59	0.0951	0.3381	0.399	25.6	0.020	0.020	0.756	0.0163
60	0.0614	0.2906	0.300	26.1	0.020	0.020	0.675	0.0166
61	0.0365	0.2528	0.196	26.1	0.020	0.020	0.536	0.0169
62	0.0786	0.3123	0.349	26.1	0.020	0.020	0.728	0.0160
63	0.0722	0.3031	0.330	26.1	0.020	0.020	0.638	0.0169
64	0.0500	0.2753	0.262	26.4	0.020	0.020	0.638	0.0170
65	0.0314	0.2398	0.153	26.1	0.020	0.020	0.468	0.0170
66	0.0211	0.2259	0.100	26.1	0.020	0.020	0.376	0.0169

Channel Cross-Section on No. 8 with $\theta_{mc}=45°$ and $\theta_{fp}=90°$

Run No.	Q (m^3/s)	H (m)	α_f	T °C	Boundary Roughness MC	Boundary Roughness FP	S $*10^2$	n
1	2	3	4	5	6	7	8	9
67	0.0950	0.3386	0.40	24.5	0.020	0.020	0.787	0.0159
68	0.0538	0.2913	0.302	24.5	0.020	0.020	0.621	0.0165
69	0.0319	0.2544	0.201	24.5	0.020	0.020	0.473	0.0142
70	0.0420	0.2709	0.250	24.5	0.020	0.020	0.594	0.0165
71	0.0878	0.3388	0.400	23.3	0.020	0.017	0.586	0.0145
72	0.0510	0.2910	0.302	23.9	0.020	0.017	0.444	0.0146
73	0.0277	0.2547	0.202	23.9	0.020	0.017	0.383	0.0147
74	0.0609	0.3079	0.340	24.5	0.020	0.020	0.705	0.0165
75	0.0794	0.3217	0.368	24.5	0.020	0.020	0.744	0.0162

TABLE C.3

Experimental Data of Compound Channel with β_f=2.0 under Free-Surface Flows

Channel Cross-Section No. OPC-CS9 with ϕ_{mc}=90° and ϕ_{fp} = 90°

Run No.	Q (m^3/s)	H (m)	α_f	T °C	Boundary Roughness MC	Boundary Roughness FP	S $*10^2$	n
1	2	3	4	5	6	7	8	9
76	0.0392	0.2566	0.208	22.2	0.020	0.020	0.546	0.0139
77	0.0607	0.2904	0.300	22.6	0.020	0.020	0.552	0.0140
78	0.0946	0.3372	0.397	22.8	0.020	0.020	0.629	0.0132
79	0.0820	0.3222	0.369	23.0	0.020	0.020	0.598	0.0135
80	0.0665	0.3020	0.327	23.0	0.020	0.020	0.554	0.0133
81	0.0438	0.2693	0.245	23.0	0.020	0.020	0.492	0.0138
82	0.0278	0.2408	0.156	23.0	0.020	0.020	0.378	0.0132

Channel Cross-Section No. OPC-CS10 with ϕ_{mc}=75° and ϕ_{fp}=90°

Run No.	Q (m^3/s)	H (m)	α_f	T °C	Boundary Roughness MC	Boundary Roughness FP	S $*10^2$	n
1	2	3	4	5	6	7	8	9
83	0.0906	0.3388	0.400	22.5	0.020	0.020	0.597	0.0124
84	0.0514	0.2902	0.300	22.8	0.020	0.020	0.569	0.0139
85	0.0755	0.3239	0.373	23.3	0.020	0.020	0.525	0.0124
86	0.0702	0.3134	0.352	23.3	0.020	0.020	0.562	0.0126
87	0.0619	0.3018	0.327	23.3	0.020	0.020	0.585	0.0130
88	0.0449	0.2710	0.250	23.3	0.020	0.020	0.546	0.0138
89	0.0268	0.2430	0.164	23.3	0.020	0.020	0.467	0.0131

TABLE C.3 - cont'd.

Channel Cross-Section No. OPC-CS11 with ϕ_{mc}=60° and ϕ_{fp}=90°

Run No.	Q (m^3/s)	H (m)	α_f	T °C	Boundary Roughness MC	Boundary Roughness FP	S $*10^2$	n
1	2	3	4	5	6	7	8	9
90	0.0871	0.3395	0.401	22.8	0.020	0.020	0.567	0.0114
91	0.0506	0.2912	0.302	22.8	0.020	0.020	0.545	0.0120
92	0.0289	0.2553	0.204	22.8	0.020	0.020	0.495	0.0112
93	0.0751	0.3246	0.374	22.8	0.020	0.020	0.526	0.0112
94	0.0670	0.3113	0.347	22.8	0.020	0.020	0.552	0.0113
95	0.0544	0.2913	0.302	22.8	0.020	0.020	0.597	0.0116
96	0.0420	0.2801	0.274	22.8	0.020	0.020	0.545	0.0125
97	0.0223	0.2432	0.164	22.8	0.020	0.020	0.422	0.0114

TABLE C4

Experimental Data of Compound Channels with β_f=0.5 under Covered Surface Flows

Channel Cross-Section No. CC-CS1 with θ_{mc}=90° and θ_{fp}=90°

Run No.	Q (m^3/s)	H (m)	α_f	T °C	Boundary Roughness MC	FP	Cover	S $*10^2$	n
1	2	3	4	5	6	7	8	9	10
1	.0474	.2572	0.210	19.5	.020	.020	.020	1.112	.0278
2	.0547	.2717	0.252	20.0	.020	.020	.020	1.204	.0279
3	.0647	.2903	0.300	20.0	.020	.020	.020	1.261	.0274
4	.0500	.2605	0.220	19.0	.020	.020	.020	1.168	.0276
5	.0627	.2832	0.295	20.0	.020	.020	.020	1.235	.0276
6	.0764	.3079	0.340	20.0	.020	.020	.020	1.393	.0273

Channel Cross-Section No. CC-CS2 with θ_{mc}=75° and θ_{fp} = 90°

Run No.	Q (m^3/s)	H (m)	α_f	T °C	Boundary Roughness MC	CP	Cover	S $*10^2$	n
1	2	3	4	5	6	7	8	9	10
7	.0443	.2560	0.206	17.0	.020	.020	.020	1.090	.0265
8	.0505	.2708	0.250	17.0	.020	.020	.020	1.030	.0254
9	.0609	.2910	0.302	18.0	.020	.020	.020	1.192	.0264
10	.0491	.2620	0.224	18.0	.020	.020	.020	1.100	.0252
11	.0598	.2890	0.297	18.5	.020	.020	.020	1.165	.0262
12	.0740	.3105	0.346	18.5	.020	.020	.020	1.246	.0252

TABLE C4 - cont'd.

Channel Cross-Section No. CC-CS3 with θ_{mc}=60° and θ_{fp}=90°

Run No.	Q (m^3/s)	H (m)	α_f	T °C	Boundary Roughness MC	FP	Cover	S $*10^2$	n
1	2	3	4	5	6	7	8	9	10
13	.0476	.2702	0.248	23.5	.020	.020	.020	.887	.0221
14	.0730	.3111	0.347	23.0	.020	.020	.020	1.061	.0215
15	.0593	.2888	0.296	24.0	.020	.020	.020	.987	.0218
16	.0405	.2547	0.202	21.5	.020	.020	.020	.743	.0206
17	.0735	.3117	0.348	21.0	.020	.020	.020	.954	.0204
18	.0606	.2907	0.300	22.0	.020	.020	.020	.889	.0204
19	.0499	.2713	0.250	22.0	.020	.020	.020	.862	.0209

Channel Cross-Section No. CC-CS4 with θ_{mc}=45° and θ_{fp}=90°

Run No.	Q (m^3/s)	H (m)	α_f	T °C	Boundary Roughness MC	FP	Cover	S $*10^2$	n
1	2	3	4	5	6	7	8	9	10
20	.0456	.2646	0.232	21.7	.020	.020	.020	1.055	.0197
21	.0544	.2927	0.306	22.2	.020	.020	.020	.842	.0191
22	.0653	.3100	0.344	22.8	.020	.020	.020	.845	.0183
23	.0435	.2708	0.250	19.2	.020	.020	.017	.865	.0199
24	.0466	.2899	0.300	20.3	.020	.017	.020	.610	.0184
25	.0534	.2990	0.321	21.1	.020	.017	.020	.653	.0181
26	.0414	.2789	0.271	21.1	.020	.017	.020	.583	.0187
27	.0338	.2635	0.229	21.1	.020	.017	.020	.576	.0194
28	.0287	.2509	0.190	20.3	.020	.017	.020	.508	.0179
29	.0594	.2914	0.303	19.5	.020	.020	.017	.945	.0212
30	.0553	.3007	0.324	19.5	.020	.020	.017	.695	.0177
31	.0502	.2913	0.302	19.5	.020	.020	.017	.675	.0176
32	.0438	.2806	0.276	19.5	.020	.020	.017	.671	.0177
33	.0338	.2614	0.223	21.1	.020	.020	.017	.661	.0175
34	.0488	.2912	0.302	21.1	.020	.017	.020	.579	.0175
35	.0580	.3072	0.338	21.1	.020	.017	.020	.639	.0173
36	.0539	.1981	0.320	21.1	.020	.017	.020	.639	.0176
37	.0437	.2817	0.280	21.7	.020	.017	.020	.591	.0181
38	.0388	.2717	0.252	21.1	.020	.017	.020	.561	.0181
39	.0338	.2607	0.266	21.1	.020	.017	.020	.534	.0182

TABLE C.5

Experimental Data of Compound Channel with β_f=1.0 under Covered Surface Flows

Channel Cross Section No. CC-CS5 with θ_{mc}=90° and θ_{fp}=90°

Run No.	Q (m^3/s)	H (m)	α_f	T °C	Boundary Roughness MC	FP	Cover	S $*10^2$	n
1	2	3	4	5	6	7	8	9	10
40	.0410	.2689	.244	26.1	.020	.020	.020	1.081	.0254
41	.0534	.2907	.300	26.1	.020	.020	.020	1.270	.0254
42	.0640	.3071	.340	26.1	.020	.020	.020	1.410	.0252
43	.0273	.2490	.220	26.1	.020	.020	.020	0.742	.0260
44	.0684	.3116	.348	25.6	.020	.017	.020	1.344	.0238
45	.0552	.2907	.300	25.6	.020	.017	.020	1.228	.0235
46	.0410	.2676	.241	25.6	.020	.017	.020	1.000	.0241
47	.0296	.2492	.358	25.6	.020	.017	.020	0.709	.0290

Channel Cross-Section No. CC-CS6 with θ_{mc}=75° and θ_{fp}=90°.

Run No.	Q (m^3/s)	H	α_f	T °C	Boundary Roughness MC	FP	Cover	S $*10^2$	n
1	2	3	4	5	6	7	8	9	10
48	.0672	.3128	.350	23.90	.020	.020	.020	1.370	.0219
49	.0435	.2723	.254	23.90	.020	.020	.020	1.173	.0218
50	.0552	.2940	.308	23.90	.020	.020	.020	1.129	.0220
51	.0536	.2903	.300	23.3	.020	.020	.017	1.231	.0226
52	.0438	.2612	.222	23.3	.020	.020	.017	1.343	.0219
53	.0669	.3067	.337	23.3	.020	.020	.017	0.302	.0212
54	.0287	.2475	.179	24.0	.020	.020	.017	0.792	.0196
55	.0669	.3129	.351	24.5	.020	.017	.020	1.301	.0222
56	.0442	.2728	.255	24.5	.020	.017	.020	1.151	.0226
57	.0609	.3023	.328	24.5	.020	.017	.020	1.267	.0222
58	.0495	.2838	.284	24.5	.020	.017	.020	1.160	.0224
59	.0307	.2516	.192	24.5	.020	.017	.020	0.884	.0217

TABLE C.5 -cont'd.

Channel Cross-Section No. CC-CS7 with $\theta_{mc}=60°$ and $\theta_{fp}=90°$

Run No.	Q (m^3/s)	H (m)	α_f	T °C	Boundary Roughness MC	FP	Cover	S $*10^2$	n
1	2	3	4	5	6	7	8	9	10
60	.0564	.3033	.330	26.7	.020	.020	.020	1.110	.0200
61	.0482	.2910	.300	26.7	.020	.020	.020	1.036	.0182
62	.0398	.2797	.274	26.7	.020	.020	.020	0.950	.0212
63	.0283	.2575	.211	26.7	.020	.020	.020	0.725	.0205
64	.0524	.2902	.300	86.7	.020	.020	.017	1.065	.0189
65	.0369	.2711	.251	26.7	.020	.020	.017	0.870	.0200
66	.0574	.3060	.340	26.7	.020	.020	.017	1.048	.0197
67	.0283	.2563	.207	26.7	.020	.020	.017	0.740	.0195

Channel Cross-Section No. CC-CS8 with $\theta_{mc}=45°$ and $\theta_{fp}=90°$

Run No.	Q (m^3/s)	H (m)	α_f	T °C	Boundary Roughness MC	FP	Cover	S $*10^2$	n
1	2	3	4	5	6	7	8	9	10
68	.0589	.3128	.350	25.6	.020	.020	.020	1.34	.0191
69	.0325	.2708	.250	25.6	.020	.020	.020	1.12	.0200
70	.0696	.3255	.376	25.6	.020	.020	.020	1.374	.0184
71	.0526	.3122	.349	25.6	.020	.017	.020	1.005	.0183
72	.0312	.2725	.254	25.6	.020	.017	.020	0.825	.0182
73	.0692	.3341	.392	24.5	.020	.017	.020	1.076	.0174
74	.0408	.2900	.299	24.5	.020	.017	.020	0.882	.0178
75	.0550	.3123	.349	24.5	.020	.017	.017	1.028	.0178
76	.0727	.3347	.393	24.5	.020	.017	.017	1.145	.0171
77	.0336	.2730	.256	25.0	.020	.017	.017	0.951	.0182
78	.0621	.3117	.348	26.0	.020	.020	.017	1.274	.0175
79	.0466	.2905	.300	25.0	.020	.020	.017	1.194	.0181
80	.0336	.2667	.238	25.0	.020	.020	.017	1.071	.0179

TABLE C.6

Experimental Data of Compound Channels with $\beta_f = 2.0$ Under Covered Surface Flows

Channel Cross-Section No. CC-CS9 with $\theta_{mc}=60°$ and $\theta_{fp}=90°$

Run No.	Q (m^3/s)	H (m)	α_f	T °C	Boundary Roughness MC	FP	Cover	S $*10^2$	n
1	2	3	4	5	6	7	8	9	10
81	.0327	.2707	.250	23.3	.020	.020	.020	0.906	.0200
82	.0426	.2911	.302	23.3	.020	.020	.020	0.984	.0198
83	.0555	.3145	.354	23.9	.020	.020	.020	1.070	.0196
84	.0413	.2903	.300	23.3	.020	.020	.020	0.986	.0202
85	.0527	.3140	.353	23.6	.020	.020	.020	0.898	.0205

Channel Cross-Section No. CC-CS10 with $\theta_{mc}=75°$ and $\theta_{fp}=90°$

Run No.	Q (m^3/s)	H (m)	α_f	T °C	Boundary Roughness MC	FP	Cover	S $*10^2$	n
1	2	3	4	5	6	7	8	9	10
86	.0555	.3127	.350	22.80	.020	.020	.020	1.313	.0190
87	.0410	.2902	.300	22.80	.020	.020	.020	1.074	.0188
88	.0312	.2700	.247	23.3	.020	.020	.020	1.132	.0200
89	.0540	.3123	.349	23.3	.020	.020	.020	1.283	.0187
90	.0438	.2901	.300	23.6	.020	.020	.020	1.149	.0192
91	.0341	.2740	.258	23.9	.020	.020	.020	1.149	.0192
92	.0256	.2572	.210	23.9	.020	.020	.020	0.932	.0186

TABLE C.6 - Cont'd.

Channel Cross-Section No. CC-CS11 with $\theta_{mc}=60°$ and $\theta_{fp}=90°$

Run No.	Q (m^3/s)	H (m)	α_r	T °C	Boundary Roughness MC	FP	Cover	S $*10^2$	n
1	2	3	4	5	6	7	8	9	10
93	.0489	.3129	.351	22.8	0.02	0.02	0.02	.948	.0162
94	.0353	.2916	.303	23.3	0.02	0.02	0.02	.862	.0167
95	.0268	.2707	.247	23.2	0.02	0.02	0.02	.723	.0162
96	.0457	.3130	.350	24.0	0.02	0.02	0.02	.939	.0172
97	.0341	.2906	.300	24.5	0.02	0.02	0.02	.819	.0169
98	.0257	.2714	.251	24.5	0.02	0.02	0.02	.663	.0160

TABLE C.7

Experimental Data of Simple and Complex Channels
Under Covered Surface Flows

Rectangular Channel Cross-Section

Run No.	Q	H	Boundary Roughness				S	n
	(m^3/s)	(m)	Bed	Cover	L.S.W.	R.S.W.	$*10^2$	
1	2	3	4	5	6	7	8	9
1	0.0797	0.4200	.017	.0115	.0115	.017	.0569	.0132
2	0.0350	0.3643	.017	.017	.017	.017	.0277	.0172
3	0.0473	0.3449	.017	.017	.017	.017	.0514	.0161
4	0.0456	0.3523	.020	.017	.020	.017	.0410	.0154
5	0.0653	0.3769	.020	.017	.020	.017	.0694	.0153
6	0.0729	0.4041	.020	.017	.020	.017	.1014	.0182
7	0.0608	0.3785	.017	.017	.017	.020	.0653	.0160
8	0.0505	0.3683	.017	.017	.017	.020	.0569	.0174
9	0.0401	0.3742	.017	.0115	.017	.017	.0292	.0160
10	0.0482	0.4098	.017	.0115	.017	.017	.0396	.0176
11	0.0482	0.3495	.017	.0115	.017	.017	.0378	.0138
12	0.0417	0.3492	.017	.0115	.017	.020	.0264	.0168
13	0.0669	0.4072	.017	.0115	.017	.020	.0708	.0155
14	0.0803	0.4135	.017	.0115	.017	.020	.0833	.0154

TABLE C.7 - cont'd.

Triangular and Complex Triangular Channel Cross-Section

Run No.	Q (m^3/s)	H (m)	Boundary Roughness				S $*10^2$	n
			Bed	Cover	L.S.W.	R.S.W.		
1	2	3	4	5	6	7	8	9
15	0.0153	0.2314	.017	.017	.017	.017	.0555	.011
16	0.0252	0.2380	.017	.017	.017	.017	.1389	.0116
17	0.0399	0.2383	.017	.017	.017	.017	.3646	.0117
18	0.0187	0.2518	.017	.0115	.017	.017	.0424	.010
19	0.0470	0.2469	.017	.0115	.017	.017	.2972	.010
20	0.0522	0.3520	.017	.017	.017	.017	.0889	.0116
21	0.0692	0.3411	.017	.017	.017	.017	.1819	.0117

Trapezoidal and Complex Trapezoidal Channel Cross-Section

Run No.	Q (m^3/s)	H (m)	Boundary Roughness				S $*10^2$	n
			Bed	Cover	L.S.W.	R.S.W.		
1	2	3	4	5	6	7	8	9
22	0.0230	0.1656	.017	.017	.017	.017	.1562	.0121
23	0.0416	0.1839	.017	.017	.017	.017	.4292	.0139
24	0.0127	0.1849	.017	.0115	.017	.017	.0271	.0116
25	0.0370	0.1824	.017	.0115	.017	.017	.1417	.0088
26	0.0501	0.2811	.017	.017	.017	.017	.0743	.0107
27	0.0721	0.2916	.017	.017	.017	.017	.1667	.0119
28	0.0341	0.2832	.017	.0115	.017	.017	.0118	.009
29	0.0495	0.2824	.017	.0115	.017	.017	.0811	.006
30	0.0667	0.2822	.017	.0115	.017	.017	.1007	.010

TABLE C.8

Velocity Coefficients, E1 and E2 of Compound Channels with β_f=0.5 under Free-Surface Flows

Channel Cross-Section No. OPC-CS1 with θ_{mc}=90° and θ_{fp}=90°

Run No.	Q (m^3/s)	H (m)	α_f	R_N $*10^{-4}$	ϕ_1	ϕ_2	ϕ	E1	E2
1	2	3	4	5	6	7	8	9	10
1	.1029	.3343	.392	8.93	.312	1.412	.517	1.014	1.154
2	.0846	.3115	.348	7.95	.320	1.412	.513	1.013	1.190
3	.0679	.2924	.305	6.38	.326	1.412	.509	1.010	1.170
4	.0543	.2715	.252	5.43	.332	1.412	.506	1.014	1.182
5	.0410	.2546	.202	4.36	.336	1.412	.504	1.014	1.175
6	.0964	.3231	.371	8.95	.316	1.412	.514	1.013	1.162

Channel Cross-Section No. OPC-CS2 with θ_{mc}=75° and θ_{fp}=90°

Run No.	Q (m^3/s)	H (m)	α_f	R_N $*10^{-4}$	ϕ_1	ϕ_2	ϕ	E1	E2
1	2	3	4	5	6	7	8	9	10
7	.0820	.3129	.351	6.19	.317	1.279	.466	1.020	1.116
8	.0669	.2913	.302	5.54	.322	1.279	.463	1.014	1.089
9	.0537	.2709	.250	4.89	.327	1.279	.461	1.020	1.089
10	.1009	.3330	.390	8.12	.311	1.279	.468	1.014	1.124
11	.0752	.2537	.199	6.42	.330	1.279	.460	1.026	1.129
12	.0920	.2896	.298	8.75	.323	1.279	.463	1.024	1.073
13	.0753	.2709	.250	7.26	.327	1.279	.461	1.030	1.075
14	.0580	.2381	.147	6.35	.331	1.279	.459	1.001	1.070
15	.0681	.2540	.200	7.19	.330	1.279	.460	1.012	1.070
16	.1058	.3047	.333	10.00	.319	1.279	.465	1.015	1.065

TABLE C.8 - Con't.

Channel Cross-Section No. OPC-CS3 with θ_{mc}=60° and θ_{fp}=90°

Run No.	Q (m^3/s)	H (m)	α_f	R_N *10^{-4}	Φ_1	Φ_2	Φ	E1	E2
1	2	3	4	5	6	7	8	9	10
17	0.0602	0.2540	.200	7.04	.315	1.124	.410	1.030	0.972
18	0.0801	0.2930	.306	8.52	.312	1.124	.411	1.025	0.975
19	0.1039	0.3388	.400	10.45	.303	1.124	.415	1.028	0.955
20	0.0684	0.2905	.300	8.03	.312	1.124	.411	1.023	0.964
21	0.0454	0.2548	.203	5.77	.315	1.124	.410	1.029	0.961

Channel Cross-Section No. OPC-CS4 with θ_{mc}=45° and θ_{fp}=90°

Run No.	Q (m^3/s)	H (m)	α_f	R_N *10^{-4}	Φ_1	Φ_2	Φ	E1	E2
1	2	3	4	5	6	7	8	9	10
22	0.0690	0.2899	.300	8.02	.290	0.9124	.341	1.037	.863
23	0.0451	0.2539	.200	5.66	.286	0.9124	.343	1.034	.899
24	0.0343	0.2395	.152	4.42	.281	0.9124	.344	1.035	.858
25	0.0443	0.2576	.211	5.45	.287	0.9124	.342	1.033	.858
26	0.0644	0.2863	.290	7.43	.290	0.9124	.341	1.023	.813
27	0.0699	0.2990	.320	7.72	.290	0.9124	.341	1.031	.832
28	0.0573	0.2920	.304	6.52	.290	0.9124	.341	1.037	.817
29	0.0665	0.2883	.295	7.36	.290	0.9124	.341	1.029	.908
30	0.0548	0.2678	.241	6.28	.289	0.9124	.342	1.032	.870
31	0.0420	0.2435	.166	5.05	.283	0.9124	.344	1.040	.854
32	0.0240	0.2263	.103	3.19	.275	0.9124	.347	1.032	.818
33	0.0745	0.3325	.389	8.90	.288	0.9124	.342	1.036	.825

TABLE C.9

Velocity Coefficients E1 and E2 of Compound Channels
β_f=1.0 under Free-Surface Flows

Channel Cross-Section No. OPC-CS5 with θ_{mc}=90° and θ_{fp}=90°

Run No.	Q (m^3/s)	H (m)	α_f	R_N $*10^{-4}$	ϕ_1	ϕ_2	ϕ	E1	E2
1	2	3	4	5	6	7	8	9	10
34	0.1002	0.3376	0.398	10.30	.273	1.063	.809	1.048	1.098
35	0.0880	0.3256	0.376	9.25	.274	1.063	.808	1.054	1.122
36	0.0752	0.3101	0.345	8.14	.276	1.063	.807	1.057	1.124
37	0.0849	0.2941	0.309	7.08	.277	1.063	.806	1.053	1.134
38	0.0492	0.2731	0.256	5.73	.277	1.063	.806	1.076	1.092
39	0.0331	0.2450	0.170	4.09	.274	1.063	.808	1.060	1.128
40	0.1061	0.3375	0.398	10.78	.273	1.063	.809	1.048	1.113
41	0.0639	0.2908	0.301	7.06	.277	1.063	.806	1.053	1.151
42	0.0398	0.2538	0.199	4.78	.276	1.063	.807	1.066	1.140
43	0.1146	0.3445	0.410	11.54	.272	1.063	.810	1.050	1.107
44	0.0914	0.3239	0.373	9.54	.275	1.063	.807	1.058	1.131
45	0.0796	0.3094	0.343	8.47	.276	1.063	.807	1.056	1.141
46	0.0510	0.2714	0.251	5.89	.277	1.063	.806	1.069	1.126
47	0.0279	0.2339	0.130	3.49	.271	1.063	.811	1.102	1.132

Channel Cross-Sections No. OPC-CS6 with θ_{mc}=75° and θ_{fp}=90°

Run No.	Q (m^3/s)	R (m)	α_f	R_N $*10^{-4}$	ϕ_1	ϕ_2	ϕ	E1	E2
1	2	3	4	5	6	7	8	9	10
48	0.0587	0.2907	0.301	6.68	.271	.9277	.707	1.028	1.019
49	0.0375	0.2553	0.204	4.66	.266	.9277	.711	1.038	1.007
50	0.0609	0.2913	0.302	6.83	.271	.9277	.707	1.020	1.034
51	0.0375	0.2552	0.204	4.61	.266	.9277	.711	1.029	1.055
52	0.1044	0.3380	0.399	10.82	.269	.9277	.709	1.019	0.999
53	0.0893	0.3256	0.376	9.47	.270	.9277	.708	1.058	1.052
54	0.0751	0.3106	0.346	8.20	.271	.9277	.707	1.031	1.020
55	0.0524	0.2788	0.271	6.11	.270	.9277	.708	1.036	1.023
56	0.0751	0.3118	0.348	8.28	.271	.9277	.707	1.025	1.020
57	0.0495	0.2776	0.268	5.86	.270	.9277	.708	1.040	1.992
58	0.0280	0.2350	0.135	3.65	.259	.9277	.716	1.060	1.015

TABLE C.9 - cont'd.

Channel Cross-Sections No. OPC-CS7 with θ_{mc}=60° and θ_{fp}=90°

Run No.	Q (m^3/s)	H (m)	α_f	R_N $*10^{-4}$	Φ_1	Φ_2	Φ	E1	E2
59	0.0951	0.3381	0.399	10.48	.261	0.7751	.597	1.026	0.898
60	0.0614	0.2906	0.300	7.53	.259	0.7751	.598	1.018	0.920
61	0.0365	0.2528	0.196	4.87	.248	0.7751	.605	1.028	0.924
62	0.0786	0.3123	0.349	9.21	.261	0.7751	.597	1.030	0.878
63	0.0722	0.3031	0.330	8.63	.260	0.7751	.598	1.025	0.931
64	0.0500	0.2753	0.262	6.40	.255	0.7751	.601	1.038	0.925
65	0.0314	0.2398	0.153	3.90	.241	0.7751	.609	1.020	0.930
66	0.0211	0.2259	0.100	3.01	.232	0.7751	.615	1.052	0.878

Channel Cross-Section No. OPC-CS8 with θ_{mc}=45° and θ_{fp}=90°

Run No.	Q (m^3/s)	H (m)	α_f	R_N $*10^{-4}$	Φ_1	Φ_2	Φ	E1	E2
67	0.0950	0.3386	0.40	10.56	.244	0.5635	.441	1.022	0.793
68	0.0538	0.2913	0.302	6.60	.235	0.5635	.445	0.998	0.832
69	0.0319	0.2544	0.201	4.26	.217	0.5635	.453	1.044	0.781
70	0.0420	0.2709	0.250	4.91	.227	0.5635	.449	1.040	0.813
71	0.0878	0.3388	0.400	9.48	.244	0.5635	.441	1.023	0.788
72	0.0510	0.2910	0.302	6.18	.235	0.5635	.445	1.023	0.811
73	0.0277	0.2547	0.202	3.66	.217	0.5635	.454	1.040	0.859
74	0.0609	0.3079	0.340	7.92	.239	0.5635	.444	1.029	0.825
75	0.0794	0.3217	0.368	9.13	.242	0.5635	.442	1.036	0.802

TABLE C.10

Velocity Coefficients E1 and E2 of Compound Channels with β_f=2.0 under Free-Surface Flows

Channel Cross-Section No. OPC-CS9 with θ_{mc}=90° and θ_{fp}=90°

Run No.	Q (m^3/s)	H (m)	α_f	R_N $*10^{-4}$	Φ_1	Φ_2	Φ	E1	E2
1	2	3	4	5	6	7	8	9	10
76	0.0392	0.2566	0.208	4.33	.212	.6890	1.115	1.09	.747
77	0.0607	0.2904	9.300	6.33	.725	.6890	1.100	1.06	.750
78	0.0946	0.3372	0.397	9.05	.231	.6890	1.094	1.06	.725
79	0.0820	0.3222	0.369	8.10	.230	.6890	1.095	1.065	.730
80	0.0665	0.3020	0.327	6.83	.227	.6890	1.098	1.076	.731
81	0.0438	0.2693	0.245	4.80	.218	.6890	1.108	1.04	.743
82	0.0278	0.2408	0.156	3.24	.203	.6890	1.125	1.083	.775

Channel Cross-Section No. OPC-CS10 with θ_{mc}=90° and θ_{fp}=90°

Run No.	Q (m^3/s)	H	α_f	R_N $*10^{-4}$	Φ_1	Φ_2	Φ	E1	E2
1	2	3	4	5	6	7	8	9	10
83	0.0906	0.3388	0.400	8.96	.226	.5536	.883	1.052	.673
84	0.0514	0.2902	0.300	5.61	.216	.5536	.892	1.052	.692
85	0.0755	0.3239	0.373	7.82	.224	.5536	.885	1.046	.675
86	0.0702	0.3134	0.352	7.42	.222	.5536	.887	1.070	.670
87	0.0619	0.3018	0.327	7.76	.219	.5536	.889	1.052	.705
88	0.0449	0.2710	0.250	4.68	.208	.5536	.899	1.072	.725
89	0.0268	0.2430	0.164	3.30	.189	.5536	.917	1.044	.705

TABLE C.10 - cont'd.

Channel Cross-Section No. OPC-CS11 with θ_{mc}=60° and θ_{fp}=90°

Run No.	Q (m^3/s)	H (m)	α_f	R_N $*10^{-4}$	Φ_1	Φ_2	Φ	E1	E2
1	2	3	4	5	6	7	8	9	10
90	0.0871	0.3395	0.401	8.99	.216	.3986	.627	1.060	.619
91	0.0506	0.2912	0.30	5.78	.201	.3986	.630	1.062	.645
92	0.0289	0.2553	0.204	3.55	.178	.3986	.633	1.080	.638
93	0.0751	0.3246	0.374	7.99	.178	.3986	.628	1.044	.607
94	0.0670	0.3113	0.347	7.07	.209	.3986	.629	1.063	.615
95	0.0544	0.2913	0.302	6.21	.202	.3986	.630	1.045	.628
96	0.0420	0.2801	0.274	4.91	.196	.3986	.631	1.054	.675
97	0.0223	0.2432	0.164	2.84	.166	.3986	.635	1.044	.620

TABLE C.11

Velocity Coefficients E1 and E2 of Compound Channels with β_f=0.5 Under Covered Surface Flows

Channel Cross-Section No. CC-CS1 with θ_{mc}=90° and θ_{fp}=90°

Run No.	Q (m^3/s)	H (m)	α_f	R_N $*10^{-4}$	ϕ_1	ϕ_2	ϕ	E1	E2
1	2	3	4	5	6	7	8	9	10
1	.0474	.2572	.210	3.39	.231	1.412	.560	0.999	1.444
2	.0547	.2717	.252	3.88	.230	1.412	.561	0.996	1.464
3	.0647	.2903	.300	4.52	.229	1.412	.562	1.002	1.455
4	.0500	.2605	.220	3.50	.231	1.412	.561	1.002	1.436
5	.0627	.2832	.295	4.34	.229	1.412	.561	1.003	1.448
6	.0764	.3079	.340	5.15	.228	1.412	.562	1.001	1.440

Channel Cross-Section No. CC-CS2 with θ_{mc}=75°, θ_{fp}=90°

Run No.	Q (m^3/s)	H (m)	α_f	R_N $*10^{-4}$	ϕ_1	ϕ_2	ϕ	E1	E2
1	2	3	4	5	6	7	8	9	10
7	.0443	.2560	.206	3.05	.223	1.2785	.511	1.004	1.325
8	.0505	.2708	.250	3.41	.223	1.2785	.511	1.010	1.280
9	.0609	.2910	.302	4.04	.223	1.2785	.511	1.013	1.336
10	.0491	.2620	.224	3.40	.223	1.2785	.511	1.015	1.250
11	.0598	.2890	2.97	4.09	.223	1.2785	.511	1.012	1.320
12	.0740	.3105	.346	4.92	.223	1.2785	.512	1.010	1.285

TABLE C.11 - Cont'd.

Channel Cross-Section No. CC-CS3 with θ_{mc}=60°, θ_{fp}=90°

Run No.	Q (m^3/s)	H (m)	α_f	R_N *10^{-4}	ϕ_1	ϕ_2	ϕ	E1	E2
1	2	3	4	5	6	7	8	9	10
13	.0476	.270	.248	.152	.212	1.124	.455	1.067	1.182
14	.0730	.3111	.347	.285	.214	1.124	.454	1.005	1.169
15	.0593	.2888	.296	2.20	.213	1.124	.454	0.996	1.181
16	.0405	.2547	.202	3.24	.209	1.124	.456	1.016	1.160
17	.0735	.3117	.348	5.36	.214	1.124	.454	1.012	1.158
18	.060	.2907	.300	4.64	.213	1.124	.454	1.003	1.169
19	.0499	.2713	.250	3.93	.212	1.124	.454	1.010	1.185

Channel Cross-Section No. CC-CS4 with θ_{mc}=45°, θ_{fp}=90°

Run No.	Q (m^3/s)	H (m)	α_f	R_N *10^{-4}	ϕ_1	ϕ_2	ϕ	E1	E2
1	2	3	4	5	6	7	8	9	10
20	.0456	.2646	.232	3.70	.190	.9124	.378	1.019	1.057
21	.0544	.2927	.306	4.07	.196	.9124	.375	1.020	1.040
22	.0653	.3100	.344	5.06	.198	.9124	.375	1.030	1.995
23	.0435	.2708	.250	3.30	.192	.9124	.377	1.027	1.064
24	.0466	.2899	.300	3.59	.196	.9124	.375	1.018	1.031
25	.0534	.2990	.321	4.06	.197	.9124	.375	1.025	1.000
26	.0414	.2789	.271	3.24	.194	.9124	.376	1.024	1.023
27	.0338	.2635	.229	2.70	.190	.9124	.378	1.022	1.064
28	.0287	.2509	.190	2.35	.186	.9124	.379	1.029	1.017
29	.0594	.2914	.303	4.50	.196	.9124	.375	1.016	1.056
30	.0553	.3007	.324	4.04	.197	.9124	.375	1.020	1.049
31	.0502	.2913	.302	3.72	.196	.9124	.375	1.020	1.056
32	.0438	.2806	.276	3.30	.194	.9124	.376	1.02	1.051
33	.0338	.2614	.223	2.62	.196	.9124	.375	1.025	1.069
34	.0488	.2912	.302	3.76	.196	.9124	.375	1.022	1.024
35	.0580	.3072	.338	4.42	.198	.9124	.375	1.026	1.010
36	.0539	.1981	.320	4.11	.197	.9124	.375	1.025	1.030
37	.0437	.2817	.280	3.42	.194	.9124	.376	1.018	1.063
38	.0388	.2717	.252	3.08	.192	.9124	.377	1.033	1.050
39	.0338	.2607	.266	2.73	.189	.9124	.378	1.024	1.059

TABLE C.12

Velocity Coefficients, E1 and E2 of Compound Channels
β_f=1.0 Under Covered Surface Floods

Channel Cross-Section No. CC-CS5 with θ_{mc}=90° and θ_{fp}-90°

Run No.	Q (m^3/s)	H (m)	α_f	R_N $*10^{-4}$	Φ_1	Φ_2	Φ	E1	E2
1	2	3	4	5	6	7	8	9	10
40	.0410	.2689	.244	3.33	.192	1.063	.877	1.048	1.327
41	.0534	.2907	.300	4.20	.194	1.063	.876	1.0265	1.362
42	.0640	.3071	.340	4.93	.196	1.063	.873	1.0295	1.348
43	.0273	.2490	.220	2.43	.188	1.063	.881	1.059	1.349
44	.0684	.3116	.348	5.29	.196	1.063	.873	1.030	1.377
45	.0552	.2907	.300	4.38	.194	1.063	.876	1.0225	1.377
46	.0410	.2676	.241	3.30	.191	1.063	.878	1.050	1.384
47	.0296	.2492	.358	2.45	.188	1.063	.881	1.056	1.356

Channel Cross-Section CC-CS6 with θ_{mc}=75° and θ_{fp}=90°

Run No.	Q (m^3/s)	H (m)	α_f	R_N $*10^{-4}$	Φ_1	Φ_2	Φ	E1	E2
1	2	3	4	5	6	7	8	9	10
48	.0672	.3128	.350	5.05	.190	0.9277	.767	1.016	1.200
49	.0435	.2723	.254	3.47	.183	0.9277	.773	1.026	1.190
50	.0552	.7940	.308	4.26	.187	0.9277	.769	1.006	1.225
51	.0536	.2903	.300	4.11	.187	0.9277	.769	1.006	1.259
52	.0438	.2612	.222	3.50	.181	0.9277	.774	1.017	1.199
53	.0669	.3067	.337	5.00	.189	0.9277	.768	1.016	1.182
54	.0267	.2475	.179	2.38	.177	0.9277	.772	1.028	1.195
55	.0669	.3129	.351	5.10	.190	0.9277	.767	1.016	1.207
56	.0442	.2728	.255	3.56	.184	0.9277	.772	1.027	1.200
57	.0609	.3023	.328	4.71	.189	0.9277	.768	1.008	1.212
58	.0495	.2838	.284	3.93	.186	0.9277	.770	1.004	1.221
59	.0307	.2516	.192	2.38	.178	0.9277	.776	1.022	1.210

TABLE C.12 - Cont'd.

Channel Cross-Section No. CC-CS7 with $\theta_{mc}=60°$ and $\theta_{fp}=90°$

Run No.	Q (m^3/s)	H (m)	α_f	R_N $*10^{-4}$	ϕ_1	ϕ_2	ϕ	E1	E2
1	2	3	4	5	6	7	8	9	10
60	.0564	.3033	.330	4.73	.179	.7751	.648	1.029	1.059
61	.0482	.2910	.300	4.08	.177	.7751	.649	1.024	1.080
62	.0398	.2797	.274	3.44	.174	.7751	.651	1.033	1.109
63	.0283	.2575	.211	2.52	.166	.7751	.657	1.052	1.043
64	.0524	.2902	.300	4.03	.176	.7751	.650	1.022	1.056
65	.0369	.2711	.251	3.23	.171	.7751	.653	1.044	1.090
66	.0574	.3060	.340	4.75	.180	.7751	.647	1.032	1.095
67	.0283	.2563	.207	2.64	.166	.7751	.657	1.050	1.054

Channel Cross-Section No. CC-CS8 with $\theta_{mc}=45°$ and $\theta_{fp}=90°$

Run No.	Q (m^3/s)	G (m)	α_f	R_N $*10^{-4}$	ϕ_1	ϕ_2	ϕ	E1	E2
1	2	3	4	5	6	7	8	9	10
68	.0589	.3128	.350	4.81	.164	.5635	.478	1.158	1.016
69	.0325	.2708	.250	2.85	.150	.5635	.485	1.168	1.025
70	.0696	.3255	.376	5.59	.167	.5635	.477	1.125	0.987
71	.0526	.3122	.349	4.22	.164	.5635	.478	1.152	1.011
72	.0312	.2725	.254	2.65	.178	.5635	.472	1.115	0.978
73	.0692	.3341	.392	5.38	.181	.5635	.470	1.104	0.968
74	.0408	.2900	.299	3.59	.158	.5635	.481	1.116	0.978
75	.0550	.3123	.349	4.47	.167	.5635	.470	1.168	1.024
76	.0727	.3347	.393	5.85	.161	.5635	.470	1.145	1.004
77	.0336	.2730	.256	2.96	.178	.5635	.472	1.118	0.980
78	.0621	.3117	.348	5.04	.180	.5635	.470	1.110	0.973
79	.0466	.2905	.300	3.91	.180	.5635	.471	1.130	0.991
80	.0336	.2667	.238	2.92	.177	.5635	.472	1.130	0.991

TABLE C.13

Velocity Coefficients E1 and E2 of Compound Channels with β_f=2.0 Under Covered Surface Flow

Channel Cross-Section No. CC-CS10 θ_{mc}=90° and θ_{fp}=90°

Run No.	Q (m^3/s)	H (m)	α_f	R_N *10^{-4}	Φ_1	Φ_2	Φ	E1	E2
1	2	3	4	5	6	7	8	9	10
81	.0327	.2707	.250	2.59	.151	.6890	1.185	1.055	1.095
82	.0426	.2911	.302	3.15	.158	.6890	1.177	1.046	1.125
83	.0555	.3145	.354	4.16	.163	.6890	1.171	1.032	1.093
84	.0413	.2903	.300	3.20	.157	.6890	1.178	1.032	1.093
85	.0527	.3140	.353	4.16	.163	.6890	1.171	0.983	1.087

Channel Cross-Section No. CC-CS11, θ_{mc}=75°, θ_{fp}=90°

Run No.	Q (m^3/s)	H (m)	α_f	R_N *10^{-4}	Φ_1	Φ_2	Φ	E1	E2
1	2	3	4	5	6	7	8	9	10
86	.0555	.3127	.350	4.08	.155	.5536	.948	1.052	0.995
87	.0410	.2902	.300	3.10	.149	.5536	.954	1.042	0.985
88	.0312	.2700	.247	2.43	.141	.5536	.962	1.068	0.998
89	.0540	.3123	.349	4.42	.155	.5536	.948	1.053	1.018
90	.0438	.2901	.300	3.40	.149	.5536	.954	1.034	1.020
91	.0341	.2740	.258	2.71	.143	.5536	.960	1.072	1.014
92	.0256	.2572	.210	2.08	.135	.5536	.967	1.075	0.974

TABLE C.13 - Cont'd.

Channel Cross-Section No. CC-CS12, $\theta_{mc}=60°$, $\theta_{fp}=90°$

Run No.	Q (m^3/s)	H (m)	α_f	R_N $*10^{-4}$	ϕ_1	ϕ_2	ϕ	E1	E2
1	2	3	4	5	6	7	8	9	10
93	.0489	.3129	.351	3.73	.143	.3986	.691	1.066	.873
94	.0353	.2916	.303	2.89	.144	.3986	.690	1.044	.885
95	.0268	.2707	.247	2.06	.143	.3986	.691	1.071	.850
96	.0457	.3130	.350	3.43	.143	.3986	.691	1.067	.889
97	.0341	.2906	.300	2.69	.145	.3986	.690	1.040	.875
98	.0257	.2714	.251	2.20	.143	.3986	.691	1.065	.830

TABLE C.14

Velocity Coefficients E1 and E2 of Simple and Complex Channels Under Covered Surface Flows

Rectangular Channel Cross Section

Run No.	Q (m^3s)	H (m)	R_N $*10^{-4}$	Φ_1	E1	E2
1	2	3	4	5	6	7
1.	0.0792	0.4200	4.54	.260	1.035	0.987
2	0.0350	0.3643	2.13	.278	1.026	1.094
3	0.0472	0.3449	2.94	.285	1.030	1.022
4	0.0456	0.3523	2.81	.284	1.034	0.892
5	0.0653	0.3769	3.91	.274	1.034	0.890
6	0.0729	0.4041	4.23	.265	1.022	1.064
7	0.0608	0.3785	3.63	.274	1.030	0.978
8	0.0505	0.3683	3.05	.277	1.027	1.060
9	0.0401	0.3742	2.41	.274	1.029	1.108
10	0.048	0.4098	2.78	.264	1.022	1.110
11	0.0482	0.3495	2.98	.283	1.036	0.957
12	0.0417	0.3492	2.58	.283	1.037	0.922
13	0.0669	0.4072	3.86	.264	1.025	1.106
14	0.0803	0.4135	4.60	.263	1.029	1.017

TABLE C.14 - cont'd.

Triangular and Complex Triangular Channel Cross-Section

Run No.	Q (m^3s)	H (m)	R_N $*10^{-4}$	Φ_1	E1	E2
1	2	3	4	5	6	7
15	0.0153	0.2314	1.38	.208	1.056	0.677
16	0.0252	0.2380	2.24	.212	1.054	0.711
17	0.0399	0.2383	3.54	.212	1.052	0.731
18	0.0187	0.2518	1.62	.217	1.057	0.711
19	0.0470	0.2469	4.11	.215	1.058	0.711
20	0.0522	0.3520	3.86	.228	1.032	0.741
21	0.0692	0.3411	5.20	.229	1.031	0.720

Trapezoidal and Complex Trapezoidal Channel Cross-Sction

Run No.	Q (m^3s)	H (m)	R_N $*10^{-4}$	Φ_1	E1	E2
1	2	3	4	5	6	7
22	0.0230	0.1656	2.15	.297	1.045	0.730
23	0.0416	0.1839	3.77	.300	1.045	0.855
24	0.0127	0.1849	1.14	.300	1.055	0.645
25	0.0370	0.1821	3.36	.300	1.063	0.614
26	0.0504	0.2811	3.85	.288	1.040	0.668
27	0.0721	0.2916	5.46	.286	1.038	0.748
28	0.0341	0.2832	2.61	.288	1.042	0.698
29	0.0495	0.2824	3.80	.288	1.042	0.698
30	0.0666	0.2822	5.11	.288	1.044	0.662

TABLE C.15

Variation of Shape Factor ϕ_1(=R/H) with the Relative Depth, α_f(=h_{fp}/H) in case of Compound Channels Under Free-Surface flows

Channel Cross-Section No.	β_f	θ_{mc}	ϕ_1 = R/H			% difference	exp(ϕ_1)			% difference
			α_f=0.15	0.275	0.40	(max/min)	.015	.275	.40	(max/min)
1	2	3	4	5	6	7	8	9	10	11
OPC-CS1	0.5	90°	.339	.329	.310	9.4	1.404	1.39	1.363	3.0
OPC-CS2	0.5	75°	.330	.326	.319	6.8	1.392	1.385	1.362	2.2
OPC-CS3	0.5	60°	.314	.314	.303	3.6	1.369	1.369	1.354	1.1
OPC-CS4	0.5	45°	.281	.290	.287	3.2	1.324	1.336	1.332	0.9
OPC-CS5	1.0	90°	.273	.277	.273	1.5	1.314	1.319	1.314	0.3
OPC-CS6	1.0	75°	.261	.270	.269	3.4	1.298	1.310	1.309	0.9
OPC-CS7	1.0	60°	.241	.257	.261	8.3	1.273	1.293	1.298	2.0
OPC-CS8	1.0	45°	.205	.231	.243	18.5	1.228	1.260	1.275	3.8
OPC-CS9	2.0	90°	.201	.222	.231	14.9	1.223	1.249	1.260	3.0
OPC-CS10	2.0	75°	.186	.212	.231	14.0	1.204	1.236	1.260	4.6
OPC-CS11	2.0	60°	.162	.196	.216	33.3	1.176	1.217	1.241	5.5

TABLE C.16

Variation of Shape Factor $\Phi_1(R/H)$ with the Relative Flow Depth, $\alpha_f(h_{fp}/H)$ in case of Compound Channels Under Covered Surface Flows

Channel Cross-Section No.	β_f	θ_{mc}	Φ_1 = R/H			% difference	exp(Φ_1)			% difference
			α_f=0.15	0.275	.040	(max/min)	.015	.275	.40	(max/min)
1	2	3	4	5	6	7	8	9	10	11
OPC-CS1	0.5	90°	.230	230	.224	2.7	1.259	1.258	1.251	0.6
OPC-CS2	0.5	75°	.221	.223	.220	1.4	1.247	1.250	1.246	0.3
OPC-CS3	0.5	60°	.206	.210	.213	3.4	1.229	1.234	1.237	0.7
OPC-CS4	0.5	45°	.182	.194	.200	9.9	1.200	1.214	1.217	1.4
OPC-CS5	1.0	90°	.185	.193	.196	5.9	1.203	1.213	1.217	1.2
OPC-CS6	1.0	75°	.174	.185	.191	9.8	1.190	1.204	1.211	1.8
OPC-CS7	1.0	60°	.158	.172	.184	16.5	1.171	1.188	1.202	2.6
OPC-CS8	1.0	45°	.133	.149	.166	24.8	1.142	1.161	1.181	2.4
OPC-CS9	2.0	90°	.137	.155	.167	21.9	1.147	1.168	1.181	3.0
OPC-CS10	2.0	75°	.124	.145	.161	29.8	1.132	1.156	1.175	3.8
OPC-CS11	2.0	60°	.106	.131	.152	43.4	1.112	1.140	1.164	4.7

TABLE C.17

Average Values of Velocity Coefficients E2 with Variation of Shape of Channels in Case of Compound Channel Under Free-Surface Flows

Channel Cross-Section No.	β_f	$\exp(\phi_1)$	ϕ_2	Φ	E2	σ (E2)
1	2	3	4	5	6	7
OPC-CS1	0.5	1.390	1.4124	0.508	1.175	0.026
OPC-CS2	0.5	1.305	1.2785	0.462	1.09	0.023
OPC-CS3	0.5	1.369	1.1238	0.410	0.983	0.041
OPC-CS4	0.5	1.336	0.9124	0.341	0.853	0.029
OPC-CS5	1.0	1.319	1.0630	0.806	1.124	0.016
OPC-CS6	1.0	1.310	0.9277	0.708	1.027	0.020
OPC-CS7	1.0	1.293	0.7751	0.599	0.910	0.021
OPC-CS8	1.0	1.260	0.5635	0.447	0.810	0.012
OPC-CS9	2.0	1.249	0.6890	1.103	0.743	0.017
OPC-CS10	2.0	1.236	0.5536	0.896	0.692	0.019
OPC-CS11	2.0	1.217	0.3986	0.655	0.630	0.020

TABLE C.18

Average Values of Velocity Coefficients E2 with Variation of Shape of Channels in Case of Compound Channel Under Covered Surface Flows

Channel Cross-Section No.	β_f	$\exp(\Phi_1)$	Φ_2	ϕ	E2	σ(E2)
1	2	3	4	5	6	7
CC-CS1	0.5	1.251	1.4124	0.561	1.452	0.015
CC-CS2	0.5	1.246	1.2785	0.511	1.300	0.029
CC-CS3	0.5	1.237	1.1238	0.455	1.172	0.010
CC-CS4	0.5	1.217	0.9124	0.376	1.042	0.021
CC-CS5	1.0	1.213	1.0630	0.876	1.357	0.018
CC-CS6	1.0	1.204	0.9277	0.771	1.208	0.019
CC-CS7	1.0	1.188	0.7751	0.652	1.073	0.022
CC-CS8	1.0	1.161	0.5635	0.485	0.994	0.019
CC-CS9	2.0	1.168	0.6890	1.180	1.097	0.015
CC-CS10	2.0	1.156	0.5526	0.958	1.004	0.012
CC-CS11	2.0	1.140	0.3986	0.699	0.867	0.021

APPENDIX D

Flow Chart for the Determination of Velocity Coefficients E1 and E2

Figure FC.1. Flow Chart for the Determination of the Coefficients, E1 and E2 for Covered Flow with Vertical and Horizontal Strips Analysis.

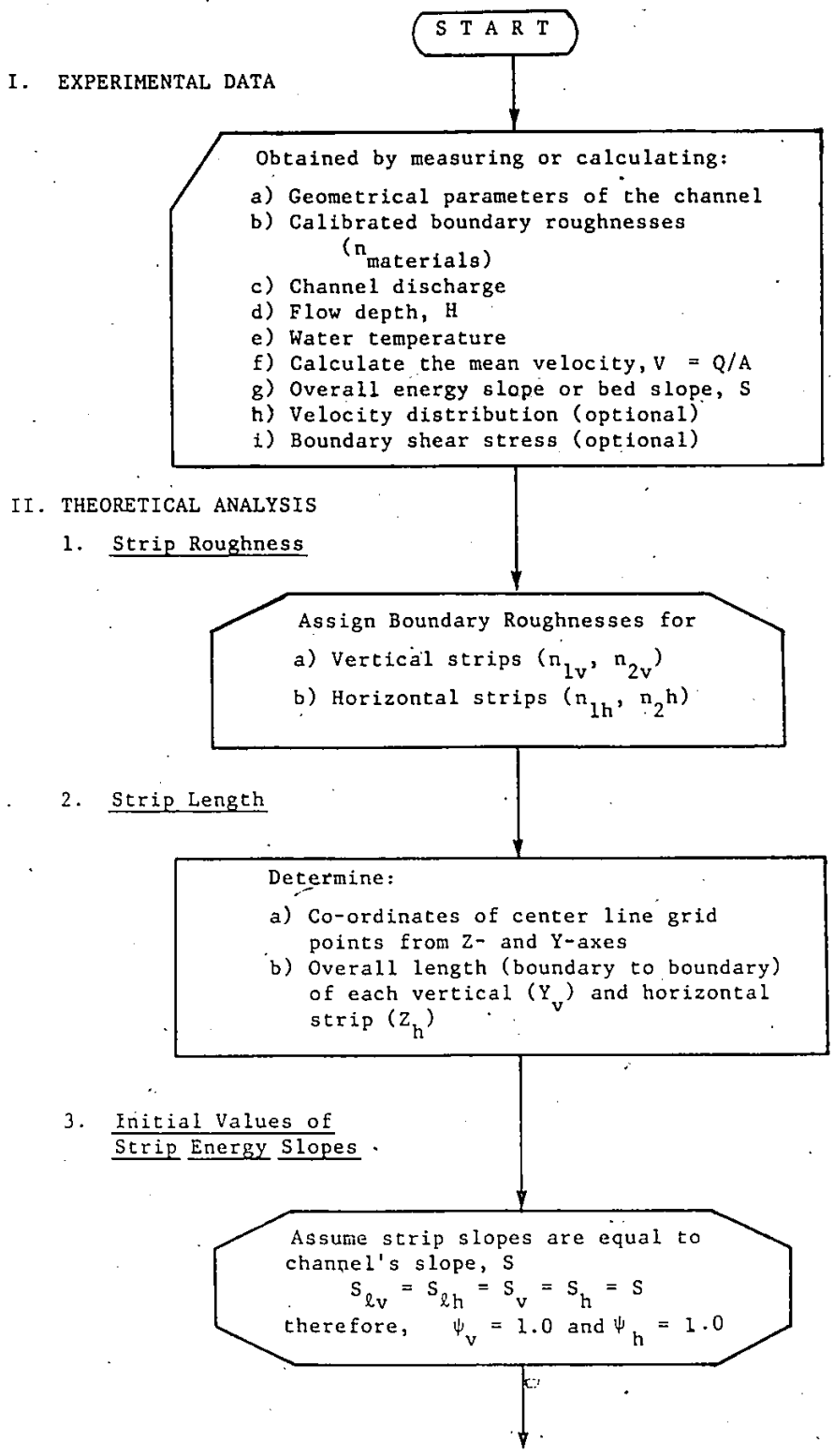
START
I. EXPERIMENTAL DATA
Obtained by measuring or calculating:
a) Geometrical parameters of the channel
b) Calibrated boundary roughnesses ($n_{materials}$)
c) Channel discharge
d) Flow depth, H
e) Water temperature
f) Calculate the mean velocity, V = Q/A
g) Overall energy slope or bed slope, S
h) Velocity distribution (optional)
i) Boundary shear stress (optional)
II. THEORETICAL ANALYSIS
1. Strip Roughness
Assign Boundary Roughnesses for
a) Vertical strips (n_{1v}, n_{2v})
b) Horizontal strips (n_{1h}, n_2h)
2. Strip Length
Determine:
a) Co-ordinates of center line grid points from Z- and Y-axes
b) Overall length (boundary to boundary) of each vertical (Y_v) and horizontal strip (Z_h)
3. Initial Values of Strip Energy Slopes
Assume strip slopes are equal to channel's slope, S
$S_{\ell v} = S_{\ell h} = S_v = S_h = S$
therefore, $\psi_v = 1.0$ and $\psi_h = 1.0$

4. Initial Value of E2

Assume,
$E2 = 1.0$
$\Delta E2 = 0.0$

5. Division Surface

Determine, λ_v and λ_h from

a) $$\frac{3\kappa}{2}\frac{Y_v^{1/6}}{n_{1v}g^{1/2}} = \frac{\lambda_v^{1/2}\psi_v^{1/2-1}}{1-\frac{n_{1v}}{n_{2v}}\lambda_v^{2/3}\psi_v^{1/2}}(1+\lambda_v)^{1/6}$$

and b) $$\frac{3\kappa}{2}\frac{Z_h^{1/6}}{n_{1h}g^{1/2}} = \frac{\lambda_h^{1/2}\psi_h^{-1}}{1-\frac{n_{1v}}{n_{2}h}\lambda_h^{2/3}\psi_h^{1/2}}(1+\lambda_h)^{1/6}$$

6. Strip Composite Roughness and Energy Slope

Determine n_v, n_h, S_v, and S_h from

a) $$\frac{n_v}{n_{1v}} = [(0.5)^{2/3}\frac{(1+\lambda_v)^{5/3}}{1+\frac{n_{1v}}{n_{2v}}\lambda_v^{5/3}\psi_v^{1/2}}][(\frac{1+\lambda_v\psi_v}{1+\lambda_v})^{1/2}]$$

b) $$\frac{n_h}{n_{1h}} = [(0.5)^{2/3}\frac{(1+\lambda_h)^{5/3}}{1+\frac{n_{1h}}{n_2h}\lambda_h^{5/3}\psi_h^{1/2}}][(\frac{1+\lambda_h\psi_h}{1+\lambda_h})^{1/2}]$$

c) $$\frac{S_v}{S_{1v}} = \frac{1+\lambda_v\psi_v}{1+\lambda_v}$$

d) $$\frac{S_h}{S_{1h}} = \frac{1+\lambda_h\psi_h}{1+\lambda_2}$$

7. Strip Mean Velocities

Determine, $V_{\ell v}$ and V_{mh} from

a) $$V_{\ell v} = \frac{1}{n_{\ell v}} Y_{\ell v}^{2/3} S_{\ell v}^{1/2}$$

and b) $$V_{mh} = \frac{1}{n_{mh}} Z_{mh}^{2/3} S_{mh}^{1/2}$$

8. Strip Dimensionless Velocity Distributions

Determine, $u_{\ell v}/V_{\ell v}$ and u_{mh}/V_{mh} from

a) $$\frac{u_{\ell v}}{V_{\ell v}} = 1 - \frac{n_{\ell v} g^{1/2}}{\kappa Y_{\ell v}^{1/6}} F_2(\epsilon_{\ell v})$$

and b) $$\frac{u_{mh}}{V_{mh}} = 1 - \frac{n_{\ell h} g^{1/2}}{\kappa Z_{mh}} F_2(\epsilon_{mh})$$

when $$F_2(\epsilon) = 2\left[\text{Ln} \frac{\epsilon^{1/2}}{1-(1-\epsilon)^{1/2}} - (1-\epsilon)^{1/2} - 1/3\right]$$

9. $$E2 = E2 \pm \Delta E2$$

10. Determine 'E1'

Determine, the coefficient, E1 from

$$E1 = \frac{A}{\left[\left(\frac{u_{\ell v}}{V_{\ell v}} \quad \frac{u_{mh}}{V_{mh}}\right) E2 \quad \Delta A\right]}$$

11. Channel Velocity Distribution

Determine, U from

$$U = E1\left[\frac{u_{\ell v}}{V_{\ell v}} \quad \frac{u_{mh}}{V_{mh}}\right]E2 \quad V$$

12. Strip Velocity Distributions

From Step 8

a) $u_{\ell v} = \frac{u_{\ell v}}{V_{\ell v}} \quad V_{\ell v}$

b) $u_{mh} = \frac{u_{mh}}{V_{mh}} \quad V_{mh}$

13. Boundary Shear Stresses

Determine

$$\tau_{\phi \ell v} = \frac{1}{N} \Sigma[\rho g S_{\ell v}(E2\frac{U}{u_{\ell v}})^2 Y_{\ell v}]$$

$$\tau_{\phi mh} = \frac{1}{M} \Sigma[\rho g S_{mh}(E2\frac{U}{u_{mh}})^2 Y_{mh}]$$

14. Sub-Strip Slopes

Determine

a) $S_{\ell v} = \tau_{\phi \ell v}/(\gamma \, Y_{\ell v})$

b) $S_{mh} = \tau_{\phi mh}/(\gamma \, Z_{mh})$

Step 5

Step 18

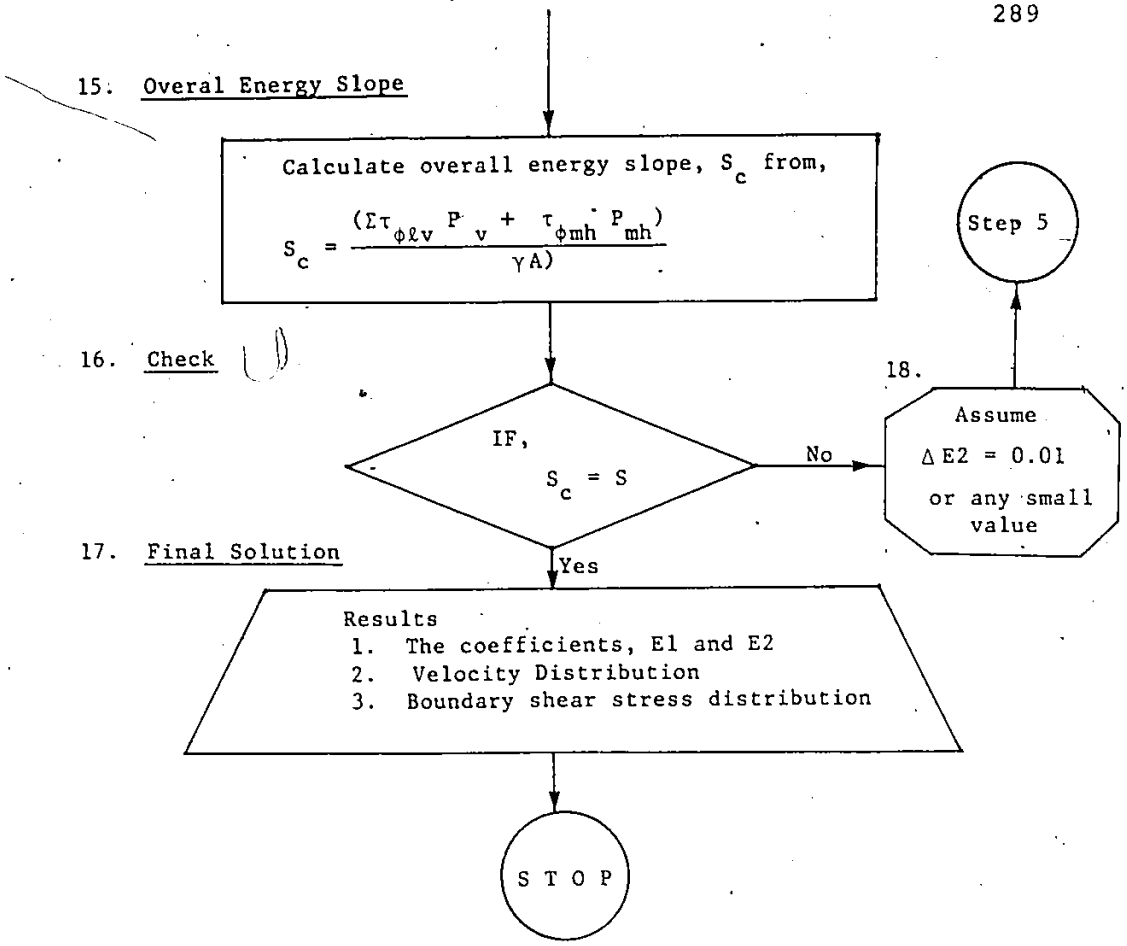
15. Overal Energy Slope
Calculate overall energy slope, S_c from,
$S_c = \frac{(\Sigma\tau_{\phi\ell v} P_v + \tau_{\phi mh} P_{mh})}{\gamma A)}$
Step 5
16. Check
18.
IF,
$S_c = S$
No
Assume
$\Delta E2 = 0.01$
or any small value
17. Final Solution
Yes
Results
1. The coefficients, E1 and E2
2. Velocity Distribution
3. Boundary shear stress distribution
S T O P

Figure FC.2. Flow Chart for the Determination of the Coefficients, E1 and E2 of Free-Surface Flow with Vertical and Horizontal Strips Analysis.

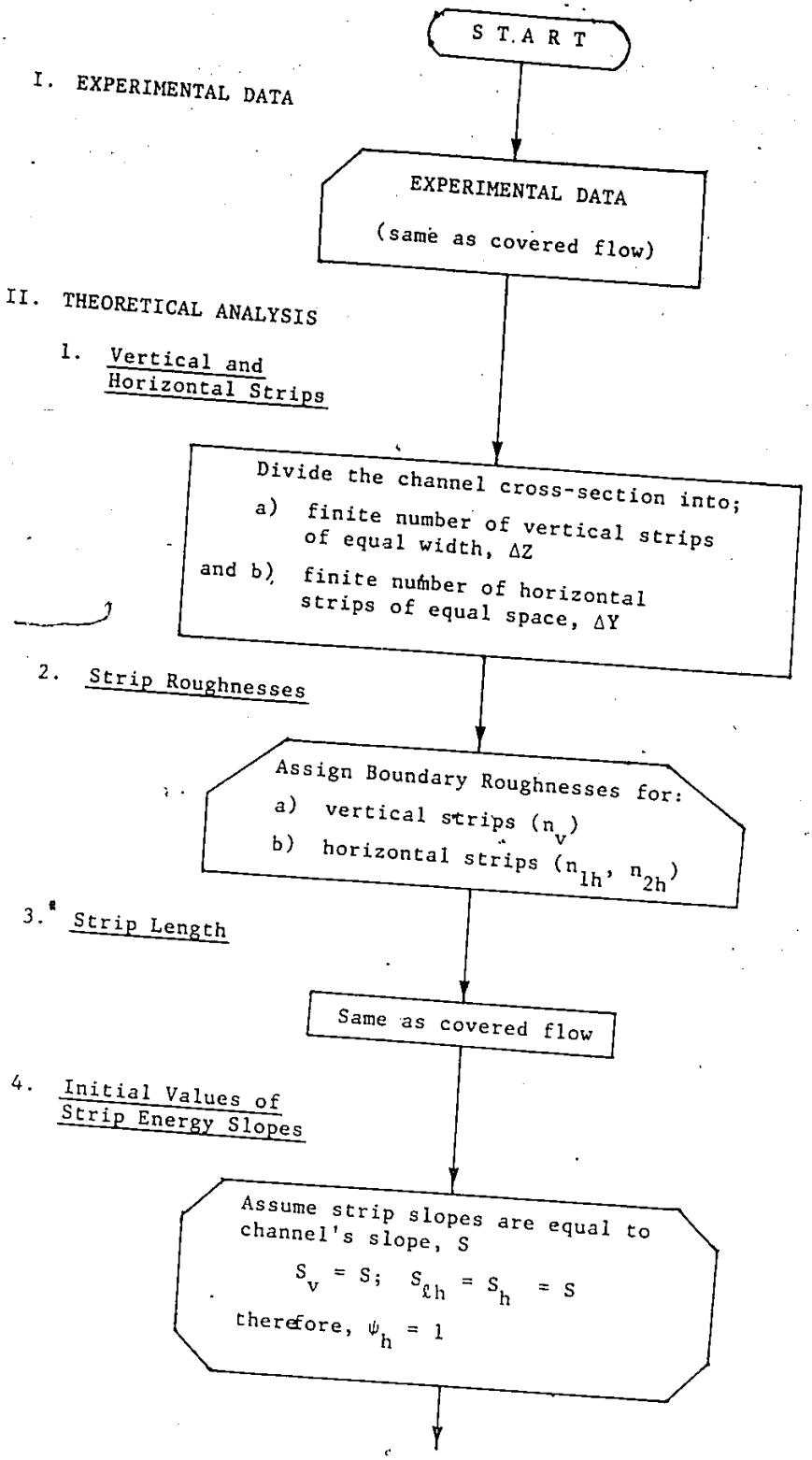
START
I. EXPERIMENTAL DATA
EXPERIMENTAL DATA
(same as covered flow)
II. THEORETICAL ANALYSIS
1. Vertical and Horizontal Strips
Divide the channel cross-section into;
a) finite number of vertical strips of equal width, ΔZ
and b) finite number of horizontal strips of equal space, ΔY
2. Strip Roughnesses
Assign Boundary Roughnesses for:
a) vertical strips (n_v)
b) horizontal strips (n_{1h}, n_{2h})
3. Strip Length
Same as covered flow
4. Initial Values of Strip Energy Slopes
Assume strip slopes are equal to channel's slope, S
$S_v = S$; $S_{\ell h} = S_h = S$
therefore, $\psi_h = 1$

5. Initial Value of 'E2'

Assume,

$E2 = 1.0;\ \Delta E2 = 0.0$

6. Division Surface

Determine, λ_h from horizontal strips from

$$\frac{3\kappa}{2}\frac{z_h^{1/6}}{n_{1h}g^{1/2}} = \frac{\lambda_h^{1/2}\psi_h^{1/2-1}}{1-\frac{n_{1h}}{n_{2h}}\lambda_h^{2/3}\psi_h^{1/2}}(1+\lambda_h)^{1/6}$$

7. Strip Horizontal Composite Roughness and Slopes

Determine n_h, S_h from

a) $$\frac{n_h}{n_{1h}} = [(0.5)^{2/3}\frac{(1+\lambda_h)^{5/3}}{1+\frac{n_{1h}}{n_{2h}}\lambda_h^{5/3}\psi_h^{1/2}}][\frac{1+\lambda_h\psi_h}{1+\lambda_h}]^{1/2}$$

b) $$\frac{S_h}{S_{1h}} = \frac{1+\lambda_h\psi_h}{1+\lambda_h}$$

8. Strip Mean Velocities

Determine V_v and V_{mh} from

a) $$V_v = \frac{1}{n_v}Y_v^{2/3}S_v^{1/2}$$

b) $$V_{mh} = \frac{1}{n_{mh}}Y_{mh}^{2/3}S_{mh}^{1/2}$$

9. Strip Dimensionless Velocity Distributions

Determine u_v/V_v and u_{mh}/V_{mh} from

a) $$\frac{u_v}{V_v} = 1 - \frac{n_v g^{1/2}}{\kappa Y_v^{1/6}} F_2(\varepsilon_v)$$

and b) $$\frac{u_{mh}}{V_{mh}} = 1 - \frac{n_{mh} g^{1/2}}{\kappa Z_{mh}^{1/6}} F_2(\varepsilon_{mh})$$

10. The Coefficient 'E2'

$$E2 = E2 \pm \Delta E2$$

11. The Coefficient, E1

Determine from

$$E1 = \frac{A}{\left[\Sigma\left(\frac{u_v}{V_u} \quad \frac{u_{mh}}{V_{mh}}\right)^{E2} \cdot \Delta A\right]}$$

12. Channel Velocity Distributions

Determine

$$U = E1\left[\frac{u_v}{V_v} \quad \frac{u_{mh}}{V_{mh}}\right]^{E2} \quad V$$

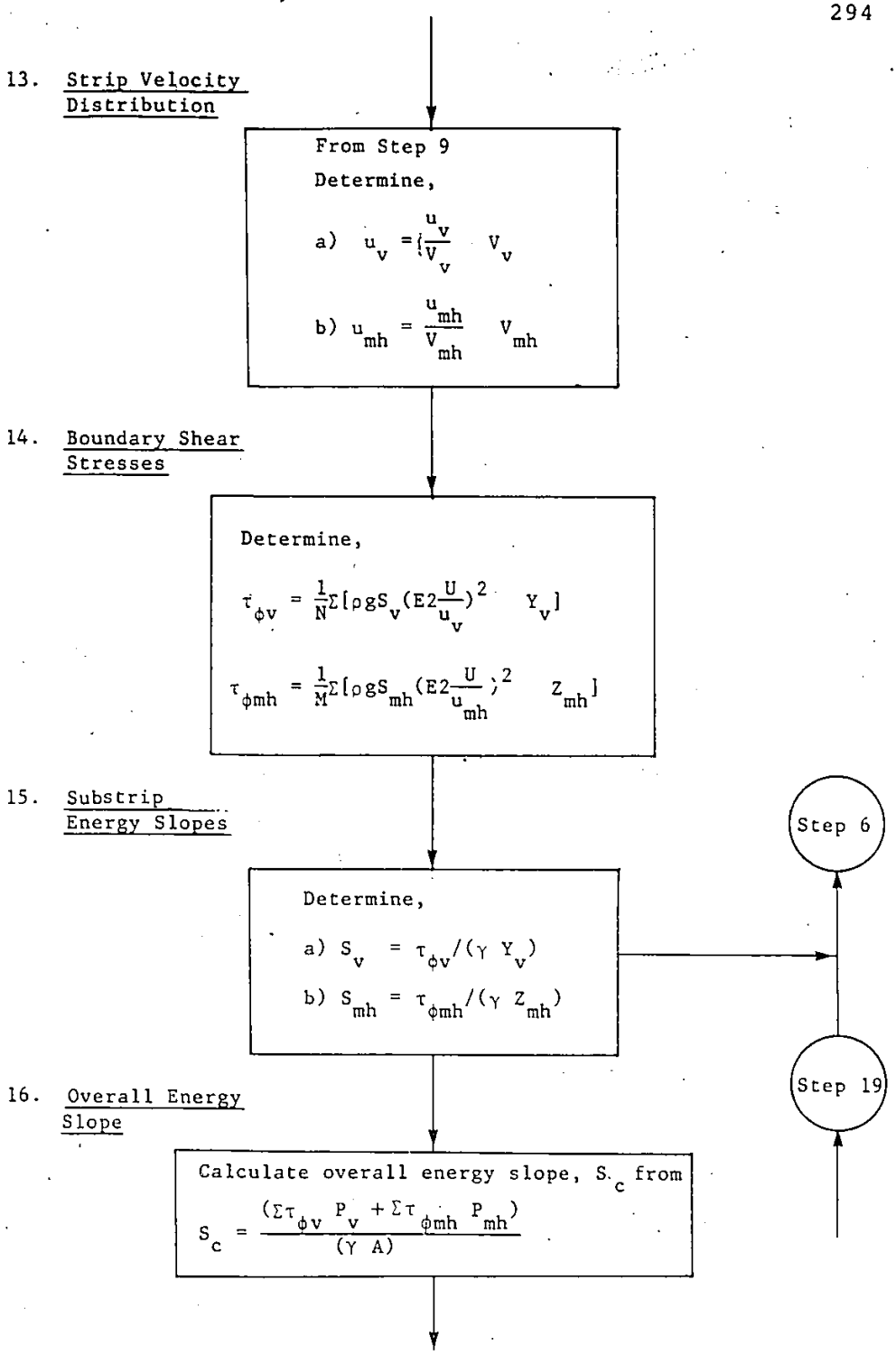
13. Strip Velocity Distribution
From Step 9
Determine,
a) $u_v = \{\frac{u_v}{V_v}\ V_v$
b) $u_{mh} = \frac{u_{mh}}{V_{mh}}\ V_{mh}$
14. Boundary Shear Stresses
Determine,
$\tau_{\phi v} = \frac{1}{N}\Sigma[\rho g S_v (E2\frac{U}{u_v})^2\ Y_v]$
$\tau_{\phi mh} = \frac{1}{M}\Sigma[\rho g S_{mh} (E2\frac{U}{u_{mh}})^2\ Z_{mh}]$
15. Substrip Energy Slopes
Determine,
a) $S_v = \tau_{\phi v}/(\gamma\ Y_v)$
b) $S_{mh} = \tau_{\phi mh}/(\gamma\ Z_{mh})$
16. Overall Energy Slope
Calculate overall energy slope, S_c from
$S_c = \frac{(\Sigma\tau_{\phi v}\ P_v + \Sigma\tau_{\phi mh}\ P_{mh})}{(\gamma\ A)}$
Step 6
Step 19

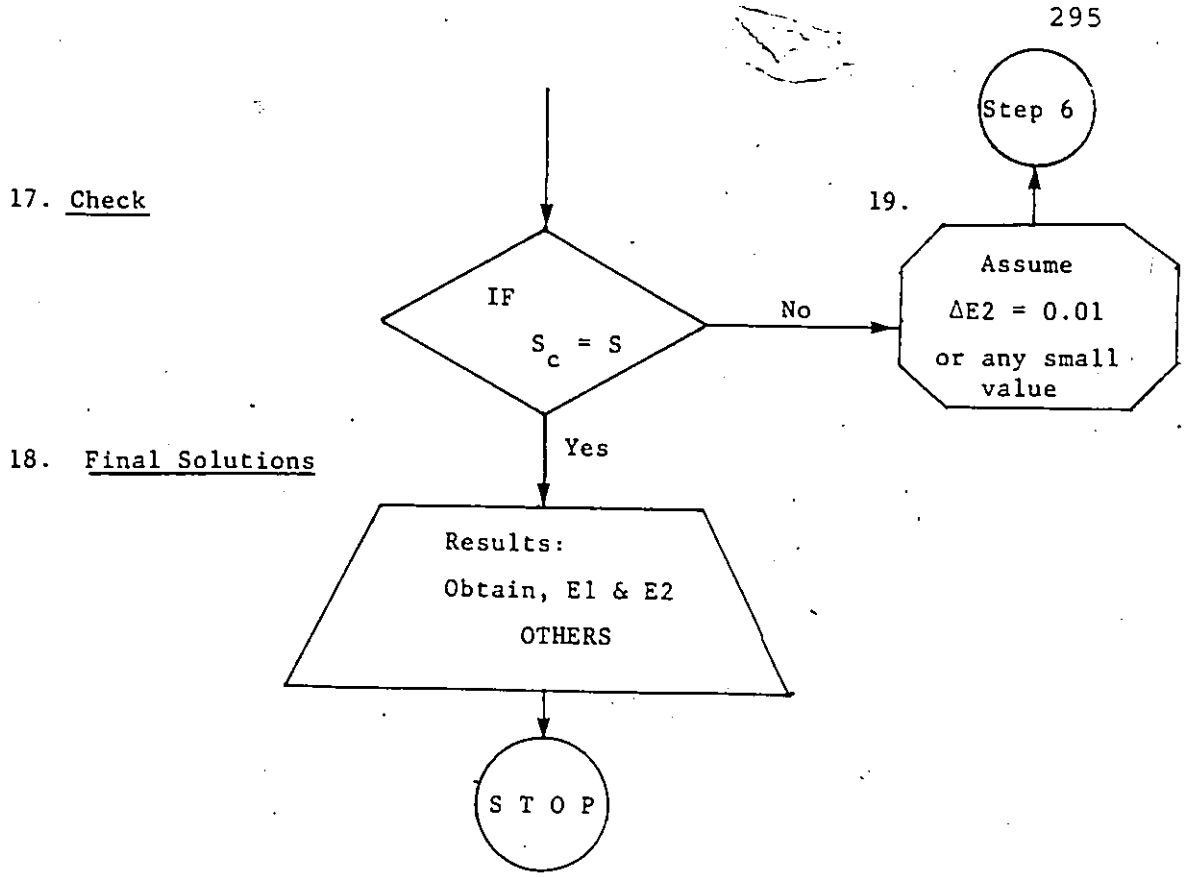

Figure FC-2. Flow Chart for the Determination of the Coefficients, E1 and E2, of Free-surface Flow with Vertical and Horizontal Strips Analysis.

Figure FC.3. Flow Chart for the Determination of the Coefficients, E1 and E2, of Covered Surface Flow with Vertical Strips Analysis.

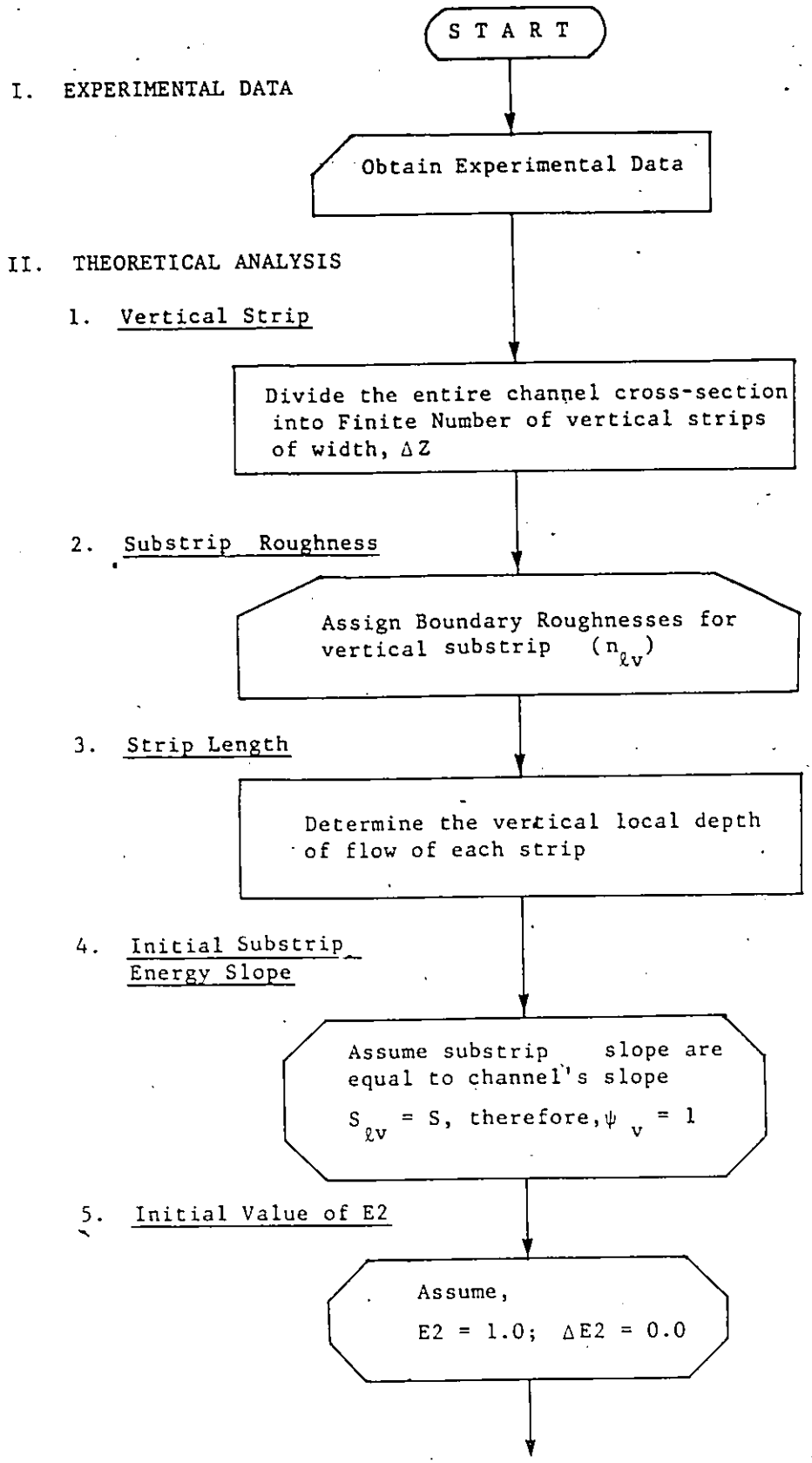
START
I. EXPERIMENTAL DATA
Obtain Experimental Data
II. THEORETICAL ANALYSIS
1. Vertical Strip
Divide the entire channel cross-section into Finite Number of vertical strips of width, ΔZ
2. Substrip Roughness
Assign Boundary Roughnesses for vertical substrip ($n_{\ell v}$)
3. Strip Length
Determine the vertical local depth of flow of each strip
4. Initial Substrip Energy Slope
Assume substrip slope are equal to channel's slope
$S_{\ell v} = S$, therefore, $\psi_v = 1$
5. Initial Value of E2
Assume,
E2 = 1.0; ΔE2 = 0.0

6. Division Surface

Determine, λ_v for vertical strips from

$$\frac{3\kappa}{2}\frac{Y_v^{1/6}}{n_{1v}g^{1/2}} = \frac{\lambda_v^{1/2}\psi_v^{1/2} - 1}{1 - \frac{n_{iv}}{n_2 n_v}\lambda_v^{2/3}\psi_v^{1/2}}(1+\lambda_v)^{1/6}$$

7. Vertical Strip Composite Roughnesses and Slopes

Determine, n_v and S_v from

$$\text{a)}\ \frac{n_v}{n_{1v}} = [(0.5)^{2/3}\frac{(1+\lambda_v)^{5/3}}{1+\frac{n_{1v}}{n_{2v}}\lambda_v^{5/3}\psi_v^{1/2}}][\frac{1+\lambda_v\psi_v}{1+\lambda_v})^{1/2}]$$

8. Substrip Velocities

For vertical strip,

$$V_{\ell v} = \frac{1}{n_{\ell v}} Y_{\ell v}^{2/3} S_{\ell v}^{1/2}$$

9. Substrip Dimensionless Velocity Distributions

For vertical strip,

$$\frac{u_{\ell v}}{V_{\ell v}} = 1 - \frac{n_{\ell v} g^{1/2}}{\kappa Y_{\ell v}^{1/6}} F_2(\epsilon_{\ell v})$$

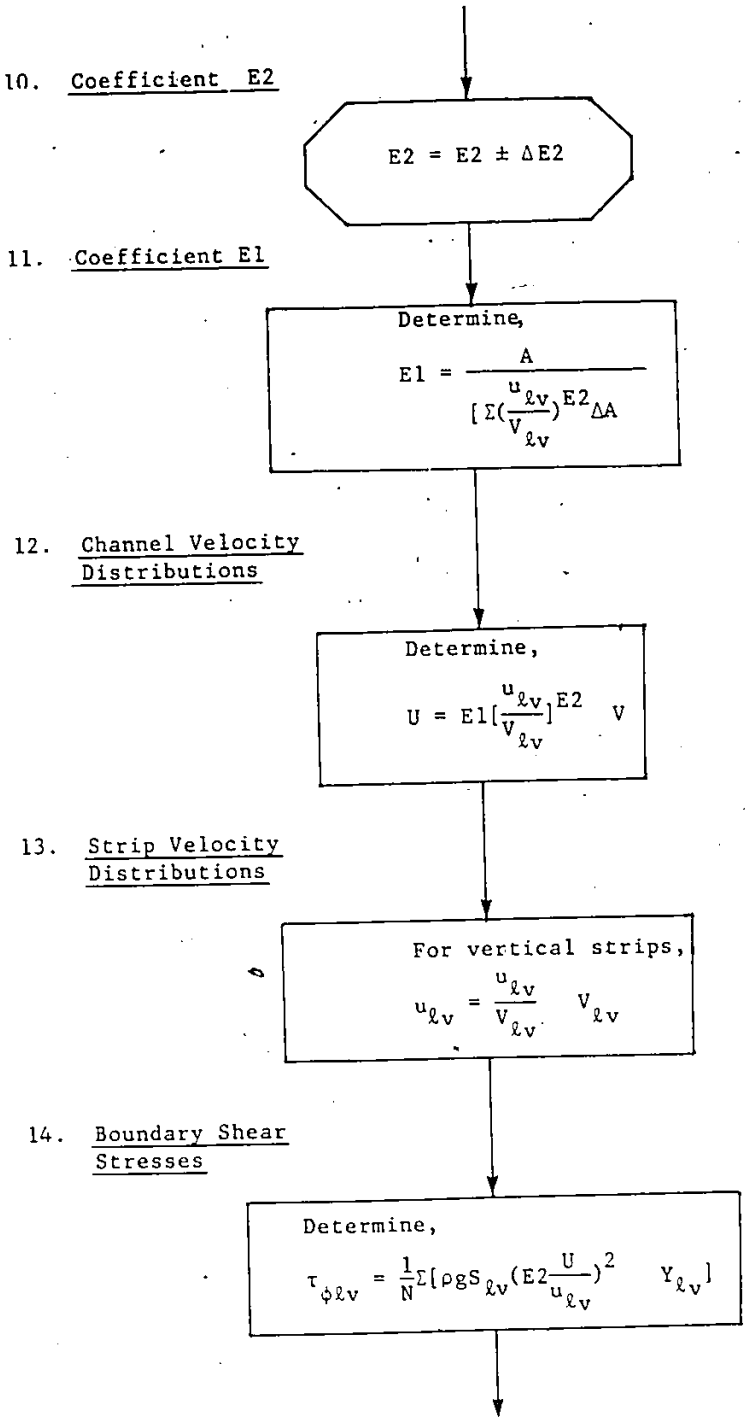
10. Coefficient E2
E2 = E2 ± ΔE2
11. Coefficient E1
Determine,
E1 = A / [Σ(u_ℓv / V_ℓv) E2 ΔA
12. Channel Velocity Distributions
Determine,
U = E1[u_ℓv / V_ℓv] E2 V
13. Strip Velocity Distributions
For vertical strips,
u_ℓv = u_ℓv / V_ℓv V_ℓv
14. Boundary Shear Stresses
Determine,
τ_φℓv = 1/N Σ[ρgS_ℓv (E2 U / u_ℓv)^2 Y_ℓv]

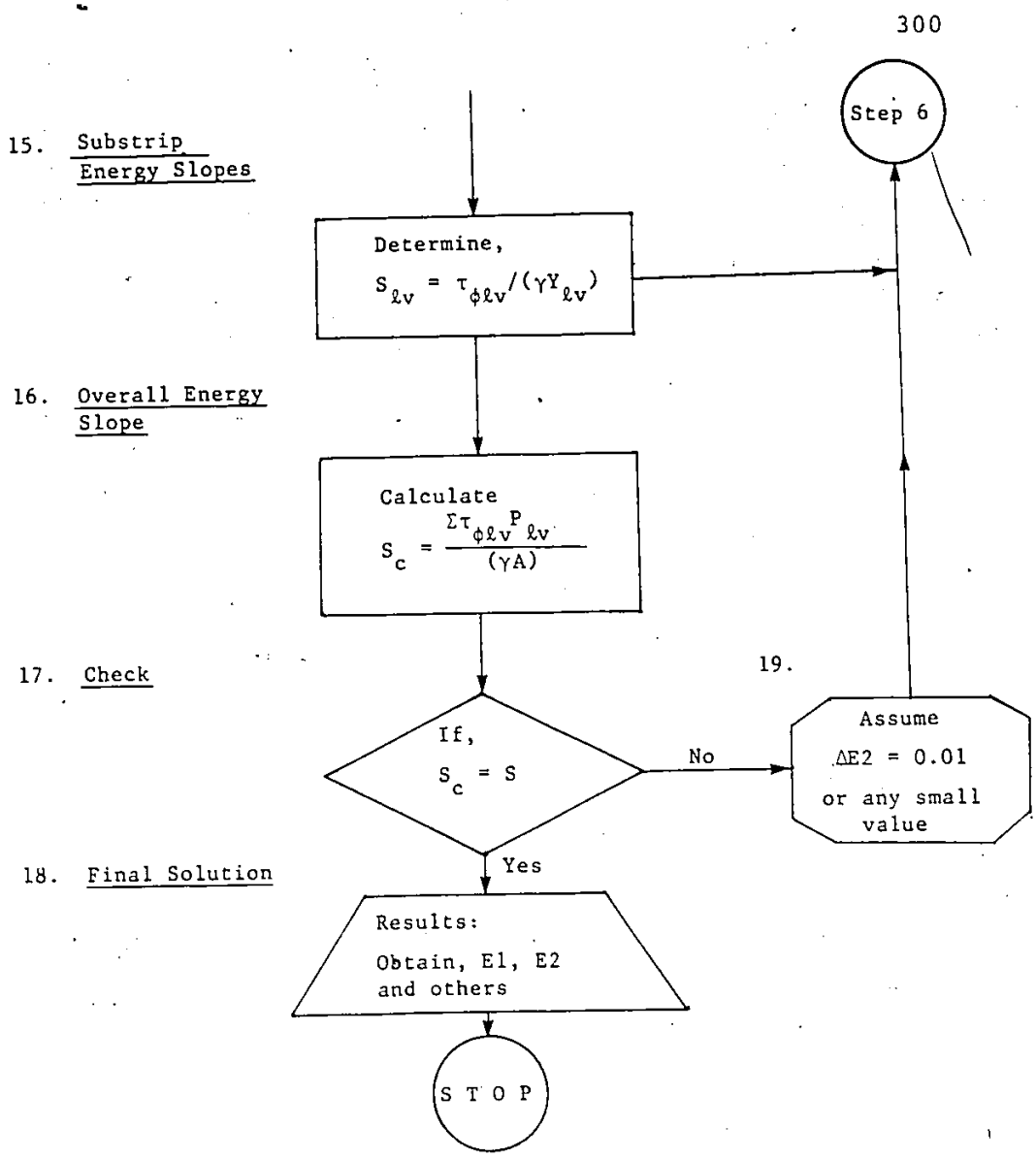

Figure FC-3. Flow Chart for the Determination of the Coefficients, E1 and E2, of Covered Surface Flow with Vertical Strips Analysis.

Figure FC.4 Flow Chart for the Determination of the Coefficients, E1 and E2, of Free-Surface Flow with Vertical Strips Analysis.

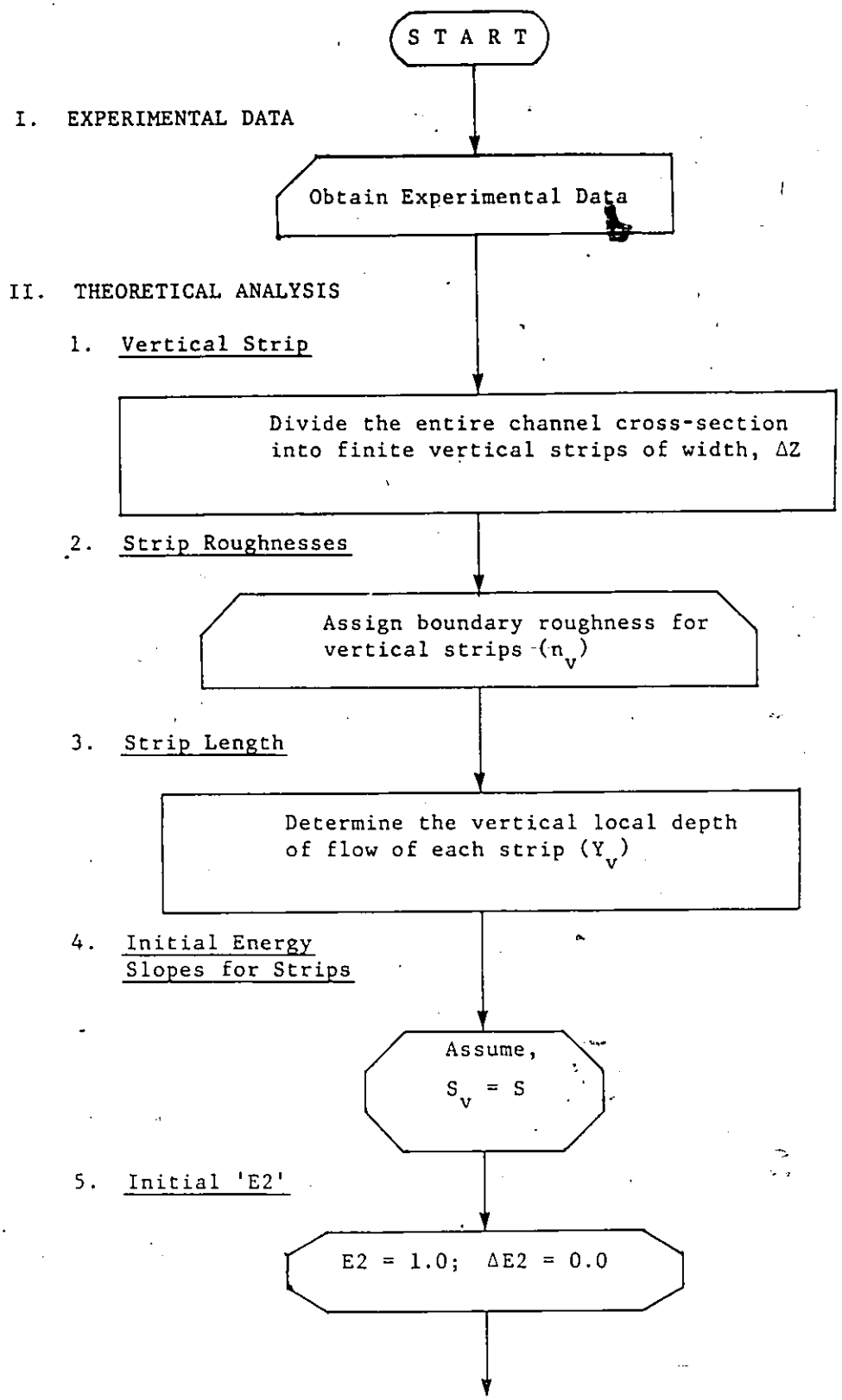
START
I. EXPERIMENTAL DATA
Obtain Experimental Data
II. THEORETICAL ANALYSIS
1. Vertical Strip
Divide the entire channel cross-section into finite vertical strips of width, ΔZ
2. Strip Roughnesses
Assign boundary roughness for vertical strips (n_v)
3. Strip Length
Determine the vertical local depth of flow of each strip (Y_v)
4. Initial Energy Slopes for Strips
Assume, $S_v = S$
5. Initial 'E2'
E2 = 1.0; ΔE2 = 0.0

6. Strip Mean Velocities

$$V_v = \frac{1}{n_v} Y_v^{2/3} S_v^{1/2}$$

7. Strip Dimensionless Velocity Distributions

$$\frac{u_v}{V_v} = 1 - \frac{n_v g^{1/2}}{\kappa Y_v^{1/6}} F_2(\varepsilon_v)$$

8. Coefficient E2

$$E2 = E2 \pm \Delta E2$$

9. Coefficient E1

$$E1 = \frac{A}{\left(\Sigma \left(\frac{u_v}{V_v}\right)^{E2} \Delta A\right)}$$

10. Channel Velocity Distributions

$$U = E1 \left(\frac{u_v}{V_v}\right)^{E2} V$$

11. Strip Velocity Distributions

$$u_v = \frac{u_v}{V_v} V_v$$

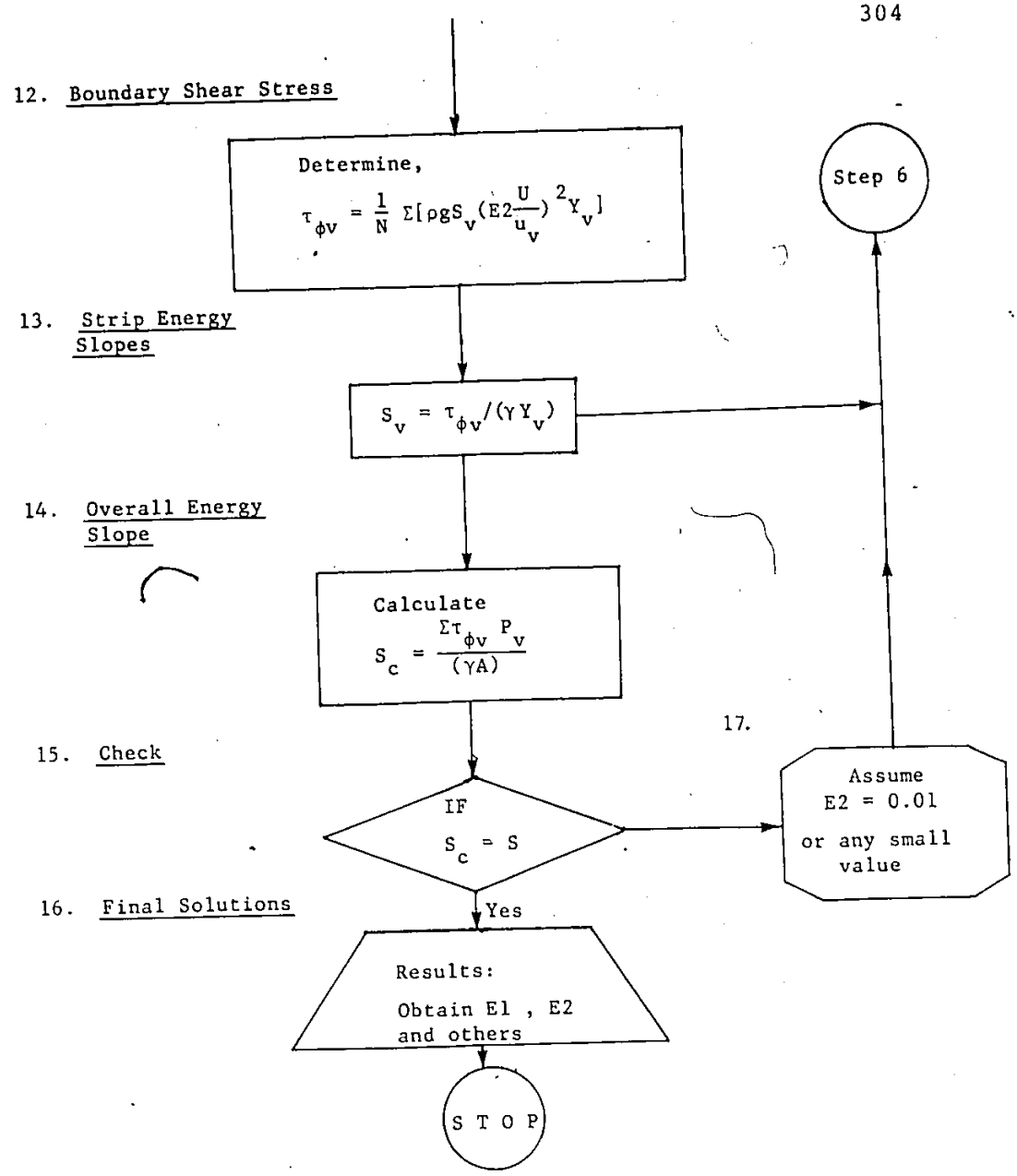

Figure FC-4. Flow Chart for the Determination of the Coefficients, E1 and E2, of Free-Surface Flow with Vertical Strips Analysis.

Figure FC.5. Extension of Flow Chart for Compound Channel.

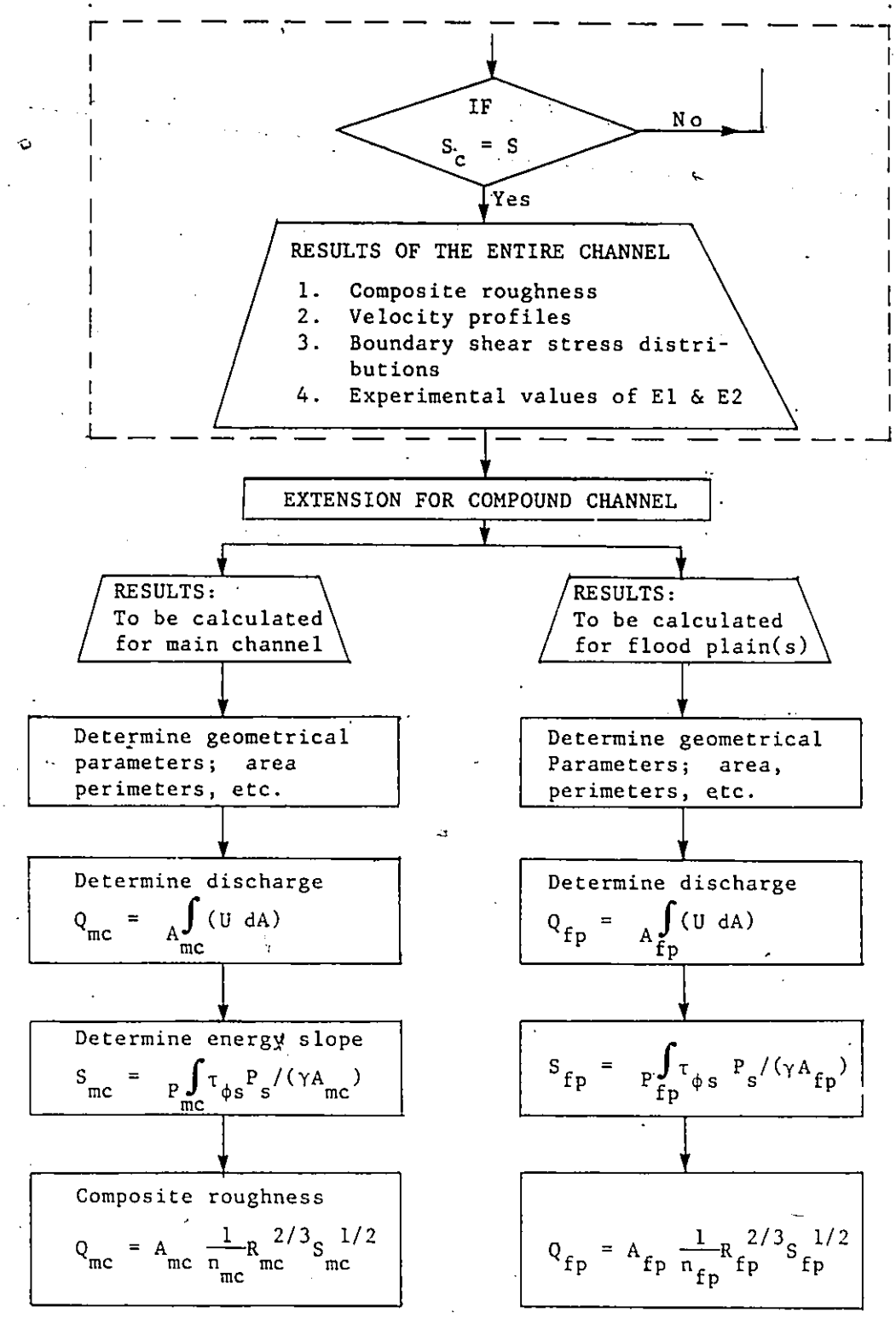

Figure FC.5 Extension of Flow Chart for Compound Channel.

REFERENCES

1. Allen, J. and Ullah, M. I., "The Flow of Water through Smooth Open Channels with Narrow Rectangular and T-shaped Cross-sections," Proceedings I.C.E., Vol. 36, February 1967, pp. 325-349.

2. Bhowmik, N. G. and Demissie, M., "Carrying Capacity of Flood Plains," Journal of the Hydraulics Division, ASCE No. HY3, March 1982, pp. 443-453.

3. Blalock, M. E. and Sturm, T. W., "Minimum Specific Energy in Compound Open Channel," Journal of the Hydraulics Division, ASCE, No. HY6, June 1981, pp. 699-717.

4. Blinco, P. and Partheniades, E., "Turbulence Characteristics in Free Surface Flows over Smooth and Rough Boundaries," Journal of Hydraulic Research, IAHR, Vol. 9, No. 1, 1971.

5. Carey, K. L., "Observed Configuration and Computed Roughness of the Underside of River Ice," U.S. Geological Survey Prof. Paper 550B, 1966, pp. B192-198.

6. Carey, K. L., "The Underside of River Ice, St. Croix River, Wisconsin, "U.S. Geological Survey Prof. Paper 575C, 1967, pp. C195-199.

7. Carey, K. L., "Analytical Approaches to Computation of Discharge of an Ice-covered Stream" U.S. Geological Survey Prof. Paper 575C, 1967, pp. C200-207.

8. Chee, S. P., Haggag, M. R., and Wong, Y. F., "Channel Configuration and Streamflow," International Conference on Water Resources Development, Taiwan, Republic of China, May 1980, pp. 651-660.

9. Chee, S. P., and Haggag, M. R., "Flow Resistance of Ice-covered Streams," (Reprinted from Canadian Journal of Civil Engineering, pp. 815-823 (1984), National Research Council of Canada, Vol. 11, No. 4, 1984, pp. 815-823.

10. Chee, S. P., and Ray, S. K., "Conveyance of Channels with Overbank Flow," IAHR, 21st Congress, August 1985, Melbourne, Australia, pp. 452-456.

11. Chee, S. P., and Ray, S. K., and Lau, A., "Rivers with Flood Plains," Proc. of CSCE Annual Conference, Vol. 2, Toronto, 1986.

12. Chee, S. P., and Ray, S. K., "Multiple Roughness Ice-covered Channels," IAHR Ice Symposium 1986, Iowa City, Iowa.

13. Chin, C. L., Hsiung, D. E. and Lin, H. C., "Three-dimensional Open Channel Flow," Journal of the Hydraulics Division, ASCE, Vol. 104, No. HY8, August 1978, pp. 1119-1136.

14. Chin, C. L. and Hsiung, D. E., "Secondary FLow, Shear Stress and Sediment Trnasport, "Journal of Hydraulics Division, ASCE, Vol. 107, No. HY7, July 1981, pp. 879-898.

15. Chin, C. L., Lin, H. C., and Kazumasa, M., "Simulation of Hydraulic Process in Open Channels," Journal of the Hydraulics Division, ASCE, Vol. 102, No. HY2, February 1976, pp. 185-206.

16. Chin, C. L., Hsuing, D. E., and Lin, H. C., "Secondary Currents under Turbulence in Open Channels of Various Geometrical Shapes," Proceedings of 18th Congress, IAHR, September 1979, pp. 10-14.

17. Chow, V. T., "Open Channel Hydraualics," McGraw-Hill Book Co., New York, 1959.

18. Coleman, N. L., and Alonso, C. V., "Two Dimensional Channel Flows over Rough Surfaces," Journal of Hydraulics Division, ASCE, Vol. 109, No. 2, Feb. 1983, pp. 184-225.

19. Dalleur, J. W., Toebes, G. H. and Udeozo, B.C., "Uniform Flow in Idealized Channel-Flood Plain Geometries," Proceedings 12th International Conference of IAHR, Fort COllins, Colorado, USA, 1967, pp. 218-225.

20. Demuren, A. O., "Prediction of Flow in Channels with Flood Plains," Proceedings of Engineering Mechanics Conference, ASCE, May 1983, Lafayette, Indiana, Vol. 2, pp. 1212-1215.

21. Elsawy, E. M. and Crory, P. M., "Effects of Interaction on a Channel with One Flood Plain," International Conference on Water Resources Engineering, Bangkok, Thailand, January 1978, pp. 597-608.

22. Ervine, D. A. and Baird, J. I., "Rating Curves for Rivers with Overbank Flow," Proceedings of I.C.E., Part 2, Vol. 73, 1982, pp. 465-472.

23. Ervine, D. A., and Baird, J. I., "Rating Curves for Rivers with Overbank Flow." Discussion, Proceeding of ICE, Part 2, 1982, 73, Dec., 849-855.

24. Ghosh, S. N., "Boundary Shear Distribution in Channels with Varying Wall Roughness," Proceedings of I.C.E., Part 2,53, December 1972, pp. 529-544.

25. Ghosh, S. N. and Kar, S. K., "River Flood Plain Interaction and Distribution of Boundary Shear Stress in a Meander Channel with Flood Plain," Proceedings of I.C.E., Part 2, 69, December 1975, pp. 805-811

26. Ghosh, S. N. and Roy, N., "Boundary Shear Distribution in Open Channel Flows," Journal of Hydraulics Division, ASCE, Vol. 96, April 1970, pp. 967-994.

27. Ghosh, S. N., "Boundary Shear Distribution in Rough Compound Channel," Synopsis, Proceedings of I.C.E., Vol. 55, June 1973, p. 487.

28. Ghosh, S. N. and Jena, S. B., "Boundary Shear Distribution in Open Channel Compound," Proceedings of I.C.E., Vol. 49, August 1971, pp. 417-430.

29. Ghosh, S. N. and Mehta, P. J., "Boundary Shear Distribution in a Compound Channel with Varying Roughness Distribution," Proceedings of I.C.E., Part 2, 57, March 1974, pp. 158-163.

30. Haggag, M. R., "Hydraulics of Floating Boundaries," Ph.D. thesis, 1980, Civil Engineering Department, University of Windsor, Ontario, Canada.

31. Henderson, F. M., "Open Channel Flow," Macmillan Service in Civil Engineering, pp. 144-145.

32. Hey, R. D., "Flow Resistance in Gravel-bed Rivers," J. of the Hyd. Divn., ASCE, No. HY4, April 1979, pp. 365-379.

33. James, M. and Brown, B., "Geometric Parameters that Influence Floodplain Flow," Research Report H-77-1, U.S. Army Eng. District, Kansas City, Missouri 64106, 1977.

34. Karasev, I. F., "Influence of the Banks and Flood Plain on Channel Conveyance," Soviet Hydrology: Selected Paper, Issue No. 5, 1969.

35. Kartha, V. C. and Leutheusser, H. J., Distribution of Tractive Force in Open Channels," Journal of Hydraulics Division, ASCE, No. HY7, July 1970, pp. 1469-1483.

36. Kazemipour, A. K. and Apelt, C. J., "Shape Effects on Resistance to Uniform Flow in Open Channels," Journal of Hydraulic Research, Vol. 17, No. 2, 1979, pp. 129-147.

36. Knight, D. W., "Boundary Shear in Smooth and Rough Channels," Journal of the Hydraulics Division, ASCE, Vol. 107, No. HY7, July 1981, pp. 839-851.

38. Knight, D. W. and Demetrious, J. D., "Flood Plain and Main Channel Flow Interaction," Journal of Hydraulics Division, ASCE, Vol. 108, No. HY8, August 1983, pp. 1073-1092.

39. Knight, D. W., Demetriou, J. D., and Hamed, M. E., "Boundary Shear in Smooth Rectangular Channels," Journal of Hydraulics Engg., ASCE, Vol. 110, NO. 4, April 1984, pp. 405-422.

40. Knight, D. W., Demetriou, J. D., and Hamed, M. E., "Stage Discharge Relationships for Compound Channels," Proc. 1st. Int. Conf. Channels & Channel Control Str. Southampton, 1984

41. Knight, D. W., and Hamed, M. E., "Boundary Shear in Symmetrical Compound Channels," Journal of Hydraulics Engineering, ASCE, Vol. 110, No. 10, October 1984, pp. 1412-1429.

42. Knight, D. W. and MacDonald, J. A., "Hydraulc Resistance of Artificial Strip Roughness," Journal of Hydraulics Division, ASCE, Vol. 105, No. HY6, June 1979, pp. 675-690.

43. Knight, D. W. and MacDonald, J. A., "Open Channel Flow with Varying Bed Roughness," Journal of Hydraulics Division, ASCE, Vol. 105, No. HY9, Sept. 1979, pp. 1167-1183.

44. Krishnamurthy, M., and Christensen, B.A., "Equivalent Roughness for Shallow Channels," Journal of Hydraulics Division, ASCE, No. HY12, Dec. 1972, pp. 2257-2263.

45. Lau, A., "Discharge and Resistance of Streams with Multiple Roughness," MA.Sc. thesis, Civil Engineering Department, University of Windsor, Windsor, Ontario, Canada, 1982.

46. Lau, Y. L. and Krishnappan, B. G., "Ice Cover Effects on Stream Flows and Mixing," Journal of the Hydraulics Division, ASCE, No. HY10, Proc. Paper 16602, Oct. 1981, pp. 1225-1242.

47. Le Van Kiyen, "Hydraulic Computation of Flood Plain Channels," Soviet Hydrology: Selected Papers,,Issue No. 4, 1968.

48. Launder, B. E. and Spalding, D. B., "The Numerical Computations of Turbulent FLow," Computer Methods in Applied Mechanics and Engineering, 1974, 3, pp. 269-289.

49. Liggett, J. A. and Chin, C. L., Secondary Currents in a Corner," Journal of the Hydraulics Division, ASCE, Vol. 91, No. HY6, November 1965, pp. 99-117.

50. Mehoute, B. L., "An Introduction to Hydrodynamics and Water Waves," Springer-Verlag, New York, Heidelberg, Berlin, 1976.

51. Marchi, E., "Resistance to Flow in Fixed-Bed Channels with the Influence of Cross-Sectional Shape and Free Surface," 12th Congress, International Association for Hydraulics Research, 1967, pp. 32-40.

52. Morris, M. H., and Wiggert, J. M., "Applied Hydraulics in Engineering," 2nd ed., New York, The Ronald Press Company, 1972.

53. Myers, W.R.C., "Momentum Transfer in a Compound Channel," Journal of Hydraulic Research, IAHR, Vol. 16, No. 2, 1978, pp. 139-150.

54. Myers, W.R.C., "Friction Factor Relationships in Compound Channels," Proceedings of the International Conf.

55. Myers, W.R.C. and Elsawy, E. M., "Boundary Shear in Channel with Flood Plain," Journal of the Hydraulics Division, ASCE, Vol. 101, July 1975, pp. 933-946.

56. Nalluri, C. and Adepoju, R. A., "Shape Effects on Resistance to Flow in Smooth Channels of Circular

Cross-Section," Journal of Hydraulic Research, Vol. 23, 1985, No. 1, pp. 37-46.

57. Noutsopoulos, G. and Hadjipanos, P., "Discharge Computations in Compound Channels," Proceedings of Intern. Conf. of IAHR, Vol. D, Moscow, September 1983, pp. 173-180.

58. Overton, D. E., "Flow Retardance Coefficients for Selected Prismatic Channels," Transactions, American Society of Agricultural Engineers, Vol. 10, No. 3, 1967.

59. Pasche, E., Evers, P. and Rouve, G., "Investigations on Hydraulic Effects of Vegetated Flood Plains in Compound Cross-section and their Influences on Discharge Capacity," Proceedings of Intern. Conf. of IAHR, Vol. D, Moscow, September 1983, pp. 489-497.

60. Petryk, S. and Grant, E. U., "Critical Flow in Rivers with Flood Plains, "Journal of the Hydraulics Division, ASCE, Vol. 104, No. HY5, May 1978, pp. 583-593.

61. Posey, C. J., "Computation of Discharge including Over-bank Flow," Civil Engineering, ASCE, April 1967, pp. 62-63.

62. Prinos, P., "A Study of Momentum Transfer Phenomena in Compound Channel Flows," Ph.D. thesis, Department of Civil Engineering, University of Ottawa, Ottawa, Ontario, Canada, 1985.

63. Prinos, P. and Townsend, D. R., "A Comparison of Methods for Predicting Discharge in COmpound Open Channels," Advance Water Resources, 1986, Vol. 7, December, pp. 180-187.

64. Prinos, P. and Townsend, D. R., "Prediction of Main Channel/Flood Plain Flow Interaction with FEM," Proceedings of 6th International Conference on Finite Elements in Water Resources, Vermont, 1984, pp. 356-361.

65. Prinos, P. and Townsend, D. R., "Estimating Discharge in Compound Open Channels," Proceedings of 6th Canadian Hydrotechnical Conference, Vol. 1, June 1983, pp. 129-146.

66. Radojkovic, M., "Mathematical Modeling of Rivers with Flood Plains," 3rd Annual Symposium of the Waterways, Harbours and Coastal Eng. Div., ASCE, Vol. 1, Rivers 1976, pp. 55-64.

67. Radojkovic, M. and Ivetic, M., "Finite Element Analysis of Momentum Transfer in Rivers of Complex Cross-section" Proceedings 4th Int. Conference on Finite Element in Water Resources, Hanover, 1982.

68. Rajaratnam, N. and Ahmadi, R. M., "Interaction between Main Channel and Flood Plain Flows," Journal of the Hydraulics Division, ASCE, Vol. 105, No. HY5, May 1979, pp. 573-588.

69. Rajaratnam, N. and Ahmadi, R., "Hydraulics of Channels with Flood Plains," Journal of Hydraulic Research, IAHR, Vol. 19, No. 1, 1981.

70. Replogle, J. A. and Chow, V. T., "Tractive Force Distribution in Open Channels," Journal of the Hydraulics Division, ASCE, Vol. 92, NO. HY2, March 1966, pp. 169-191.

71. Rice, C. E., "Hydraulics of Main Channel Flood Plain Flows," Research Project Technical Completion Report, Oklahoma State Univ., 1974.

72. Rouse, H., "Critical Analysis of Open-Channel Resistance," Journal of the Hydraulics Division, ASCE, Vol. 91, No. HY4, July 1965, pp. 1-25.

73. Sarma, K.V.N., Lakshminarayana, P., and Rao, N.S.L., "Velocity Distribution in Smooth Rectangular Open Channels," Journal of Hydraulics Division, ASCE, Vol. 109, No. 2, Feb. 1983, pp. 270-293.

74. Sinotin, V. J., "Velocity Structures of Flow under Ice Cover," 11th Congress, International Association for Hydraulics Research, Leningrad, 1965, pp. 435-437.

75. Sumbal, J. and Komora, J., "Determination of the Tangential Stress Acting on the Ice Cover in a Rectangular Flume," 12th Congress, International Association for Hydraulics Research, 1967, pp. 255-259.

76. Tingsanchali, T. and Ackermann, N. L., "Effects of Overbank Flow in Flood Computations," Journal of the Hydraulics Division, ASCE, Vol. 102, No. HY7, July 1976, pp. 1013-1025.

77. Toebes, G. H. and Sooky, A. A., "Hydraulics of Meandering Rivers with Flood Plains," Journal of Waterways and Harbours, ASCE, Vol. 93, May 1967, pp. 213-236.

78. Tracy, H. J., "Turbulent FLow in a Three-Dimensional Channel," Journal of the Hydraulics Division, ASCE, No. HY6, Proc. Paper 4530, Nov. 1965, pp. 9-35.

79. Tracy, H. J., "The Structure of a Turbulent Flow in a Channel of Complex Shape," U.S. Geological Survey, Prof. Paper 983, 1976, 25p.

80. Uzuner, M. S., "The Composite Roughness of Ice Covered Streams," Journal of Hydraulics Research, IAWH, No. 1, 1975, pp. 79-102.

81. Vreugdenhil, C. B. and Wijbenga, J.H.A., "Computation of Flow Patterns in Rivers," Journal of the Hydraulics Division, ASCE, November 1982, HY11, pp. 1296-1309.

82. Vreugdenhil, C. B. and Wijbenga, J.H.A., "Closure on Computation of Flow Patterns in Rivers," Journal of the Hydraulics Division, ASCE, January 1984, HY1, pp. 90-91.

83. Weiss, H. W. and Midgley, D. C., "Suite of Mathematical Flood Plain Models," Journal of the Hydraulics Division, ASCE, Vol. 104, No. HY3, March 1978, pp. 361-375.

84. Wong, Y. F., "Influence of Cross-Sectional Shape on Channel Flow with a Floating Boundary," MA.Sc. thesis, Civil Engineering Department, University of Windsor, Windsor, Ontario, Canada, 1979.

85. Wormleaton, P. R., Allen, J. and Hadjipanos, P., "Effects of Shear Stresses in Compound Channels," Proceedings of the International Conference on Water Resources Development, Taipei, Taiwan, Republic of China, May 12-14, 1980.

86. Wormleaton, P. R., Allen, J. and Hadjipanos, P., "Discharge Assessment in Compound Channel Flow," Journal of the Hydraulics Division, ASCE, Vol. 108, NO. HY9, September 1982, pp. 975-993.

87. Wright, R. R. and Carstens, M. R., "Linear-Momentum Flux to Overbank Sections," Journal of the Hydraulics Division, ASCE, VOl. 96, No. HY9, September 1970, pp. 1781-1793.

88. Yen, C. L. and Overton, D. E., "Shape Effects on Resistance in Flood-Plain Channels," Journal of the Hydraulics Division, ASCE, Vol. 99, No. HY1, January 1973, pp. 219-238.

VITA AUCTORIS

It was the historical year, when India achieved sovereignty, that the author was born. The year was 1947 and the date was the 2nd day of June.

In 1971 the author completed his first degree in Civil Engineering with first class standing from Jadarpur University, Calcutta, India and in 1975 he was honoured with a Master degree in the field with specialization in Structural Engineering from Regional Engineering College, Durgapur, W.B. India.

In 1974 he joined Calcutta Metropolitan Development Authority (CMDA), Government of West Bengal, as an Assistant Engineer and served the Authority till the date (January 1980) of his arrival to this country at Ottawa. The author has years of experience in the professional field through working with several reputable organizations in Calcutta before he joined CMDA.

Had built up a sound background in the sphere of water resources (SWM) by completing several graduate course works and through research works at the University of Ottawa during 1980-81. During 1981-82 he worked at the Civil Engineering Department of the Royal Military College, Kingston as a full-time Research Assistant (Structural Engg.) on a project fully funded by the Department of National Defence. In 1983 he resumed his graduate studies at the University of Windsor.